Vibration Suppression in Flexible Structures using Hybrid Active and Semi-active Control

The University Of Sheffield.

Irfan Ullah Khan

Supervisor: Prof. D. Wagg and Prof. N. D. Sims

Department of Mechanical Engineering

University of Sheffield

This dissertation is submitted for the degree of

Doctor of Philosophy

June 2017

I would like to dedicate this work to my parents.

Declaration

I hereby declare that all the work presented in this thesis is original unless otherwise stated or referred and has not been submitted anywhere else to attain a degree. The thesis meets the university requirements and has less than 80,000 words including appendices, references, footnotes, equations, tables. The work presented here is my own work and has not been done in collaboration with any institute or group.

Irfan Ullah Khan

June 2017

Acknowledgements

First of all, I would like to thank my parents and family for their support and belief in me. Without their support, it would not be feasible for me to reach up to this stage. I would like to express my deep gratitude to my supervisors Prof. David Wagg and Prof. Neil Sims for their guidance and help. Weekly discussions with my supervisors and their continuous feedback helped me a lot in every step of my research. I acknowledge and appreciate Prof. David Wagg, who has provided me with various opportunities to present my work in different conferences. He has associated me with Engineering Nonlinearity (ENL) group as well, where I have presented my work in the form of posters and presentations. This platform has also given me an opportunity to interact with people linked with academia and industry. I also want to thank everyone from the Dynamic Research Group (DRG) for their support. I would like to acknowledge Mr. Les Morton help during redesigning of rig in the lab and Mr. Richard Kay, who provided his expertise along with the Oddy hydraulics people for fault identification in the hydraulic system. I am thankful to all my friends who supported, tolerated and encouraged me throughout this journey. Last but not the least, a special gratitude to Melanie Fitzgerald and Numaira Khan for the support and help with the proof read.

Abstract

This thesis presents a new hybrid active and semi-active control method for vibration suppression in flexible structures. The method uses a combination of a semi-active device and an active control actuator situated elsewhere in the structure to suppress vibrations. The key novelty is to use the hybrid controller to enable the semi-active device to achieve a performance as close to a fully active device as possible. This is accomplished by ensuring that the active actuator can assist the semi-active device in the regions where energy is required. Also, the hybrid active and semi-active controller is designed to minimise the switching of the semi-active controller. The control framework used is the immersion and invariance control technique in combination with a sliding mode control. A two degree-of-freedom system with lightly damped resonances is used as an example system. Both numerical and experimental results are generated for this system and then compared as part of a validation study.

The experimental system uses hardware-in-the-loop simulation to simulate the effect of both the degrees-of-freedom. The results show that the concept is viable both numerically and experimentally, and improved vibration suppression results can be obtained for the semi-active device that approaches the performance of an active device. To illustrate the effectiveness of the proposed hybrid controller, it is implemented to keep the contact force constant in the pantograph-catenary system of high-speed trains. A detailed derivation is given after which the simulation results are presented.

Then a method to design a reduced order observer using an invariant manifold approach is proposed. The main advantage of this approach is that it enables a systematic design approach, and (unlike most nonlinear observer design methods), it can be generalised over a larger class of nonlinear systems. The method uses specific mapping

functions in a way that minimises the error dynamics close to zero. Another important aspect is the robustness property which is due to the manifold attractivity: an important feature when an observer is used in a closed loop control system. The observer design is validated using both numerical simulations and hardware-in-the-loop testing. The proposed observer is then compared with a very well known nonlinear observer based on the off-line solution of the Riccati equation for systems with Lipschitz type nonlinearity. In all cases, the performance of the proposed observer is shown to be excellent.

Table of contents

List of figures

List of tables

Nomenclature

Greek Symbols

α_s stiffness variation coefficient in a span

$\beta = [\beta_1, \beta_2, \beta_3]^T$ mapping function vector

η_{smc} SMC design parameter

γ Lipschitz constant

$\hat{\eta} = [\hat{\eta}_1, \hat{\eta}_2, \hat{\eta}_3]^T$ observer state vector

$[\lambda_1, \lambda_2]$ SMC controller gains

$\phi = [\phi_1, \phi_2, \phi_3]^T$ mapping function vector

$\pi = [\pi_1, \pi_2, \pi_3, \pi_4]^T$ mapping function vector

$\xi = [\xi_1, \xi_2]^T$ target system state vector

Other Symbols

$\hat{x}$ observer state vector

$\mathscr{M}$ manifold

$\tilde{x}$ error dynamics state vector

A system matrix

A^T transpose of matrix A

C	system matrix
C^T	transpose of matrix C
C_1	damping coefficient between the fixed support and m_1
C_2	damping coefficient between m_1 and m_2
E	potential energy function
e	error in sliding mode control
e_p	position error in PI controller
e_v	velocity error in PI controller
f	nonlinear function
f_a	active actuator output
f_n	normalized control signal
f_c	contact force between pantograph and catenary
$f_{i\&i}$	I and I controller output
f_{sa}	semi-active device (MR damper) output
f_{smc}	SMC controller output
g	nonlinear function
I	identity matrix
I_{MR}	MR damper input current
$K(t)$	time varying stiffness function for catenary
K_1	spring stiffness coefficient between the fixed support and m_1
k_1, k_2	I and I controller gains

K_2 spring stiffness coefficient between m_1 and m_2

K_3 cubic stiffness coefficient

K_a fluid compressibility of MR damper

K_0 average equivalent stiffness coefficient of catenary

K_{cat} constant catenary stiffness coefficient

K_{max} maximum stiffness value in a span

K_{min} minimum stiffness value in a span

K_{smc} SMC design parameter

K_s pantograph shoe stiffness coefficient

$[Ki, Kv, Kp]$ PI controller gains

L gain matrix

L_s span length

m_1 base mass of 2DOF system

m_2 top mass of 2DOF system

m_a fluid mass of MR damper

m_b piston head mass of MR damper

R damping function

R_{MR} MR damper internal resistance

S sliding surface

t time

U_d excitation signal

V Lyapunov function

v_r relative velocity

V_t train speed

V_z Lyapunov function for observer error dynamics

$V_{i\&i}$ Lyapunov function for I and I controller

V_{smc} Lyapunov function for SMC controller

$x = [x_1, x_2, x_3, x_4]^T$ 2DOF system state vector

X_1 displacement of m_1

X_2 displacement of m_2

x_a displacement of m_a

x_b displacement of m_b

$z = [z_1, z_2]^T$ error dynamics state vector

Acronyms / Abbreviations

2-DOF Two Degree Of Freedom

A Ampere

ADC Analog to Digital Converter

AMD Active Mass Damper

ARE Algebric Riccati Equation

ATMD Active Tuned Mass Damper

C Centigrade

cm Centimeter

DAC Digital to Analog Converter

DC Direct Current

DSP Digital Signal Processor

ER Electro-Rheological

g Gram

h Hour

HIL Hardware In Loop

HMD Hybrid Mass Damper

I & I Immersion and Invariance

kg Kilogram

km Kilometer

LAN Local Area Network

LQR Linear Quadratic Regulator

LVDT Linear Variable Differential Transformer

MIMO Multi-Input-Multi-Output

m Meter

mm Millimeter

MR Magneto-Rheological

NI National Instruments

N Newton

PCB Printed Circuit Board

PID Proportional Integral Derivative

PIFD Proportional Integral Feedforward Derivative

PI Proportional Integral

psi Pounds per Square Inch

RAM Random Access Memory

SASD Semi-Active Stiffness Damper

SDOF Single Degree Of Freedom

sec Second

SMC Sliding Mode Control

TLCD Tuned Liquid Column Damper

TMD Tuned Mass Damper

VSC Variable Structural Control

Chapter 1

Introduction

Vibrations in mechanical systems are normally undesirable, because they can cause wear and tear, can affect the controller performance and in a worst case scenario they can destroy the complete system. In many applications it is imperative to observe these vibrations including environmental disturbances and keep them under control all the time. Much research has been done on vibrations attenuation [1–5]. In the literature different control techniques, both linear and nonlinear have been developed for this purpose. Oscillation in any system is considered as vibration. There are two main types of oscillations; free and forced. There is also a third type called self-excited oscillations e.g flutter. In the free oscillations there is no external forced involved and eventually, they die out because of the system damping. In the forced oscillations, the external force keeps the system oscillating all the time.

In the past, vibrations caused some of the devastating incidents and one of the most famous is the Tacoma Narrows suspension bridge shown in Figure 1.1. This bridge was constructed in 1940 and was the longest suspension bridge at that time. A phenomenon called flutter (or aeroelastic instability) completely destroyed the bridge. In this phenomenon, the structure starts simple harmonic motion, and the net damping goes to zero either suddenly or gradually. If the net damping goes to zero suddenly, then it is called hard flutter otherwise it is soft flutter. The damping caused by the aerodynamic forces cancels the structure's positive damping, which makes the net damping zero, so any further decrease in the damping can lead to structural damage.

Fig. 1.1 Tacoma narrows suspension bridge [1]

1.1 Vibration in Civil Structures

Civil structures include bridges, buildings, dams and towers. The main sources of vibrations for these structures are earthquakes, wind, ground vibration coming from machines, humans and vehicles. It is unavoidable to keep the structure isolated completely from these vibrations. However, for the safety of the structures and the people working in or around them, the vibrations need to be limited within a certain range to avoid permanent damage. As buildings have become taller over the years, the vibrations induced by the wind have become more of a problem.

For bridges, wind also becomes the most important effect as the bridges become longer. Another issue is the ground vibration caused by the humans and the vehicles and for that very reason when a troop is crossing a bridge they have to break the rhythm of their steps, otherwise it can excite the structure at its resonant frequency which can lead to significant vibrations. Similarly, if there is a gym on the ground floor of a building, when in heavy use, these activities can also lead to noticeable vibration in the structure.

In the early days, researchers have focused mainly on using passive damping techniques to deal with vibration in civil structures. They are still used, but provide less vibration reduction than either active or semi-active devices. An advantage of passive dampers is that they do not require external power to operate. Different passive dampers

[1] http://seattletimes.com/html/localnews/2003787138_narrowstimeline13m.html

are utilised in the construction of earthquake resistant structures in U.S, Japan, New Zealand, Italy, China, Canada and Colombia. The University of Southern California teaching hospital is one of the buildings that survived in 1994 earthquake out of 10 other hospitals because of base isolation is shown in Figure 1.2.

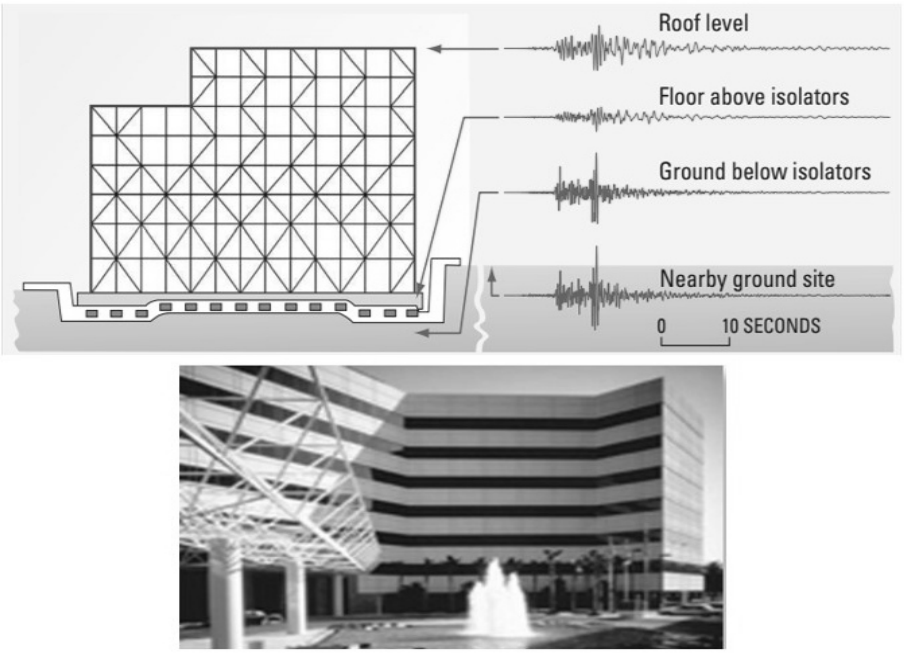

Fig. 1.2 Base isolation in USC teaching hospital [2]

There are numerous other examples of passive damping application like the use of metallic yield dampers in the Ski-Dome in Chiba, Japan, viscoelastic dampers in the building of Columbia Seafirst, train stations in Taipei Chien-Tan Taiwan, the Amolanas Bridge, Chile [6]. Figure 1.3 shows the base isolation implementation in the San Diego County Emergency Communications Center.

There was a hesitation in using the active control techniques with active actuators because there is a possibility that system can go to unstable regions with the active actuator. So instead of moving to the active actuators, the trend shifted to the semi-active devices, the reason being that both passive and semi-active devices are fail-safe. However, with the advancement in the active control techniques and especially in the area of nonlinear control, active actuators are now used in the civil structures. In some cases, the active actuators have been combined with the passive device and in other

[2]http://pubs.usgs.gov/fs/2003/fs068-03/fs068-03.pdf

situations, the semi-active devices are combined with the passive devices for better performance.

Fig. 1.3 Base isolation in San Diego County Emergency Communications Center [3]

The problem with passive damping devices is that they cannot adapt to circumstances. In order to tackle this issue semi-active devices have replaced the passive devices in many applications. The main advantage of the semi-active device is the ability to vary the damping. There are mainly two types of semi-active dampers, electro-rheological (ER) and magneto-rheological (MR). In MR dampers the damping is modified by varying the magnetic field around the magneto-rheological fluid, whereas in ER dampers the damping changes by varying the electric field. MR dampers can provide more damping as compared to ER dampers but the response time of ER dampers is faster than MR dampers. Another advantage of the semi-active devices is that they need low actuation power, but the disadvantage is that they cannot inject energy into the system, they can only dissipate energy from the system. The output power generated by semi-active devices is also limited as compared to active actuators. Some of the examples of the MR dampers used in civil engineering structures are the National

[3] http://www.sdsheriff.net/ccweb/building.htm

Museum of Emerging Science and Innovation, Tokyo, Dongting Lake Bridge, Hunan, China and Binzhou Yellow River Bridge, China.

The third type of device used recently in many structures for vibration damping is that of active actuators. Some examples of this include the Kyobashi Center, and the Research Institute No. 21 Sendagaya INTES in Tokyo, Japan, the Applause Tower in Osaka, Japan, Porte Kanazawa, Kanazawa, Japan and Nanjing Tower, Nanjing, China. Active actuators can inject energy into the system and can also dissipate energy out of the system. The main issue that needs addressing while using active actuators is the stability of the closed loop system because energy is also going into the system. The other problems usually faced are the actuator size and the actuation power required by the actuators.

1.2 Vibration in Aerospace Industry

Vibrations are caused by various sources in an aeroplane. Some of them originate from the structure itself, and some are due to the external forces on the structure. Again these vibrations need to be controlled because of the risk of structural damage and also to avoid discomfort to the aircrew and passengers. One of the primary sources of vibration in aeroplanes is the engine. Due to unbalanced forces in the engine, the vibrations can be transmitted to the whole structure through the mounting mechanism. Hence much work has been done on the mounting mechanism to isolate the engine from the rest of the structure, to minimise the vibrations.

To reduce the amplitude of the transmitted vibration from the engine, the natural frequency of mounting mechanism should be lower than the fundamental frequency of the disturbance force that is causing the vibrations in the engine. The problem is that the frequency of the disturbance force is usually very low. It means that the mounting mechanism should have further lower natural frequency and for that purpose, the mounting mechanism needs to be flexible, which is practically not possible in aeroplanes [7]. So these vibrations are inevitable and cannot be eliminated. Hence advanced control techniques are required to control these vibrations.

There are also other sources of vibration in an aeroplane. One of them is the regular air flow, however, these vibrations are considered as normal vibrations or background noise. Vibrations resulting from turbulent flow are more prominent but again regarded as normal vibrations. There is another phenomenon called flutter or aeroelastic instability, which as explained earlier can cause very damaging vibrations in the structure. During the design phase, extensive testing is done to make the structure flutter free within the aeroelastic stability region. Another phenomenon very close to flutter is limit cycle oscillation (LCO), but the difference is the LCO is self-excited and self-sustaining oscillation with limited amplitude. Mainly LCO is caused by the free play within the flight control surfaces. The first ever plane crashed due to flutter was the Handley Page O/400 bomber in 1916 in the UK.

(a) AS350 helicopter [4] **(b)** Alouette III helicopter [5]

Fig. 1.4 Vibration effects in helicopters

Vibrations in a helicopter are more crucial as compared to the aeroplane. The current level of vibrations in helicopters is between 0.05-0.1 g, which is much higher than the vibration levels in aeroplanes i.e. 0.01 g. These vibrations have adverse effects on the structure, control panel, instruments, etc. and more importantly the aircrew and passengers' health and safety. They have long lasting effects on the aircrew health both physically and mentally. The helicopter has rotating parts which are the main sources of vibration. The vibrations that come from the main rotor transmit to the structure components and the aircrew through seats. The tail rotor has the same effect on the

[4]https://www.youtube.com/watch?v=0FeXjhUEXlc
[5]http://www.aviafora.com/forums/forum/helicopter-fora/gazelles

structure. The unbalance, flexibility and misalignment in the rotating parts generate the vibrations.

Aerodynamics can also make one blade work harder than the other or uneven mass distribution in the blades can also lead to vibration. The vibration coming from the gears can also have severe effects on the structure. The AS350 helicopter suffered from excessive vibrations in the air and those vibrations developed into destructive ground resonance after the aircraft touched the ground. The Alouette-III helicopter also suffered from ground resonance. Both the incidents are shown in Figure 1.4, which depicts that it is critical to control all these vibrations.

Vibrations in spaceships or rockets are serious concern as well. They can make the avionics, instruments, etc. malfunction and again can have a severe effect on the human body. The level of vibrations in a spaceship are much higher than both in the helicopter and aeroplane. In the first stage, the vibrations that are produced by the thrust force causing rhythmic oscillations in the form of waves. In addition to effect the performance of the avionics, they can shut down the main engine too.

1.3 Vibration in Automobiles

In the automobile industry vibration control has always been an important topic and lots of literature is available regarding the effects and control of vibrations. Vibrations coming from any source in the automobile affect the whole structure as well as on the passengers. The main sources of vibrations are the engine, or electric motors in case of hybrid electric vehicles, drive-train and road roughness/bumps. Regarding the vehicle, these vibrations can affect the performance of the engine or electric motor, fuel consumption and wear and tear in the drive train. Another vital impact of these vibrations is on the ride comfort for the driver and passengers.

In a vehicle, vibrations are transmitted to the human body through the seat. Vibrations have very adverse effects on the human body both physically and mentally depending on the nature and duration of the vibrations. A human body exposed to vibrations can lead to neck and back pain, drowsiness, fatigue, heart rate variability,

an effect on vision, and tension in muscles. Mental alertness is a very crucial factor for the drivers, especially during long drives. Generally, in automobiles, the vibrations transmitted to the human body through seat are below 60 Hz. The human body resonates at a frequency below 15 Hz. Exposure to vibrations between 4-10 Hz can cause pain in the chest, vibrations between 8-12 Hz can cause pain in the back, vibrations between 10-20 Hz can cause a headache, effect on vision, discomfort in the bladder and intestines [8].

1.4 Vibration in Robotics

With the advancement in the field of robotics, vibration is the key concern. In some applications like surgery, car manufacturing and PCB soldering, precision is crucial. A small vibration can lead to a huge disaster and can cost lives. To achieve high performance and in breaking new ground, structures are becoming more lightweight and flexible, but at the cost of vibration. So again vibration control techniques play a paramount role in achieving these goals. In the field of robotics mostly active actuators are used for the control purpose in contrast to the civil or automobile industry. Vibration in industrial machines like pumps, motors, gears, robotics arms, rolling mills etc. are also of great concern. Some application may have less concern about vibration than others, but the concern is always there. Figure 1.5 shows the damage done by the vibration in industrial machines.

(a) Damaged motor shaft **(b)** Destroyed coupling

Fig. 1.5 Torsional vibration effects [6]

[6]http://nisee.berkeley.edu/lessons/kelly.html

1.5 Motivation

In today's world structures in the fields of civil, aeronautical and mechanical engineering are becoming more flexible because of the design constraints and also in order to achieve better performance, but flexibility correlates with vibrations, which can have catastrophic effects on a structure. Active control devices (actuators) provide the best solutions, and depending on the context; there is a broad range of both linear and nonlinear design approaches that can be applied [9–14]. However, there are often restrictions on using active actuators, such as size or weight, power consumption, mechanical design constraints, robustness issues, and lack of passive fail-safety. An alternative is to use a semi-active device that is smaller in size with less power consumption, and often has a passive fail-safety. However, it is not possible to get the same performance from a semi-active device because they can only operate by dissipating energy.

Hybrid control has frequently been used in the literature to describe the combination of two control techniques or devices. For example, active and passive control [15, 16], or semi-active and passive control [17, 18]. However, to the authors' knowledge, a hybrid combination of active and semi-active control has not been previously studied in detail in this context. The novelty presented in this thesis is to show how an active actuator, placed at a different location in the structure (e.g., at the base of the structure) can assist the semi-active device at the remote position to achieve the performance as close to that of a fully active actuator as possible. The clipping phenomenon, typical of semi-active control, is reduced to a large extent by the proposed hybrid controller. The immersion and invariance methodology along with sliding mode control is used to create the hybrid controller. The result is that as the semi-active controller switches off in the hybrid controller, the active actuator injects the required energy into the system. A two degree of freedom system with cubic stiffness is used as an example system. Both simulation and experiment data are presented to demonstrate the usefulness of the proposed idea.

After the controller design and validation, there is another very active research area that has been explored in this thesis namely nonlinear observers. One of the

major issues with nonlinear observers is that most of them do not possess a structured design methodology and if they do then some of the conditions are very hard to meet. Secondly, most of them are designed for a specific class of systems. A method to design a reduced order observer using an invariant manifold approach is explored. The main advantages of this method are that it enables a systematic design approach, and (unlike most nonlinear observer design methods), it can be generalized over a larger class of nonlinear systems.

The theory for observers developed by Astolfi *et al.* [19] has been implemented on many systems, such as ball and beam system, range estimation in a vision system and magnetic levitation system. The present contribution builds upon these previous studies by demonstrating application of the observer to a real mechanical system both in open loop and closed loop, so that the robustness to parameter variation, external disturbance and measurement noise can be explored for the first time. Therefore, the idea presented by Astolfi *et al.* [19] is further extended to systems with nonlinear stiffness The method uses specific mapping functions in a way that minimises the error dynamics close to zero. Another important aspect is the robustness property which is due to the manifold attractivity: an important feature when an observer is used in a closed loop control system. The observer design is validated using numerical simulation. Then experimental validation is carried out using hardware-in-the-loop testing.

1.6 Aims and Objectives

The overall objective of the thesis is

- To achieve fully active type control performance using hybrid active and semi-active control.

The additional objectives are

- To understand how an active actuator can assist the semi-active device to achieve the desired performance.

- To design a nonlinear robust controller for both active actuator and semi-active device.
- To implement the proposed hybrid active and semi-active controller on a test rig using hardware-in-the-loop (HIL) configuration.
- To design a nonlinear observer for the system under consideration.
- To implement the proposed observer on a test rig using hardware-in-the-loop (HIL) configuration both in the open and closed-loop.
- To consider practical application of the proposed controller in different real-time applications.

1.7 Thesis Outline

- In Chapter 2, a detailed literature review is presented. First the passive damping devices used for the vibration suppression and vibration isolation are discussed. Then the semi-active devices are discussed and MR damper is described in detail. A comparison between MR and ER dampers is presented. Active control devices are then discussed briefly. After that the control techniques that has been used in the literature for the MR damper and for the active actuators are discussed in detail. Finally the two control techniques i.e. the sliding mode control and immersion & invariance control are explained in detail.
- In Chapter 3, the hybrid active and semi-active controller design methodology is discussed in detail. An Immersion and Invariance (I & I) methodology is used to design the controller for the active actuator and sliding mode control (SMC) is used to design the controller for the semi-active device. A 2-DOF nonlinear spring damper system is used to validate the designed controller.
- In Chapter 4, the test rig is introduced for the hardware-in-the-loop testing. The hybrid active & semi-active controller that has been presented in Chapter 3,

is validated using HIL testing. The results from HIL testing has shown good results in achieving the control objectives. The switching time of the semi-active controller has been reduced to a large extent by the hybrid active & semi-active controller because the active actuator injects the desired energy as the semi-active controller switches off, following which the semi-active device returns to the dissipative region. The proposed control technique is then compared with semi-active and hybrid active & passive controllers.

- In Chapter 5, the hybrid active and semi-active controller applicability is discussed. In this Chapter, an application of the hybrid controller is demonstrated. The hybrid control methodology, is implemented on pantograph-catenary system of high speed trains. The control objective is to keep a constant contact force between the pantograph and catenary. The proposed controller has shown promising results both under normal conditions and in the presence of the band-limited white noise, which demonstrates the robustness of the controller. Then the robustness was also checked against variable train speed with different slope variations and the results are satisfactory.

- In Chapter 6, a nonlinear reduced order observer is designed for the same system using the notion of invariant manifold theory. The designed observer is tested in simulation. After satisfactory results, it is tested on the rig both in the open and closed loop with the proposed hybrid active and semi-active controller. Finally, the proposed observer is compared with a benchmark observer based on Lipschitz type nonlinearity.

- In Chapter 7, a summary of the thesis, conclusion, overview of the original contribution and future work is presented.

Chapter 2

Literature Review

In Chapter 1 the effects of vibrations in different fields were discussed and some of the methods to damp the vibration were introduced. In this chapter, a literature review is presented, related to the passive damping devices, semi-active devices and active actuators used for the vibration suppression. After that the control techniques that have been used in the literature both for the MR damper and the active actuators are discussed in detail.

In general, systems for which mathematical modelling is possible, are modelled as linear or nonlinear systems. The primary difference between linear and nonlinear system is that the linear systems follow the superposition and homogeneity principles whereas that is not the case in nonlinear systems. Linear systems are easier to control, and the control laws are well established in linear theory [20, 21]. Mathematical modelling is performed to check the behaviour of the system and to verify the control algorithms designed for it in the simulation. To get the same results in practice, the mathematical model should be close enough to the actual system.

All real systems are nonlinear, or in other words, it will be fair to say that in reality, nothing is linear. So the question arises that why the systems are modelled as linear? The answer to this issue is for some systems the linear approximation of the nonlinear system works well, or the domain of work is restricted in such a way that nonlinear system in that field behaves as linear. Another question that arises from here is why all the systems are not modelled as nonlinear? The answer to this question is because

the nonlinear systems are not easy to model and control. Nonlinear control is an open research area [22–25] and a lot of investigation is going on in this field. In both linear and nonlinear systems, there are mainly two types of uncertainties, i.e., structural and unstructural uncertainties. The structural uncertainties come from errors in the system parameter estimations or perturbation, and the unstructural uncertainties come from the un-modeled system dynamics [26]. To deal with these uncertainties systems require a robust controller design.

In nonlinear systems, the nonlinearity comes from the plant or the controller. In either case, it is critical to deal with the nonlinearity. Most of linear control theory focuses on a small range of operation, where linear control techniques can be implemented. However, if the range of operation is increased then the linear control technique performance starts deteriorating [27]. In these cases, a need for a nonlinear controller comes in.

Mainly there are two types of nonlinearities; smooth and non-smooth. Smooth nonlinearities are easy to deal with; however, that is not the case in non-smooth nonlinearities. Some of the smooth nonlinear problems can be modified to linear problems using feedback control. Smooth nonlinearities include continuous nonlinear functions, products, power law functions, etc. Non-smooth nonlinearities are difficult to handle because they do not have globally definable inverse. Non-smooth nonlinearities include backlash, friction, actuator saturation limits or slew rate limit [27].

2.1 Vibration Suppression Using Passive Devices

One of the earliest solutions for vibration suppression was passive damping. Passive dampers were used both for vibration suppression and base isolation. It is vital to distinguish between the vibration suppression and vibration isolation. In vibration suppression, the response of the system near the resonance is damped whereas in vibration isolation the vibrating part of the system is isolated from the rest of the system.

Some of the advantages of passive damping are; it is fail-safe, no external power is required, and there is no need to design a control algorithm. However, the downside is that it is not adaptable to the variations either in the system parameters or the external circumstances. One of the examples of passive damping is the linear Tuned Mass Damper (TMD) as shown in Figure 2.1.

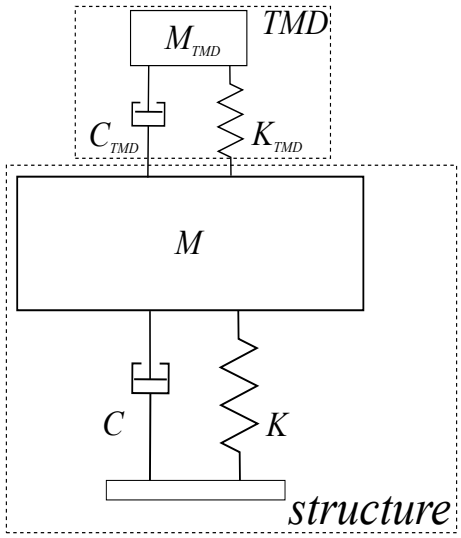

Fig. 2.1 Tuned Mass Damper, where M, K, C represents the mass, stiffness, damping coefficient of the structure respectively, M_{TMD}, K_{TMD}, C_{TMD} represents the mass, stiffness, damping coefficient of the TMD respectively

A linear TMD consist of a damper, a linear spring and a mass. It is attached to a primary structure, in which the vibrations need to be suppressed near resonant frequency. A TMD can be tuned to a single frequency i.e. the resonant frequency of the structure, to dissipate the energy. In a TMD the majority of the amplitude reduction is caused by splitting the resonant peak.

The TMD was introduced in 1883 by Watts [28]. In 1909, Frahm patented the idea of TMD [29]. Frahm implmented this idea to reduce the rolling motion of ships. In 1928 Ormondroyd and Den Hartog made the first analytical contribution on TMD [30]. For harmonic loading Den Hartog presented an optimal design for TMD [31]. TMDs work well for regular excitation or when the structure fundamental frequency is dominant during vibration, but the performance under irregular vibration or during high ground motion when the other modes are significant in vibration is not satisfactory. Figure 2.2 shows the application of a nested pendulum TMD design for Park Tower located in

Chicago, USA. The nested design has been adapted to overcome the insufficient height available for simple pendulum TMDs [32].

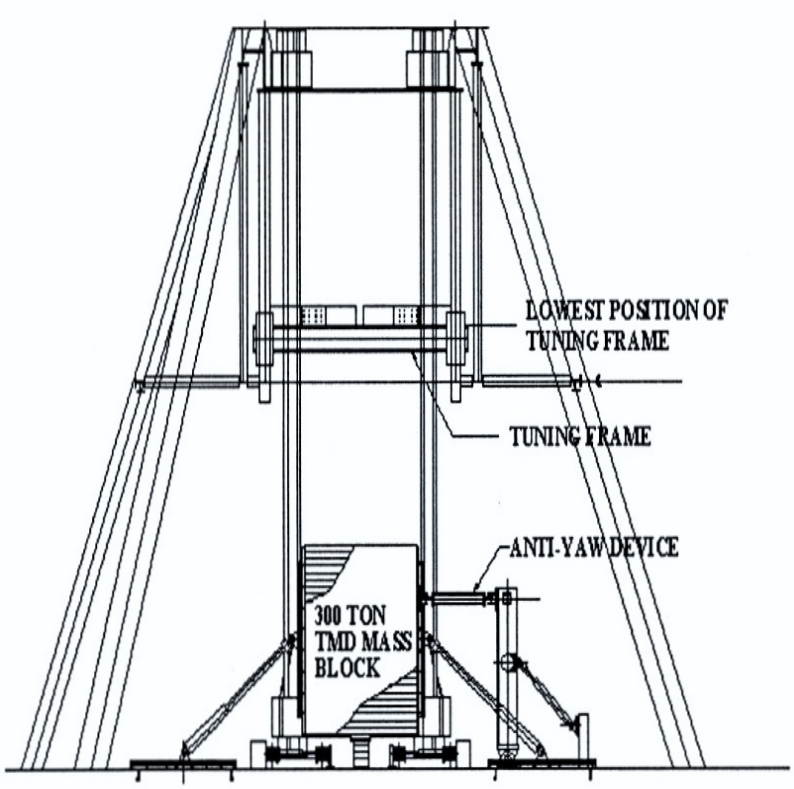

Fig. 2.2 Nested pendulum Tuned Mass Damper design for Park Tower [32]

The Tuned Liquid Column Damper (TLCD) is another passive damping device used in civil structures to damp the vibrations caused by wind and earthquake. Its working principle is same as of TMD. In TLCD instead of using a large mass, water in a storage container is used as a mass. TLCDs are more economical, easily implementable and need less maintenance as compared to TMDs. Figure 2.3 shows the cross sectional view of Wall Center located in Vancouver, BC, with TLCD [32].

Figure 2.4 shows another example of passive damping as vibration isolation [33], in which the main frame is isolated from the base foundation through passive damping device. These isolators are optimized to reduce the level of vibration in the main structure up to certain acceptable level [34].

Passive damping devices have also been used in low speed trains or trams where the maximum speed reaches to 60-70 km/h, to keep the contact force constant between the pantograph and catenary. The current from the catenary system flows to the train

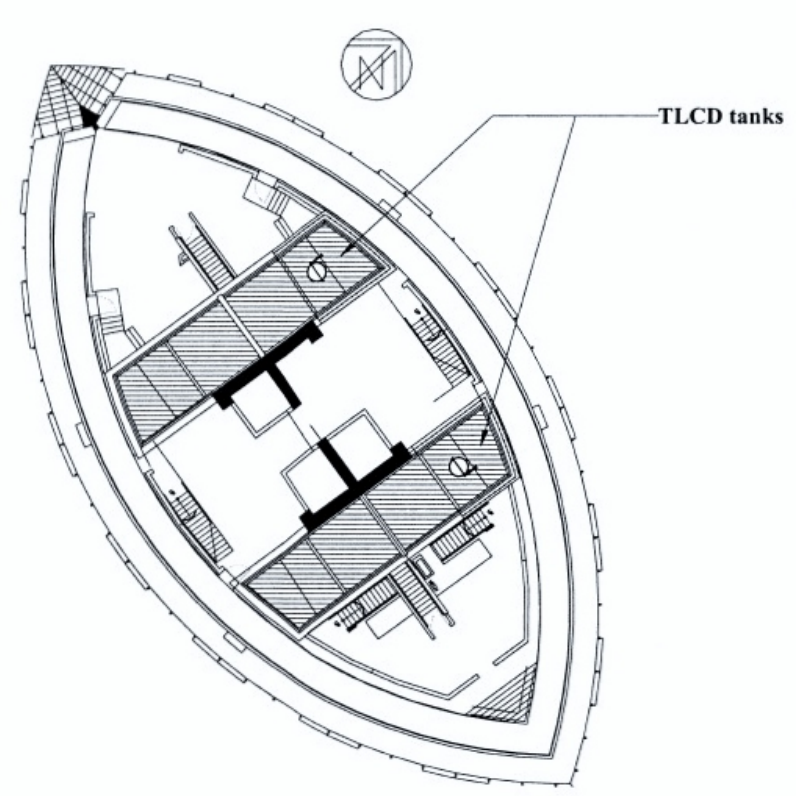

Fig. 2.3 Cross-sectional view of Wall Center with TLCD in Vancouver [32]

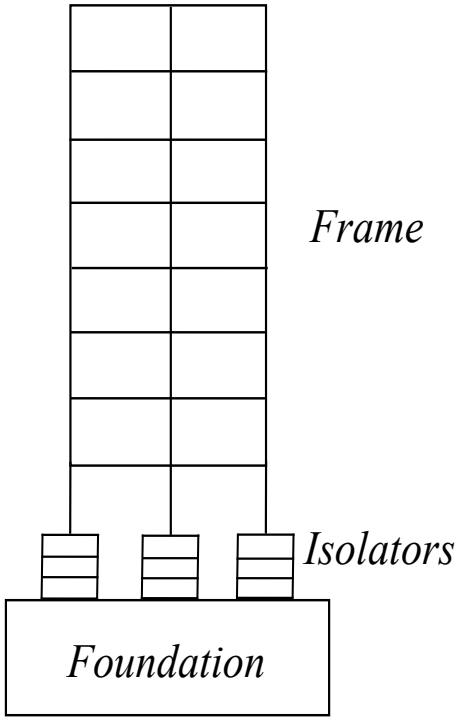

Fig. 2.4 Base isolation, where the isolators are used to isolate foundation from the frame

transformer through pantograph. It is very important to keep the contact force constant between pantograph and catenary. Vibrations can cause loss of contact, arcing, abrasion

and deterioration of quality of current collection. For high speed trains it is not possible for the passive dampers to keep the contact force constant, so active pantograph-catenary systems are proposed to deal with this issue [35–37]. In this thesis to overcome some of the problems with the active pantograph-catenary system, a hybrid method is proposed to keep the contact force constant between pantograph and catenary system. Figure 2.5 shows the pantograph-catenary system of a tram.

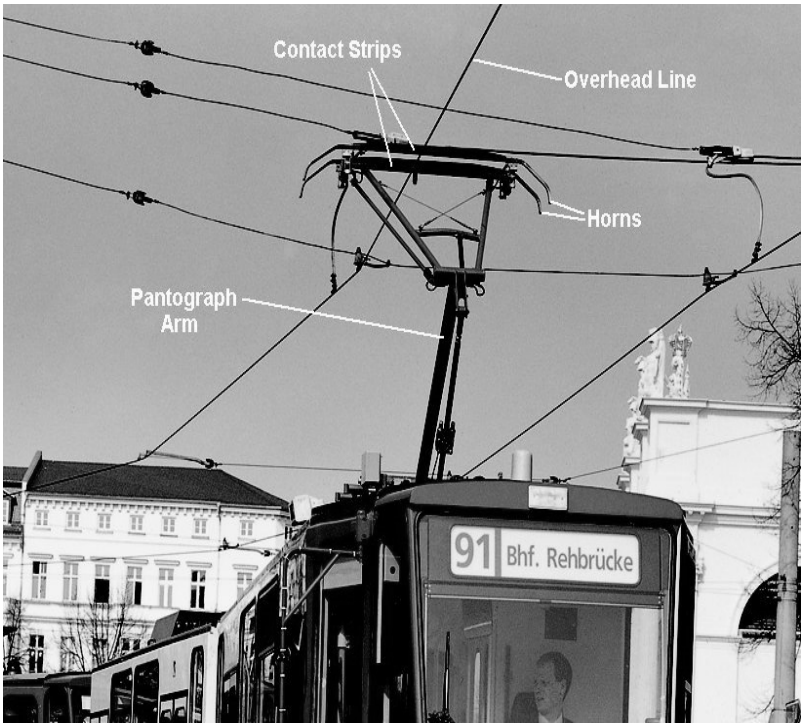

Fig. 2.5 Pantograph-catenary system showing the pantograph arm, overhead line, contact strips and horns [7]

Another very important passive device is an inerter. The idea of an inerter came from the concept of the force-voltage analogies between mechanical and electrical systems. The analogues of the inductor, resistor and capacitor of electrical systems are the spring, damper and mass of mechanical systems. Mass is a one terminal element for which the displacement, velocity and acceleration are measured relative to the ground, unlike others. The electrical systems with ungrounded capacitors do not have a direct analogy to mechanical systems. The inerter was proposed as an ideal mechanical two-terminal element to substitute or replace the mass. Malcolm Smith proposed the idea of inerter in 2002 [38]. The inerter was introduced with the property that the applied force at the

[7]http://www.railway-technical.com/etracp.shtml

terminals is directly proportional to the relative acceleration between them. The idea was illustrated with a rack and pinion as shown in Figure 2.6.

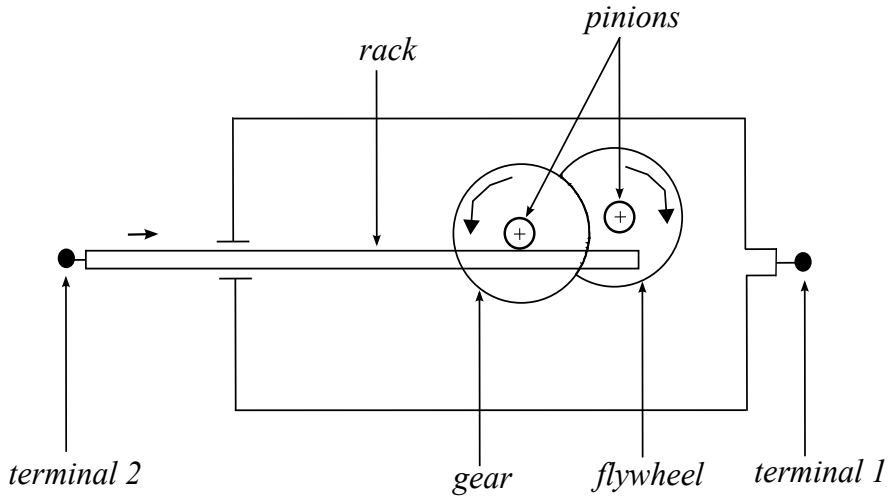

Fig. 2.6 Schematics of a mechanical model of an inerter [38]

The idea was to store the kinetic energy using the flywheel. A large amount of energy could be captured and released with a very small mass. In Figure 2.6 one terminal of the inerter is connected to the housing and the second terminal is on the end of the rack that rotates the flywheel through the gear. The gear is used to rotate the flywheel at higher speed. Figure 2.7 shows the ballscrew inerter made at the Cambridge University by Smith in 2003 with a mass of 1 kg and adjustable inertance between 60-180 kg.

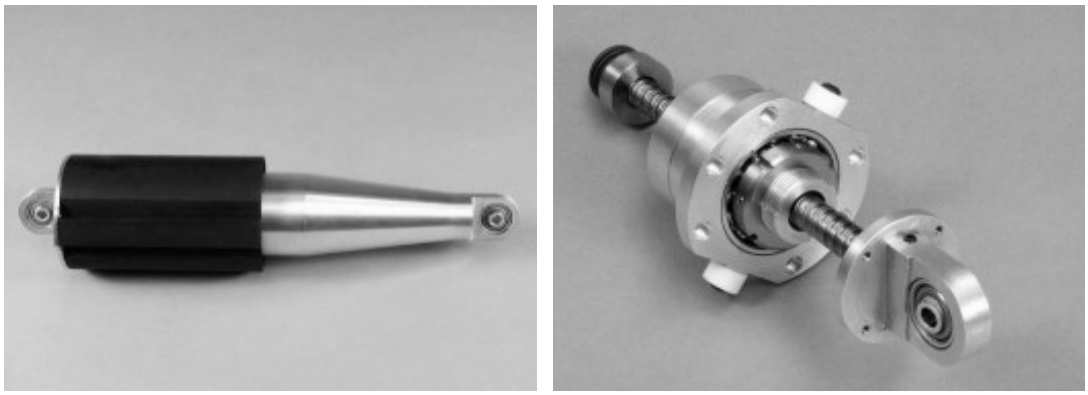

(a) **(b)**

Fig. 2.7 Ballscrew inerter made at Cambridge University [8], (a) with flywheel, (b) without flywheel

[8]http://www.icms.org.uk/downloads/Function/Smith.pdf

Actually this idea of the inerter by Smith was underlined in 1997 and was used with a secret name of the J-Damper by Mclaren as a suspension device in Formula 1 race for the first time in 2005 [39]. Its an active research area and some of the work done on different inerter designs and their applications in car suspension system, vibration control of civil structures, train suspensions are presented in [40–45]. In the next section, different semi-active devices used for vibration suppression are discussed in detail.

2.2 Vibration Suppression Using Semi-active Devices

Semi-active devices have the ability to dynamically vary their properties with a small amount of external power. A semi-active device like the passive device is fail-safe, but needs a small amount of external power to change properties, via a control algorithm. Semi-active devices without any doubt perform much better than passive devices, but the downside of semi-active devices is the passivity constraint. The passivity constraint means that they can only dissipate energy from the system. The idea of semi-active damping was first introduced by Karnopp and Crosby in 1974 [46], to use it for vibration isolation in the automobile industry. The method proposed was to change the damping force by controlling the valve of a fluid damper. Unlike passive damping, semi-active devices also require a control law as the damping force is adaptable. In this section, different types of semi-active devices that have been used for vibration control are presented.

Semi-active stiffness dampers (SASD) have a cylinder filled with viscous fluid (oil), a piston and a controlled valve. The valve is controlled by a small motor to change the damping coefficient by changing the rate of fluid flow [47]. Another version of such dampers is resetting semi-active stiffness dampers (RSASD), in which the position of the piston is periodically reset to add stiffness (valve closed) or to dissipate the absorbed energy (valve open) [48]. One more version is the switched semi-active stiffness damper (SSASD). The SSASD has the same way of operation as RSASD, but in this case, an open valve means there is no damping, and it behaves like SASD when the valve is closed [49].

The working principle of a semi-active tuned mass damper is similar to a passive tuned mass damper as discussed in section 2.1 with one modification i.e. the passive damper is replaced with a variable damping device as shown in Figure 2.8.

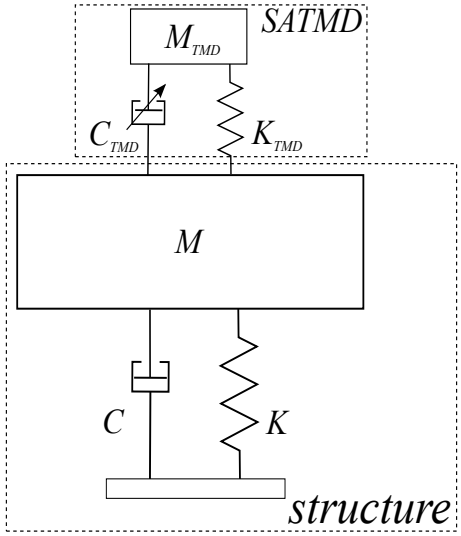

Fig. 2.8 Semi-active Tuned Mass Damper, where M, K, C represents the mass, stiffness, damping coefficient of the structure respectively, M_{TMD}, K_{TMD}, C_{TMD} represents the mass, stiffness, damping coefficient of the semi-active TMD respectively

The semi-active tuned liquid column damper is another semi-active device in which the damping force is controlled by the flow of liquid through an orifice. The tuning frequency, can be easily controlled by changing the length of the liquid column [50] as shown in Figure 2.9.

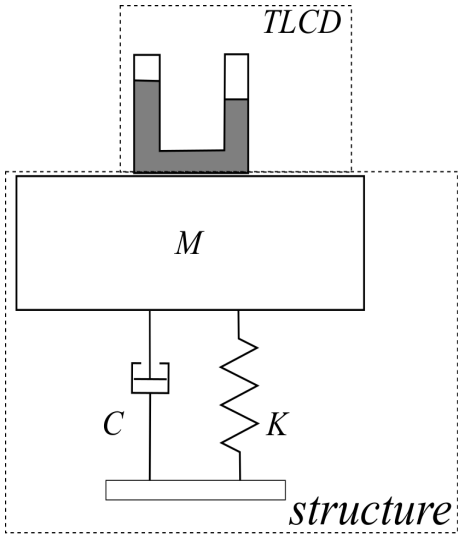

Fig. 2.9 Semi-active Tuned Liquid Column Damper, where M, K, C represents the mass, stiffness, damping coefficient of the structure respectively

Piezoelectric dampers are also used as semi-active devices. As evident by the name they use piezoelectric materials which create stress or strain based on the applied current. When the piezoelectric material is strained, mechanical energy is converted to electrical energy. Then the electrical energy can be dissipated as a heat energy by shunting an appropriate circuit to the piezoelectric material [51] as shown in Figure 2.10.

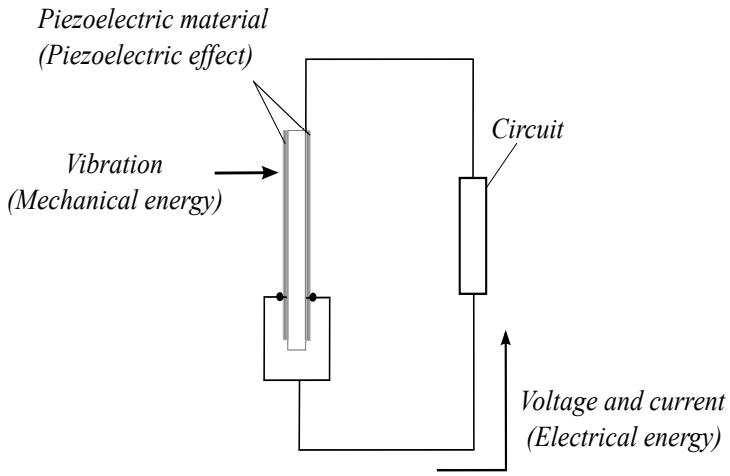

Fig. 2.10 Schematic of a piezoelectric material [51]

The variable orifice damper comprises of a viscous fluid damper with a by-pass pipe that has a variable orifice and a controlled valve, which controls the damping. The by-pass tube controls the flow of the fluid between the chambers of the piston through the valve. The damping is at its lowest value when the valve is completely open and is at its highest value when the valve is completely closed. The idea of variable orifice damper was first proposed in 1990 by Feng and Shinozuka [52]. Figure 2.11 shows the schematic representation of a variable orifice damper.

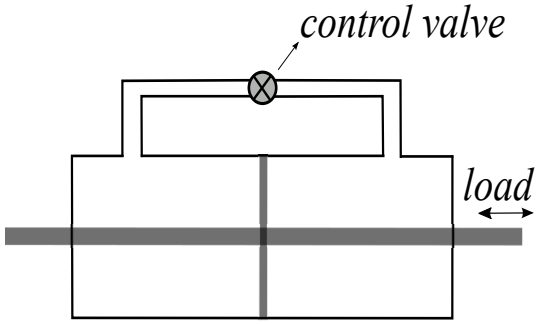

Fig. 2.11 Variable orifice damper with a controlled valve

Among all these semi-active devices, the two most popular and widely used semi-active devices are rheological dampers. There are two types of rheological dampers based on the types of the fluid, i.e., magneto-rheological (MR) dampers and electro-rheological (ER) dampers. MR fluids have iron particles suspended in a carrier fluid like mineral/synthetic oil, water, etc. ER fluids, on the other hand, have non-conducting particles in an electrically insulating fluid. The damping is varied by changing the viscosity of the fluid, while the viscosity of the fluid is modified by applying either the magnetic or electric fields.

Among the two, MR dampers are widely used in different fields for vibration suppression. The reasons are that [53, 54]

- The MR damper is easy to control because the rheological equilibrium can be achieved in milliseconds.
- The MR fluids are more robust to changes in the temperature.
- The MR fluids have a higher yielding stress as compared to ER fluids.
- The power requirement of MR damper is also less than ER dampers.
- The cost of production of MR damper is lower because MR fluid in not sensitive to contaminants.

The history of MR and ER fluids can be traced back to 1940. The first discovery and initial development of MR fluid was proposed by Jacob Rabinow in 1940 [55, 56]. Rabinow patented his MR fluid discovery in 1947 [57]. The fluid used in clutches today is similar to that of MR fluid made by Rabinow. From 1950 to early 1960 the MR fluid was considered to be the most focused research interest.

In late 1960's, the concentration of research moved from MR fluids to ER fluids. Most of the universities and companies were seeking to accomplish research on ER fluids by 1980's. Finally, it was concluded that ER fluids cannot meet the required yield strength [58]. It was considered quite low for the practical implementations. The revival of MR fluid and its applications began in the early 1990's [59], which offered the required yield strength along with the ability to function in low and high temperatures.

It did not require high voltages for the magnetic field. The electromagnets in the MR fluid devices could be directly powered by low voltages power supplies or batteries.

Lord Corporation did a lot of research on the MR fluid and brought it to the commercial market. Figure 2.12 shows the demonstration of the operation of MR fluid. Lord Corporation developed large MR dampers for civil structures, after the MR dampers had produced incredible results in the auto industry.

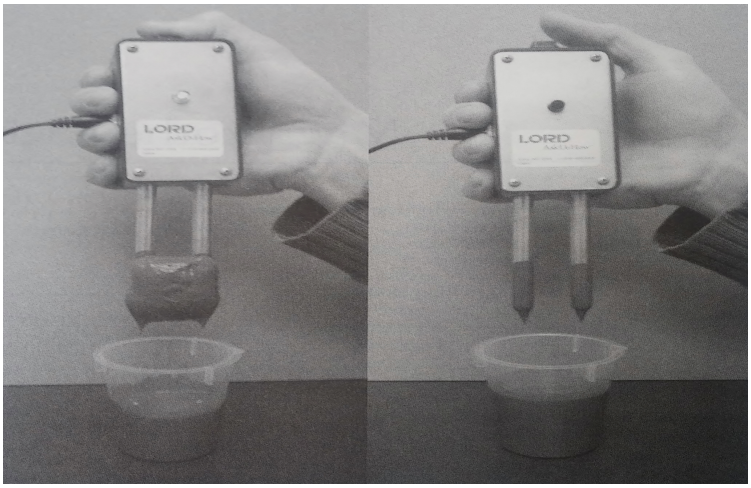

Fig. 2.12 Demonstration of the operation of MR fluid. On the right, the magnetic field is off. On the left, the magnetic field is generated between the two steel prongs of MR probe by energizing the electromagnet [58]

The MR damper is a nonlinear device. Its force-velocity curve shows a hysteresis behaviour, which leads to difficulty in the mathematical modelling of the device and can also cause problems in the control. Figure 2.13 shows the force-velocity behaviour of the Lord Corporation damper.

Both MR and ER fluids can operate in three different modes i.e. flow mode, shear mode and squeeze mode as shown in Figure 2.14. The flow mode is the first most fundamental configuration of small fluid devices. In the flow mode, the magnetic poles or the electrode plates are fixed. The fluid is compelled to flow between two fixes poles/electrodes. The implementation of the device can be accommodated through control of an electric/magnetic field, which is vertical to the flow direction. The applied field acts as a flow control valve. Many applications for instance damping devices, actuators and prosthesis devices use this type of configuration extensively [10,25]. In the shear mode, the magnetic poles or the electrode plates move in parallel to one

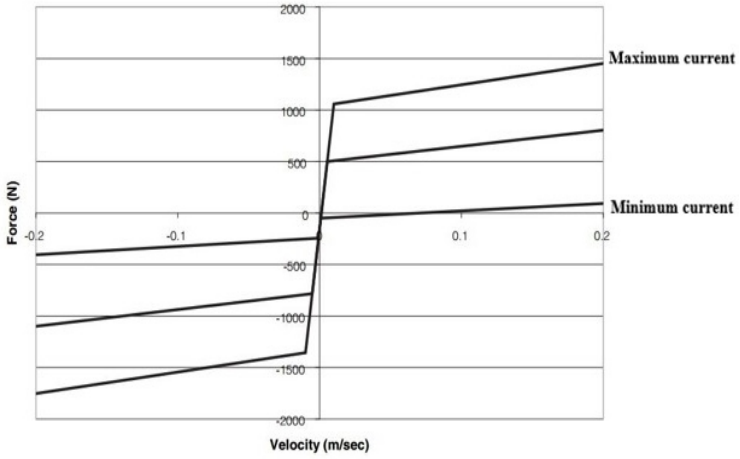

Fig. 2.13 Lord Corporation MR damper force-velocity curve [9]

another. The fluid is placed between these moving poles. The shear mode is used when the required damping force is small like in clutches and brakes. In the squeeze mode, the magnetic poles or the electrode plates move towards each other. This mode is not used very often.

The MR dampers are classified into two categories in terms of modelling; parametric models and non-parametric models. Parametric modelling uses the analytical tools such as the mathematical relation of friction and viscosity to describe the dynamic behaviour of MR damper. In non-parametric modelling instead of mathematical tools, soft computing methodologies such as fuzzy logic or neural networks are used. The model is trained on the experimental data. In the next section, the active devices used for vibration control are discussed briefly.

2.3 Vibration Suppression Using Active Devices

Active actuators have been used extensively in different fields for vibration suppression. In the civil engineering field, active control was first implemented in 1993 in Tokyo on Kyobashi Seiwa Building [60]. Both the actuators were placed on the top of 10 storey building. One actuator that was put at the centre of gravity was used to control the fundamental mode and the second one was placed at the edge of the building to control

[9] http://www.lordmrstore.com/lord-mr-products/rd-8040-1-mr-damper-short-stroke

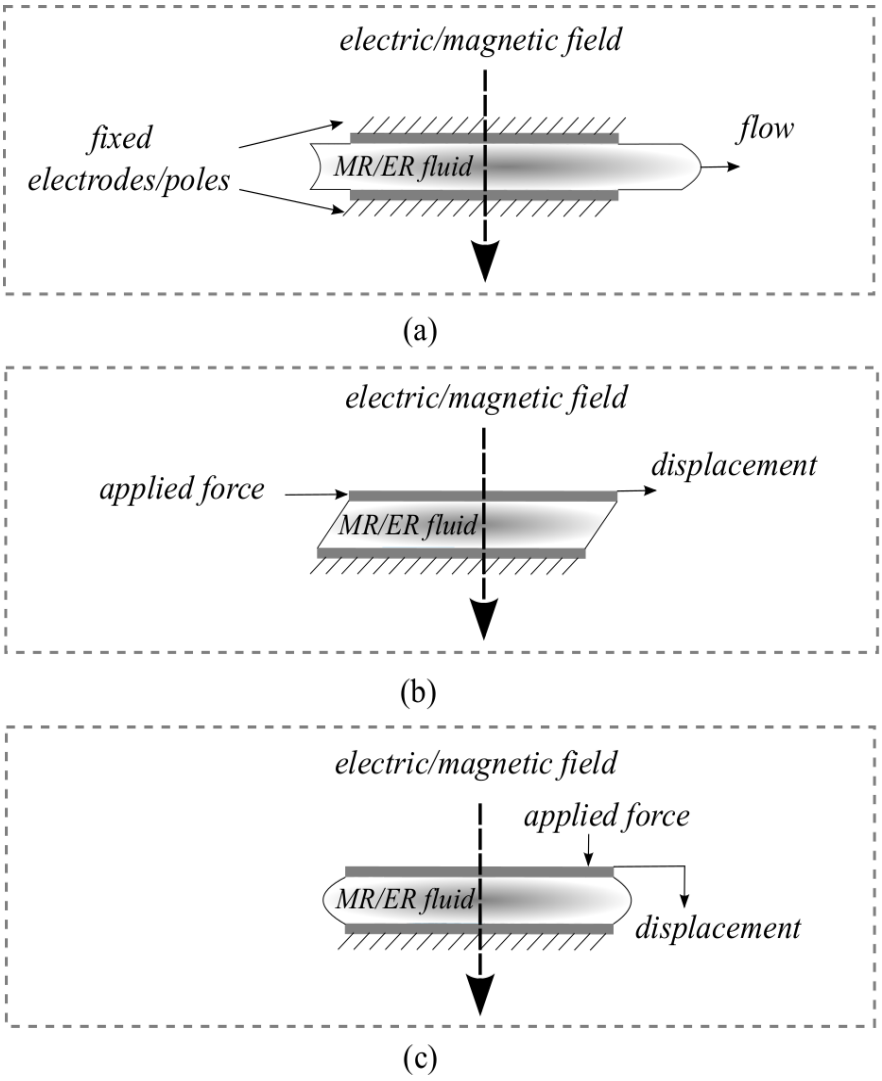

Fig. 2.14 *MR/ER damper modes, (a) flow mode, (b) shear mode, (c) squeeze mode*

the torsional vibration. Later on, active actuators were used in a lot of structures for vibration suppression.

Active tendon control is one of the most widely used active vibration suppression technique for large civil structures. A tendon connects the two corners of the ground floor to the two corners of the first floor. The tendon is already part of the structure, and there is no need of any modification in the structure. The actuator in the ground floor can pull the tendon to oppose the motion in the case of earthquake [61]. The actuators used in this type of control are hydraulic actuators as they can provide a very significant amount of force. The disadvantages are; the size of actuator, power consumption, power cutoff during the seismic vibration and instability. The active tendon control configuration is shown in Figure 2.15.

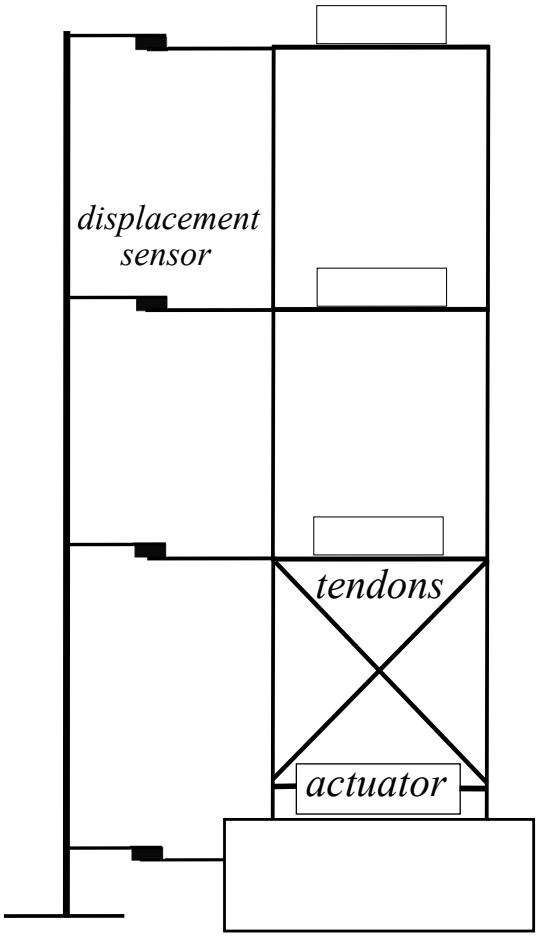

Fig. 2.15 Active tendon control configuration showing the actuator with a feedback loop at the base with tendons

Another commonly used technique in active vibration suppression of civil structures is active mass damper (AMD). In this method, an active actuator is placed on the top of the structure. During the vibration, it opposes the vibration to maintain the centre of mass of the structures at the equilibrium. This type of control is useful against wind disturbance but for high seismic waves, this method is not that effective as compared to active tendon control because the vibrations originate from the ground, and the actuator is located on the top of the building. The actuators used in AMD are usually hydraulic, or servo motors. The active control implemented on Kyobashi Seiwa Building in Tokyo for vibration suppression is based on AMD technique. In the next section, the control techniques used in the literature for the semi-active devices and the active actuators for vibration control are discussed.

2.4 Control Methodologies

Skyhook control is mostly used to design the controller for semi-active dampers. In 1974 Karnopp *et al*. proposed a skyhook controller for the MR damper to be used in the vehicle suspension system [46]. The skyhook configuration is shown in Figure 2.16. In skyhook control, the damper is considered to be connected to a imaginary inertial reference point. Now this configuration is not possible in practice and is fictional. It was shown by Karnopp *et al*. that the performance of the vehicle suspension has been improved as compared to the passive system for a single DOF system.

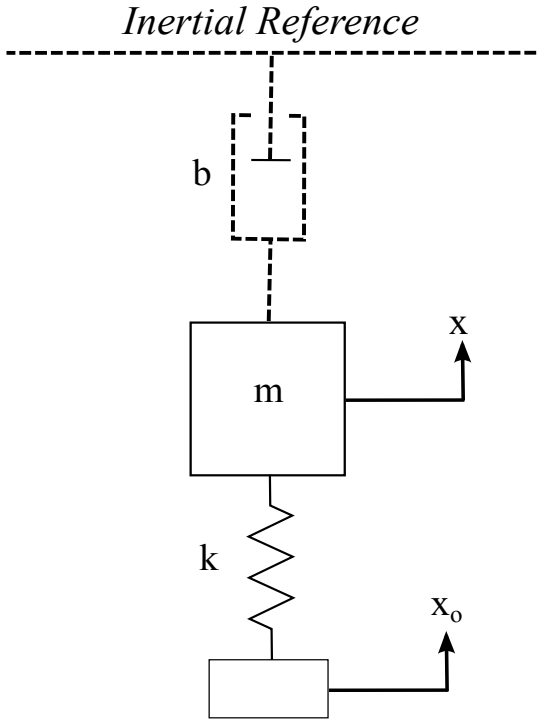

Fig. 2.16 *Skyhook control configuration presented by Karnopp et al. in [46]*

The interpretation of the skyhook control for the quarter car is explained in [62] and is shown in Figure 2.17. It requires two measurement signals; first one is the acceleration of the sprung mass $\ddot{y}_1$ and second one is the relative displacement between sprung and unsprung masses y_{12}. The skyhook control signal is then given by

$$F_{sa} = \begin{cases} G\dot{y}_1 & \dot{y}_1\dot{y}_{12} > 0 \\ 0 & otherwise \end{cases} \tag{2.1}$$

where $\dot{y}_1$ is the velocity of the sprung mass, $\dot{y}_{12}$ is the relative velocity between sprung and unsprung masses and G is the gain. Later on, much research has been done to improve the performance of the skyhook control [63–68].

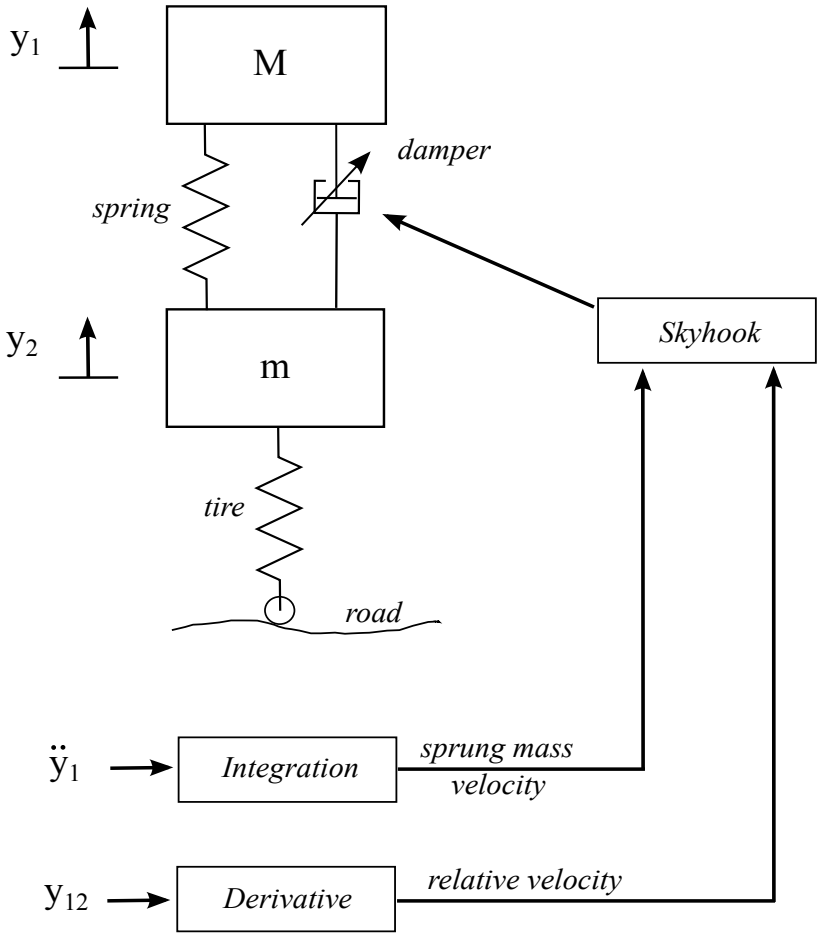

Fig. 2.17 *Two sensor based skyhook control configuration [62]*

Clipped optimal control has also been proposed for the MR damper with acceleration feedback [69]. The idea behind proposing this control technique was that acceleration feedback can easily be attained from structures during seismic vibration as compared to other techniques that require full state feedback i.e displacement or velocity, which is difficult to achieve especially when the foundation of the structure is moving with the ground. Accelerometers can easily obtain acceleration at arbitrary locations in the structure. In this technique, an optimal linear controller is designed to calculate the desired forces vector based on the feedback from the structure.

It is not always possible to generate the desired force because of the passivity constraint. When the optimal desired force and the actual force generated by the MR

damper are the same, then the controlled signal to the MR damper, i.e., either current or voltage remains constant at the same level. If the two forces have the same sign but the actual MR damper force is less than the desired optimal force than the controlled signal is increased to match the desired and the actual force. In all other scenarios, the controlled signal is set to zero.

In [70], a comparison is made between different control techniques which include a Lyapunov controller, a decentralised bang-bang controller, a homogenous friction controller, a clipped optimal controller for an MR damper. A six-story building model with four MR dampers is used to make a comparison. All the results are shown in the simulation. Two MR dampers are placed rigidly between the ground and the first floor, and two MR dampers are positioned rigidly between first and second floor. The Lyapunov controller, homogenous friction controller and clipped optimal controller have shown a better performance in different scenarios.

A bang-bang controller has also been designed for a MR damper [69]. A bang-bang controller is also called an on-off controller because it switched between two states. When the relative displacement and relative velocity of the semi-active device have the same sign, then the bang-bang controller provides a maximum value of control force and acts as a brake to dissipate energy. When the relative displacement and relative velocity are in opposite direction, then the controller provides a minimum value of the control signal, so that the device can move quickly with minimum friction. The control algorithm can be defined as

$$u_t = \begin{cases} u_{max} & \text{sign}(x) = \text{sign}(\dot{x}) \\ u_{min} & \text{sign}(x) = -\text{sign}(\dot{x}) \end{cases} \tag{2.2}$$

where u_{max} and u_{min} are the maximum and minimum control signals, x and $\dot{x}$ represents the relative displacement and relative velocity across the semi-active device.

Fuzzy logic control comes under the umbrella of computationally oriented control techniques. It does not require an accurate model of the system, unlike other analytically

oriented control methods. The controller design is divided into three main steps, which includes fuzzification of the control inputs, implementing the rule of the controller and lastly defuzzification of the output [71].

In the first phase, a member function is defined for each input. There are different shapes of the membership functions and they are chosen depending upon the problem under consideration. In the second step, before establishing the rules, first the membership functions for the outputs need to defines as well. Later, a table can be computed based on the combination of inputs to define an output. In the last step, the fuzzy output generated in the second phase is de-fuzzified into a crisp output. There are different methods available for defuzzification, and some of them include the weighted average method, mean-max membership method, etc.

In 1960, Kalman presented the linear quadratic feedback control, which later contributed to the foundation of the Linear Quadratic Regulator (LQR) control [72]. This idea of the feedback control to minimise the integral of the tracking error square dates back to 1943 by Hall [73] and 1949 by Wiener [74]. In LQR control technique a quadratic objective function is defined based on the weighted energy of all the state variables and control signals. The aim is to minimize the objective function given as

$$J_{lqr} = \lim_{t\to\infty} \int_0^t \left(x^\intercal Q x + u^\intercal R u \right) dt \tag{2.3}$$

The matrices Q and R are design parameters and can be tuned to shift the emphasis between different objectives in the cost function. The optimal controller to minimize the objective function is given as

$$u(t) = -K_{lqr} x(t) \tag{2.4}$$

where K_{lqr} is the feedback gain matrix and is given as

$$K_{lqr} = R^{-1} B^\intercal P_{lqr} \tag{2.5}$$

where P_{lqr} is solution of the Algebraic Riccati Equation (ARE) given as

$$A^{\top}P_{lqr} + P_{lqr}A - P_{lqr}BR^{-1}B^{\top}P_{lqr} + Q = 0. \tag{2.6}$$

where A and B are system matrices.

One of the issues with LQR is that it requires all the states to be available, which is not feasible in most of the practical problems because of various constraints. In 1961 Kalman proposed an optimal state observer in the sense of least squares [75], which lead to the development of Linear Quadratic Gaussian (LQG) control. In LQG, the control task is divided into two parts. One part is the optimal estimation of the states that are not available and the second part of optimal regulation remains unaffected. A Kalman filter is used as an optimal estimator. Stability margins are guaranteed in the LQR, but that is not the case in LQG because of the Kalman filter [76, 77]. Different techniques have been proposed in the literature to deal with this issue of robustness.

LQG control that was briefly explained earlier is similar to H_2 control. In H_2 control algorithm, the aim is to find an optimal controller gains that will minimise the H_2 norm of the transfer function matrix between the disturbances and the regulated signals. The formulation of the problem is different, but the basic idea is the same.

Unlike LQG control techniques the H_∞ controller takes into account the robustness in the optimal design framework. Bounds are imposed on the amplitude of uncertainty and optimisation is done for the uncertainty with maximum amplitude within the imposed limits i.e. the worst case scenario.

2.4.1 Sliding Mode Control

Sliding mode control (SMC) is a class of variable structural control (VSC) [78], that can be accommodated within the I & I framework and is, therefore, ideal for a hybrid scheme. The theory of VSC was started in the late 60's by SV Emelyanov. Early studies were undertaken by [79, 80], and more recent surveys are given in [81–83]. VSC has a switching logic that changes the structure dynamics. A survey [79] was presented by Vadim I. Utkin in 1977 about variable structure systems with the sliding mode. Later on,

more work on variable structure systems has been carried out by Utkin [80]. Another survey on variable structure control and sliding mode in 1993 was presented in [81]. In [82] a brief overview of the work done on sliding mode control up to 1999 is discussed in the context of practical implementation. Sliding mode control has previously been used to design controllers for both active [84–86] and semi-active devices [87–89].

The control design explained in Appendix B is called first order sliding mode control because the sliding surface is defined in such a way that it has a relative degree of one [90]. It means that after first differentiation, the input should appear in $\dot{S}$, where S is the sliding surface. There is also second order sliding mode control, in which the relative degree of the sliding surface is two [91–94]. The second order sliding surfaces have been used mainly to avoid the chattering effect [95–97]. The robustness property in SMC is because of the discontinuous part in the control. The discontinuous part switches the control action as the system crosses the sliding surface and pushes the system back towards the sliding surface.

In the early stages, SMC has been used to design the controller for active actuators but later on it has also been used for semi-active devices with a passivity constraint. In [98], SMC is used to design a controller for an active suspension system for a quarter car model. A reference system has been defined with a skyhook configuration, and the reference system does not require the road input from the actual system. SMC has been designed to control the vibrations in the sprung mass. In both the actual and the reference system, the un-sprung mass dynamics are considered to be same, and the error is defined in terms of the dynamics of the sprung mass. The sliding surface is defined in terms of the error dynamics, and the SMC is forcing the actual system to behave as a reference system. In simulations, the SMC is compared with the self-tuning control, and it is shown that SMC shows better results to discrete road inputs.

In [84], an SMC is used to damp the vibration in a flexible beam with an active actuator. Its simulation and experimental results are shown. A comparison of an SMC is made with a PD controller, and the SMC has shown better performance. A low pass filter has been used in the controller output and the feedback signal. In [99], a

nonlinear model is designed for hydropneumatic spring, then the model is linearized using feedback linearization. SMC is used to create the controller for the linear model. The SMC combined with the feedback linearization has shown better performance in terms of robustness and accuracy.

In [85], an SMC is designed for a n-DOF robot arm. It is mentioned that an SMC with a saturation function and a fuzzy SMC have difficulty with unstructured model uncertainties. To deal with this issue, a mathematical error based tuning method with a fuzzy SMC is proposed. The sliding surface gain is adapted online by updating a factor defined as the sliding surface slope. At the end, a comparison is made between an SMC, a fuzzy SMC and the proposed method. All results are shown in simulations. The proposed method has shown better performance in terms of disturbance rejection and steady state error. In [100], an SMC is used to design a controller for active suspension system. The sliding surface is defined as proportional-integral rather than conventional proportional-derivative. The proposed controller is compared with the passive and LQR controller in simulations and has shown better results for vibration damping. The system is a 2-DOF quarter car model, and the controller is designed for an active actuator to damp the vibrations in a sprung mass.

In [101], an SMC is designed for a single degree of freedom system to control the vibration in the sprung mass. The controller design methodology is the same as the one used in [98]; the difference is that in [98] the actuator is active but in [101] the actuator is semi-active. The SMC is compared with the on-off controller, and the SMC has shown better performance. All the results are shown in the simulation.

In [89], the 2-DOF actual system and the reference skyhook based system are defined in the same way as discussed before. The actuator is an MR damper, and a passivity constraint is imposed on it after designing the controller using an SMC. The SMC is compared with passive and skyhook control. Both simulation and experimental results are shown. Figure 2.18 shows how the reference model concept has been used in designing the SMC. In [102] the SMC is used to create the controller for a sprung mass. The 2-DOF quarter car system and the reference system defined in this paper

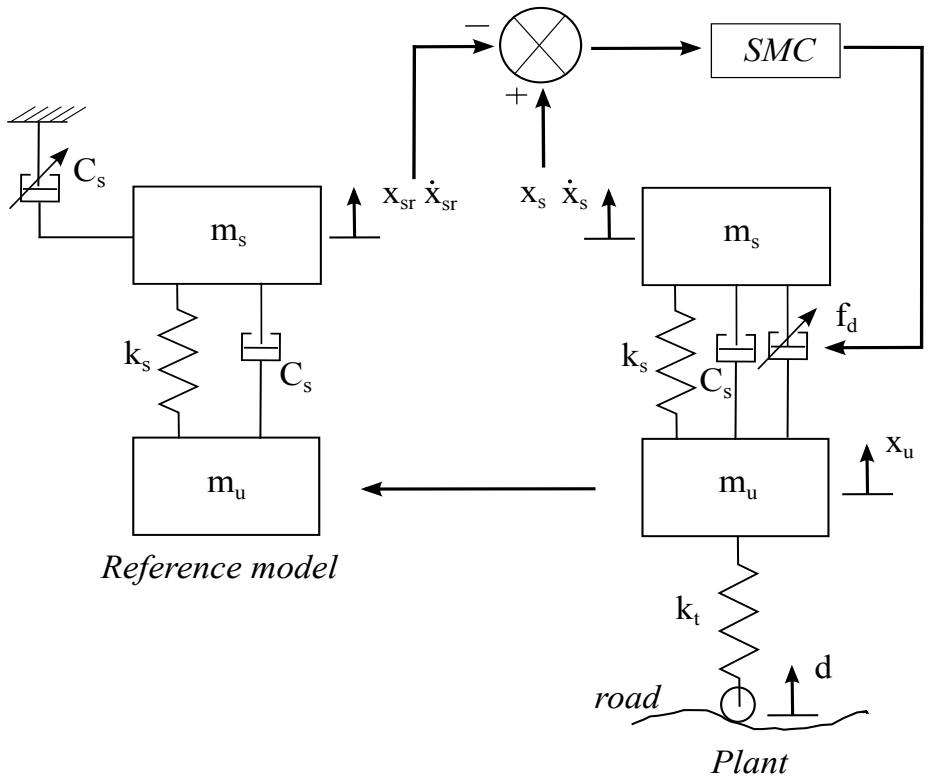

Fig. 2.18 Reference model based sliding mode control [89]

are the same as [98], the difference here again is the semi-active device, but the design methodology is the same. Then a comparison is made with passive, fully active and ideal semi-active systems. All the results are shown in simulations.

One of the shortcomings of SMC is the chattering effect, which is caused by the discontinuous nature of the control during the sliding phase across the sliding surface. To make SMC efficient for practical implementation, different techniques have been proposed to minimise or eliminate the chattering effect. One of the most widely used solutions to avoid chattering is to use a saturation function. In this proposed solution a boundary layer is defined across the sliding surface with some thickness. When the system trajectories enter into this region, the switching control law is replaced with a linear approximation. The problem with this approach is that the tracking error will still be there and if the trajectories come out of that region because of some disturbance, then the switching control will again be activated.

Other techniques, used to deal with the chattering are observer design [103], frequency shaping [104], second order sliding surface [105–115]. Different books have

been written on sliding mode control to discuss each aspect in detail. The first book about sliding mode control was written by Utkin and Vadim in 1992 [116]. Another book by the same authors was published in 1999 [117]. Another interesting book about SMC was published in 2002 [118].

2.4.2 Immersion and Invariance Control Methodology

Immersion and Invariance (I & I) control methodology was first introduced in [119], and the work was further extended by the same authors in [120, 121]. A detailed explanation of I & I controller can be found in [122], and further examples are given in [123–127].

The first step in I & I is the definition of the target system, which should be reduced order and should be asymptotically stable. Then the next step is to derive the nonlinear mapping functions for off-the-manifold dynamics. There can exist more than one mapping function, but they should follow certain conditions. Then the third step is defining a manifold regarding the error dynamics between the off-the-manifold dynamics and the nonlinear mapping functions. The final step is to design a controller that will bring the error dynamics to zero and then the actual system will start behaving as the target/reference system.

The aim is to make the actual system emulate the target system, and meanwhile to be certain that the actual system (as modelled) will be asymptotically stable. The concept of immersion is to transform a system into another system with pre-specified properties. Meanwhile, a manifold is a topological space that locally resembles Euclidean space. If a manifold is invariant under the action of a dynamical system, then it is an invariant manifold.

The concept of invariant manifolds, and of mapping, can be related to the mathematical topic of algebraic topology. This involves the study of shapes, their properties, and (in particular) the way in which these properties are modified when a form is transformed. Algebraic topology is the study of shapes and their properties, which are not dependent on continuous deformation, and the primary interest is that what is maintained when the shapes are continuously deformed. One of the famous examples

in topology is that a doughnut or torus is same as the coffee cup topologically because they can be continuously transformed into each other. They are geometrically different but homomorphically or topologically they are same. In the same way, a higher order system can be transformed into a lower order through appropriate nonlinear mapping.

2.5 Hybrid Control

The term hybrid control used for vibration suppression mainly in the civil structure is the combination of either passive and semi-active devices or passive device and active actuators. One of the examples is hybrid mass damper (HMD) used for vibration control in a building. It combines the AMD with TMD. Both have been explained before in the literature separately. It has shown almost similar results like pure AMD, but the energy consumption in the hybrid case is less. The first HMD was installed in a 14 story building Ando Nishickiki in Japan. Another example of hybrid control is hybrid base isolation. Here the active tendon control or AMD is combined with passive base isolation.

In [128], a review of the control techniques implemented in civil structures like buildings, bridges and towers from 1989 to 2002 has been covered. A list of 40 buildings and ten bridges that have implemented active or hybrid (active+passive) control is provided with all the details, and then the semi-active devices used in civil structures including variable orifice dampers, smart TMD, variable friction dampers, controllable fluid dampers have been discussed in detail. In [129], the passive energy dissipation devices used in the civil structures that include metallic yield dampers, friction dampers, viscoelastic dampers, viscous fluid dampers, TMD and then active control devices like active mass dampers (AMD), hybrid mass dampers (HMD) and in the end semi-active devices are discussed. These are presented with the civil structure examples in which they are used all over the world.

In July 2015, Demetriou and Nikitas proposed a hybrid semi-active TMD [130], in which semi-active TMD is used in conjunction with an active element. The groudhook control technique is used for the semi-active device and LQR is used for the active

element. Only simulation results are presented in the paper without considering the seim-acticve device and active actuator models and constraints. It is claimed in the paper that the proposed hybrid device performs better than TMD and STMD. Later on, the same idea is explained in detail by Demetriou and Nikitas in a journal paper [131] published on 30 November 2016. Again, only the simulation results are presented.

2.6 Summary

Firstly, in the literature, the passive damping devices used for the vibration suppression and vibration isolation have been discussed. The Tuned mass damper, tuned liquid column damper, piezoelectric dampers, inerter were reviewed in detail with their applications in different fields for vibration control. At the end of this section, the limitations of the passive devices were explained.

In the next section, semi-active devices including semi-active TMD, variable orifice damper, MR/ER dampers have been explored. The MR damper has been examined in detail as the semi-active device that has been used in the current work is an MR damper. A comparison between MR and ER dampers was presented and how the research has shifted from ER to MR dampers has also been mentioned. Different application of the MR dampers in different fields have been elaborated.

In the next section, active control devices have been explained briefly. After that the control techniques that has been used in the literature both for the MR damper and the active actuators have been discussed in detail. First, a very well known skyhook control that has been used a lot in the literature to design controller for the MR damper has been reviewed along with the clipped optimal control and bang bang control that has also been used in the literature for the MR dampers and other semi-active devices. After that fuzzy logic, LQR, LQG, H_2 and H_∞ control techniques have been discussed very briefly. These controller techniques have been used in the literature to design the controller for both semi-active and active devices. Towards the end the two control techniques i.e. the sliding mode control and immersion and invariance control have been explored in detail.

2.7 Thesis Contribution in the Literature

The term hybrid control is either used for the combination of semi-active and passive or active and passive in the literature. In this thesis, the hybrid control in the sense of active and semi-active will be explored and how an active actuator can assist the semi-active actuator so that the whole system can achieve the performance, very close to a fully active system. Now this combination of active and semi-active can be beneficial in different scenarios. A hybrid combination of active and semi-active control has not been previously studied in detail in this context.

The semi-active devices need small actuation power and are smaller in size, so they can be incorporated anywhere in the structure to control the vibration, but the drawback of such devices is that they can only dissipate energy from the system, which limits their performance. On the other hand, the active actuator can do both the energy injection and energy dissipation, however; the size of the actuator and actuation power requirement limits their capability to position them anywhere in the structure. So the idea behind the work done in this thesis is that how an active actuator that is located somewhere else in the structure can assist the semi-active device to achieve the performance close to an active actuator.

Most of the time, it is not possible or it is difficult to measure all the states of the system. So the observer or estimator design is vital. The theory of observer design was started in 1958 by Kalman and Bertram and then in 1964 by Luenberger. The observer for linear systems has been developed using the linear theory approach but when the same observer was implemented on the nonlinear systems, the results were not satisfactory, which has opened the door for a new research area, i.e., nonlinear observer design. A lot of research has been done, and different techniques have been developed in the last two decades for nonlinear observers, but this area is still not fully explored.

One of the major issues with nonlinear observers is that most of them did not give a structural design methodology and if they do, then some of the conditions are very hard to meet. Secondly, most of them are designed for a particular class of systems. In this work a reduced order observer using the notion of an invariant manifold is designed.

The proposed observer is not restricted to any class of system as long as an invariant manifold exists and it also provides a structured design methodology.

2.7.1 Publications Outcome

The following articles [132–135] have been published from the current work.

From Chapters 3 and 4

- I. U. Khan, D. Wagg, and N. D. Sims, "Improving the vibration suppression capabilities of a magneto-rheological damper using hybrid active and semi-active control," *Smart Materials and Structures*, vol. 25, no. 8, p. 085045, 2016.
- I. U. Khan, D. Wagg and N. D. Sims "Hybrid active and semi-active control for vibration suppression in flexible structures," *Dynamic Systems and Control Conference*, ASME, Oct 2016.

From Chapter 5

- I. U. Khan, D. Wagg and N. D. Sims "Hybrid active and semi-active control for pantograph-catenary system of high-speed train," *27th International Conference on Noise and Vibration*, ISMA, Sept 2016.

From Chapter 6

- I. U. Khan, D.Wagg, and N. D. Sims, "Nonlinear robust observer design using an invariant manifold approach," *Control Engineering Practice*, vol. 55, pp. 69–79, 2016.

Chapter 3

Hybrid Controller – Design Methodology

3.1 Introduction

In this Chapter, results from an example hybrid system that contains an active actuator and semi-active damping device are presented. The context for such a combination of control devices is the need to suppress unwanted vibrations in lightweight structures in application areas such as aeronautical and mechanical engineering.

The unwanted vibrations are a by-product of the increasingly lightweight and therefore flexible nature of these structures. The increased flexibility is often driven by pressure to improve performance and efficiency, for example, by reducing weight or improving dynamic performance. As a result, the associated unwanted vibrations in flexible structures are increasingly difficult to suppress, and this has led to an increasing reliance on control devices. Different controllers, both linear and nonlinear have been designed for vibration control.

In this Chapter, I & I is used in designing the controller for the active actuator and an SMC is used to create the controller for the semi-active device using the same target/reference system. The reason behind combining these two control techniques is that they share the same design approach, and a common target system can be

defined for both the controllers. In an I & I design, first step is to define a target system, which should be reduced order and should be asymptotically stable. Then the nonlinear mapping functions are derived for off-the-manifold dynamics. In the third step a manifold is defined with respect to the error dynamics between off-the-manifold dynamics and the nonlinear mapping functions. Finally, the control law is derived that will bring off-the-manifold dynamics onto the manifold.

In SMC, a sliding surface is defined based on the error dynamics between the actual and the reference system states that need to be controlled. In this work, a first order sliding mode controller [90] is used for control of the semi-active device because the sliding surface is defined in such a way that it has a relative degree of one. This means that the input should appear at the first derivative of the sliding surface.

There is also a second order sliding mode control, in which the relative degree of the sliding surface is two. Second order sliding surfaces have been used mainly to avoid the chattering effect [95–97]. The robustness property in the SMC is because of the discontinuous part in the control. The discontinuous part switches the control action as the system crosses the sliding surface and pushes the system back towards the sliding surface. The underlying phenomenon of the manifold/sliding surface and the target/reference system is the same in both the design methodologies.

In Section 3.2 the example system is introduced. The details of I & I and SMC methodologies and controller design for the example system is given in Section 3.3. The results are presented in Section 3.4 and Section 3.5, and further discussion and summary are given in Section 3.6 and Section 3.7.

3.2 System Under Consideration

The example system under consideration is the multi-input-multi-output (MIMO) two-degree-of-freedom (2-DOF) nonlinear spring damper system shown in Figure 3.1. The nonlinearity in the system is a weak cubic stiffness that comes in from the spring between mass m_1 and the fixed support. As mentioned above, the weak non-linearity is introduced in the system to represent the behaviour associated with large deflections

in a flexible structure. The system is subjected to an excitation signal, U_d, that creates unwanted vibrations of the two masses.

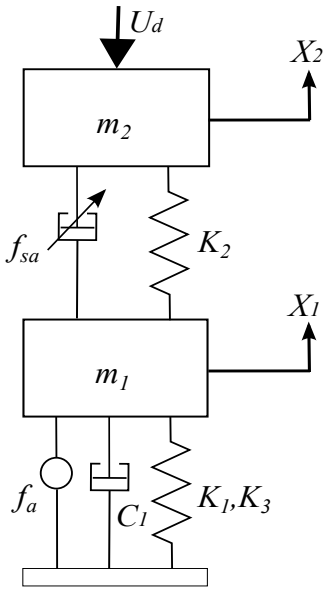

Fig. 3.1 *2-DOF mass-spring-damper system, where f_a represents the force of an active actuator and f_{sa} represents the force of a magneto-rheological damper. m_1, m_2 represent the masses, K_1, K_2 are the liner spring stiffness, K_3 is the nonlinear spring stiffness, C_1 is the damping coefficient and U_d is an excitation signal*

The control objective is to minimise the motion of the masses using the combined action of the active and semi-active control devices. An MR damper is used as a semi-active device because it is both reliable and widely available. To simulate the situation in flexible structures that suffer from unwanted vibrations, the damping constants are chosen such that the two-degree-of-freedom system is under-damped. As a result, the open-loop system has two lightly damped resonances.

$$\begin{bmatrix} m_1 & 0 \\ 0 & m_2 \end{bmatrix} \begin{bmatrix} \ddot{X}_1 \\ \ddot{X}_2 \end{bmatrix} + \begin{bmatrix} C_1 & 0 \\ 0 & 0 \end{bmatrix} \begin{bmatrix} \dot{X}_1 \\ \dot{X}_2 \end{bmatrix} + \begin{bmatrix} K_1+K_2 & -K_2 \\ -K_2 & K_2 \end{bmatrix} \begin{bmatrix} X_1 \\ X_2 \end{bmatrix} = \begin{bmatrix} -K_3 \\ 0 \end{bmatrix} X_1^3 + \begin{bmatrix} f_a - f_{sa} \\ f_{sa} - U_d \end{bmatrix} \tag{3.1}$$

The equation of motion for the two degree-of-freedom system is given by (3.1), where X_1 and X_2 represent the displacement of masses m_1 and m_2, respectively, f_a represents

the force of the active actuator, f_{sa} represents the force of the semi-active device (MR damper), m_1, m_2 represent the masses, K_1, K_2 are the linear spring stiffness, K_3 is the nonlinear spring stiffness, C_1 is the damping coefficient and U_d is an excitation signal.

The system can be represented in state space form as

$$\begin{aligned}
\dot{x}_1 &= x_2, \\
\dot{x}_2 &= \frac{1}{m_1}\Big(f_a - f_{sa} - K_1 x_1 - C_1 x_2 - K_2(x_1 - x_3) - K_3 x_1^3\Big), \\
\dot{x}_3 &= x_4, \\
\dot{x}_4 &= \frac{1}{m_2}\Big(f_{sa} - K_2(x_3 - x_1) - U_d\Big),
\end{aligned} \tag{3.2}$$

where x_1 and x_2 are the position and velocity of mass m_1 respectively, and x_3 and x_4 are the position and velocity of mass m_2 respectively.

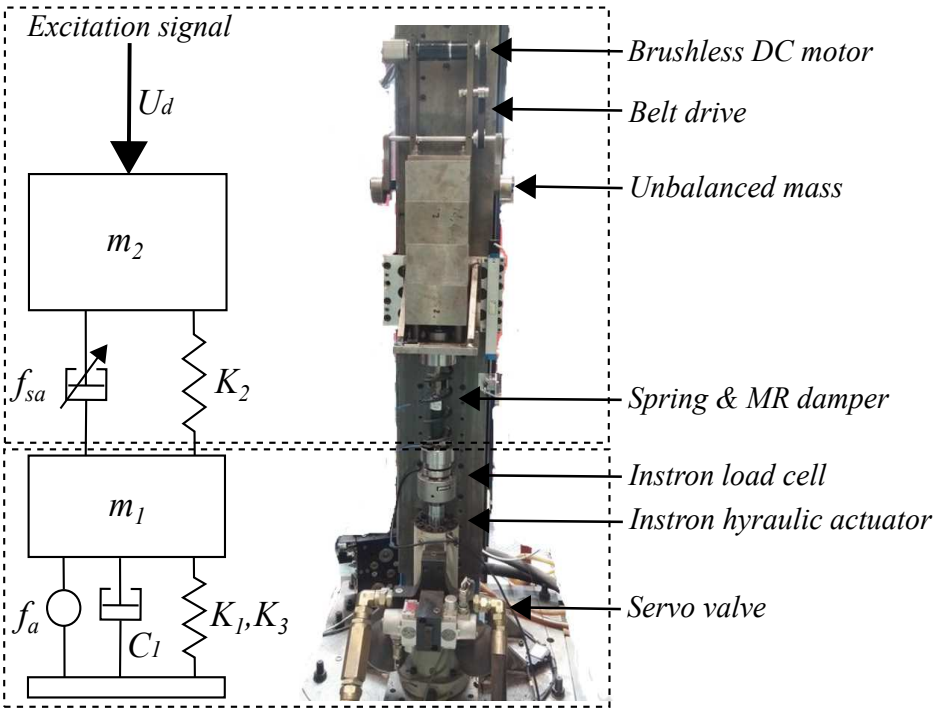

Fig. 3.2 *Hardware-in-the-loop (HIL) test set-up, where f_a represents the force of the active actuator and f_{sa} represents the force of the magneto-rheological damper. m_1, m_2 represent the masses, K_1, K_2 are the linear spring stiffness, K_3 is the nonlinear spring stiffness, and C_1 is the damping coefficient*

Figure 3.2 shows that how each of the term in Figure 3.1 is realised practically. The practical tests are performed as hardware-in-the-loop (HIL) tests. The physical part of the HIL test is the degree-of-freedom that includes mass m_2, the MR damper and

the linear spring. The other degree-of-freedom that includes the mass m_1, the active actuator, linear damper C_1 and nonlinear spring is the non-physical part of the HIL test. This is simulated numerically and applied to the physical system via a force applied by the Instron hydraulic actuator. The displacement of mass m_1 from Simulink goes into the Instron 8400 controller via a National Instruments data acquisition card. The control signal from the Instron 8400 controller goes to the Instron hydraulic actuator via servo valves, and the LVDT gives the displacement feedback signal.

3.3 Hybrid Active and Semi-active Controller Design

In this Chapter the standard, I & I approach is used [122]. The objective in the I & I theorem is to find a manifold $\mathscr{M} = \{x \in \mathbb{R}^n \,|x = \pi(\xi),\ \xi \in \mathbb{R}^p\}$ based on the actual system, target system and the mapping functions. The manifold will be defined in terms of z coordinates, where z represents the error between the mapping functions and off-the-manifold dynamics. The order of target system is lower than the order of the actual system, and the mapping functions are defined as virtual dynamics, to represent the actual system dynamics (off-the-manifold) that are not present in the target system.

The philosophy behind a sliding mode control (SMC) resembles that of an I & I methodology. In SMC, instead of the manifold, a sliding surface is defined. The sliding surface can be linear or nonlinear. The system trajectories are forced towards the sliding surface during the reaching mode and once on the sliding surface, the system trajectories are pushed towards an asymptotically stable equilibrium point during the sliding mode. One of the differences mentioned in the literature between an SMC and an I & I is that in the SMC the sliding surface needs to be reached by the trajectories whereas in an I & I this is not necessary [122]. The reason behind combining these two control techniques is that they share the same design approach, and we can define a common target system for both the controllers. In the next subsection, the I & I conditions are explained.

3.3.1 I & I Conditions

Consider a nonlinear system

$$\dot{x} = f(x) + g(x)u \tag{3.3}$$

where $x \in \mathbb{R}^n$ is the system state, $u \in \mathbb{R}^m$ is the input signal, $f(x)$ and $g(x)$ are nonlinear functions of x and an over-dot represents the differentiation with respect to time. The equilibrium point to be stabilized is denoted $x^\star \in \mathbb{R}^n$.

The following properties should hold.

(H1) The system

$$\dot{\xi} = \alpha(\xi) \tag{3.4}$$

with transformed state vector $\xi \in \mathbb{R}^p$ has an asymptotically stable equilibrium at $\xi^\star \in \mathbb{R}^p$, and

$$x^\star \in \pi(\xi^\star).$$

where $\alpha : \mathbb{R}^p \to \mathbb{R}^p$ and $\pi : \mathbb{R}^p \to \mathbb{R}^n$ are smooth mapping functions with $p < n$.

(H2) For all $\xi \in \mathbb{R}^p$, substituting a smooth mapping $x = \pi(\xi)$ in (3.3) leads to

$$f(\pi(\xi)) + g(\pi(\xi))\, c(\pi(\xi)) = \frac{\partial \pi}{\partial \xi}\alpha(\xi). \tag{3.5}$$

where $c : \mathbb{R}^p \to \mathbb{R}^m$ is the control signal that renders the manifold invariant.

(H3) The set identity holds

$$\{x \in \mathbb{R}^n \mid \phi_m(x) = 0\} = \{x \in \mathbb{R}^n \mid x = \pi(\xi),\ \xi \in \mathbb{R}^p\}. \tag{3.6}$$

where $\phi_m : \mathbb{R}^n \to \mathbb{R}^{n-p}$ represents the manifold. From (3.6), the manifold $\phi_m(x) = 0$, when $x = \pi(\xi)$, and $z = x - \pi(\xi)$, where z represents the distance between off-the-manifold coordinates and the manifold.

(H4) All trajectories of the system

$$\dot{z} = \frac{\partial \phi_m}{\partial x}[f(x) + g(x)\psi(x,z)], \tag{3.7}$$

$$\dot{x} = f(x) + g(x)\psi(x,z), \tag{3.8}$$

are bounded and satisfy

$$\lim_{t\to\infty} z(t) = 0. \tag{3.9}$$

where $\psi : \mathbb{R}^{n\times(n-p)} \to \mathbb{R}^m$ is the equivalent control signal and right hand side of (3.7) is $\dot{\phi}_m$.

Then x^* is an asymptotically stable equilibrium of the closed loop system

$$\dot{x} = f(x) + g(x)\psi(x,\phi_m(x)). \tag{3.10}$$

Once the closed loop system (3.10), trajectories converge to the manifold such that $z = 0$ then $\psi(\pi(\xi),0) = c(\pi(\xi))$. The I & I methodology defines a set of conditions, for the existence of three features: an *invariant manifold*, a *mapping function*, and a *target system*. In the next two subsections, the controller design and detailed derivation is explained.

3.3.2 I & I Controller Design

The first step in the control design is to define a target/reference system. The target system should be realisable and should also consider the physical constraints of the actual system [122]. In this example, the objective to control the vibrations in the mass m_2. Therefore the target system is defined to reduce the flexible dynamics to a single degree-of-freedom (SDOF) such that, in effect, the other degrees-of-freedom will behave as a rigid body motion. This means that the flexibility in the structure is reduced. It also aligns with the I & I methodology where the target system should be at least one degree less than the actual system.

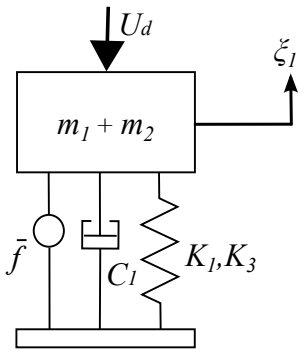

Fig. 3.3 *Target system, where ξ_1 and ξ_2 represents the position and velocity of the mass (m_1+m_2), $\bar{f}$ will be computed after defining the mapping functions, K_1 is the linear spring stiffness, K_3 is the nonlinear spring stiffness, C_1 is the damping coefficient and U_d is an excitation signal*

As a result the nonlinear SDOF system shown in Figure 3.3 is defined as the target system. The aim of the controller design is to damp out the vibrations introduced by U_d at m_2. The dynamics of the target system are given as

$$\begin{aligned}\dot{\xi}_1 &= \xi_2,\\ \dot{\xi}_2 &= \frac{1}{(m_1+m_2)}\Big(\bar{f} - K_1\xi_1 - C_1\xi_2 - K_3\xi_1^3 - U_d\Big),\end{aligned} \tag{3.11}$$

where ξ_1 and ξ_2 represent the position and velocity of the mass (m_1+m_2) respectively, and $\bar{f} = \mathscr{W} + u$, u represents the controller signal and $\mathscr{W}$ is the function that will be computed after defining the mapping functions. The next step is to design a controller for the target system. Any controller can be designed for the target system as long as it can achieve the desired performance for the defined mapping functions. A proportional plus integral (PI) controller is designed in the same way as in [136]. The implementation of the PI controller in the target system is given by

$$u = K_i \int e_v dt + K_v e_v$$

where $e_v = K_p e_p - \xi_2$, and the PI control signal is given as

$$u = K_a e_p + K_b \int e_p dt - K_c \xi_2 - K_d \xi_1 \tag{3.12}$$

where, K_i, K_v & K_p are control gains, e_v is the velocity error, e_p is the position error, and $K_a = K_v K_p$, $K_b = K_i K_p$, $K_c = K_v$, $K_d = K_i$.

It is difficult to solve the partial differential equation (3.5). Since the target system dynamics (3.11) resembles the part of actual system dynamics (3.2), so the solution of (3.5) can be obtained by setting $\pi_3(\xi_1, \xi_2) = \xi_1$. As $\dot{x}_1 = x_2$, hence $\pi_4(\xi_1, \xi_2) = \xi_2$. Therefore, the mapping functions $\pi_1(\xi_1, \xi_2)$, $\pi_2(\xi_1, \xi_2)$ are derived from

$$\dot{\xi}_2 = \dot{\pi}_4. \tag{3.13}$$

and

$$\frac{1}{m_1 + m_2}\Big(\bar{f} - K_1\xi_1 - C_1\xi_2 - K_3\xi_1^3\Big) = \frac{1}{m_2}\Big(-C_2(\xi_2 - \pi_2) - K_2(\xi_1 - \pi_1)\Big) \tag{3.14}$$

The selection of the mapping functions is a non trivial task and it is possible for more then one mapping function to exist. However, they should always satisfy (3.14) and by using these mapping functions, the target system should have an asymptotically stable equilibrium at the origin. Therefore the mapping functions selected are

$$\pi_1 = -\alpha_1 \frac{m_2 K_3 \xi_1^3}{K_2(m_1 + m_2)} - \frac{m_2 K_1 \xi_1}{K_2(m_1 + m_2)} + \xi_1 + \alpha_2 e_p + \alpha_3 \int e_p dt + \alpha_4 \xi_2 + \alpha_5 \xi_1, \tag{3.15}$$

$$\pi_2 = \Big(-\alpha_1 \frac{3 m_2 K_3 \xi_1^2}{K_2(m_1 + m_2)} - \frac{m_2 K_1}{K_2(m_1 + m_2)} + 1\Big)\xi_2 - \alpha_2 \xi_2 + \alpha_3 e_p + \alpha_4 \dot{\xi}_2 + \alpha_5 \xi_2. \tag{3.16}$$

$\bar{f}$ is defined as

$$\bar{f} = -\frac{C_2(3K_3\xi_1^2 + K_1)\xi_2}{K_2} + C_1\xi_2 + u \tag{3.17}$$

where C_2 is taken to be a linear approximation of the MR damping constant. Substituting π_1, π_2 and $\bar{f}$ in (3.14) gives

$$\frac{1}{m_1+m_2}\Bigg[-\frac{C_2(3K_3\xi_1^2+K_1)\xi_2}{K_2}+C_1\xi_2+K_ae_p+K_b\int e_p dt-K_c\xi_2-K_d\xi_1-K_1\xi_1 -C_1\xi_2-K_3\xi_1^3\Bigg]=\frac{1}{m_2}\Bigg[-C_2\Bigg(\xi_2-\Big(\big(-\alpha_1\frac{3m_2K_3\xi_1^2}{K_2(m_1+m_2)}-\frac{m_2K_1}{K_2(m_1+m_2)}+1\big)\xi_2 -\alpha_2\xi_2+\alpha_3e_p+\alpha_4\dot{\xi}_2+\alpha_5\xi_2\Big)\Bigg)-K_2\Bigg(\xi_1-\Big(-\alpha_1\frac{m_2K_3\xi_1^3}{K_2(m_1+m_2)} -\frac{m_2K_1\xi_1}{K_2(m_1+m_2)}+\xi_1+\alpha_2e_p+\alpha_3\int e_p dt+\alpha_4\xi_2+\alpha_5\xi_1\Big)\Bigg)\Bigg] \tag{3.18}$$

Using (3.18), we now compare coefficients to find out the five unknowns α_1, α_2, α_3, α_4, α_5.

$$\begin{bmatrix} 0 & 0 & 0 & \frac{C_2(K_d-K_1)}{m_2(m_1+m_2)} & \frac{K_2}{m_2} \\ 0 & \frac{K_2}{m_2} & \frac{C_2}{m_2} & \frac{K_aC_2}{m_2(m_1+m_2)} & 0 \\ 0 & 0 & \frac{K_2}{m_2} & \frac{K_bC_2}{m_2(m_1+m_2)} & 0 \\ 1 & 0 & 0 & \frac{C_2}{m_2} & 0 \\ 0 & \frac{C_2}{m_2} & 0 & -\frac{C_2}{m_2(m_1+m_2)}\frac{-K_1C_2-K_cK_2}{K_2}-\frac{K_2}{m_2} & -\frac{C_2}{m_2} \end{bmatrix}\begin{bmatrix} \alpha_1 \\ \alpha_2 \\ \alpha_3 \\ \alpha_4 \\ \alpha_5 \end{bmatrix}= \begin{bmatrix} \frac{K_d}{m_1+m_2} \\ \frac{K_a}{m_1+m_2} \\ \frac{K_b}{m_1+m_2} \\ 1 \\ \frac{K_c}{m_1+m_2} \end{bmatrix} \tag{3.19}$$

To check the asymptotic stability of the target system, the target system dynamics are compared with a single mass system dynamics (3.20). From the Lagrangian formulation the dynamics of a single mass are

$$\begin{aligned}\dot{\xi}_1 &= \xi_2 \\ \dot{\xi}_2 &= -E^{'} - \xi_2 R\end{aligned} \tag{3.20}$$

where E is the potential energy function and R is the damping function and a dash represents differentiation with respect to the state vector.

Comparing (3.11) and (3.20) gives

$$E^{'} = \frac{K_1\xi_1 + K_3\xi_1^3}{(m_1+m_2)} \tag{3.21}$$

$$R = \frac{C_2(3K_3\xi_1^2 + K_1)}{K_2(m_1+m_2)} \tag{3.22}$$

and

$$E = \frac{K_1\xi_1^2}{2(m_1+m_2)} + \frac{K_3\xi_1^4}{4(m_1+m_2)}. \tag{3.23}$$

A Lyapunov function is defined as a generalized energy function

$$V_{i\&i} = \frac{1}{2}{\xi_2}^2 + E. \tag{3.24}$$

The target system dynamics will have an asymptotically stable equilibrium at the origin if the following conditions are satisfied by the Lyapunov function defined in (3.24)

$$V(0,0) = 0 \tag{3.25a}$$

$$V(\xi_1,\xi_2) > 0, \text{ in } D - \{0\}. \quad D \to \mathbb{R}^p \tag{3.25b}$$

$$\dot{V}(\xi_1,\xi_2) < 0, \text{ in } D - \{0\}. \tag{3.25c}$$

where $V(\xi_1, \xi_2)$ is the energy function, and D is the subset of $\mathbb{R}^p$ in which the Lyapunov function is defined.

As a result

$$\dot{V}_{i\&i}(\xi_1, \xi_2) = \xi_2 \dot{\xi}_2 + E^{'} \xi_2,$$

$$\dot{V}_{i\&i}(\xi_1, \xi_2) = \xi_2 \left(\dot{\xi}_2 + E^{'} \right),$$

and

$$\dot{V}_{i\&i}(\xi_1, \xi_2) = -R{\xi_2}^2. \tag{3.26}$$

The first two conditions (3.25a) and (3.25b) are satisfied by the Lyapunov function defined in (3.24). The third condition (3.25c), where $\dot{V}_{i\&i}(\xi_1, \xi_2)$ should be negative definite, is satisfied when R is positive. As it can be seen from (3.22), R is always positive. Therefore, the selected target system has an asymptotically stable equilibrium at the origin. The error between the off-the-manifold dynamics and the mapping functions is defined as

$$z = x_1 - \pi_1 \tag{3.27}$$

and the manifold is defined as

$$\mathscr{M} = -k_1 z - k_2 \dot{z} \tag{3.28}$$

where $\dot{z} = x_2 - \pi_2$. The gains k_1 and k_2 are chosen in such a way that $(s^2 + k_2 s + k_1)$ is Hurwitz.

The last step in the I & I methodology is to compute the control law, which is done using

$$\ddot{z} = \dot{x}_2 - \dot{\pi}_2 \tag{3.29}$$

and

$$\ddot{z} = \frac{1}{m_1}\Big(f_a - f_{sa} - K_1 x_1 - C_1 x_2 - K_2(x_1 - x_3) - K_3 x_1^3\Big) - \frac{\partial \pi_2}{\partial x_3}\dot{x}_3 - \frac{\partial \pi_2}{\partial x_4}\dot{x}_4. \quad (3.30)$$

The control signal f_a is given by

$$f_a = \left[-k_1 z - k_2 \dot{z} + \frac{\partial \pi_2}{\partial x_3}\dot{x}_3 + \frac{\partial \pi_2}{\partial x_4}\dot{x}_4\right] m_1 + K_1 x_1 + C_1 x_2 + K_2(x_1 - x_3) + C_2(x_2 - x_4) + K_3 x_1^3 \quad (3.31)$$

where

$$\frac{\partial \pi_2}{\partial x_3} = -\frac{6\alpha_1 K_3 m_2 x_3 x_4}{K_2(m_1 + m_2)} - \alpha_3 - \frac{\alpha_4 K_2}{m_2}, \quad (3.32)$$

$$\frac{\partial \pi_2}{\partial x_4} = \frac{(-3\alpha_1 K_3 x_3^2 - K_1)m_2}{K_2(m_1 + m_2)} + 1 - \alpha_2 - \frac{\alpha_4 C_2}{m_2} + \alpha_5 \quad (3.33)$$

The expressions in (3.32) and (3.33) gives the partial derivative of the mapping function π_2, with respect to x_3 and x_4. In the next subsection, SMC controller design is derived.

3.3.3 SMC Controller Design

The controller for MR damper is designed using the SMC. A sliding surface is defined on which the system will be forced to slide. In order to make sure that the sliding surface has an asymptotic stable equilibrium point, a Lyapunov candidate function is defined. To add robustness, a discontinuous control is added to the equivalent control and finally to avoid the chattering phenomenon the signum function is replaced with a hyperbolic tangent function. The sliding mode control is designed to control the semi-active device. The error dynamics are defined as

$$e = x_3 - \xi_1. \quad (3.34)$$

The sliding surface is defined in terms of the error dynamics as

$$S = \lambda_1 e + \lambda_2 \dot{e} \tag{3.35}$$

where λ_1, λ_2, are the design parameters, which will determine how fast the error dynamics will go to zero and $\dot{e} = x_4 - \xi_2$. In the next step the control signal is derived using (3.35) to give

$$f_{sa} = f_n - \frac{m_2}{\lambda_2}\Big(K_{smc}\text{sgn}(S)\Big) \tag{3.36}$$

where K_{smc} is a design parameter and strictly positive and f_n is given as

$$f_n = \frac{m_2}{\lambda_2}\Bigg(-\lambda_1(x_4 - \xi_2)\Bigg) + m_2\dot{\xi}_2 + K_2(x_3 - x_1). \tag{3.37}$$

The SMC control signal has two parts. One part represents the normalized control f_n and the second part represents the discontinuous (signum function) control, which is responsible for robustness. To make sure that the sliding surface has an asymptotically stable equilibrium at the origin towards which the system will slide, a Lyapunov function is defined as

$$V_{smc} = \frac{1}{2}S^2. \tag{3.38}$$

The sliding surface will have an asymptotically stable equilibrium if (3.38) satisfies the conditions in (3.25). The first two conditions (3.25a) and (3.25b) are satisfied by the Lyapunov function defined in (3.38), for the third condition (3.25c) to be satisfied, $\dot{V}_{smc}$ needs to be analyzed, where

$$\dot{V}_{smc} = S\dot{S}$$

and

$$S\dot{S} < 0$$

To make sure that the system will reach the sliding surface in finite time, a more strict condition is imposed on $S\dot{S}$

$$S\dot{S} \leq -\eta_{smc}|S| \tag{3.39}$$

where η_{smc} is strictly positive. Then

$$S\dot{S} \leq -\eta_{smc}S\text{sgn}(S)$$

and

$$\dot{S} \leq -\eta_{smc}\text{sgn}(S)$$

such that

$$K_{smc} \geq \eta_{smc}. \tag{3.40}$$

For the third condition to be satisfied for an asymptotically stable equilibrium, K_{smc} should be greater than η_{smc}. The MR damper can only dissipate energy from the system. The controller will be switched-on, when the relative velocity v_r across the MR damper and the control signal f_{sa} have opposite signs and will be switched-off otherwise. This condition is imposed on f_{sa} in (3.41) and is called the passivity constraint:

$$f_{sa} = \begin{cases} f_n - \dfrac{m_2}{\lambda_2}\Big(K_{smc}\text{sgn}(S)\Big) & f_{sa}v_r < 0 \\ 0 & f_{sa}v_r > 0 \end{cases} \tag{3.41}$$

where $v_r = x_4 - x_2$.

To avoid chattering, we have used the approximation that the signum function can be replaced with the tangent hyperbolic function

$$\text{sgn}(x) \approx \tanh(kx) \tag{3.42}$$

where $k >> 1$ for smooth approximation. In order to validate the designed controller, simulation results are shown in the next section.

3.4 Simulation Results without Actuator Dynamics

Figure 3.4 shows the block diagram implementation of the hybrid control without including the actuator dynamics. In this block diagram f_{smc} is the control signal of the SMC controller, $f_{i\&i}$ is the control signal of the I & I controller, and $f_{smc} = f_{sa}$, $f_{i\&i} = f_a$, as there are no actuator dynamics involved. All the other state variables and system parameters that are shown in the block diagram have already been defined.

Figure 3.5 shows the I & I controller block diagram. First the mapping functions are defined for off-the-manifold dynamics and then the manifold is defined as the error between the mapping functions and off-the-manifold dynamics. The output of *Mapping and Manifold* block is z_1 and z_2, which have already been defined in the controller design. The output of the *PI controller* block is u. This is the same PI controller that was designed for the target system. Then the *Immersion & Invariance control law* block, which has the input z_1, z_2, and u, generates the final control signal $f_{i\&i}$.

Figure 3.6 shows the SMC controller block diagram. In the SMC block diagram the *Sliding surface* block inputs are the states of the target system and the actual system. The sliding surface is defined in this block. *Sliding mode control law* block inputs are the sliding surface and the state variables from the actual and the target system. The control law is defined in this block, which gives the final control signal f_{smc}. The *Target system* block input is u, which is the output of the *PI controller* block. Both the equivalent and the discontinuous part of f_{smc} are defined here. To validate the analytical results via simulation, Matlab/Simulink is used. The resonant frequencies of the 2-DOF system are 2.76 Hz and 6.8 Hz. To check the controller performance, initially in the simulations an excitation signal at 3 Hz with an amplitude of 100 N is given to the 2-DOF system at mass m_2. In the first two seconds the system is vibrating in open-loop after which the controller is switched on.

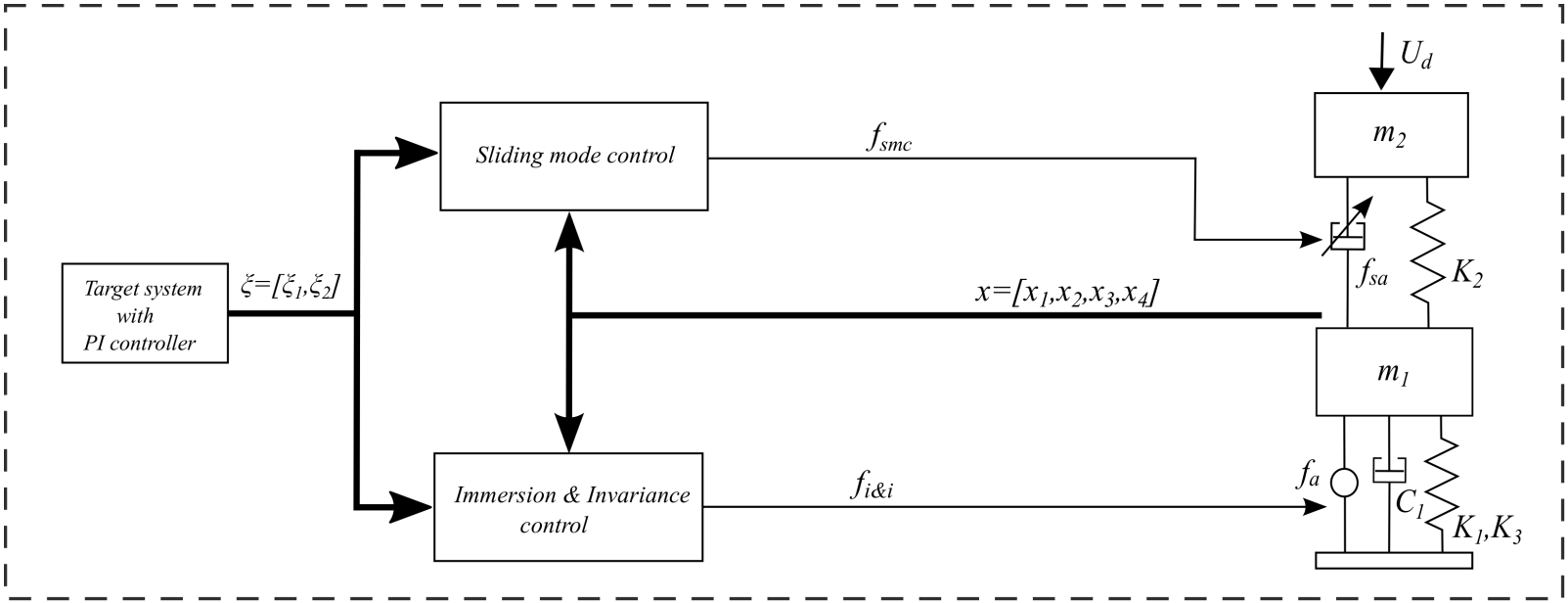

Fig. 3.4 *Block diagram implementation of hybrid active & semi-active control without actuators dynamics, where x_1 and x_2 are the position and velocity of mass m_1 respectively, x_3 and x_4 are the position and velocity of mass m_2 respectively, $f_{i\&i}$ is the I & I control signal, f_{smc} is the control signal of SMC controller*

Table 3.1 shows the parameters of the 2-DOF system and Table 3.2 shows the gains designed for the PI, I & I and SMC controllers. Figure 3.7 shows the displacement and velocity of mass m_2 being controlled to follow the reference system in which a single mass, $m_1 + m_2$, is assumed. It can be seen that the simulated system is following the reference system and when the proposed hybrid active & semi-active controller is turned on at 2 seconds, the error between x_3 and ξ_1 is reduced by 98.6%. Figure 3.8 shows the displacement and velocity of mass m_1, and it is also following the reference system and the error between x_1 and ξ_1 is reduced by 95%.

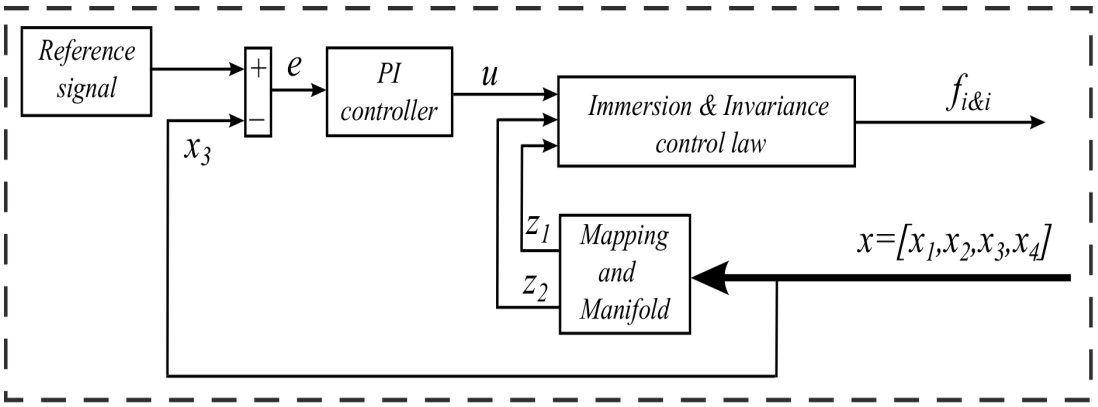

Fig. 3.5 *Block diagram implementation of the I & I controller, where x_1 and x_2 are the position and velocity of mass m_1 respectively, x_3 and x_4 are the position and velocity of mass m_2 respectively, $f_{i\&i}$ is the I & I control signal, z_1 and z_2 are the error dynamics in the I & I controller, u is output of the PI controller, e is error between reference and desired signal*

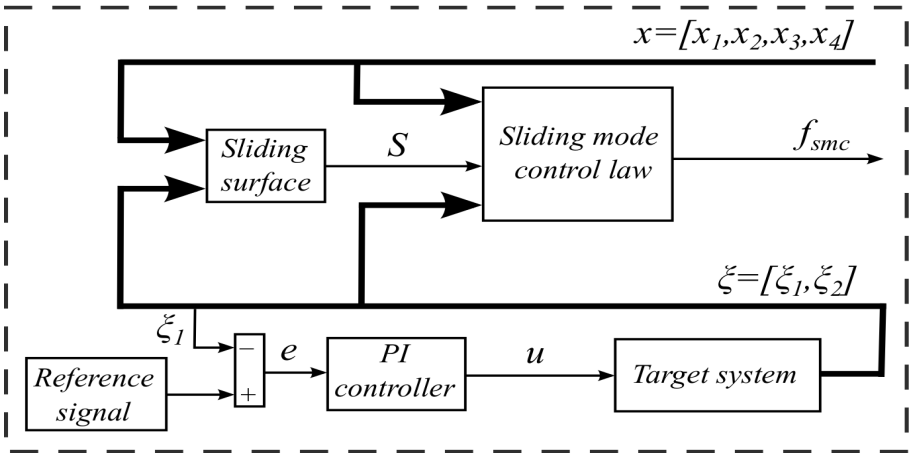

Fig. 3.6 *Block diagram implementation of the SMC controller, where x_1 and x_2 are the position and velocity of mass m_1 respectively, x_3 and x_4 are the position and velocity of mass m_2 respectively, u is output of the PI controller, e is error between reference and desired signal, f_{smc} is the output of the SMC controller, S is the sliding surface, ξ_1 and ξ_2 represent the position and velocity of the mass $(m_1 + m_2)$, respectively*

Table 3.1 System parameters

mass (kg)	stiffness (Nm^{-1})	damping (Nsm^{-1})
$m_1 = 100$	$K_1 = 100000$	$C_1 = 1000$
$m_2 = 112$	$K_2 = 63000$	$C_2 = 1000$

Table 3.2 Controller gains

PI controller	I&I controller	SMC controller
$K_p = 5.43$	$k_1 = 1000$	$K_{smc} = 1$
$K_v = 7420$	$k_2 = 15.00$	$\lambda_1 = 1$
$K_i = 67722$		$\lambda_2 = 1$

The active control signal is shown in Figure 3.9a. The controller is in the off state for the first two seconds and after that as the controller is switched-on, the active control signal goes to -1500 N to bring off-the-manifold dynamics to the manifold. After the transient response, the active control signal goes to steady state. The same phenomenon is followed by the semi-active control signal as shown in Figure 3.9b, the semi-active control signal goes to a maximum value of 300 N, and after the transient response the control signal goes to a steady state phase.

In the next step of validation process, a sinusoidal chirp signal with a frequency range of 0.1-10 Hz and an amplitude of 100 N is given to the system at mass m_2. The open-loop frequency response of the system is shown in Figure 3.10. The system resonates at 2.76 Hz and 6.8 Hz. The closed loop frequency response of the system is shown in Figure 3.11. The performance of the hybrid controller is evident. In the next section, the simulations will be repeated after adding the actuator dynamics.

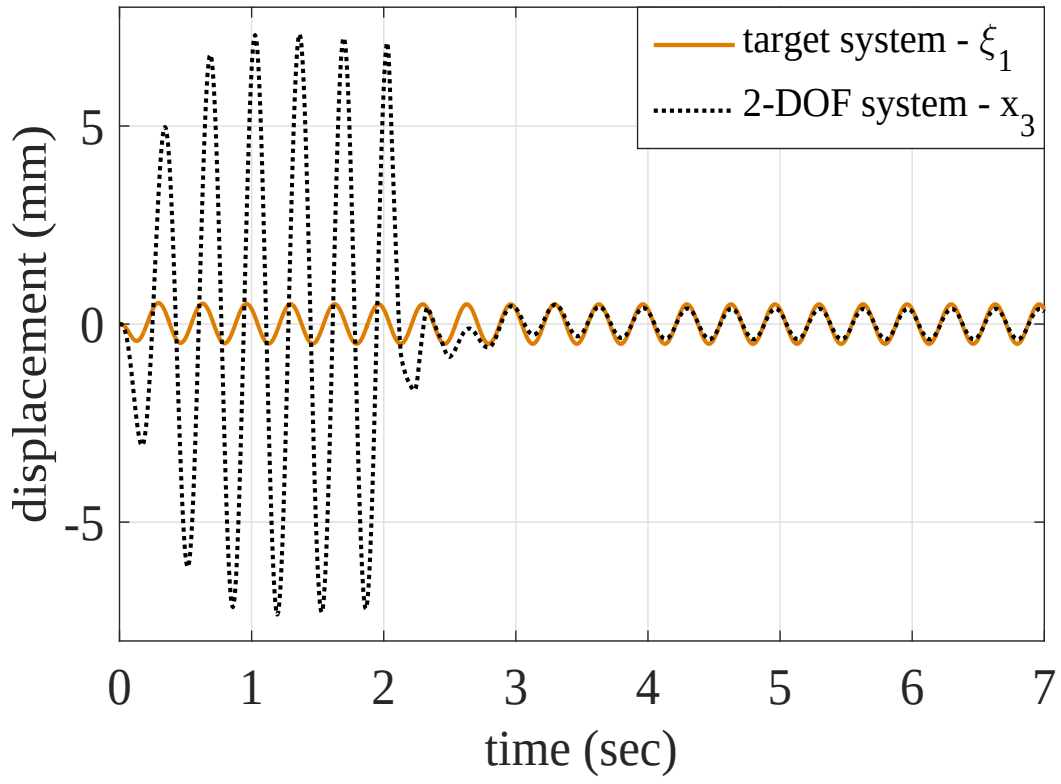

(a)

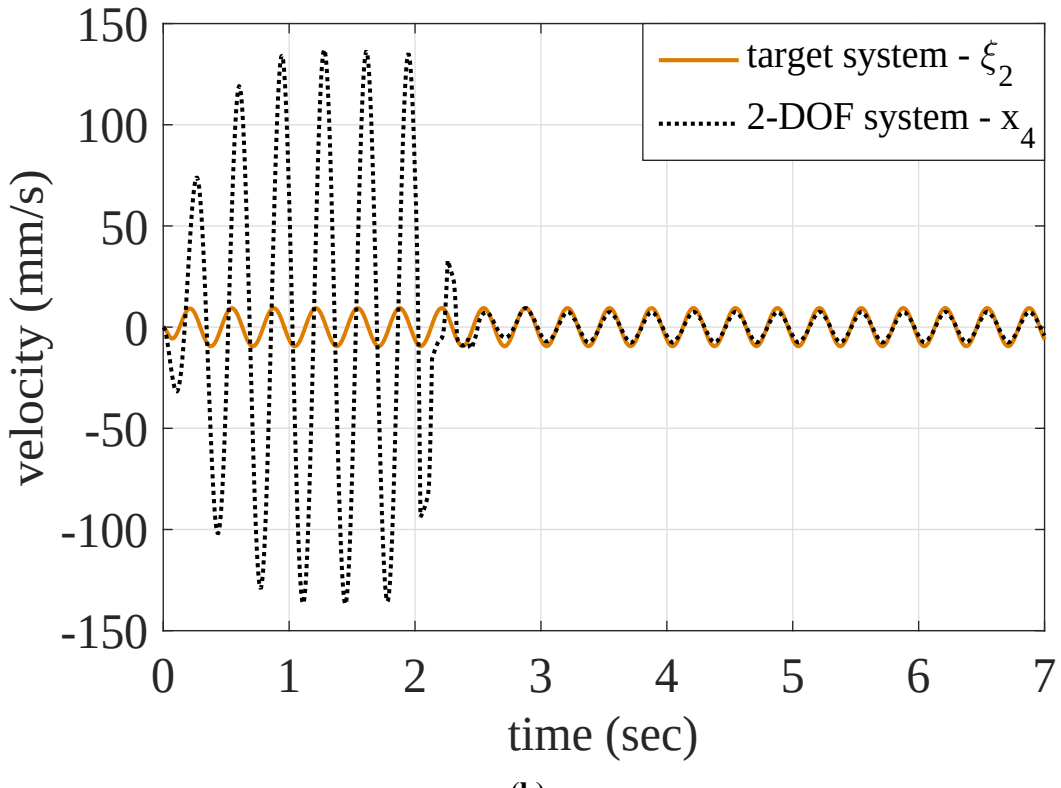

(b)

Fig. 3.7 *Displacement and velocity of mass m_2 controlled to follow the reference system with the hybrid active & semi-active controller without actuators dynamics. The hybrid controller is switched-on at time 2 seconds, (a) displacement, (b) velocity*

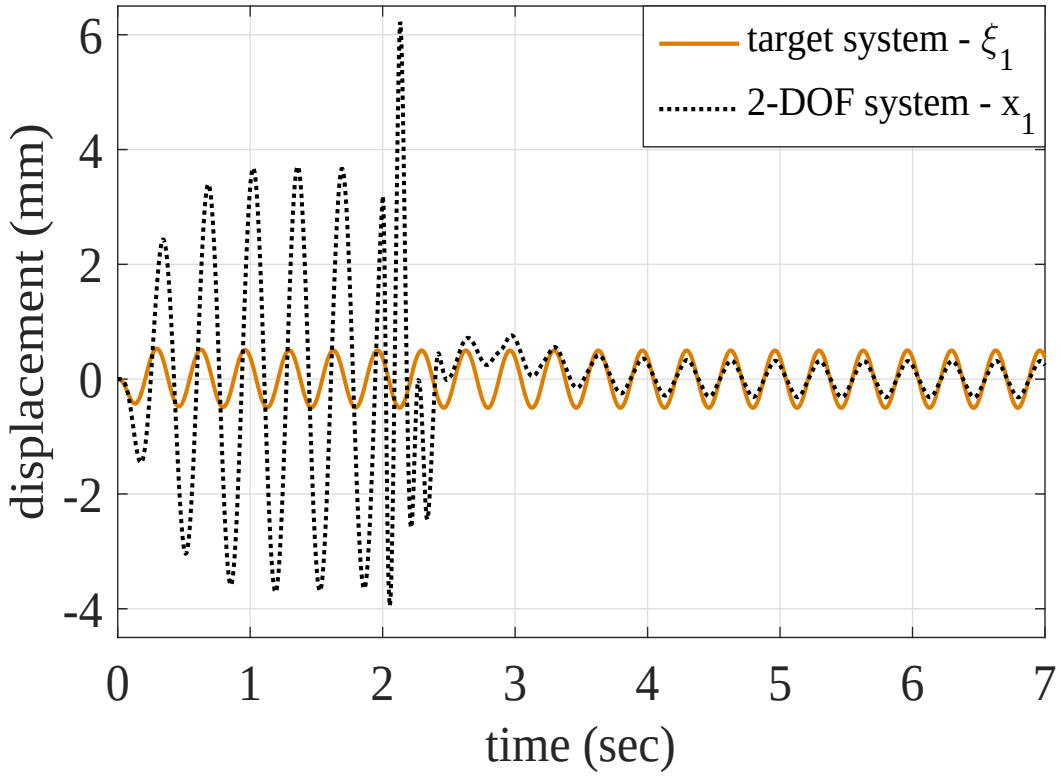

(a)

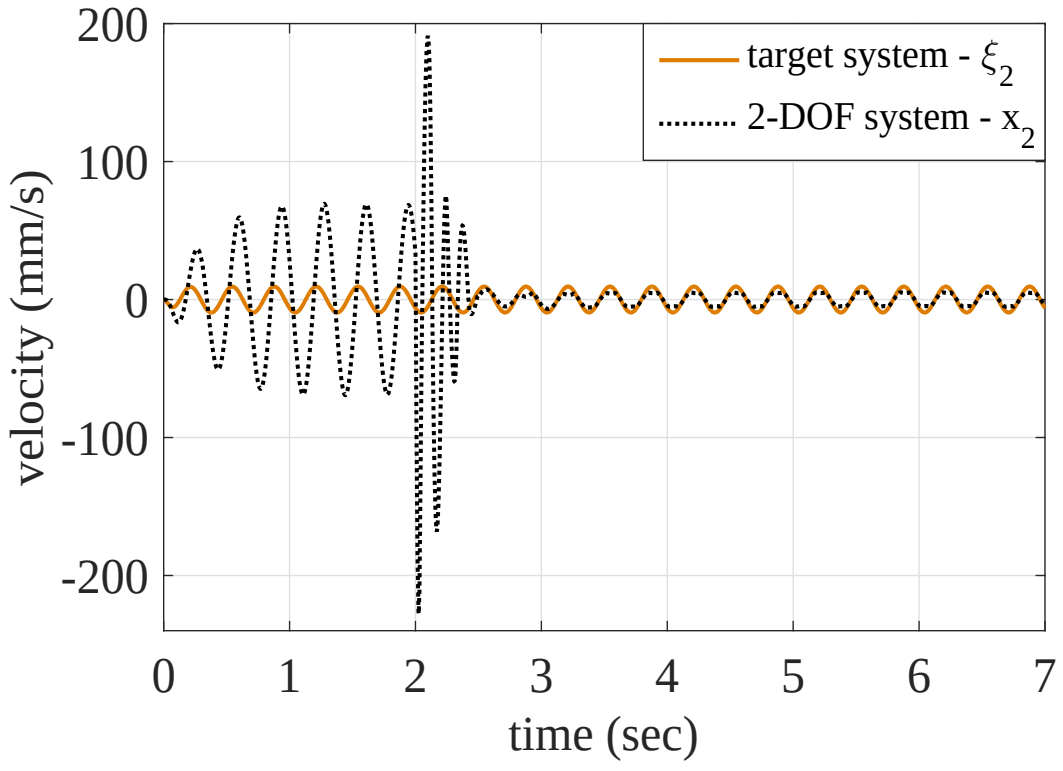

(b)

Fig. 3.8 *Displacement and velocity of mass m_1 controlled to follow the reference system with the hybrid active & semi-active controller without actuators dynamics. The hybrid controller is switched on at time 2 seconds, (a) displacement, (b) velocity*

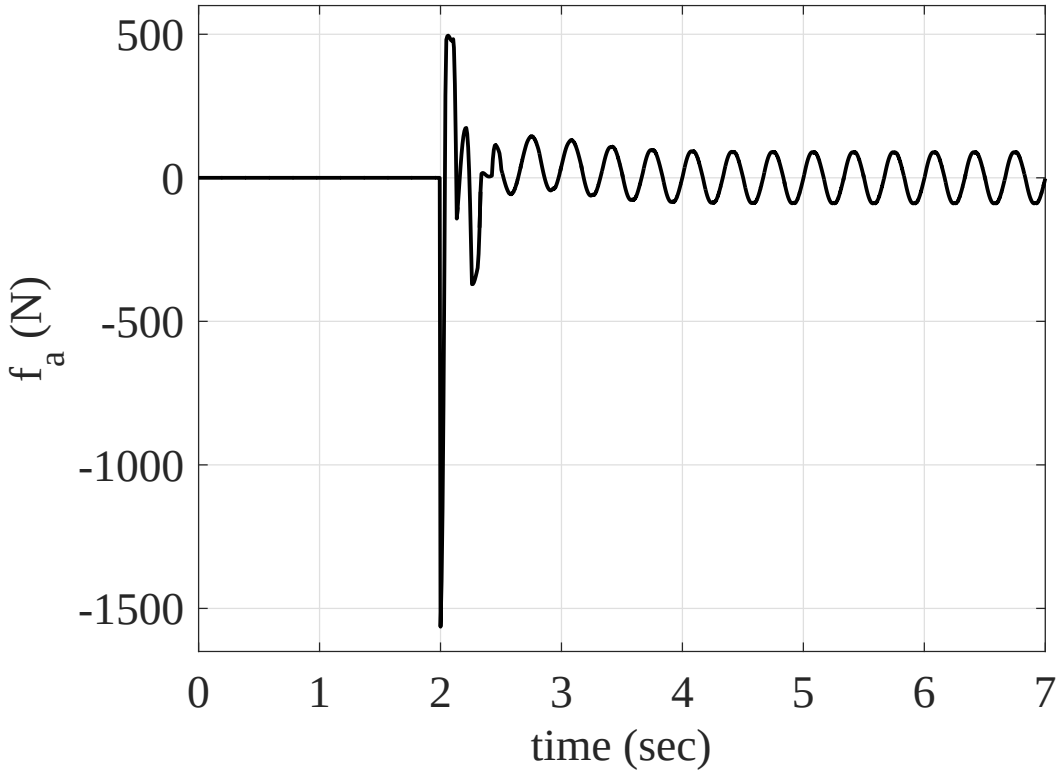

(a)

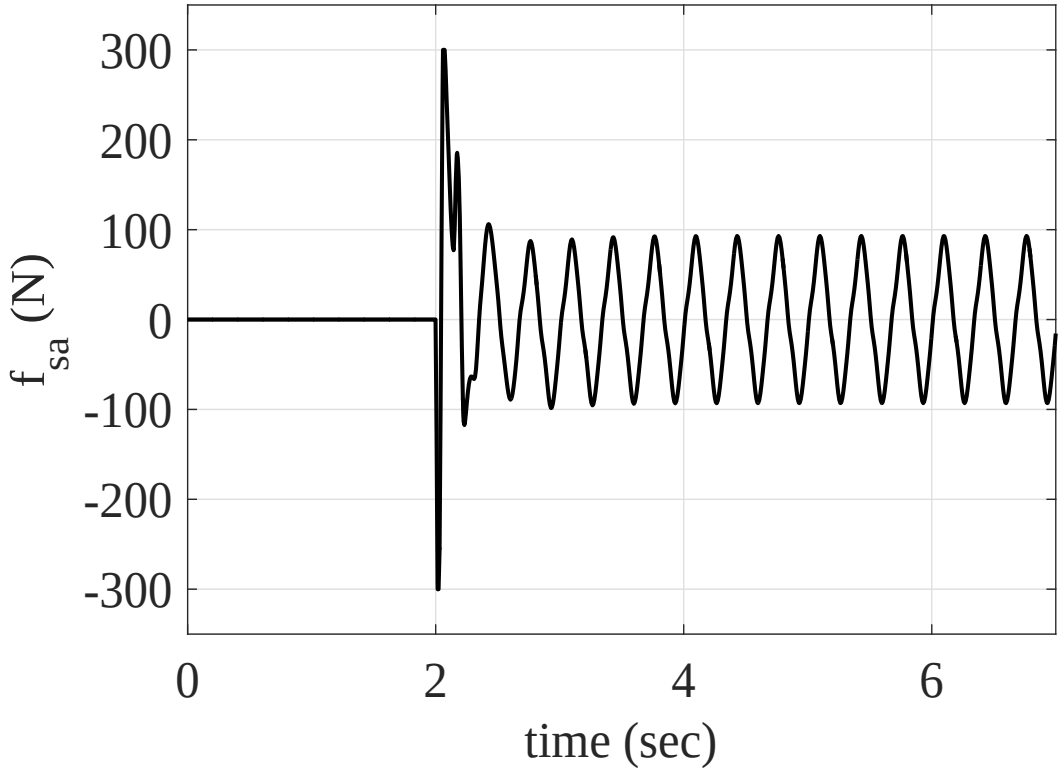

(b)

Fig. 3.9 *Control signals in hybrid active & semi-active controllers without actuators dynamics. The hybrid controller is switched on at time 2 seconds, (a) active control signal, (b) semi-active control signal*

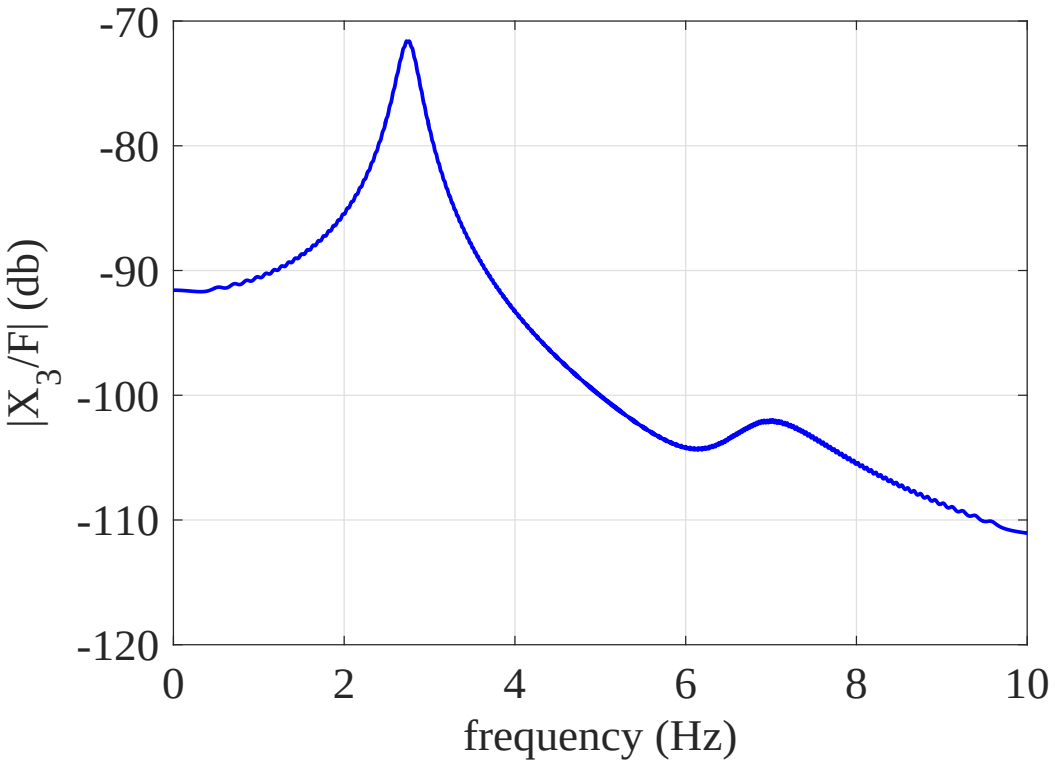

(a)

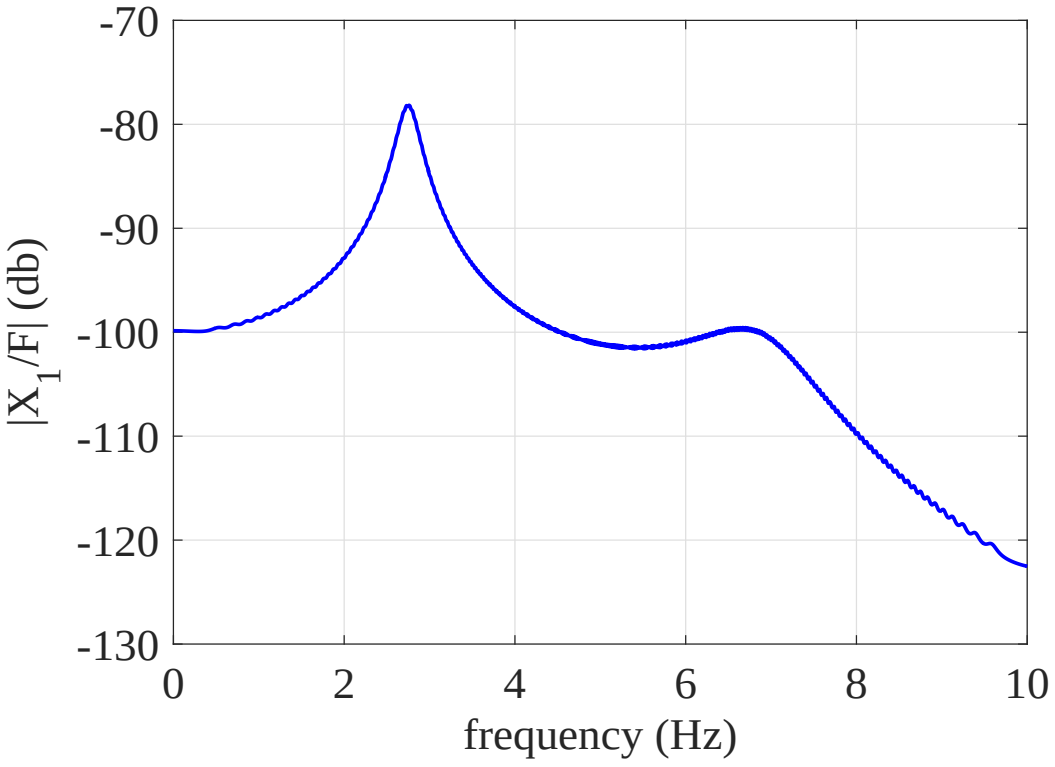

(b)

Fig. 3.10 *Open-loop frequency response of the actual system showing resonance peaks at 2.7 and 6.8 Hz, (a) displacement of mass m_2, (b) displacement of mass m_1*

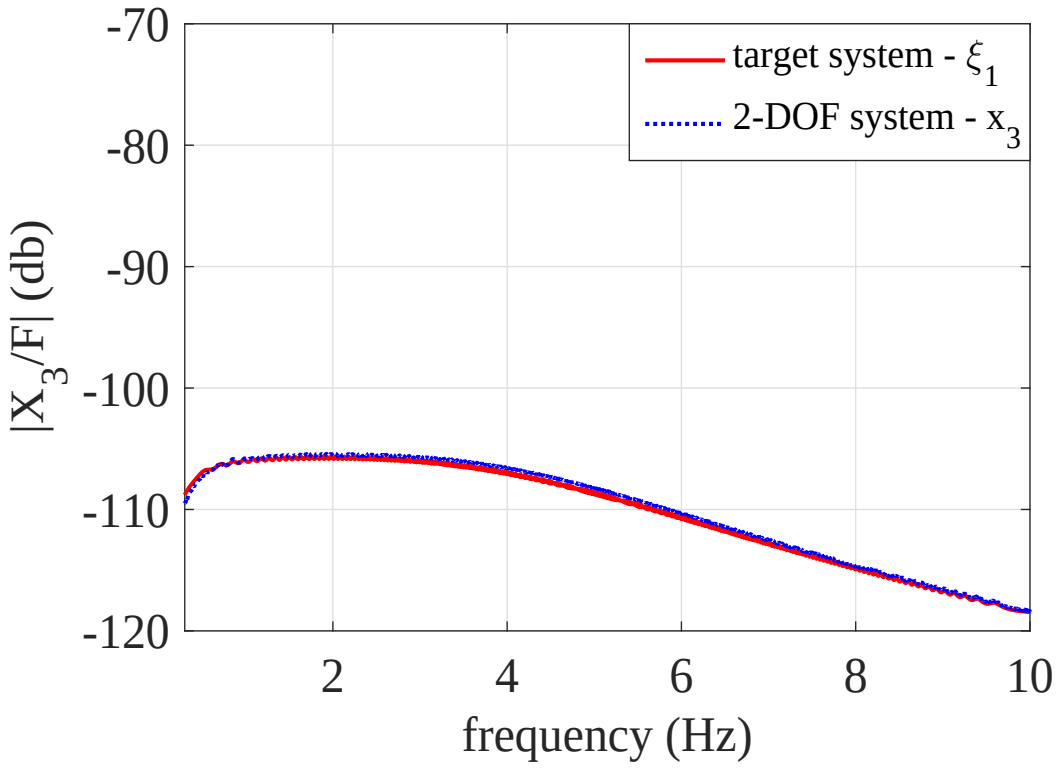

(a)

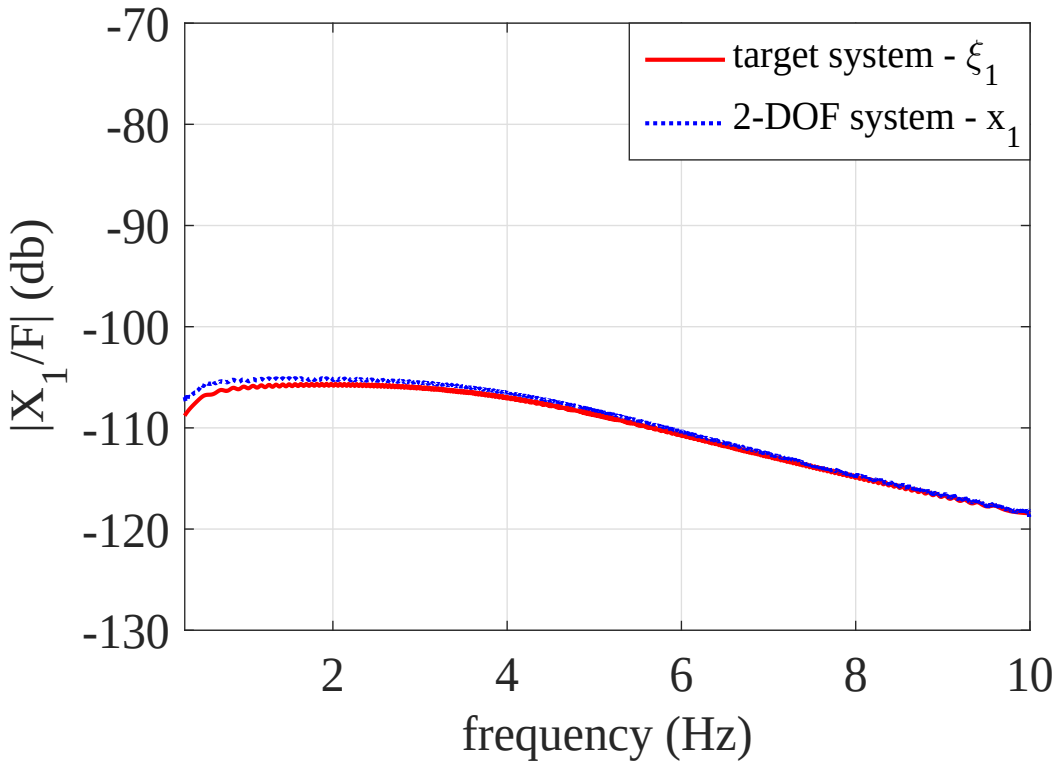

(b)

Fig. 3.11 *Closed loop frequency response of the actual system, (a) displacement of mass m_2, (b) displacement of mass m_1*

3.5 Simulation Results with Actuator Dynamics

So far the controller has been analytically designed and tested in simulation without the actuator dynamics. The performance of the controller is satisfactory, however; to implement it in practice the actuator dynamics need to be incorporated in the simulations. The test rig that will be used for hardware-in-the-loop testing has a hydraulic actuator and an MR damper. As a part of hardware-in-the-loop testing, the hydraulic actuator will be used to replicate one degree of freedom in a 2-DOF system. The MR damper will be utilised as a semi-active device and to introduce the active actuator dynamics in the simulation; a second order low-pass filter with the cutoff frequency of 50 Hz is incorporated in the simulation with saturation limits of $\pm$ 250 N. The actuators need to be modelled and tested in the simulation with the controller, before the HIL testing.

The MR damper is a nonlinear device, with hysteresis behaviour. This means that the current output not only depends on the current input and states but also on the history. Different models have been developed for the MR damper with different complexity levels. MR damper models are categorised in two distinct ways. The first categorization is based on the modelling techniques. i.e parametric or non-parametric. In parametric modelling the design is accomplished mathematically whereas is non-parametric modelling, experimental data is used for designing the model. The second categorization is based on the model estimation i.e. Quasi-steady state models or dynamical models. Quasi-steady state model estimates the behaviour only in the steady state whereas the dynamical model estimates the behaviour in both the transient and steady states.

Dynamical models are well suited for control applications. One of the simple models is the Bingham plastic model, which estimates the behaviour in the steady state. Bingham plastic model assumes that the fluid is in post yield phase and does not take into account the pre yield behaviour [137], which is important for dynamical models. Later, the Bouc-Wen model was proposed [53]. In this model, a non-parametric element is added to account for the hysteresis. The visco-elastic plastic model was also proposed for the MR damper, in which nonlinear shape functions determine the pre-yield and

post-yield behaviour. Some models from non-parametric design methodology include Chebyshev polynomials and sixth order polynomials, fitted to the experimental data.

In [138] a general MR model has been presented with a quasi-steady state model in series with two masses and a linear spring. The design approach is general rather than for a particular MR damper. The behaviour of the damper has been thoroughly studied in previous literature; in the present work, the MR damper model presented in [138] is used. Figure 3.12 shows a schematic representation of a unified MR damper model [138] that has been used in our simulations. The corresponding equations for the unified MR damper are given as

$$K_a(x_b - x_a) - \chi_a(\dot{x}_a, I) = m_1\ddot{x}_a \tag{3.43}$$

$$f_{sa} - K_a(x_b - x_a) = m_2\ddot{x}_a \tag{3.44}$$

Here m_a is fluid mass, m_b is piston head mass, K_a is fluid compressibility, χ_a is a quasi-steady damping function, x_a is displacement of m_a, x_b is displacement of m_b, and f_{sa} is the output force. The quasi-steady damping function is defined as

$$\chi_a(\dot{x}_a, I) = \begin{cases} C_{pre}\dot{x}_a & \dot{x}_a \leq \dfrac{F_y}{C_{pre}} \\ C_{post}\dot{x}_a + F_y \text{sgn}(\dot{x}_a) & \dot{x}_a > \dfrac{F_y}{C_{pre}} \end{cases} \tag{3.45}$$

where

$$\begin{aligned} C_{pre} &= 4.1357 + 99.4736\tanh(1.0697I) \\ C_{post} &= -0.6167 + 3.7383\tanh(1.3629I) \\ F_y &= -0.0115 + 1.3063\tanh(1.1946I) \end{aligned} \tag{3.46}$$

All the values in (3.46) are calculated by curve fitting in [138].

The input to this MR damper model is a current signal. For that, the control signal from SMC first needs to be converted to a current signal and then the MR damper

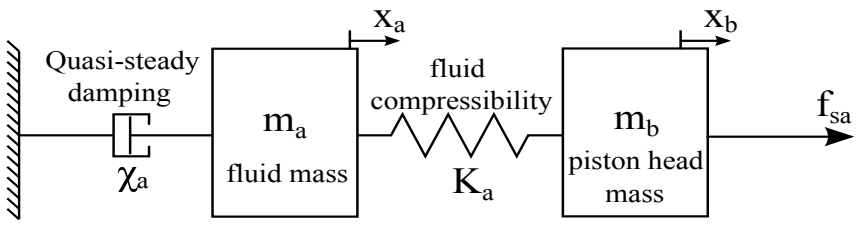

Fig. 3.12 *Schematic representation of the unified MR damper model [138], where m_a is fluid mass, m_b is piston head mass, K_a is fluid compressibility, χ_a is quasi-steady damping function, x_a is displacement of m_a, x_b is displacement of m_b, f_{sa} is the output force*

model will generate the desired control signal. To do that, an inner loop controller design is required that will convert the control signal from SMC to a current signal. A feed-forward controller has been designed to convert the control signal to the current signal. Figure 3.13 shows the current controller. The input of current controller is the relative velocity and the desired force/control signal from the SMC controller.

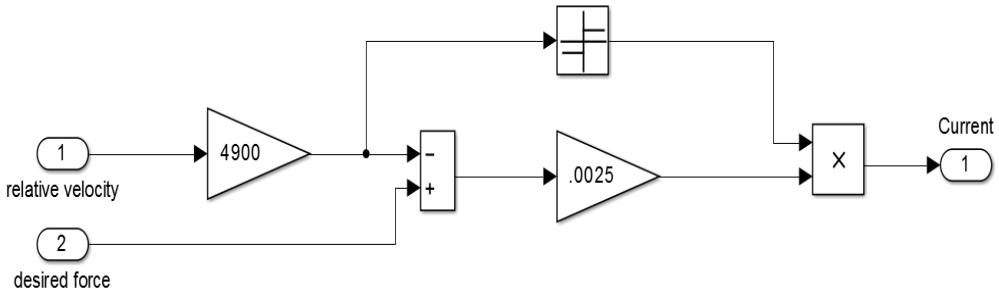

Fig. 3.13 Feed-forward controller to convert the control signal from SMC to a current signal

An Instron PLL25K servo-hydraulic actuator used in the HIL testing system is controlled by Instron 8400 controller. The Instron actuator is driven by two Moog servo values and it converts the hydraulic energy to mechanical energy. A built-in inductive displacement transducer gives the position of the piston as a feedback signal to the controller. The Instron actuator is hysteresis free in cyclic and quasi-static operations up to a nominal value. These type of actuators are used for vibration testing and fatigue testing.

The Simulink models employed in the simulations for the Instron PLL25K servo-hydraulic actuator and Instron 8400 controller are provided by the manufacturer. Figure 3.14 shows the block diagram implementation of the hybrid controller with the actuator dynamics. In this block diagram, the SMC control signal f_{smc} is converted to current

signal I_{MR} by the current controller. The current signal I_{MR} goes into the MR damper model, which eventually generates the control signal f_{sa}. The input to simulated DOF is $f_{i\&i}$, which eventually gives the displacement x_1 as an output. This displacement signal x_1 is the desired or reference signal for Instron controller. The Instron controller generates a control signal based on the error between the desired signal and feedback from the LVDT, which measures the displacement of the hydraulic actuator. This control signal forces the Instron actuator to achieve the desired displacement.

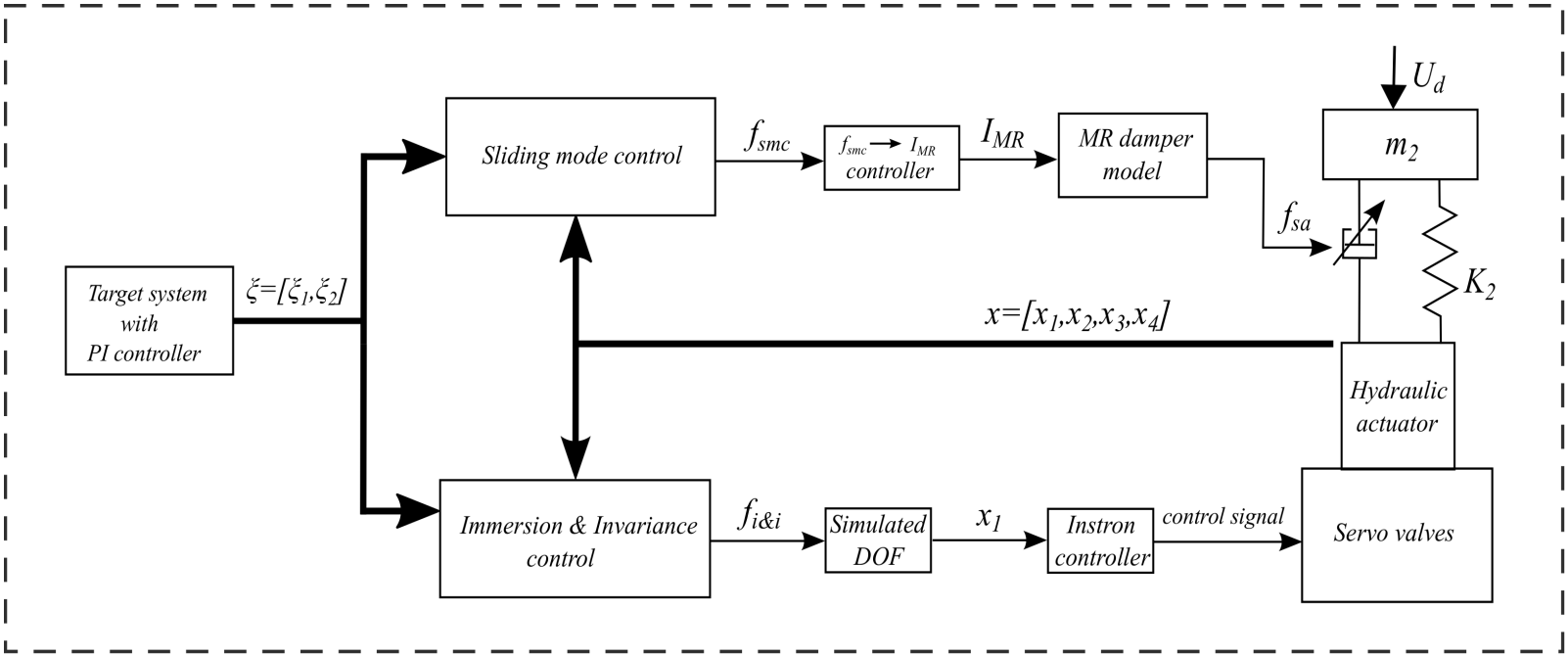

Fig. 3.14 *Block diagram implementation of hybrid active & semi-active control with actuators dynamics, where x_1 and x_2 are the position and velocity of mass m_1 respectively, x_3 and x_4 are the position and velocity of mass m_2 respectively, $f_{i\&i}$ is the I & I control signal, f_a is force of the active actuator, f_{sa} is force of the MR damper, I_{MR} is output of the controller that converts the SMC control signal f_{smc} to the current signal for MR damper*

The same simulations are repeated with a sinusoidal excitation signal at 3 Hz and an amplitude of 100 N at mass m_2. The results are shown in Figures 3.15 and 3.16, which are very close to the simulation results without the actuator dynamics that were shown in the previous section. The error between x_3 and ξ_1 is reduced by 95.8%, as shown in Figure 3.15a. The error between x_1 and ξ_1 with the actuator dynamics is reduced by 98% as shown in Figure 3.16a. There are two active control signals shown in Figure 3.17a. One is the output of the I & I controller, which goes into the second order low pass filter and the second one is the output of the low pass filter. The filter is adding a delay and saturation limits to the signal. The semi-active control signals shown in Figure 3.17b, are the output of the SMC controller and the MR damper. In the first two seconds when the controller is in the off state, the MR damper is acting as a passive damper and the output can be seen in Figure 3.17b.

The convergence of off-the manifold dynamics to the manifold when the controller is switched-on is shown in Figure 3.18a during the transient phase and the steady state phase is shown in Figure 3.18b. The error dynamics convergence is shown in Figure 3.19, both in the transient and steady state phase.

So far it was assumed that the excitation signal is known and the same excitation signal is given to the target system. Now to take it one step further, the same excitation is considered as unknown, so in this case the target system is not given any excitation as it is unknown. The simulation results are shown in Figure 3.20. It can be seen that the performance is satisfactory, hence the controller is robust against unknown excitation signal or disturbance. Figure 3.21 shows the active and semi-active control signals for unknown excitation case.

Finally, the last test was conducted, where the excitation signal is again considered unknown but random instead of sinusoidal. The results are shown in Figures 3.22 and the performance of the controller is impressive. This demonstrated that whether the excitation is sinusoidal or random, known or unknown, in all the cases the controller is performing very well, which is desirable in practice.

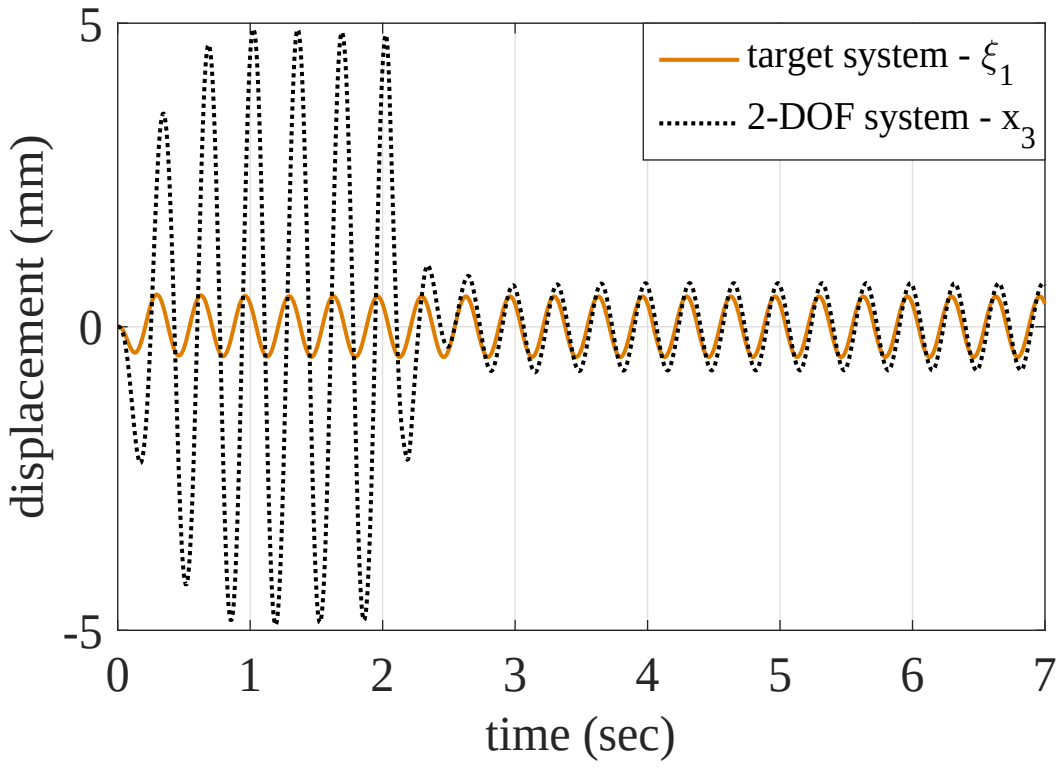

(a)

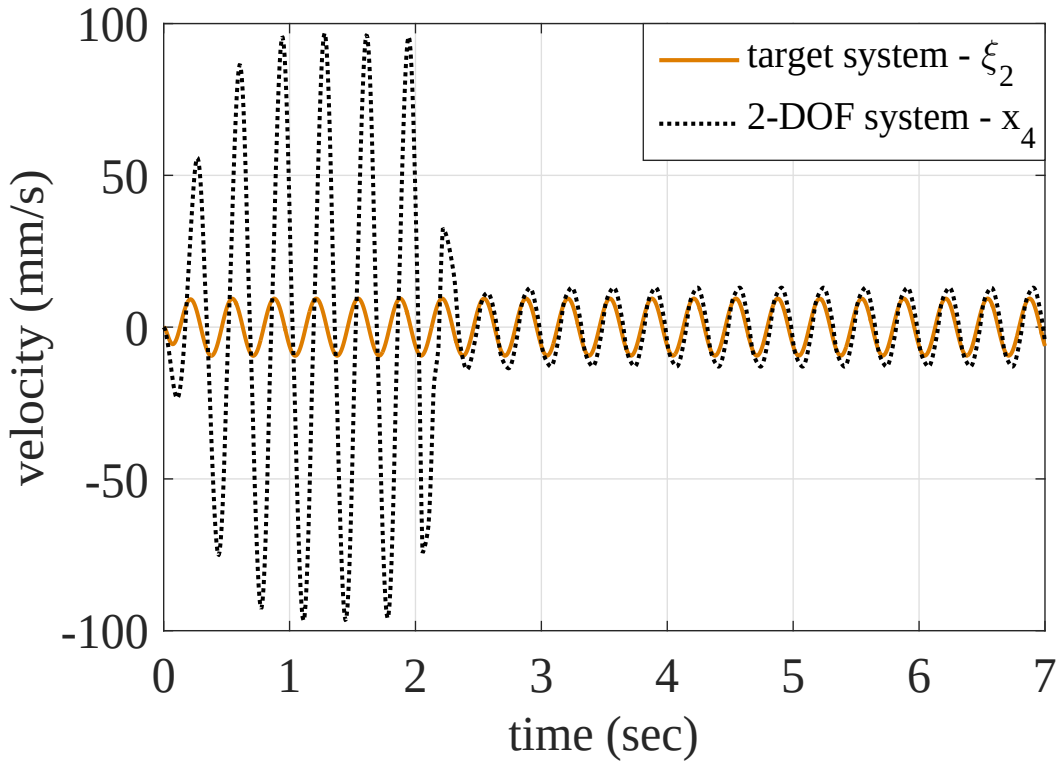

(b)

Fig. 3.15 *Displacement and velocity of mass m_2 controlled to follow the reference system with the hybrid active & semi-active controller with actuators dynamics. The hybrid controller is switched on at time 2 seconds, (a) displacement, (b) velocity*

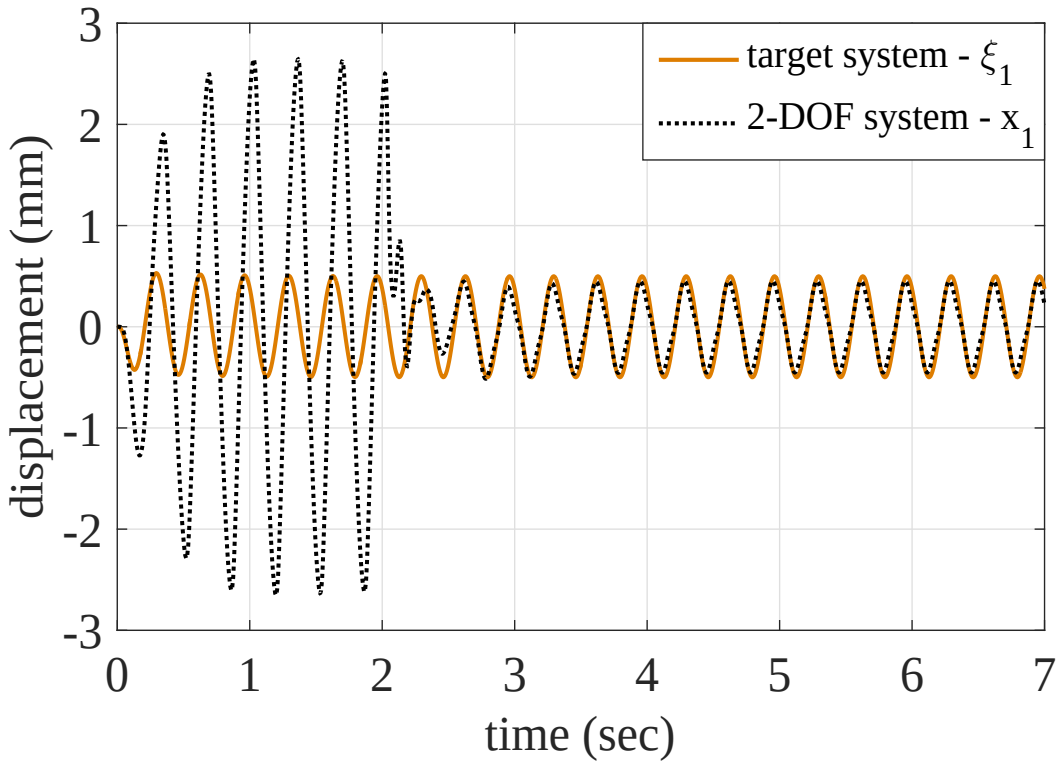

(a)

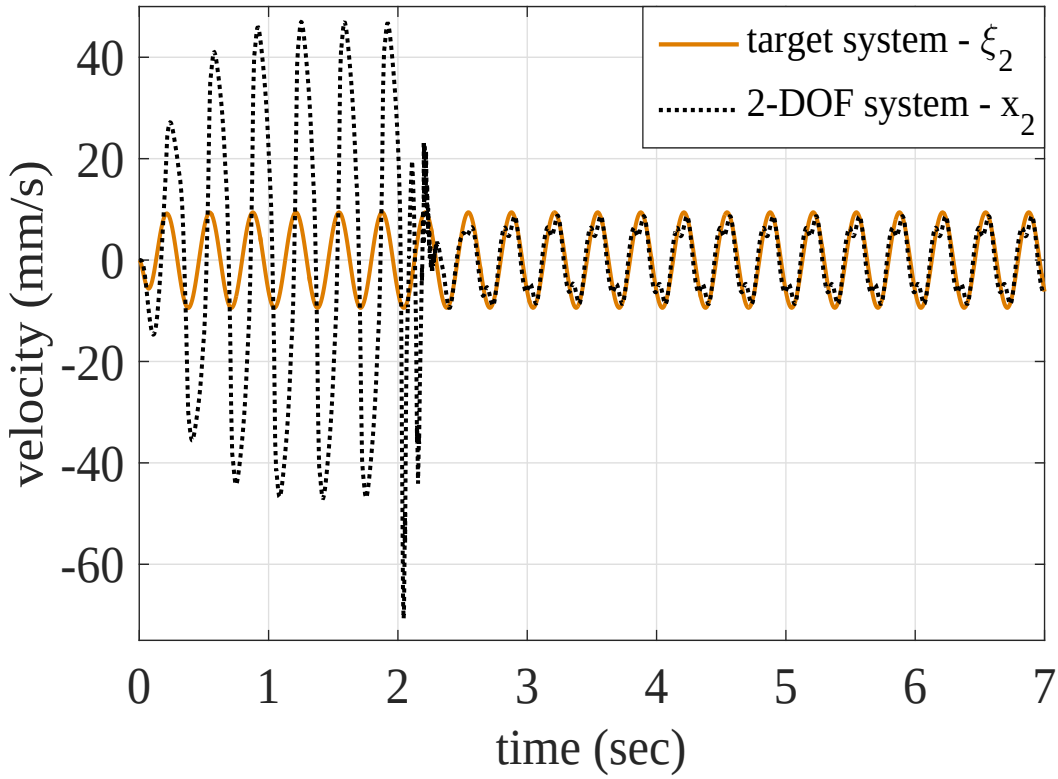

(b)

Fig. 3.16 *Displacement and velocity of mass m_1 controlled to follow the reference system with the hybrid active & semi-active controller with actuators dynamics. The hybrid controller is switched on at time 2 seconds, (a) displacement, (b) velocity*

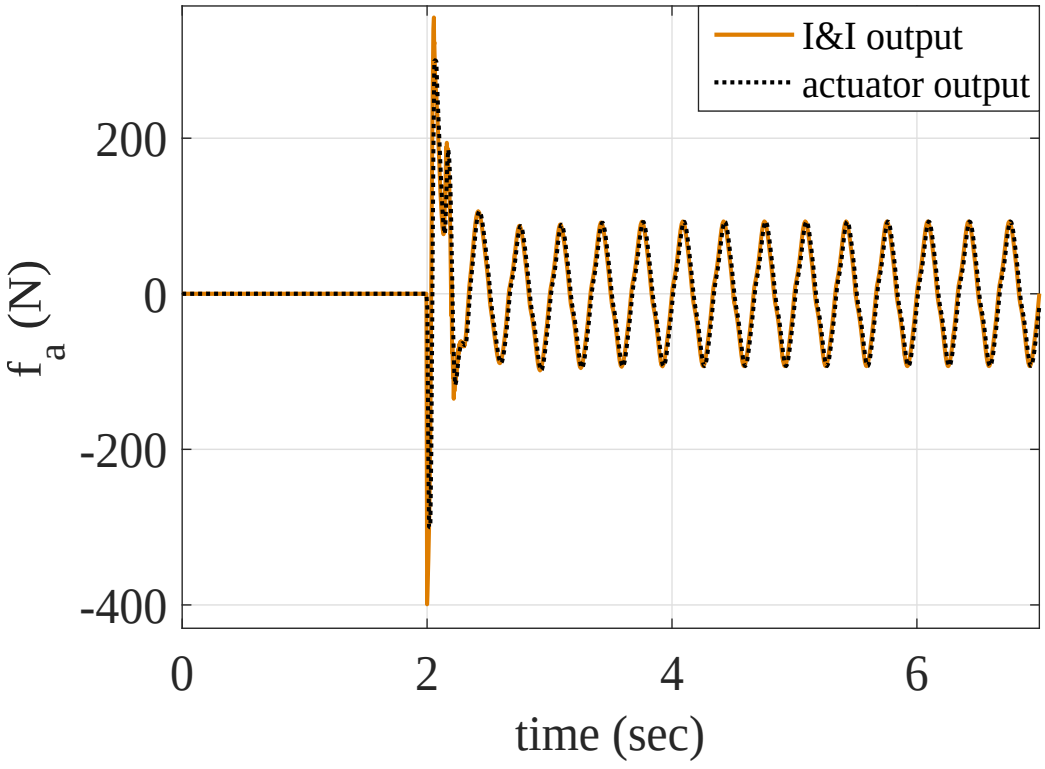

(a)

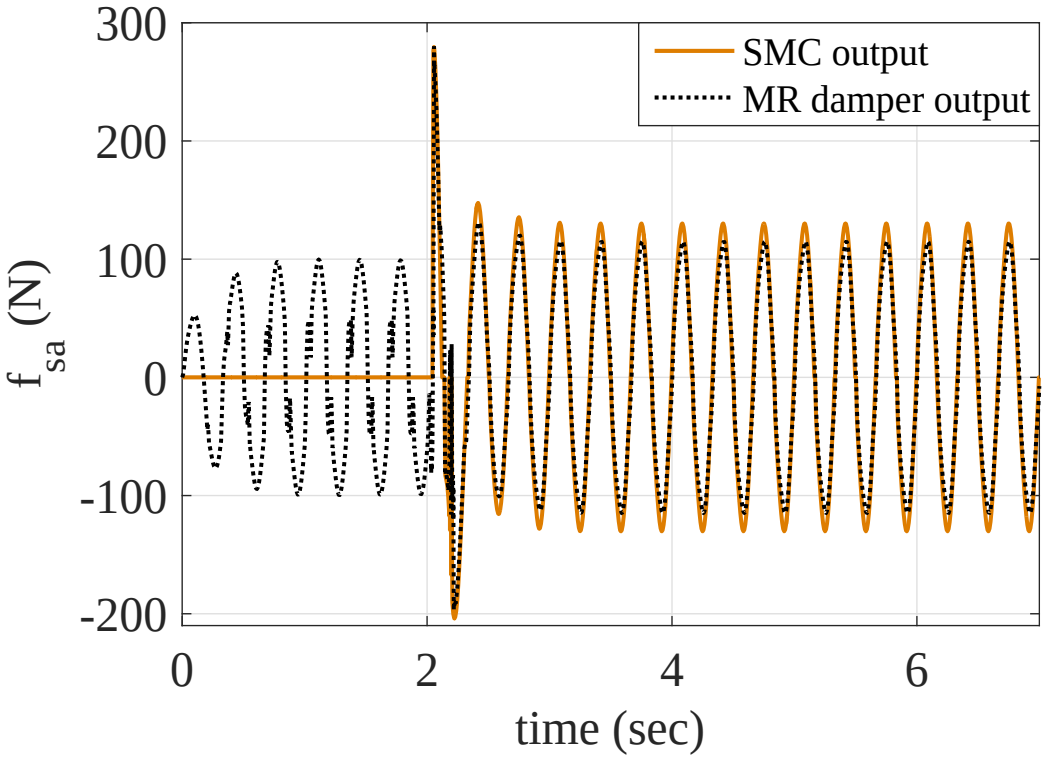

(b)

Fig. 3.17 *Control signals in hybrid active & semi-active controllers with actuators dynamics. The hybrid controller is switched on at time 2 seconds, (a) active control signal, (b) semi-active control signal*

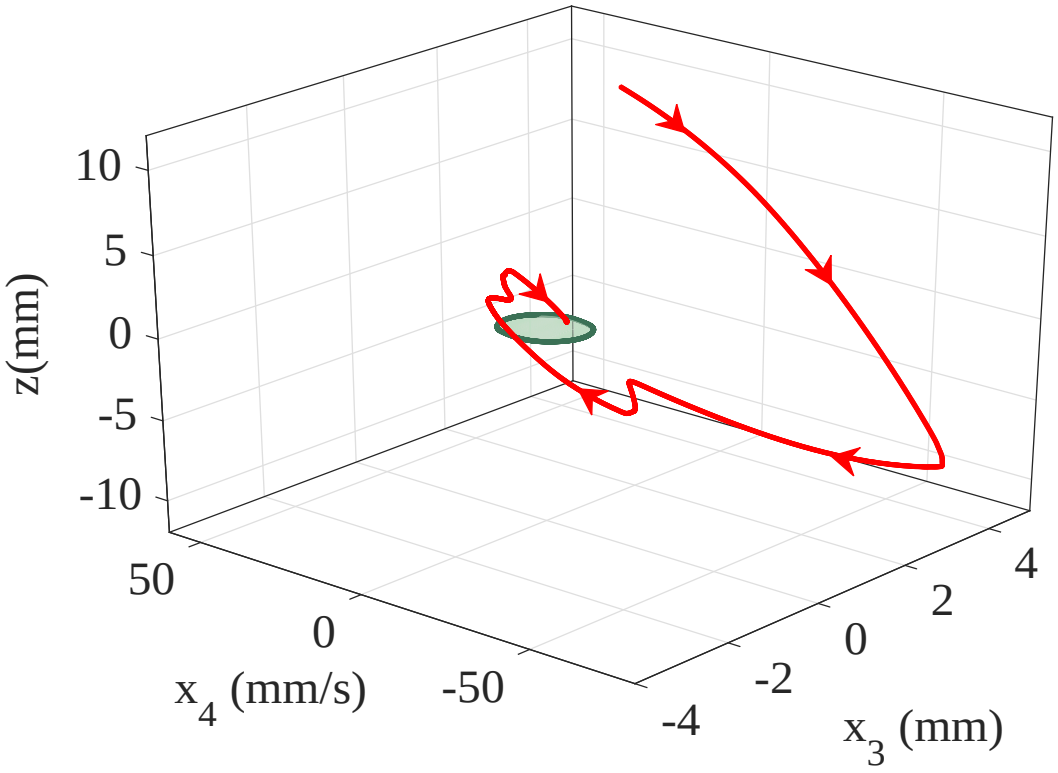

(a)

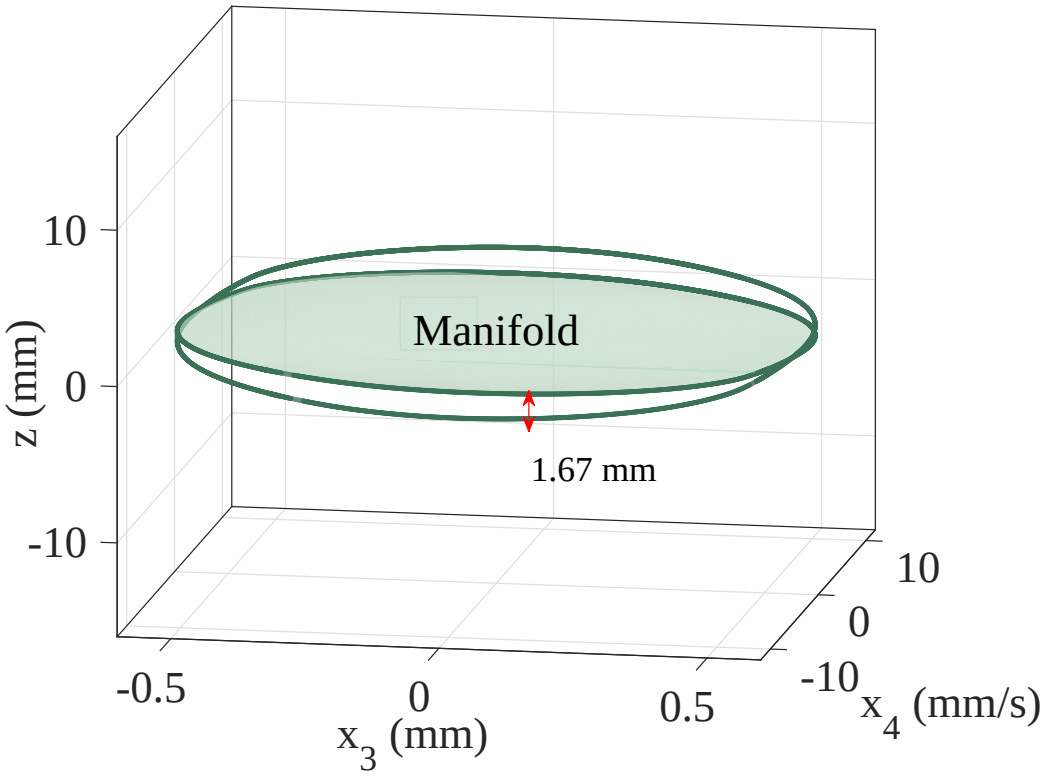

(b)

Fig. 3.18 *Manifold with off-the-manifold dynamics (a) transient phase, (b) steady state phase*

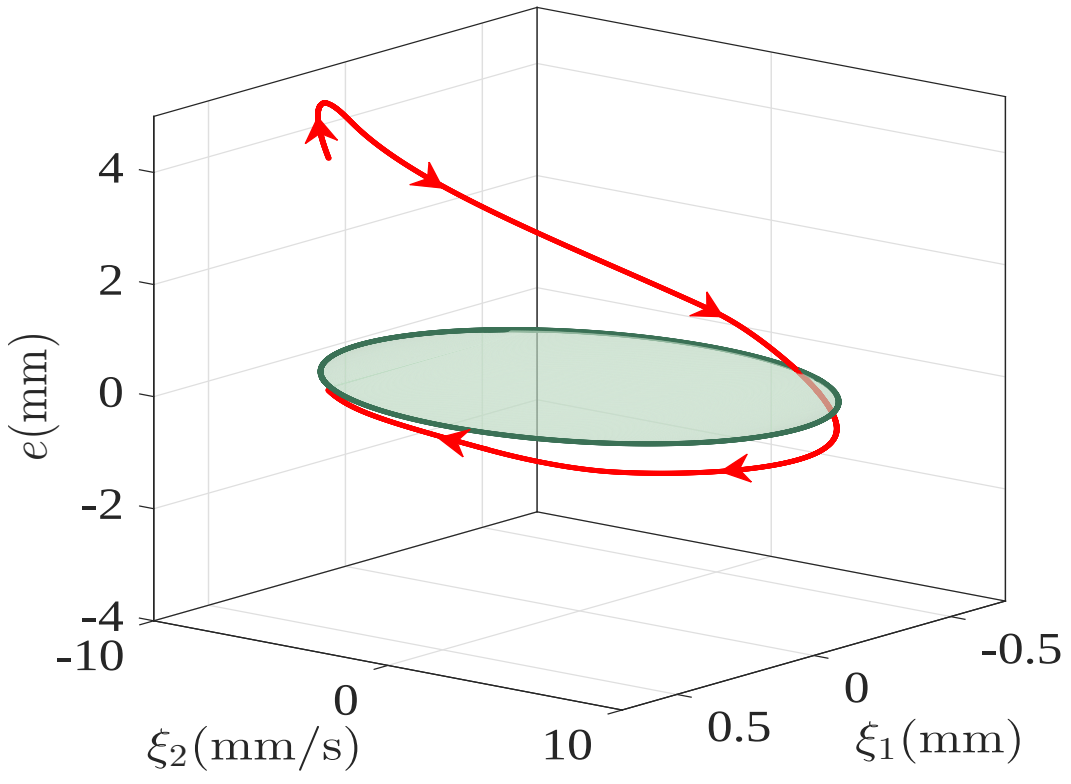

(a)

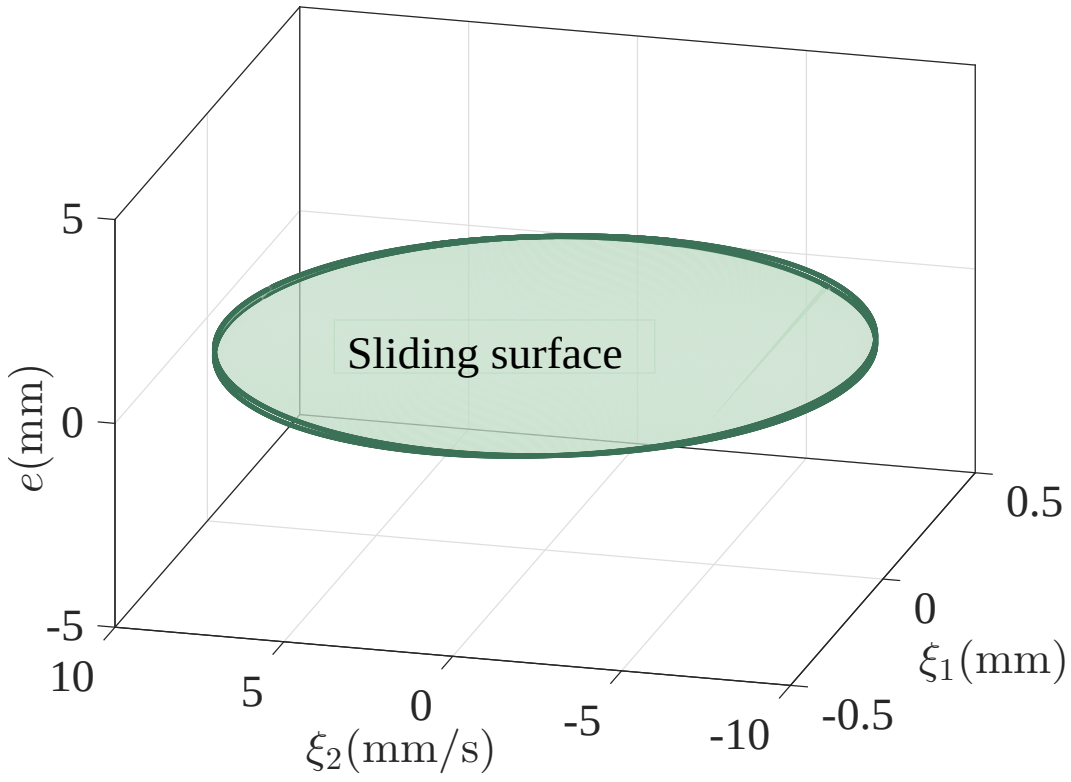

(b)

Fig. 3.19 *Sliding surface with error dynamics (a) transient phase, (b) steady state phase*

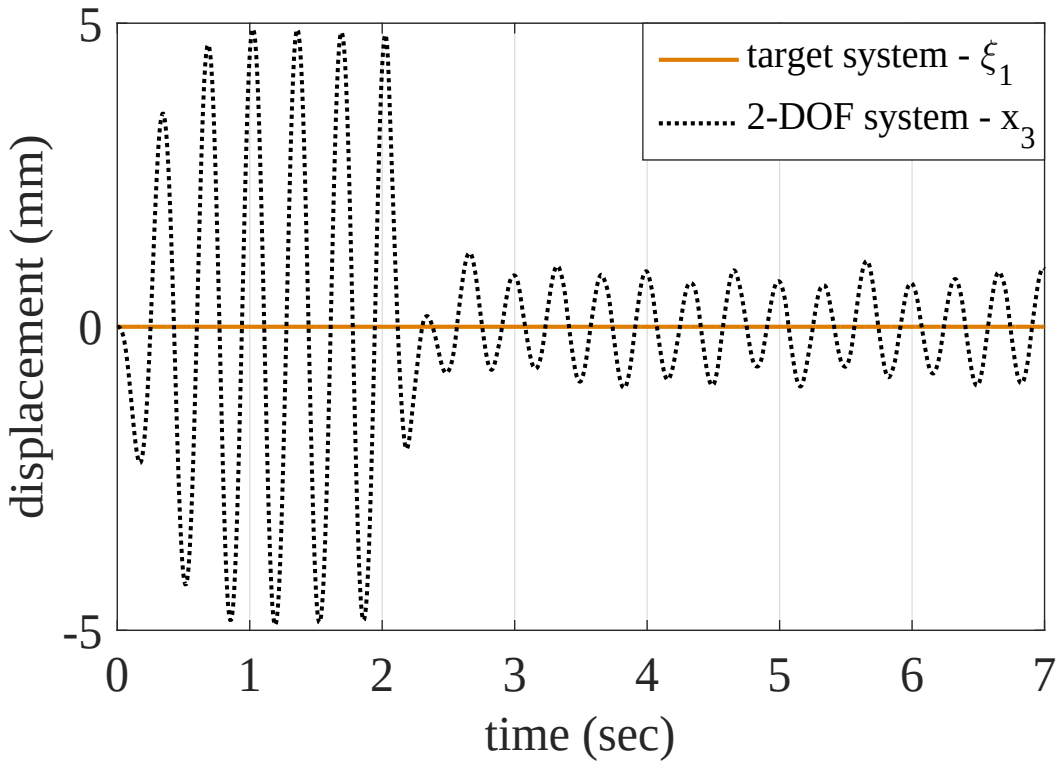

(a)

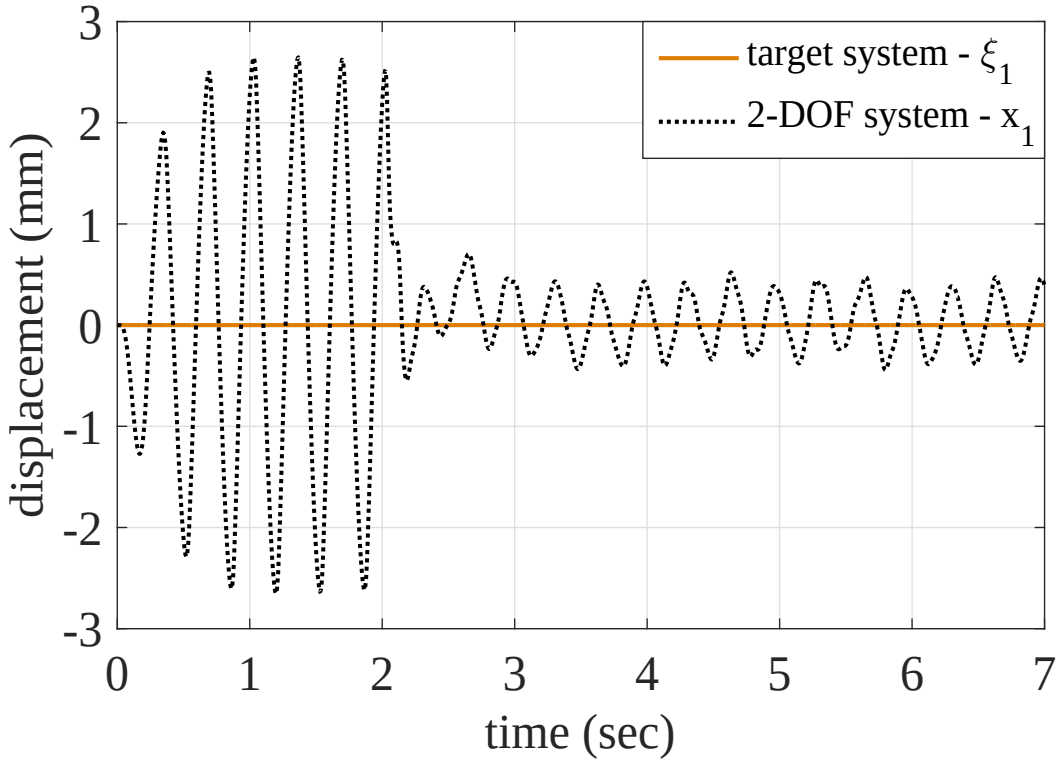

(b)

Fig. 3.20 *Displacement of mass m_1 & m_2, controlled to follow the reference system with the hybrid active & semi-active controller with actuators dynamics and unknown excitation signal. The hybrid controller is switched on at time 2 seconds, (a) displacement of mass m_2, (b) displacement of mass m_1*

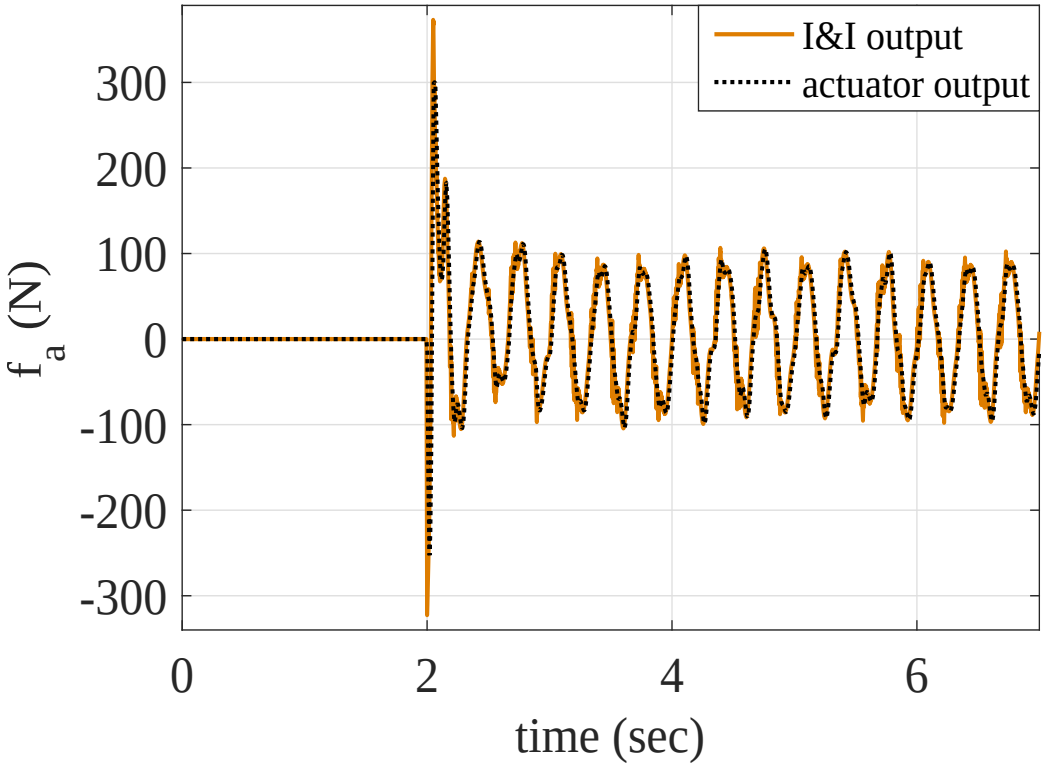

(a)

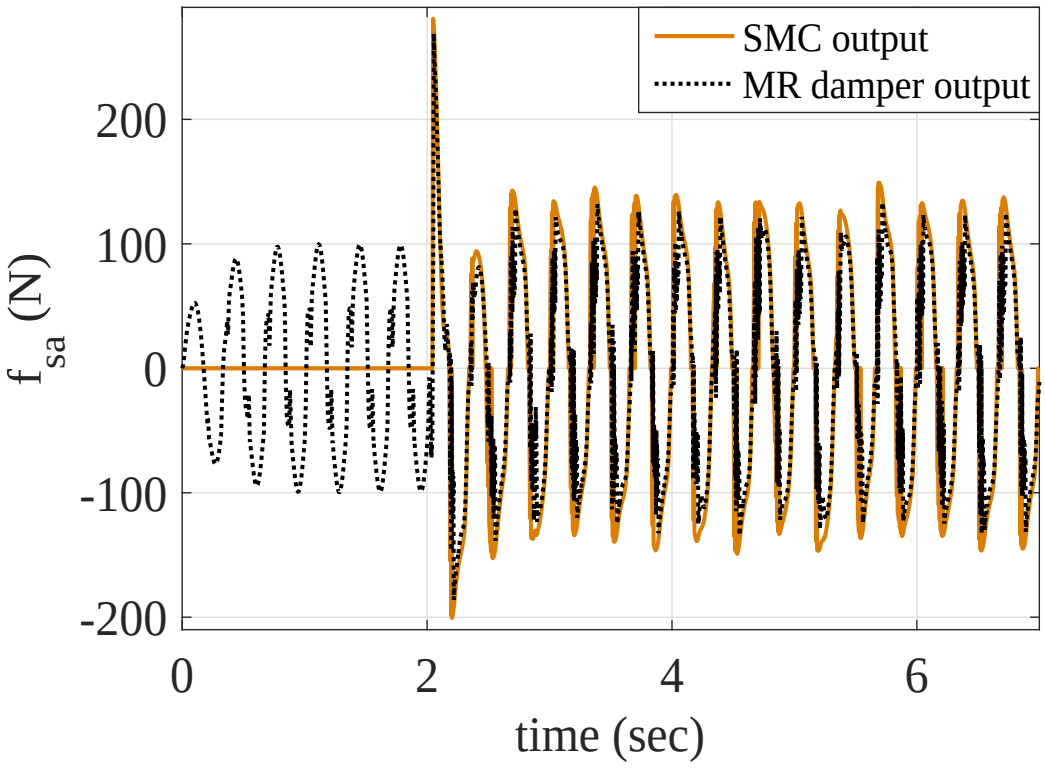

(b)

Fig. 3.21 *Control signals in hybrid active & semi-active controllers with actuators dynamics. The hybrid controller is switched on at time 2 seconds, (a) active control signal, (b) semi-active control signal*

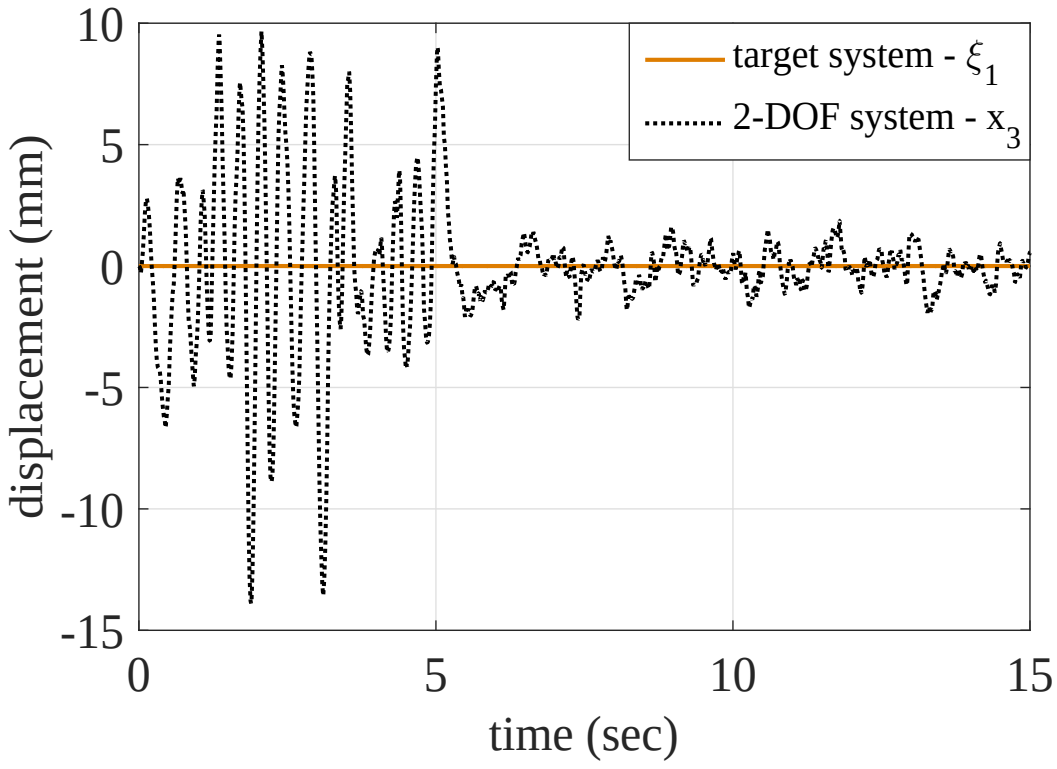

(a)

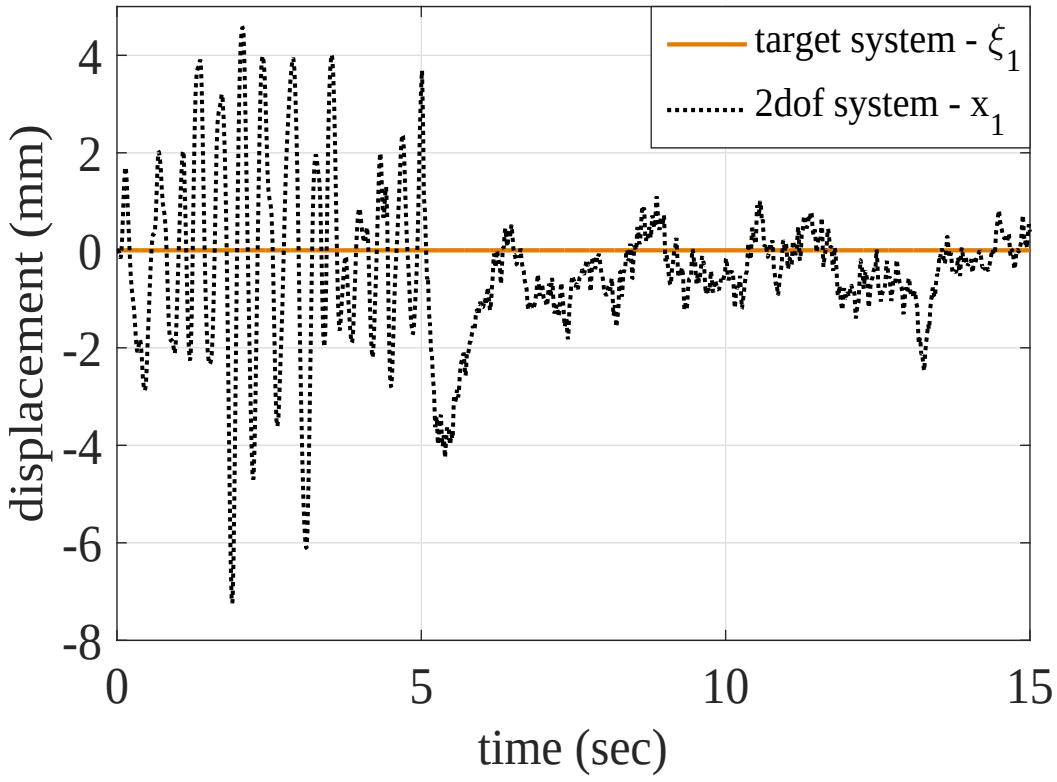

(b)

Fig. 3.22 *Displacement of mass m_1 & m_2, controlled to follow the reference system with the hybrid active & semi-active controller with actuators dynamics and random excitation signal. The hybrid controller is switched on at time 2 seconds, (a) displacement of mass m_2, (b) displacement of mass m_1*

3.6 Discussion

Semi-active devices have been used for the past few decades for vibration control in different applications. There are a lot of advantages to semi-active devices, and some of them are; they have smaller size, have less power consumption and are passive fail-safe, etc. The only disadvantage of this device is that it can only dissipate energy, and that is because of the passivity constraint. So the technique proposed in this Chapter is focused on the question of how can the capabilities of a semi-active device be further enhanced with the help of another active actuator. The hybrid active and semi-active controller is designed in a way that an active actuator, placed somewhere else in the structure, can assist the semi-active device when the energy is required to be injected into the system. Then the whole system behaves as close to the fully active system as possible.

After the analytical design of the controller, in which the I & I is used for designing the controller for the active actuator and the SMC is used to create the controller for the semi-active device, the simulations are performed without actuator dynamics to check the controller performance. The simulation results have shown promising results. It can be seen in Figure 3.7a, that when the proposed hybrid active & semi-active controller is turned on at 2 seconds, the error between x_3 and ξ_1 is reduced by 98.6%. The error between x_1 and ξ_1 is reduced by 95% as shown in Figure 3.8a . After that, the next step was to do HIL testing and check that whether the controller will perform the same way. To do this, some further simulations are required that will include the actuator dynamics as well, which is a significant step because this will bring different constraints in the simulation, to replicate the actual system as closely as possible. Again It can be seen in Figure 3.15a, the error with the actuator dynamics between x_3 and ξ_1 is reduced by 95.8%. The error between x_1 and ξ_1 with the actuator dynamics is reduced by 98% as shown in Figure 3.16a.

Details of the MR damper and hydraulic actuator models used for the simulation have not been provided because that work has been done previously and has already been explained in greater detail in the references provided. The focus of this work is in controller design and its performance. Now one thing that needs to be kept in

mind is that the same goals i.e. an active actuator assisting a semi-active device can be achieved with different control strategies. The reason why these particular control design techniques are chosen is because a robust controller was required to damp the vibrations and they share the same design approach, and we can define a common target system for both the controllers.

3.7 Summary

A new robust hybrid active & semi-active control technique has been introduced in which an active actuator is assisting the semi-active device to achieve the performance close to a fully active system. The I & I and SMC methodologies have been used for controller design, as both the design methods share the same design approach. The I & I has been used to design the controller for active actuator and the SMC is used to design the controller for the semi-active device. After the analytical design of the controller, it has been validated in the simulation without the actuator dynamics. To implement the controller in practice, the actuator dynamics need to be first incorporated into the simulation. For that purpose, the unified MR damper model [138] has been used along with the current controller which converts the SMC control signal to current control signal.

The ultimate goal is to perform the HIL testing, in which one DOF will be simulated and represented by the hydraulic actuator. The hydraulic actuator model provided by the manufacturer has been used in the simulation and is controlled by an Instron controller. The model of the Instron controller utilised in the simulation is also provided by the manufacturer. After making all these changes, the simulations were run again, and the results were very close to the one without the actuator dynamics. Now the controller is ready for HIL testing. In the next Chapter, the experimental setup is described in detail. Later the HIL implementation of the controller is validated.

Chapter 4

Hybrid Controller – Validation Using Experimental Analysis

4.1 Experimental Setup

In this Chapter, the experimental setup is explained in detail. The overview of the complete experimental setup is shown in Figure 4.1. The Simulink file is transferred from host PC to xPC target through LAN. The data are sent in and out in real time from xPC target through an N.I. DAC card. The current control signal I_{MR}, first goes to the Kepco amplifier and then to the MR damper. The displacement of mass m_1 goes from interface board to the Instron 8400 controller. This displacement signal x_1 is the desired or reference signal for Instron controller. The Instron controller then generates a control signal based on the error between the desired signal and feedback from the LVDT, which measures the displacement of the hydraulic actuator. This control signal forces the Instron actuator to achieve the desired displacement. The accelerometer feedback signal goes to the xPC target through an amplifier.

The load cell gives the combined force of spring and damper that is sent to the xPC target. The laser displacement sensor is used to measure the displacement of the mass m_2. The excitation signal is generated by rotating unbalanced masses with a brushless DC motor, whose speed is controlled through a separate motor speed controller.

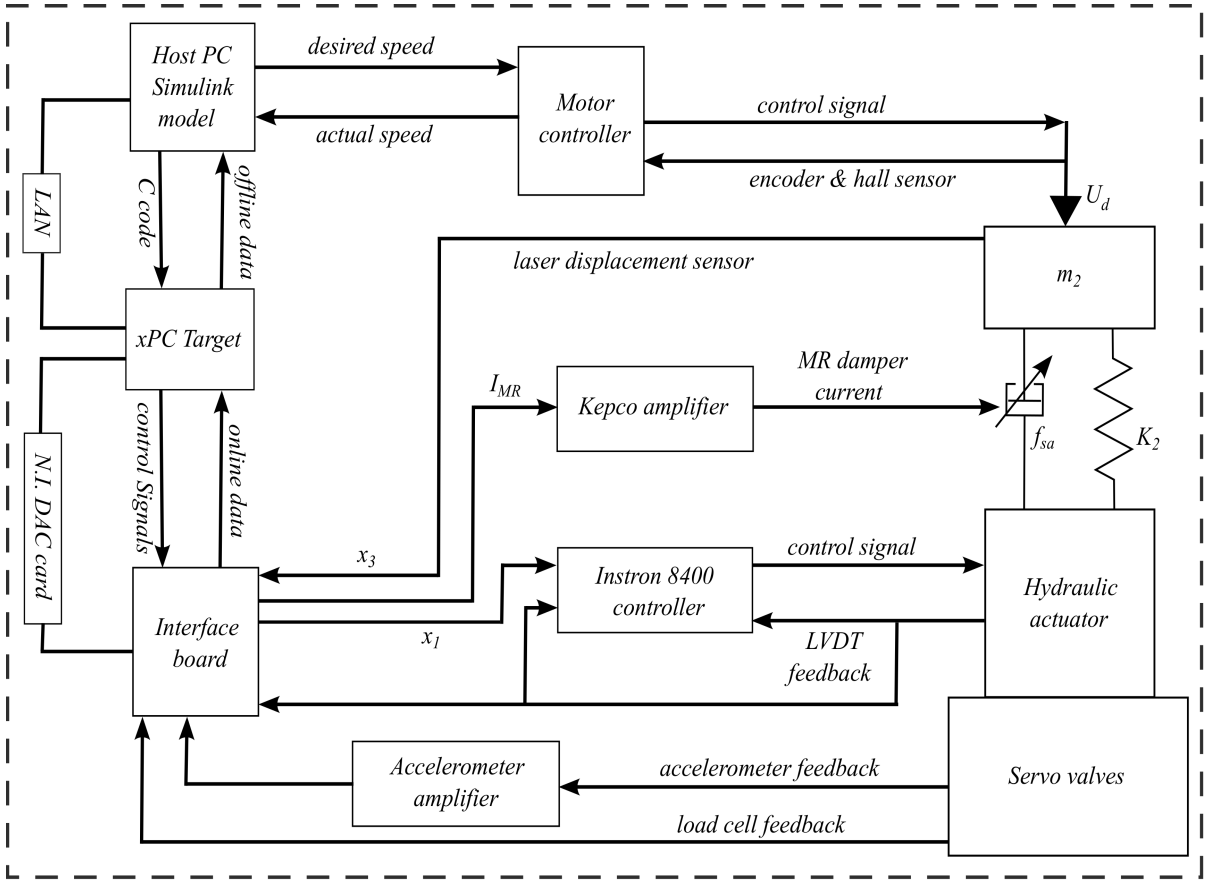

Fig. 4.1 *Experimental setup, where the Simulink file is transferred from host PC to xPC target through LAN. The data is sent in and out in real time from the xPC target through an N.I. DAC card, I_{MR} is the current control signal that first goes to the Kepco amplifier and then to the MR damper, x_1 is the displacement of mass m_1 which goes to the Instron 8400 controller. The accelerometer feedback signal goes to the xPC target through an amplifier. The load cell that gives the combined force of spring and damper that is sent to the xPC target. Laser displacement sensor is used to measure the displacement of the mass m_2. The excitation signal is generated by rotating unbalanced masses with a brush-less DC motor, whose speed is controlled through a separate motor speed controller*

The semi-active device is an MR damper, manufactured by Lord Corporation. Lord Corporation manufactures two types of MR dampers, LORD RD-8040-1 and LORD RD-8041-1. LORD RD-8040-1 is the short stroke damper, and the LORD RD-8041-1 is the long stroke damper. The MR damper used in the experimental setup is LORD RD-8040-1 shown in Figure 4.2 along with the linear spring. The damping can be continuously changed by changing the yield strength of the MR fluid via the magnetic field. The response time of both the dampers is less than 15 ms. The LORD dampers are monotube shocks with high-pressure nitrogen gas at 300 psi. The maximum input current for continuous 30 sec is 1 A. At irregular intervals it can also sustain a maximum of 2 A. The input voltage is 12 V DC. Other specifications of LORD RD-8040-1 are given in Table 4.1 [10]. The maximum nominal damper stroke is set to 27.5 mm. The spring nominal compression, because of 112 kg mass, is 15 mm.

Fig. 4.2 LORD RD-8040-1 MR damper along with the linear spring

An Instron PLL25K servo-hydraulic actuator, shown in Figure 4.3 is used in the HIL testing system and is controlled by Instron 8400 controller. The actuator is driven by an electrical pump along with two Moog servo valves, and it converts the hydraulic

[10]http://www.lordmrstore.com/_literature_192929/Data_Sheet_DS_RD-8040-1_and_RD-8041-1

Table 4.1 LORD RD-8040-1 specifications

Properties	LORD RD-8040-1 MR damper
Stroke (mm)	55
Extended Length (mm)	208
Body Diameter (mm)	42.1
Shaft Diameter (mm)	10
Tensile Strength (N)	8896
Damper Forces (N) peak to peak 5 cm / sec @ 1 A 20 cm / sec @ 0 A	 2447 667
Operating Temperature (C)	71

energy to mechanical energy. A built-in inductive displacement transducer gives the position of the piston as a feedback signal to the controller. The actuator is hysteresis free in cyclic and quasi-static operations up to a nominal value. These type of actuators are typically used for vibration testing and fatigue testing. The specifications of Instron PLL25K servo-hydraulic actuator are given in Table 4.2 [11].

Fig. 4.3 Instron PLL25K servo-hydraulic actuator

[11] http://www.instron.com

Table 4.2 Instron PLL25K servo-hydraulic actuator specifications

Properties	Instron PLL25K servo-hydraulic actuator
Force (kN)	± 25
Displacement (mm)	± 50
Velocity (m/s)	± 01

The Labtronics Instron 8400 is a digital servo-hydraulic controller shown in Figure 4.4, which is used in the experimental setup to control the servo-hydraulic actuator. It is a standalone single axis controller with its display. It has an alpha numeric keypad and special function keys for user-friendly operations. It has two DSP processors, one for loop closure and the other for signal conditioning. There are two control modes; one is with position feedback and the other with load feedback. The control loop is a digital PID (Proportional, Integral, Differential) with a feed forward gain (PIDF). A programmable lag term is also available to deal with the resonance.

It can also be used as a function generator to generate signals like sine, triangle, square, ramp, etc. as a reference signal and can also accept external signals such as a reference or command signal. It has four digital inputs and four digital output to communicate with other devices. Programmable peak detectors are used to read maximum and minimum peaks, programmable limit detectors are used to check the limits on each transducer signals, two cycle counter are used to count cycles and five programmable event detectors to detect different conditions.

Fig. 4.4 Instron 8400 controller

The reference current generated from the Matlab/Simulink does not have enough power to drive the MR damper. A Kepco BOP 20-5M amplifier shown in Figure 4.5, is

used to amplify the current signal which is then given to the MR damper. The Kepco BOP 20-5M operates in all four quadrants of the voltage-current axes and because of that its output as current or voltage can be controlled smoothly and linearly over the entire range. The BOP 20-5M can function both as a source and a sink. It has high power bipolar operational amplifiers, so its frequency bandwidth is much higher than the standard power supply. To check the full potential of BOP 20-5M, the load should be resistive. In the case of inductive load, it must be slowed down to avoid oscillations.

The Matlab/Simulink is installed in host PC. The controller is designed in Simulink, and real-time implementation is done through xPC target. The host PC is connected to the target PC through LAN. The target PC has a National Instrument PCI-MIO-16XE-10 data acquisition card and a RAM of 128 Mb. A C compiler is used to download the Simulink model as a C programme in the target PC. The interface board is connected to the target PC and has 8 A/D channels and 2 D/A channels for the real-time interface. The data is stored on the target PC RAM and is then transferred to a host PC after the test for further analysis.

Fig. 4.5 Kepco BOP 20-5M amplifier

4.2 Experimental Results

For the experimental results, in the first five seconds the system is vibrating in open-loop after which the controller is switched-on. Before showing the results of the hybrid controller, Figure 4.6, is comparing the displacement of the simulated DOF with the LVDT feedback from the hydraulic actuator. It is clearly evident that the simulated DOF is represented in the HIL testing by the hydraulic actuator. Figure 4.7 shows the displacement and velocity of mass m_2 being controlled to follow the reference system

in which a single mass, $m_1 + m_2$, is assumed. It can be seen that the simulated system followed the reference system more closely than the experimental results.

The reason is that in simulation, the excitation signal was a perfect sine wave at 2.8 Hz with a known phase. In the experimental test, the excitation signal was generated by a rotating unbalanced masses with a brush-less DC motor, whose speed is controlled through a separate motor speed controller. The speed controller keeps the speed of the motor close to the desired speed but there is a small variation in the speed, so its not a perfect single frequency sine wave, and the phase is also unknown. Despite these issues, the results are very good which suggests that the behavior is sufficiently robust to the uncertainties in the experimental excitation signal. Figure 4.8 shows the displacement and velocity of mass m_1. Again, the results are satisfactory. Then the control signals are shown in Figure 4.9. As the controller is switched-on at 5 seconds, both active and semi-active control signals go to their maximum value to bring off-the-manifold dynamics and error dynamics to the manifold and sliding surface respectively. The same phenomenon was observed in the simulation results.

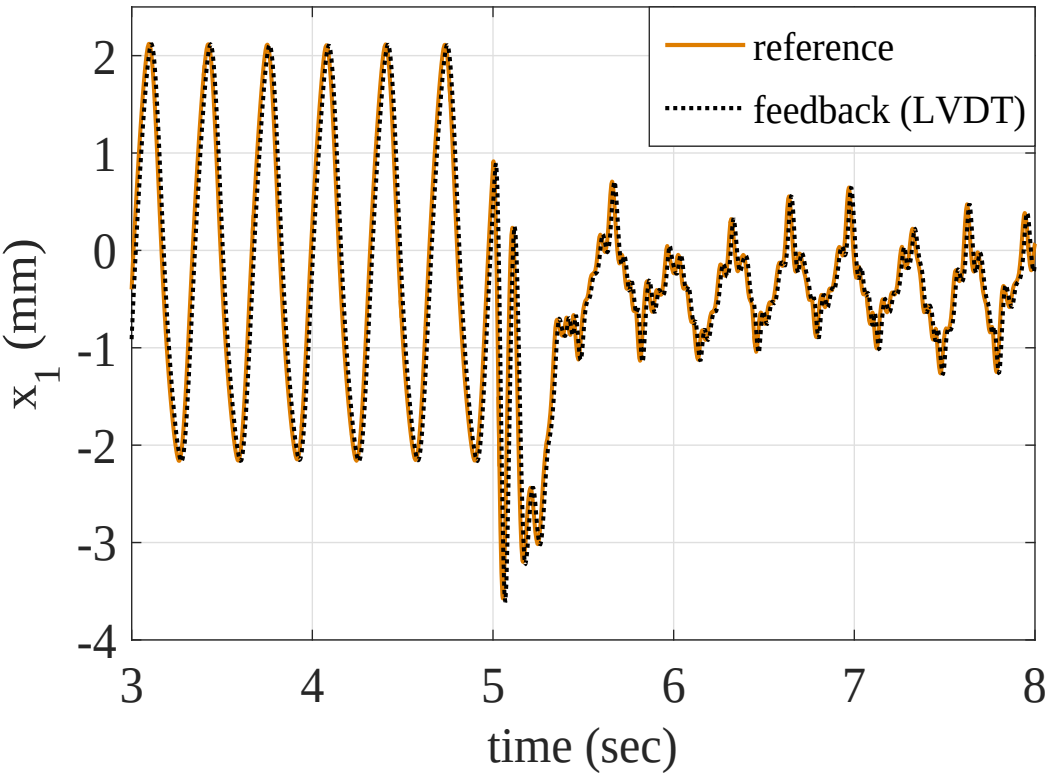

Fig. 4.6 *Comparing the simulated DOF displacement with the hydraulic actuator displacement from LVDT. The hybrid controller is switched on at time 5 seconds*

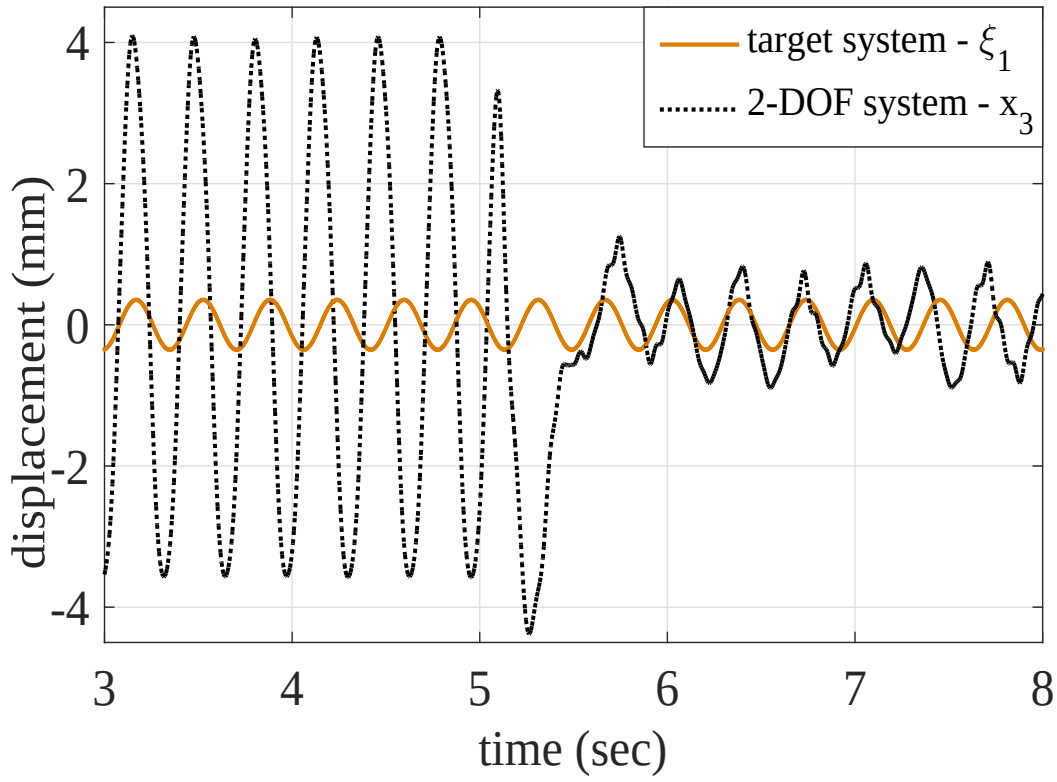

(a)

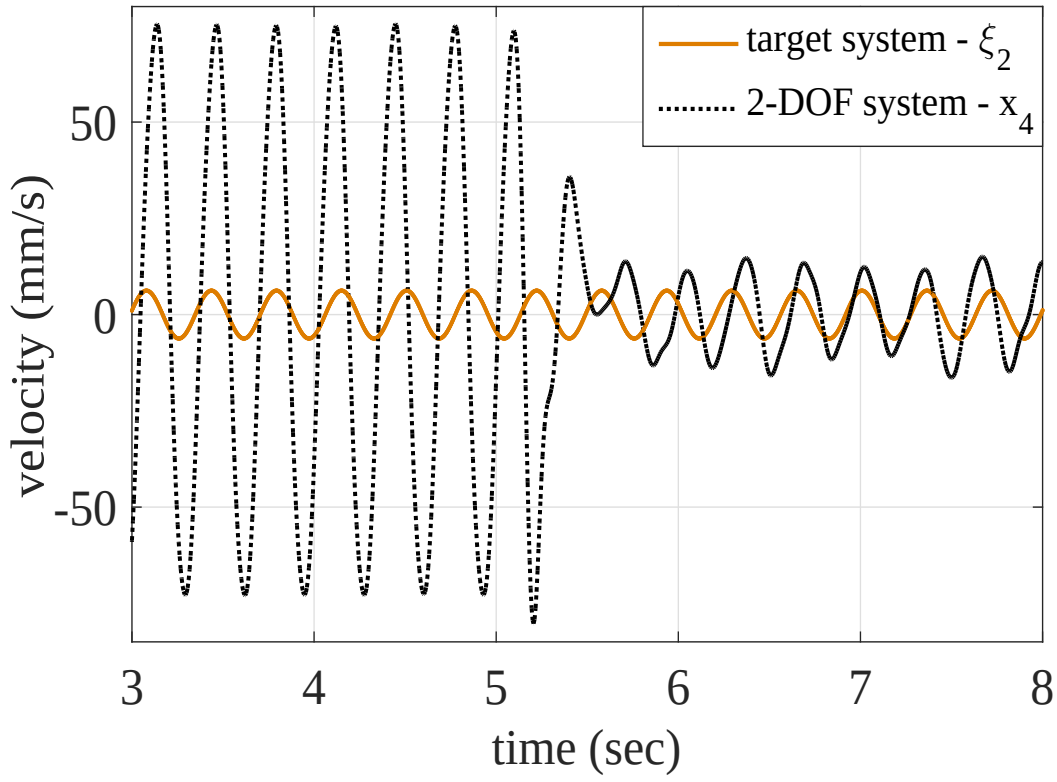

(b)

Fig. 4.7 *Displacement and velocity of mass m_2 controlled to follow the reference system with the hybrid active & semi-active controller. The hybrid controller is switched on at time 5 seconds, (a) displacement, (b) velocity*

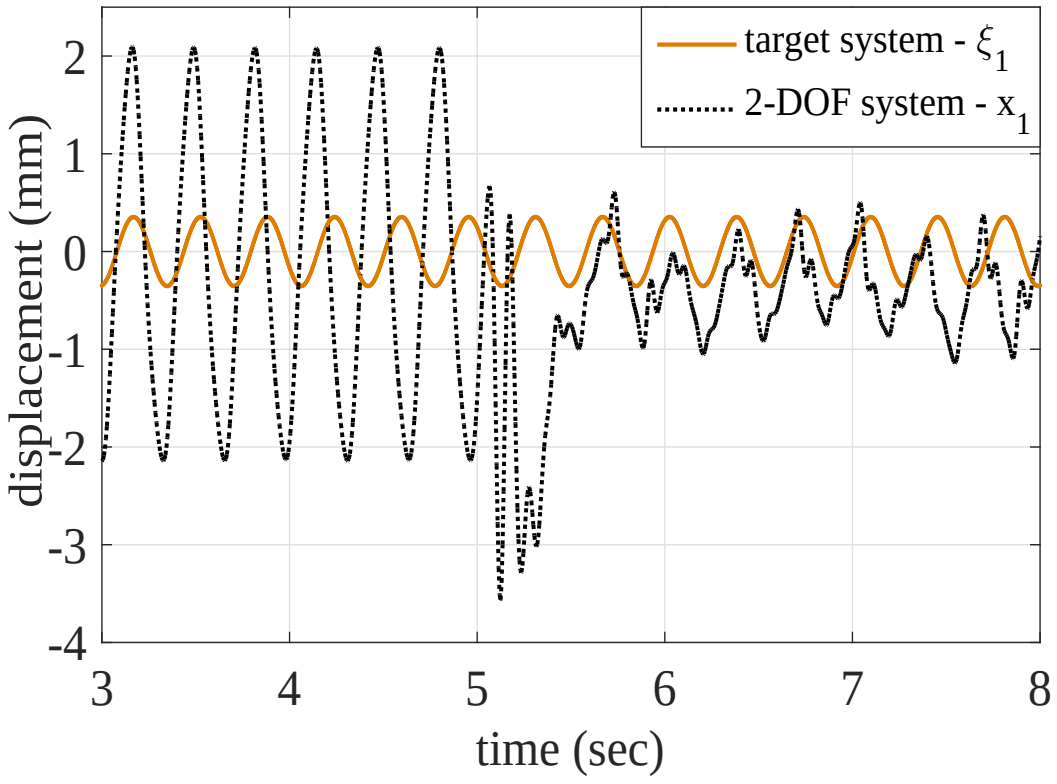

(a)

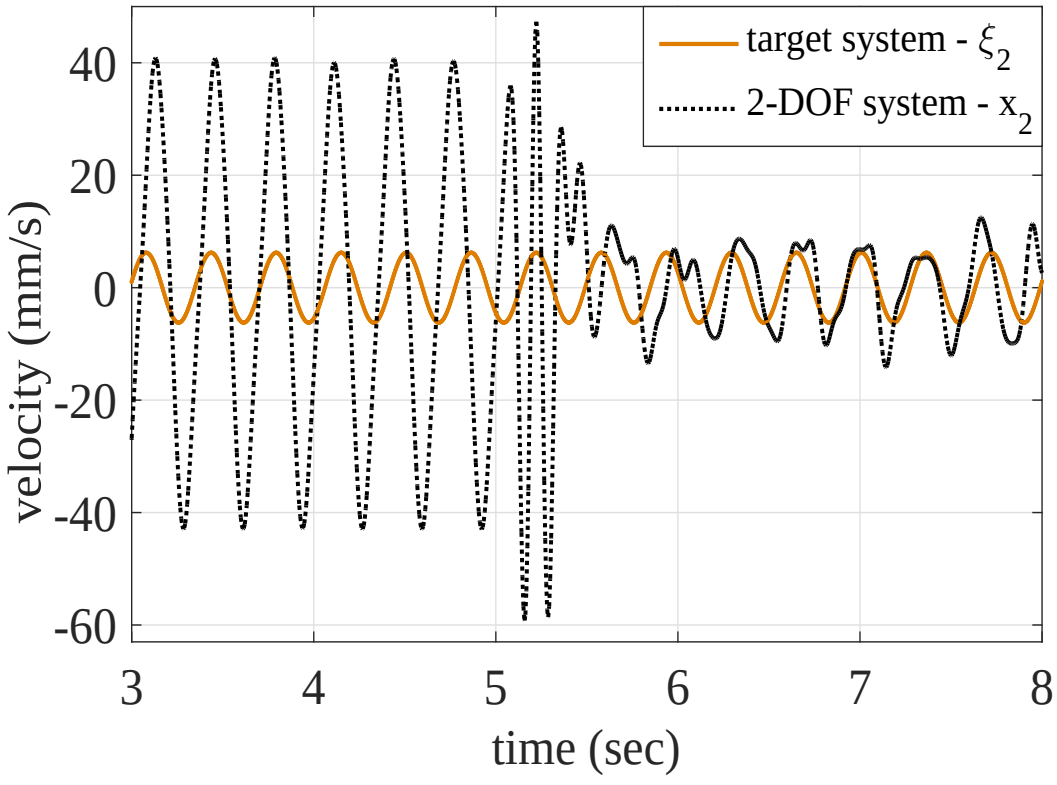

(b)

Fig. 4.8 *Displacement and velocity of mass m_1 controlled to follow the reference system with the hybrid active & semi-active controller. The hybrid controller is switched on at time 5 seconds, (a) displacement, (b) velocity*

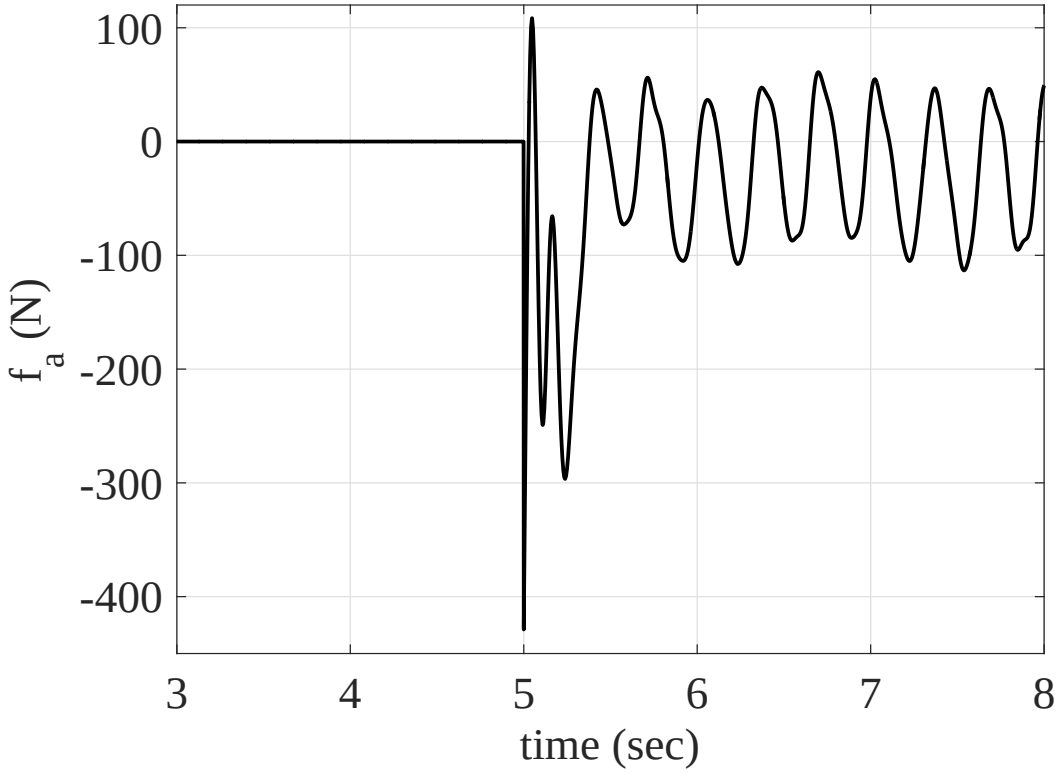

(a)

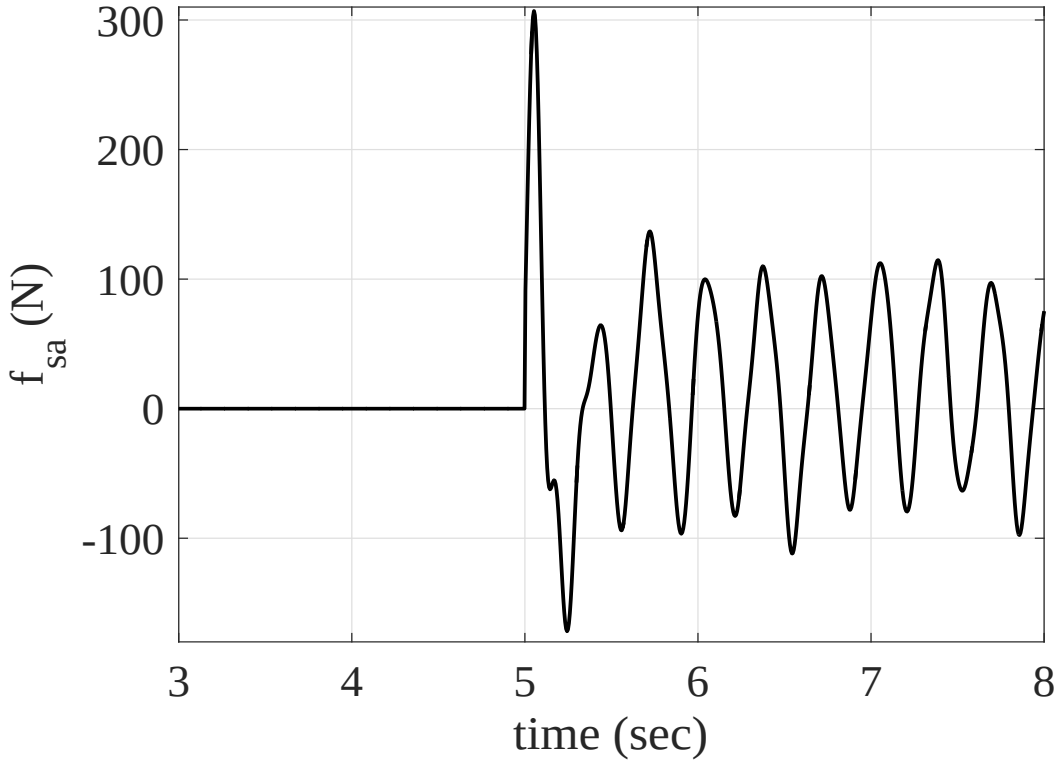

(b)

Fig. 4.9 *Control signals in hybrid active & semi-active controller. The hybrid controller is switched on at time 5 seconds, (a) active control signal, (b) semi-active control signal*

4.3 Comparison With Other Controllers

To illustrate the effectiveness of proposed hybrid active & semi-active controller, the proposed hybrid controller is compared to two straightforward scenarios with reference to Table 4.3. The hybrid active & passive controller involves using the MR damper as a purely passive device. For the semi-active controller, the active actuator is completely absent from the system. Figure 4.10 shows the active and semi-active control signal in the hybrid active & semi-active controller. Here, the MR damper can only work in the dissipative region and when energy is required to be injected into the system then the active actuator is assisting the semi-active device.

One of the biggest problems with the semi-active controller is "clipping" [139], which occurs when the semi-active device is unable to inject energy into the system and so the control is switched off. Figures 4.11a and 4.11b show the semi-active control signals with respect to the relative velocity, time in hybrid active & semi-active and semi-active controllers respectively. The clipping is reduced to a large extent in the hybrid active & semi-active controller as compared to the semi-active controller, because as the controller switches off in the hybrid active & semi-active controller, the active actuator injects the desired energy and the semi-active device returns to the dissipative region.

Figure 4.12a shows the experimental displacement of mass m_2 with the semi-active controller. After 5 seconds the controller is turned on, and the actual system cannot achieve the target system. Figure 4.12b also shows the displacement of mass m_2 with a hybrid active & passive controller, its performance is better than the semi-active

Table 4.3 Simplified controller architecture used for comparison

	Hybrid (active & semi-active)	Hybrid (active & passive)	Semi-Active
Hydraulic Actuator	I & I	I & I	Absent
MR Damper	SMC	Off (Passive)	SMC

controller, but still it cannot achieve the target system. However, the proposed hybrid active & semi-active controller can achieve the target system as shown in Figure 4.7a. Figures 4.13a and 4.13b show the error dynamics in the simulation and experiment respectively. It can be seen that the hybrid active & semi-active controller performance is significantly better than the other two controllers. If the amplitude of the excitation signal is increased from 70 N to 1000 N, then the difference in the performance of the controller can be seen more clearly in Figure 4.13c.

Figures 4.14 and 4.15 show the manifold with the off-the-manifold dynamics and sliding surface with error dynamics respectively in three different cases. In the first case both the controllers are in the off state. In the second case, the semi-active controller is turned on, and the distance between the manifold and off-the-manifold dynamics is decreased. In the third case, the hybrid controller is turned on, and off-the manifold dynamics comes very close to the manifold. The same pattern is followed by the error dynamics in Figure 4.15.

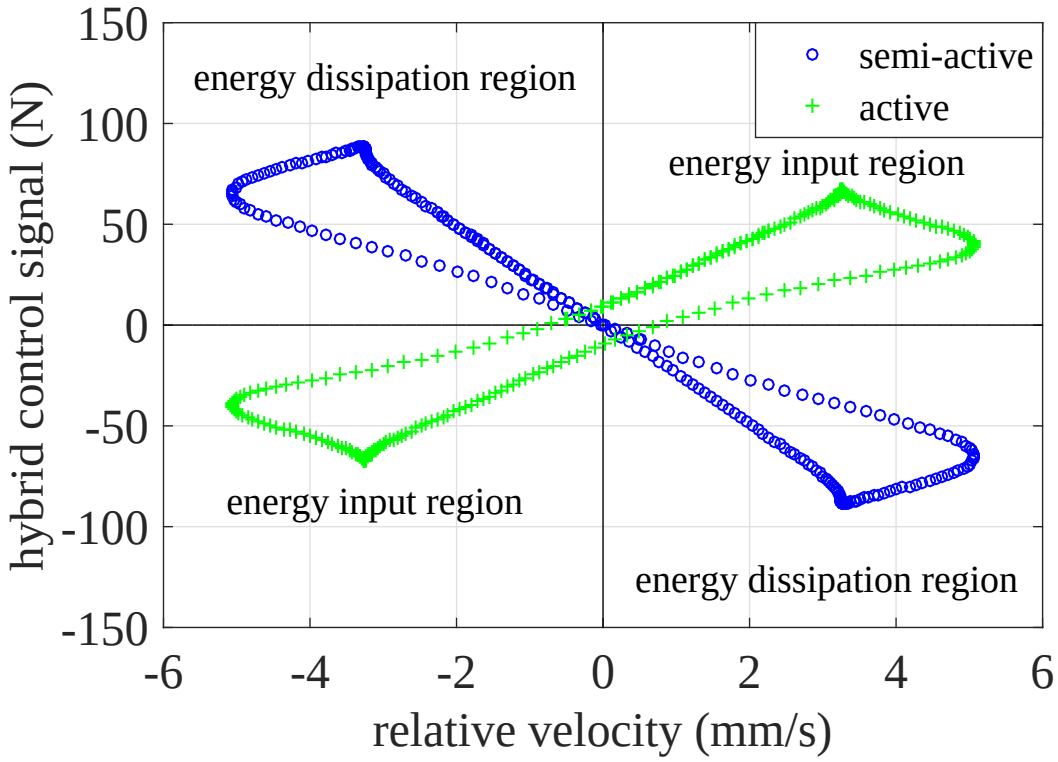

Fig. 4.10 *Active & semi-active control signals in hybrid active & semi-active controller. Active control signal is in the energy injection region and semi-active control signal is in the energy dissipation region without clipping*

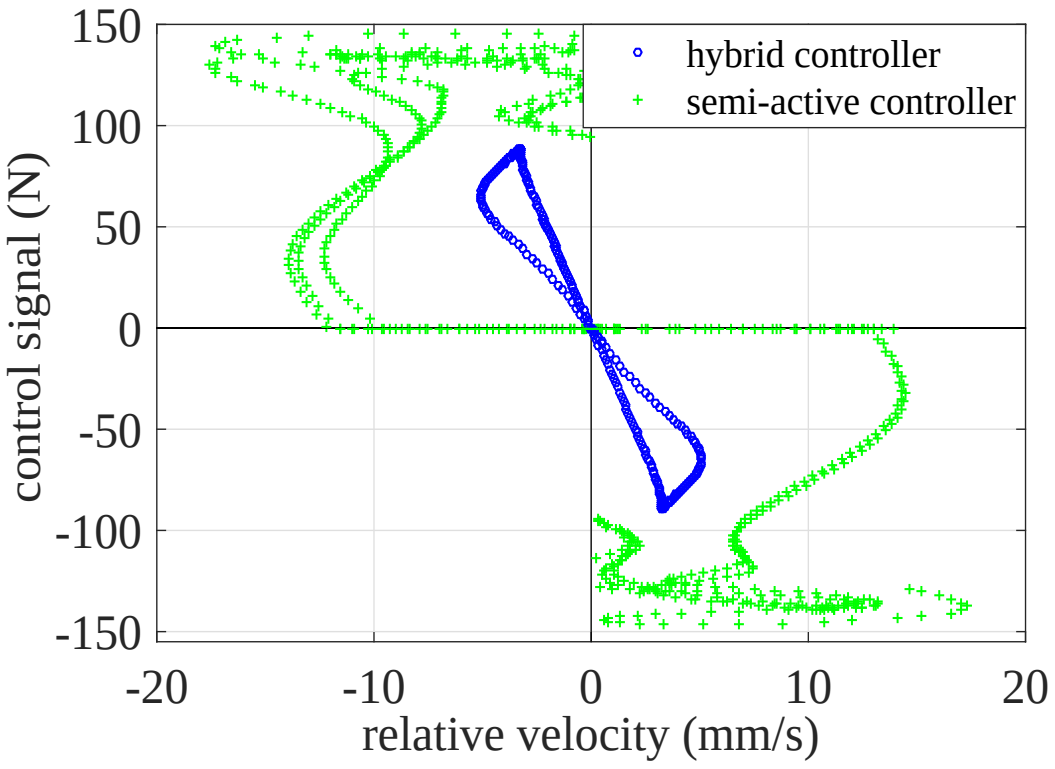

(a)

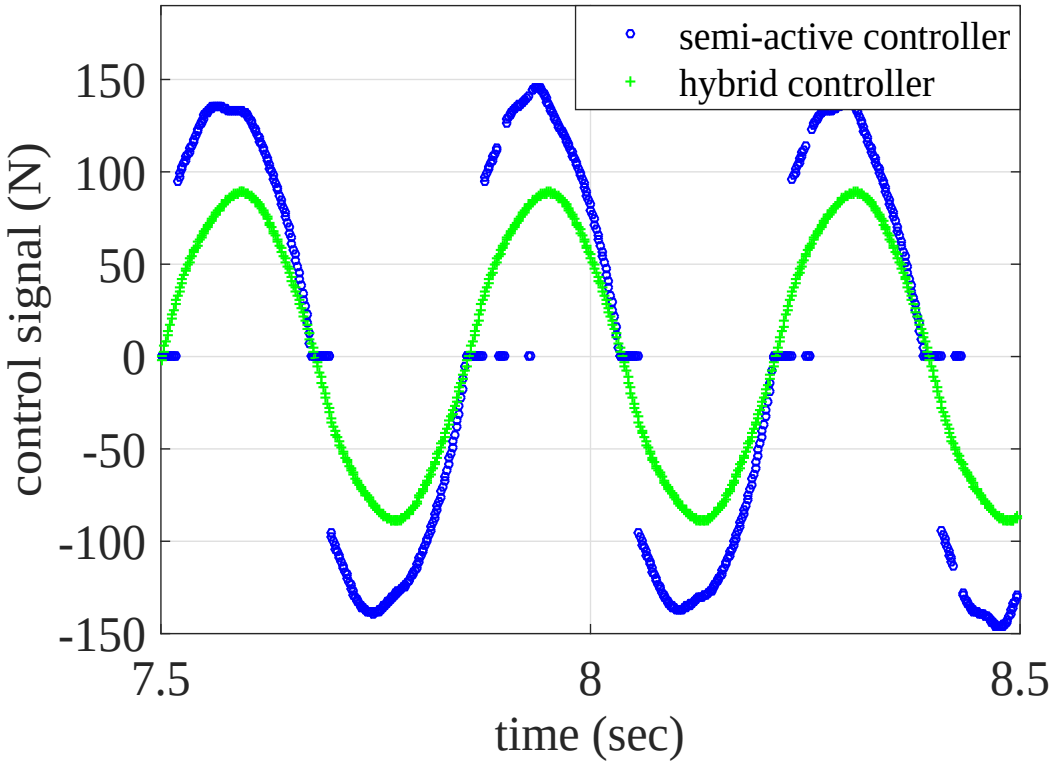

(b)

Fig. 4.11 *Semi-active control signal in hybrid active & semi-active and semi-active controllers, (a) with respect to the relative velocity, (b) with respect to the time*

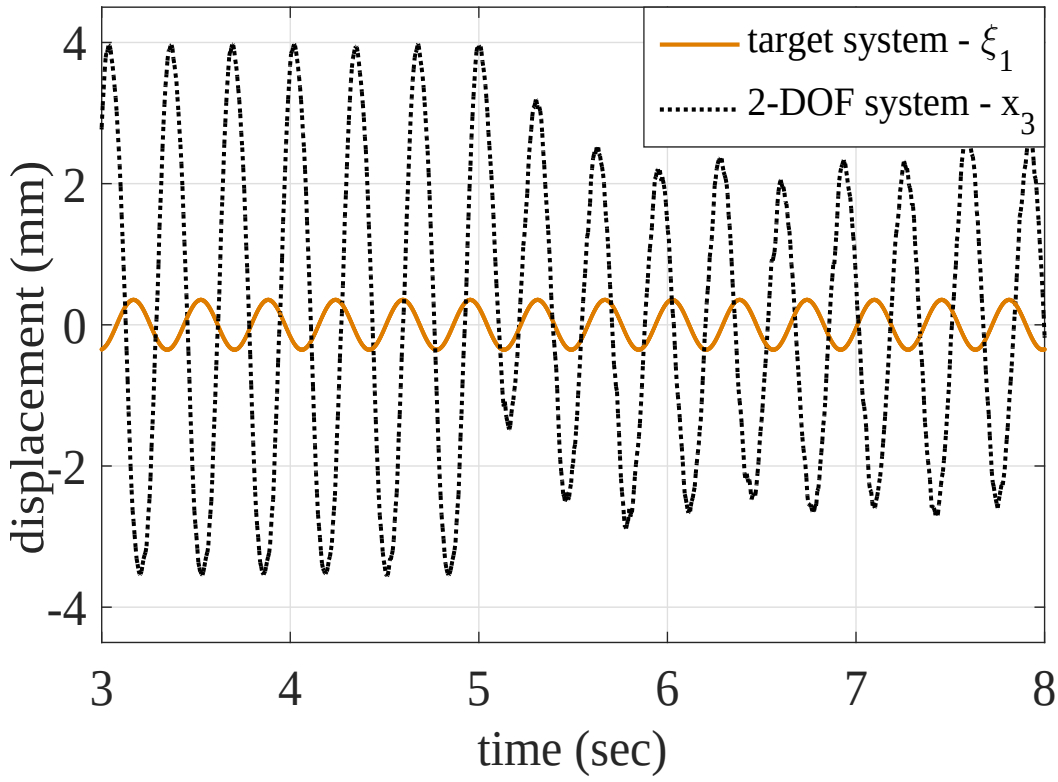

(a)

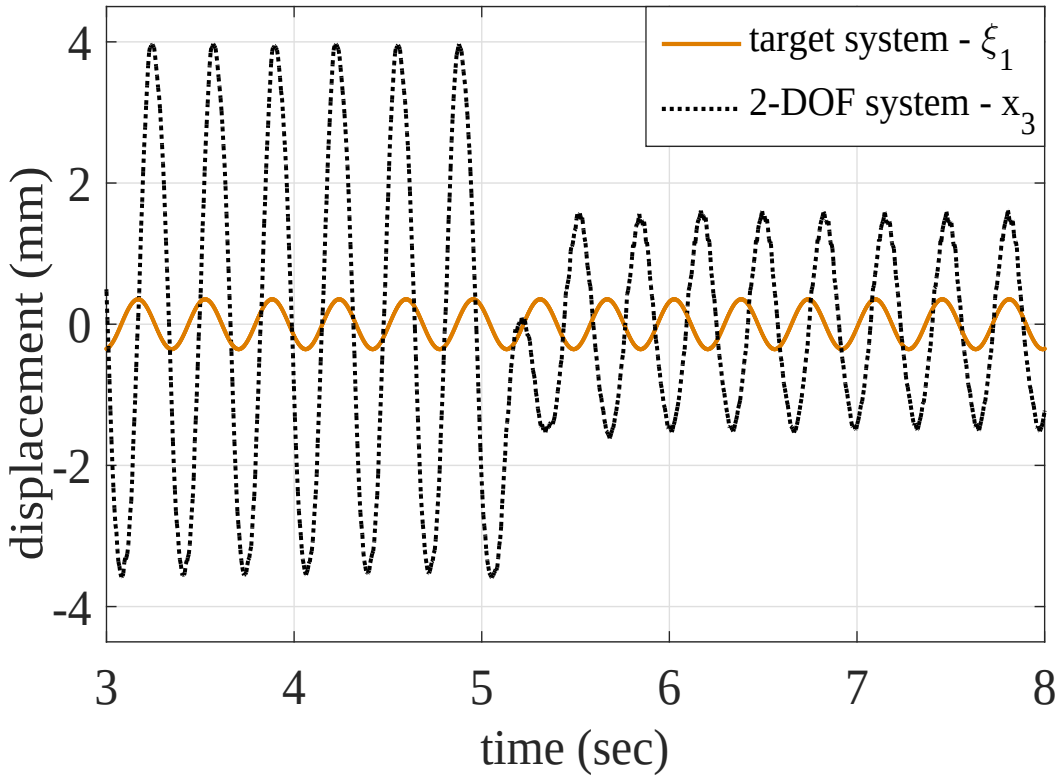

(b)

Fig. 4.12 *Displacement of mass m_2 controlled to follow the reference system, (a) with a semi-active controller, (b) with hybrid active & passive controller*

One of the advantages of an MR damper is its low energy consumption, which comes with the cost of passivity constraint. Figure 4.16a shows the energy consumption of the MR damper in passive, semi-active and hybrid control regions. The energy consumption of the MR damper is taken to be:

$$E_C = R_{MR} \int_0^t i^2 \mathrm{dt} \tag{4.1}$$

where i is the input current to the MR damper, R_{MR} is the MR damper internal resistance, and E_C is the energy consumption of MR damper over the time t. In the passive mode, the current input to the MR damper is zero. One of the important observations to note is that the energy consumption in the semi-active region is greater than that in the hybrid region whereas the performance is better in the hybrid region. Hence the proposed hybrid controller has further reduced the energy consumption of the MR damper in addition to the performance enhancement.

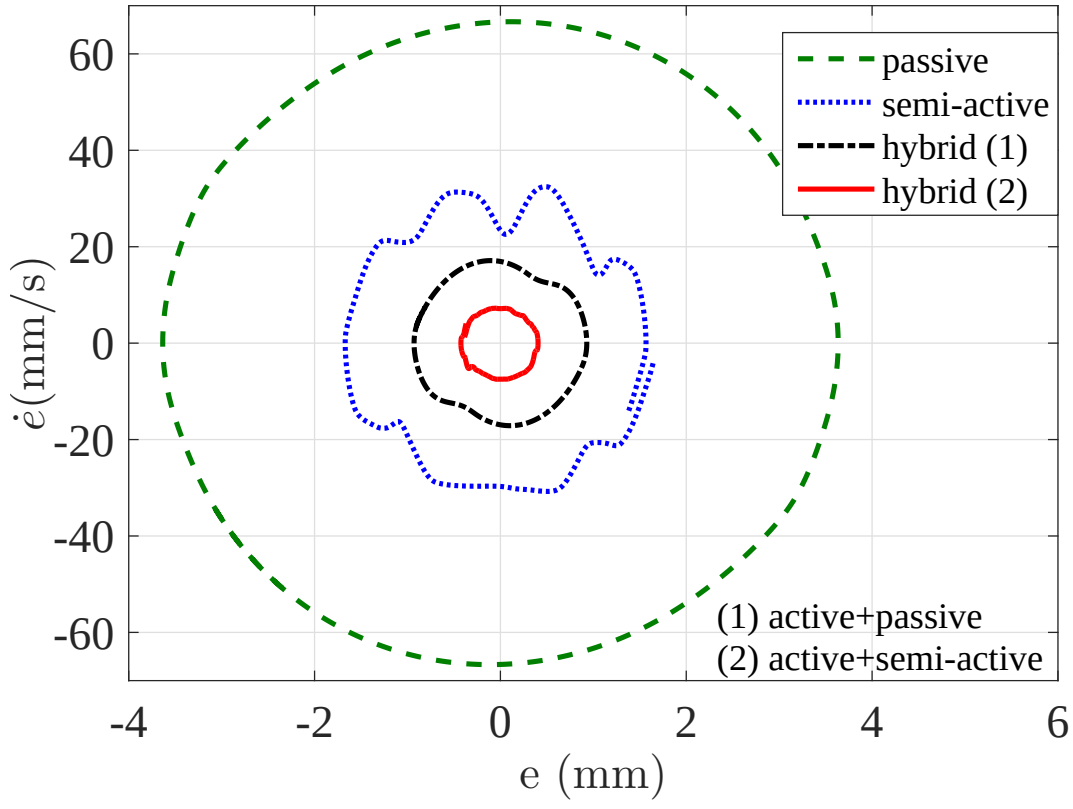

(a)

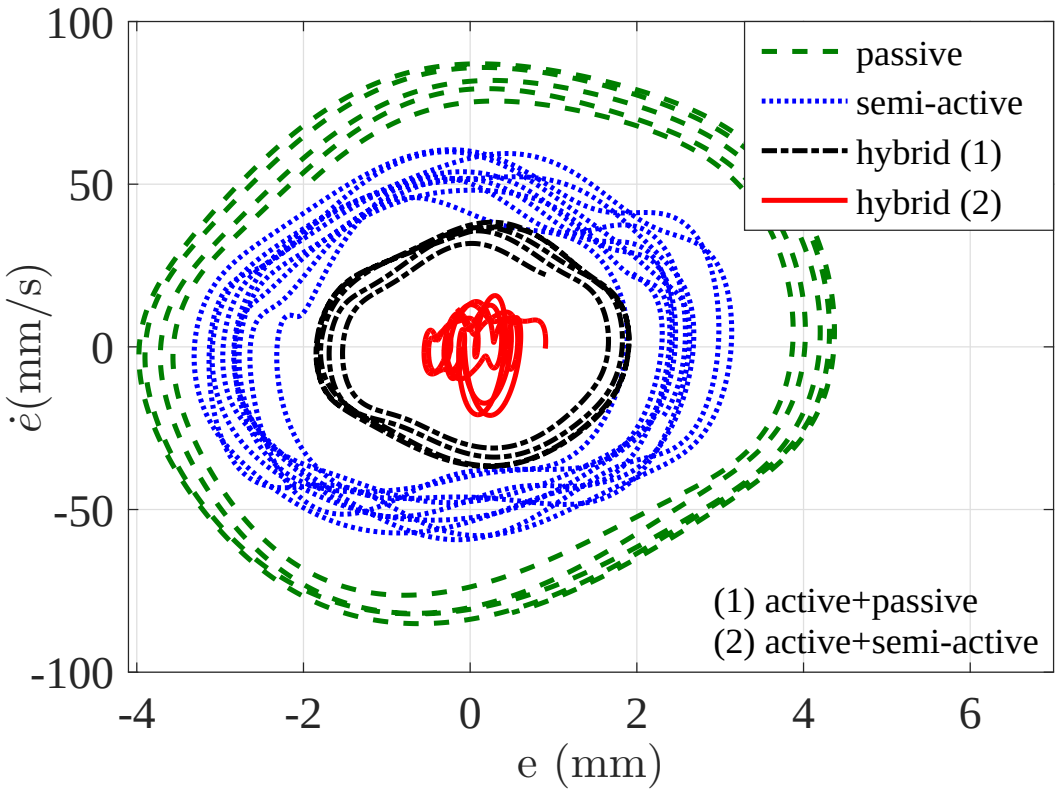

(b)

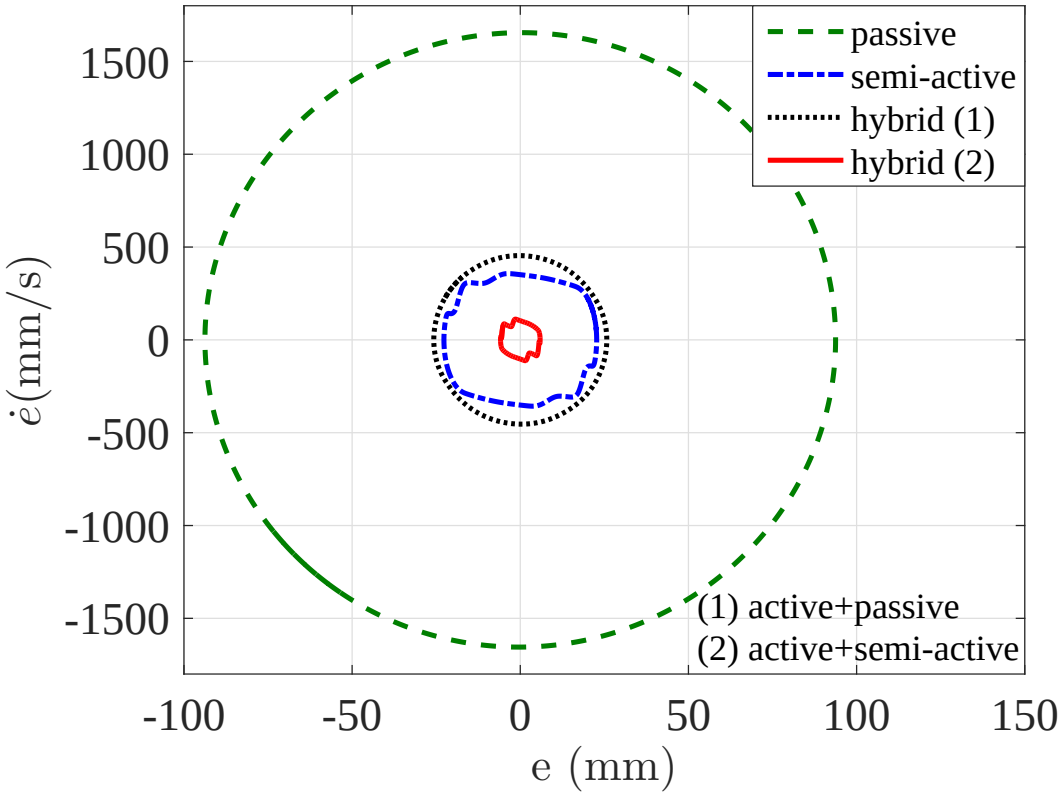

(c)

Fig. 4.13 *Error dynamics (a) error dynamics with U_d=70 N (simulation), (b) error dynamics with U_d=70 N (experiment), (c) error dynamics with U_d=1000 N (simulation)*

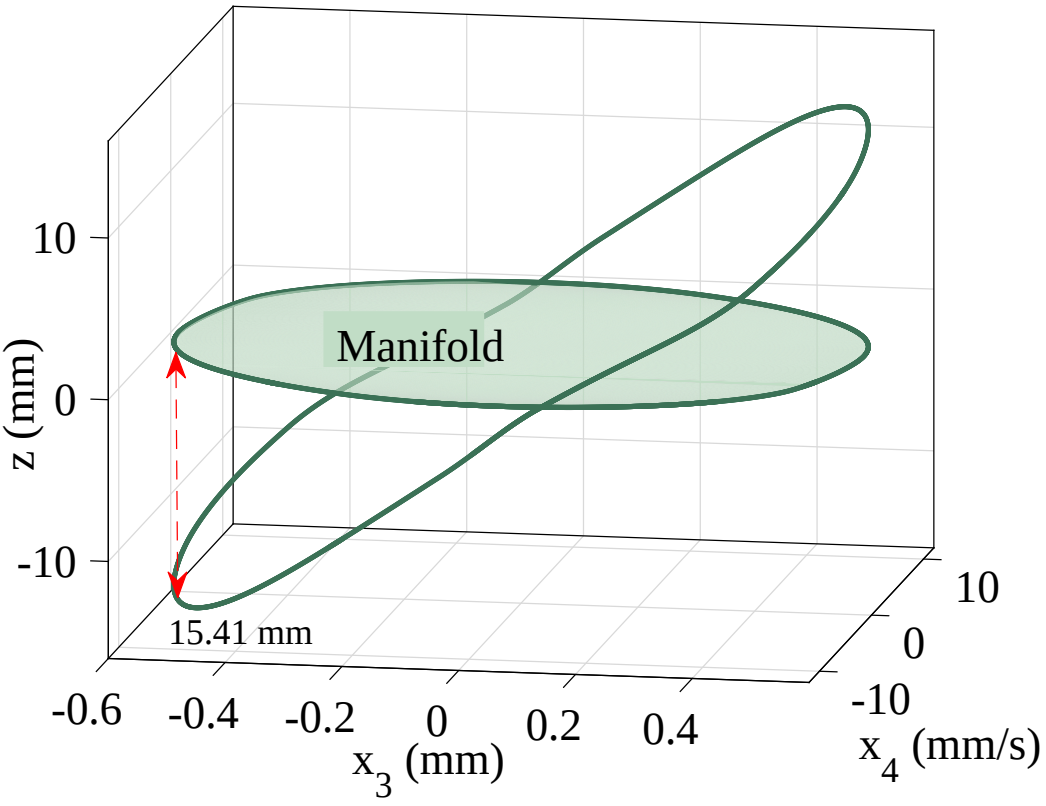
Manifold
15.41 mm
z (mm)
10
0
-10
-0.6
-0.4
-0.2
0
0.2
0.4
x3 (mm)
10
0
-10
x4 (mm/s)

(a)

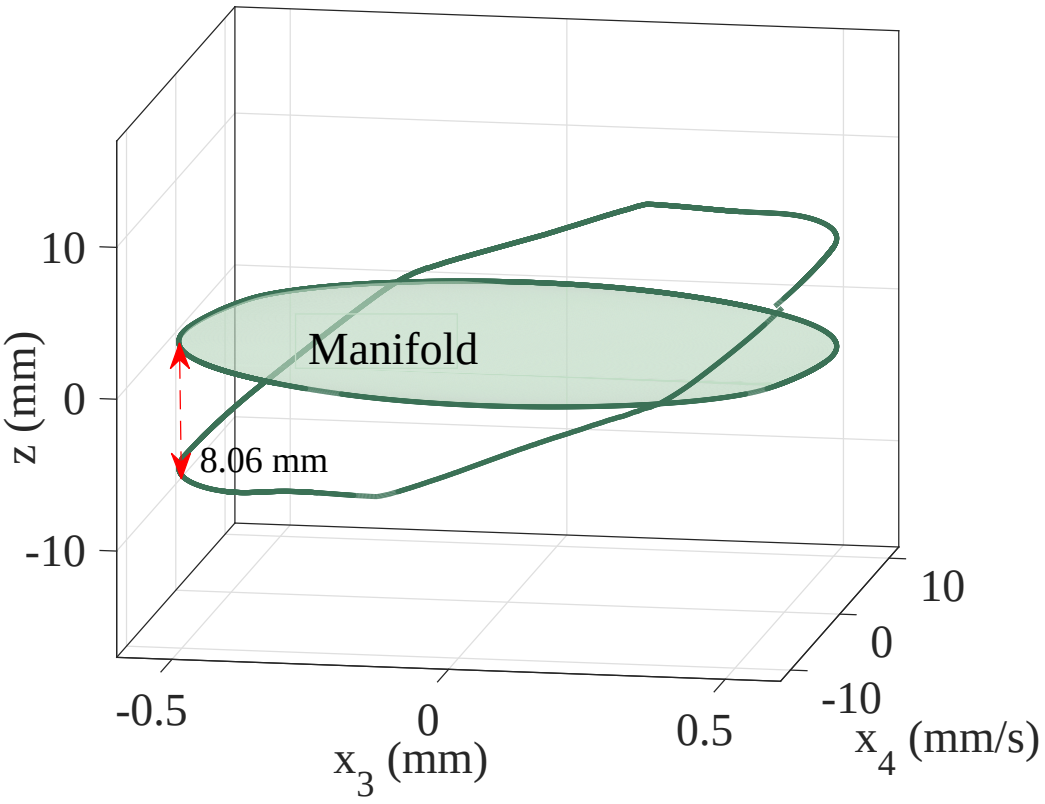
Manifold
8.06 mm
z (mm)
10
0
-10
-0.5
0
0.5
x3 (mm)
10
0
-10
x4 (mm/s)

(b)

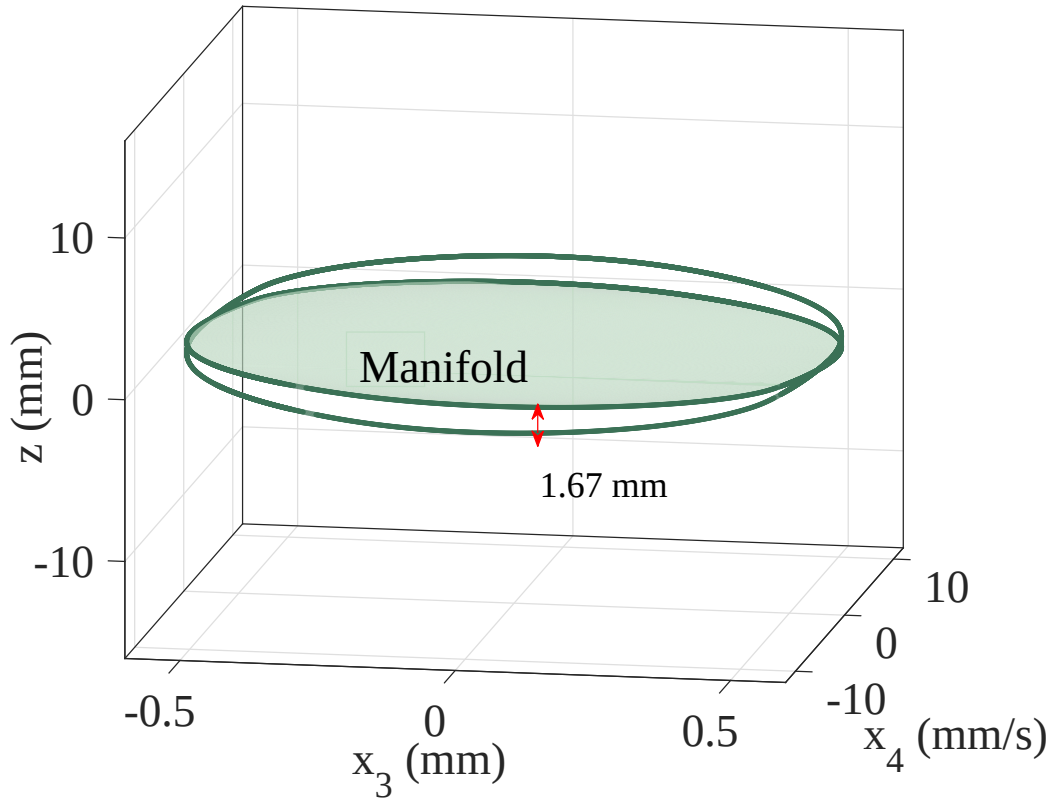

(c)

Fig. 4.14 *Manifold with off-the-manifold dynamics (a) in open-loop , (b) with semi-active controller, (c) with hybrid controller*

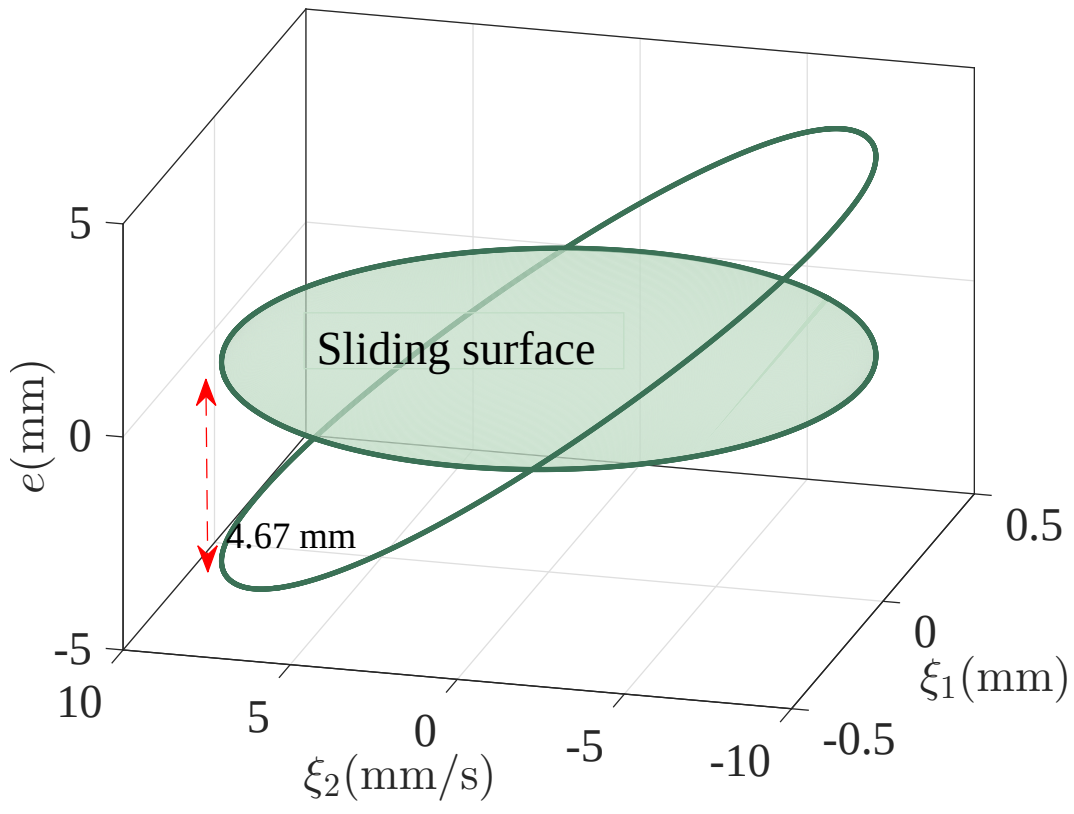

(a)

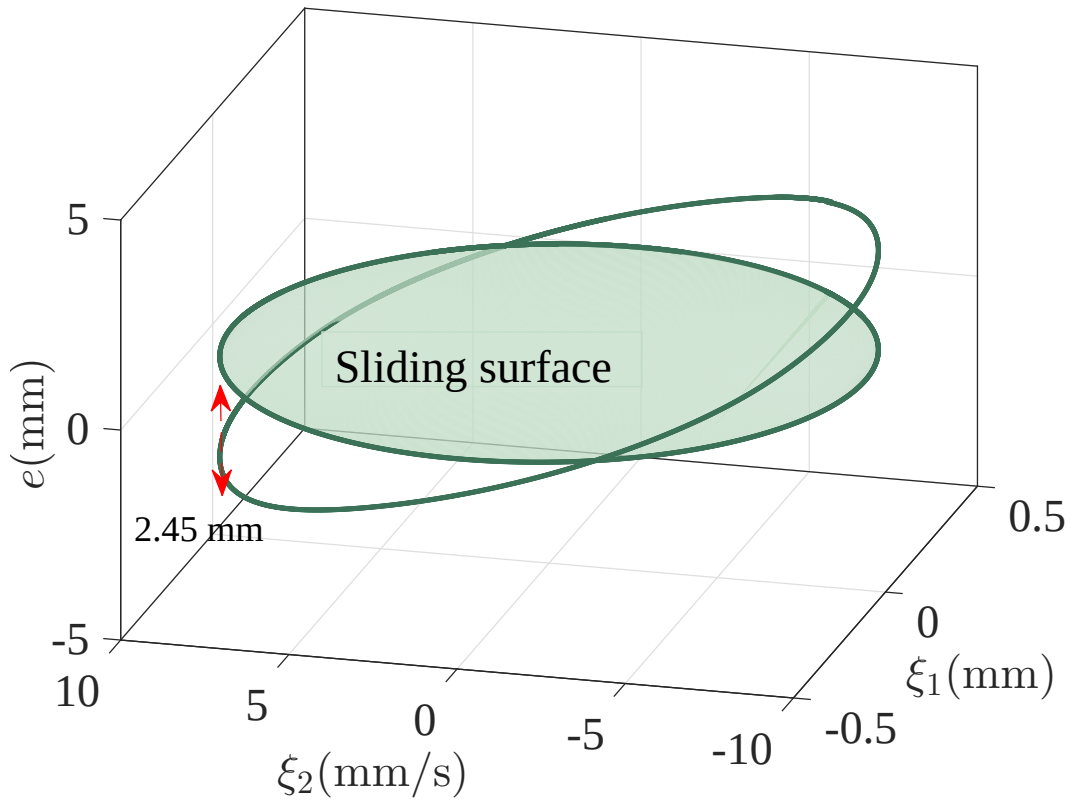

(b)

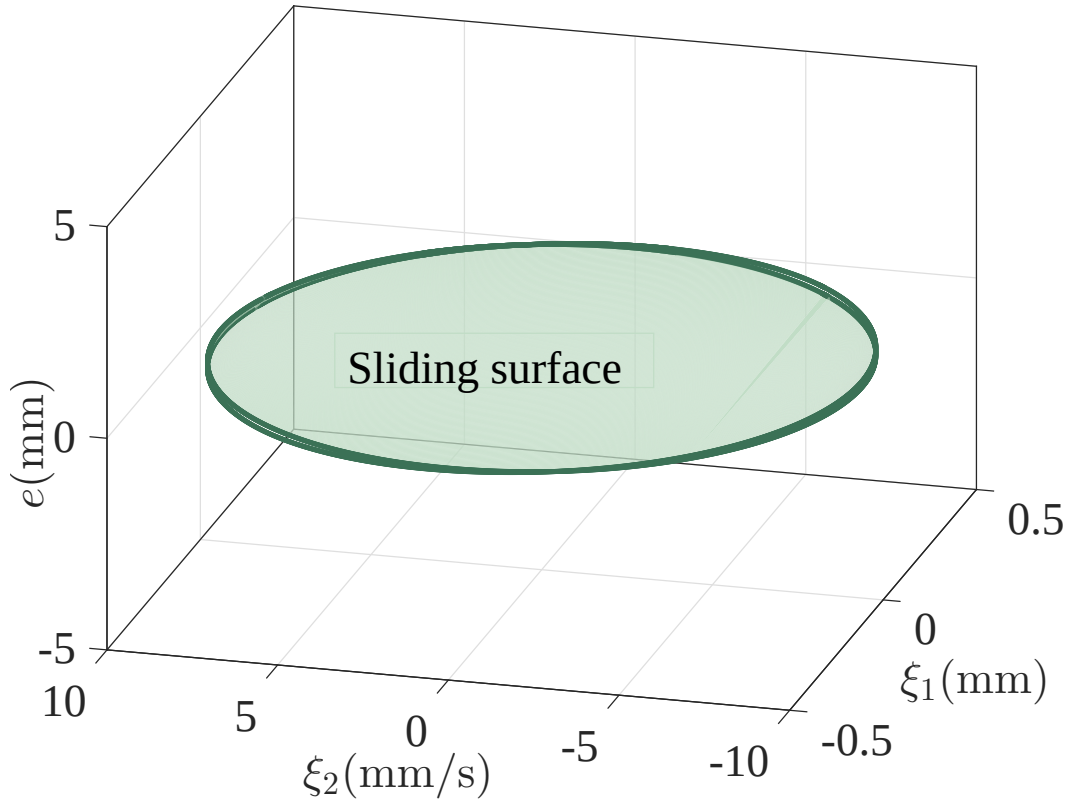

(c)

Fig. 4.15 *Sliding surface with error dynamics (a) in open-loop , (b) with semi-active controller, (c) with hybrid controller*

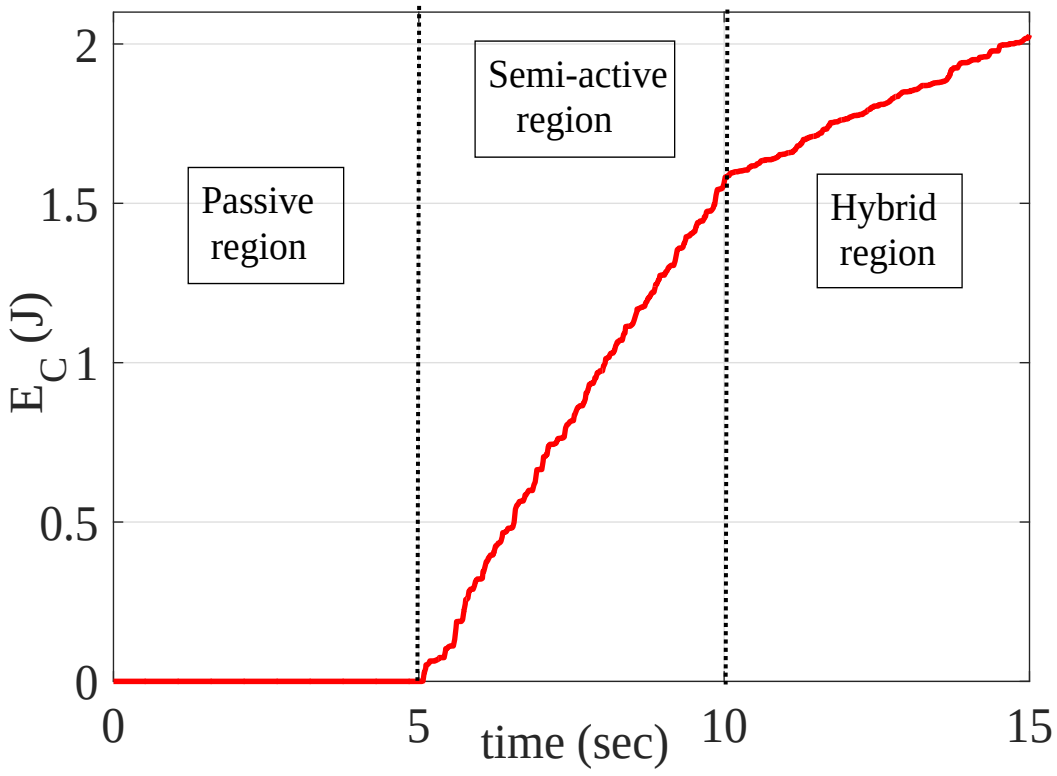

(a)

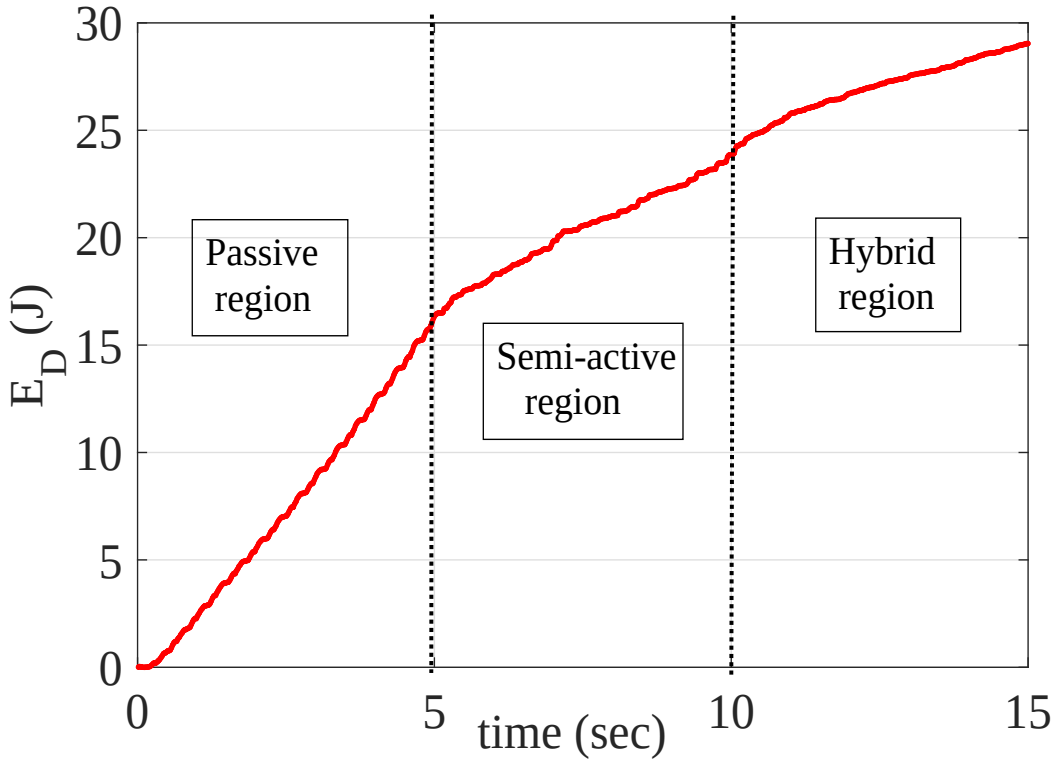

(b)

Fig. 4.16 *MR damper energy consumption & energy dissipation, (a) MR damper energy consumption, (b) MR damper energy dissipation*

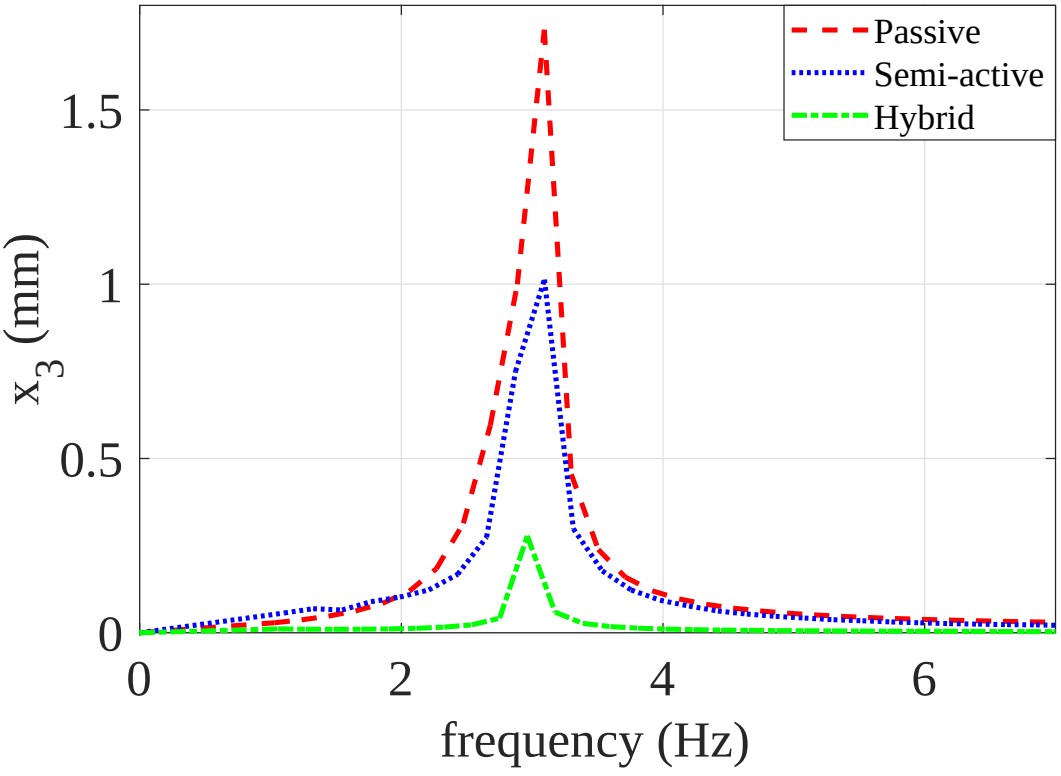

(a)

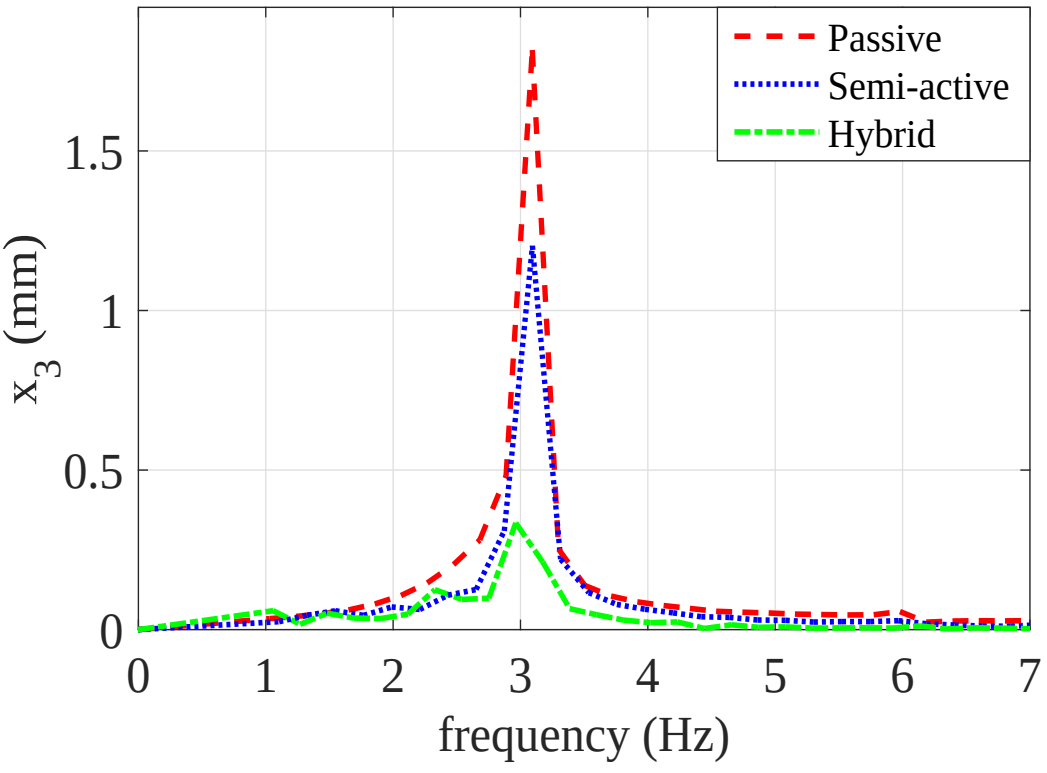

(b)

Fig. 4.17 *Frequency response, (a) simulation, (b) experimental*

Figure 4.16b shows the energy dissipation of the MR damper which is given as:

$$E_D = \int_0^t f_{sa} v_r \mathrm{dt} \tag{4.2}$$

where f_{sa} is the MR damper output force, v_r is relative velocity across the MR damper and E_D is MR damper dissipated energy. The dissipated energy keeps on decreasing as we move from passive to semi-active and finally to the hybrid region. On the other hand, the performance keeps on showing significant improvement. Figure 4.17 show the frequency response in simulation and experiment. It can be seen that the hybrid controller shows significant attenuation in the vibration.

4.4 Discussion

This research concluded that the performance of a semi-active device could be improved with the assistance of an active actuator located somewhere else in the system via the proposed hybrid active & semi-active control methodology. The results obtained both in the simulation and experiment have reinforced the proposed idea. As previously mentioned, it should be noted that the simulation and experimental results are not exactly the same because the excitation signal in the experiment is generated through an unbalanced rotating mass. There is a small variation in the speed of the rotating motor, and the phase is also unknown. In spite of these issues, the results are very good, which demonstrates the robustness of the hybrid active & semi-active controller for the example system.

For a quantitative analysis of the three controllers as compared in Figure 4.13, a performance index is defined as an absolute value of the radius of phase plane shown in Figure 4.13. It can be seen that when the proposed hybrid active & semi-active controller is turned on, the error is reduced by 88%. In comparison, the other two controllers i.e. hybrid active & passive and semi-active, the error is reduced by 73% and 41% respectively. In Figure 4.13, the amplitude of the excitation signal has been

increased from 70 N to 1000 N. The proposed hybrid active & semi-active controller has reduced the error by 92%, and the other two controllers have reduced the error by 68%. Therefore the performance of the proposed hybrid active & semi-active controller is better than the other two controllers in both the cases of low and high amplitude excitation signals. In the case of the high amplitude excitation signal, the performance index of the proposed hybrid active & semi-active controller has been further increased by 4%.

This idea is general and is not restricted to either the controller methodologies or the example presented in this Chapter. The same results might be achieved by combining different control techniques; however, this is beyond the scope of the current proof-of-concept study. HIL testing is used because there is a freedom to change the system parameters in the simulated part of the model which in this study included the non-linearity.

4.5 Summary

It is always vital to implement the analytical design on a practical system because at the end of the day it needs to deal with real world problems. The experimental setup that is used for HIL testing is described in detail. The hybrid active & semi-active control technique that has been introduced in Chapter 3, is validated using HIL testing in which an active actuator is assisting the semi-active device to achieve performance close to that of a fully active system. The switching time of the semi-active controller has been reduced to a large extent by the hybrid active & semi-active controller because the active actuator injects the desired energy as the semi-active controller switches off, following which the semi-active device returns to the dissipative region.

The proposed control technique has been compared with semi-active and hybrid active & passive controllers. Based on the performance index defined in Section 4.4, the proposed controller performance is better than the other two controllers. The idea has been implemented on a 2-DOF mass-spring-damper example system that also includes

a cubic stiffness nonlinearity. The results from HIL testing has shown good results in achieving the control objectives.

Chapter 5

Hybrid Controller Application

5.1 Introduction

In this Chapter the practical applicability of the hybrid controller designed in Chapter 3 is illustrated by considering its application to a pantograph-catenary system. The use of high-speed trains not only improves the efficiency of transportation but also has a very positive impact on the environment in terms of controlling air pollution. High-speed trains can achieve a speed around 350-450 km/h. Hence it is crucial to have a permanent contact between pantograph and catenary. The electric current from catenary to train transformer flows through the pantograph. In an ideal scenario, the contact between pantograph and catenary should be permanent, but due to the flexibility in the structure of catenary and pantograph, as the train speed increases the oscillations keeps on rising and the contact is not guaranteed, which results in electric arcs and eventually deteriorating the current collection from catenary.

One solution to avoid loss of contact is to increase the contact force, but this will result in wear and tear due to the excessive contact force. It is vital to keep the contact force constant without causing any damage to the pantograph-catenary system. Another solution is to increase the tension in the contact wire which means increasing the equivalent stiffness. This solution is very expensive. The catenary presents a time varying stiffness, which is dependent on the train speed. To solve this problem different control strategies have been proposed using active actuators.

There are mainly three types of pantograph-catenary models used in the literature for control purposes. In [35–37, 140] the pantograph is modelled as a 2-DOF mass spring damper system and the catenary is designed as a time varying spring. In [141–145] the pantograph is modelled as a 2-DOF mass spring damper system and catenary is modeled as spring with fixed stiffness. In addition to that, a spring with fixed stiffness is added to represent the pantograph shoe. In [146–148] the pantograph is modelled as a 3-DOF mass spring damper system, and the catenary is designed an SDOF mass spring damper system with time varying mass, time varying stiffness and time varying damping.

To evaluate the performance of the proposed controller, the first two pantograph-catenary models are used. The hybrid controller is designed in a way that an active actuator is assisting a semi-active device in achieving a performance close to a fully active system. The semi-active device can only work in the dissipative energy region. In the energy injection region, the semi-active controller has to be switched off, and the semi-active device behaves as a passive device. In the proposed control methodology, when the semi-active controller is about to switch off before going into the energy injection region, the active actuator injects the required energy into the system and pushes the semi-active device back into the dissipative region.

In Section 5.2 the pantograph-catenary models are introduced. The hybrid controller design is presented with detail in Section 5.3. The simulation results are presented in Section 5.4 with detailed discussion, and conclusions are given in Section 5.5.

5.2 Pantograph-Catenary System

Two models of the pantograph-catenary system are used in this study. In the first model shown in Figure 5.1b, the pantograph is represented as a 2-DOF mass spring damper system with a time varying stiffness representing the catenary behaviour. In the second model shown in Figure 5.1c, the pantograph design is the same, and the catenary is modelled as a spring with constant stiffness. Additionally, the pantograph shoe is represented with a linear spring.

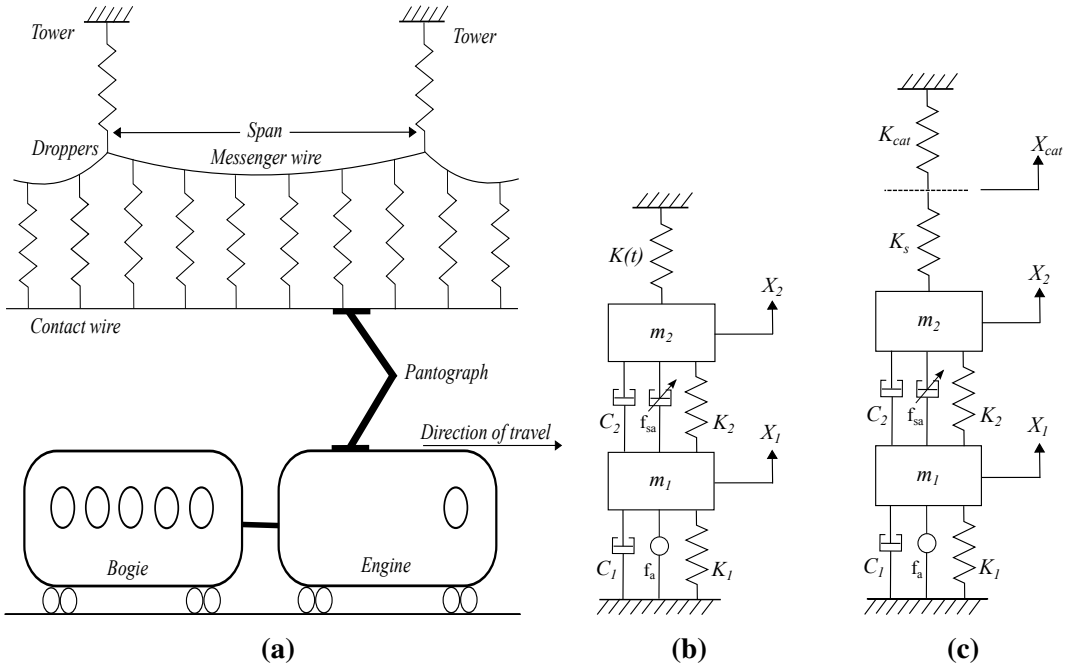

Fig. 5.1 *Pantograph-catenary system, where f_a represents the force of an active actuator and f_{sa} represents the force of a semi-active device. m_1 & m_2 represent the masses, K_1 and K_2 are the linear spring stiffness, $K(t)$ is the time varying catenary stiffness, C_1 and C_2 are the damping coefficients,K_s is the pantograph shoe stiffness, K_{cat} is the constant catenary stiffness. (a) pantograph-catenary system, (b) 2-DOF pantograph-catenary model with time varying catenary stiffness, (c) 2-DOF pantograph-catenary model with constant catenary stiffness*

The system can be represented in state space form as

$$\begin{aligned}
\dot{x}_1 &= x_2, \\
\dot{x}_2 &= \frac{1}{m_1}\Big(f_a - f_{sa} - K_1x_1 - C_1x_2 - K_2(x_1 - x_3) - C_2(x_2 - x_4)\Big), \\
\dot{x}_3 &= x_4, \\
\dot{x}_4 &= \frac{1}{m_2}\Big(f_{sa} - K_2(x_3 - x_1) - C_2(x_4 - x_2) - K(t)x_3\Big),
\end{aligned} \tag{5.1}$$

where x_1 and x_2 are the position and velocity of mass m_1 respectively, x_3 and x_4 are the position and velocity of mass m_2 respectively, f_a represents the force of the active actuator, f_{sa} represents the force of the semi-active device, m_1, m_2 represent the masses, K_1, K_2 are the linear spring stiffness, $K(t)$ is the nonlinear spring stiffness, C_1 and C_2 are the damping coefficients. $K(t)$ is defined as

$$K(t) = K_0\Big(1 + \alpha_s\cos(\frac{2\pi V}{L}t)\Big) \tag{5.2}$$

where V is the train speed, L is the span length, K_0 is average equivalent stiffness, α_s is stiffness variation coefficient in a span. K_0 and α_s has been identified using (5.3).

$$K_0 = \frac{K_{max} + K_{min}}{2}, \qquad \alpha_s = \frac{K_{max} - K_{min}}{K_{max} + K_{min}} \tag{5.3}$$

5.3 Hybrid Controller Design

As two models of the pantograph-catenary system are defined, hence two target systems are shown in Figure 5.2. First the controller is designed for the system shown in Figure 5.1b, with the corresponding target system shown in Figure 5.2a. The order of the target system is lower than the order of the actual system, and the mapping functions are defined as virtual dynamics, to represent the actual system dynamics (off-the-manifold) that are not present in the target system.

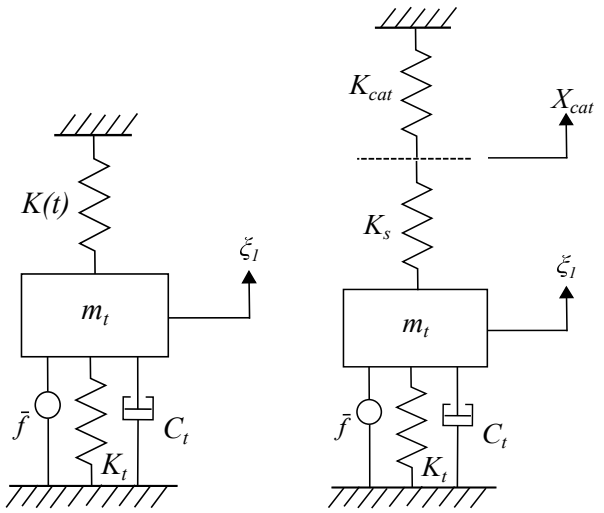

Fig. 5.2 *Target system, where ξ_1 and ξ_2 represents the position and velocity of the mass m_t, $\bar{f}$ will be computed after defining the mapping functions, K_t is the linear spring stiffness, C_t is the damping coefficient. (a) target system for 2-DOF system with time varying catenary stiffness, (b) target system for 2-DOF system with constant catenary stiffness*

The dynamics of the target system are given by

$$\begin{aligned} \dot{\xi}_1 &= \xi_2, \\ \dot{\xi}_2 &= \frac{1}{m_t}\Big(\bar{f} - K_t\xi_1 - C_t\xi_2 - K(t)\xi_1\Big), \end{aligned} \tag{5.4}$$

where ξ_1 and ξ_2 represent the position and velocity of the mass m_t respectively, and $\bar{f} = \mathscr{W} + u$, u represents the controller signal and $\mathscr{W}$ is the function that will be computed after defining the mapping functions.

The next step is to design a controller for the target system. The same PI controller is used here, as defined in Chapter 3. The PI controller is given as

$$u = K_a e_p + K_b \int e_p dt - K_c \dot{f}_c - K_d f_c \tag{5.5}$$

where $K_a = K_v K_p$, $K_b = K_i K_p$, $K_c = K_v$, $K_d = K_i$, K_i, K_v & K_p are control gains, and e_p is the error.

The mapping functions that need to be defined are given by

$$\pi(\xi) = \begin{bmatrix} \pi_1(\xi_1, \xi_2) \\ \pi_2(\xi_1, \xi_2) \\ \pi_3(\xi_1, \xi_2) \\ \pi_4(\xi_1, \xi_2) \end{bmatrix} \tag{5.6}$$

where $\pi_1(\xi_1, \xi_2)$, $\pi_2(\xi_1, \xi_2)$ need to be defined for off-the-manifold coordinates and $\pi_3(\xi_1, \xi_2) = x_3(\pi_1, \pi_2)$, $\pi_4(\xi_1, \xi_2) = x_4(\pi_1, \pi_2)$.

As the target system dynamics (5.4) resembles the dynamics of the actual system (5.1), in which the vibration needs to be controlled, hence $\pi_3(\xi_1, \xi_2) = \xi_1$. As $\dot{x}_1 = x_2$, so we can write $\pi_4(\xi_1, \xi_2) = \xi_2$. Based on (5.7), the mapping functions $\pi_1(\xi_1, \xi_2)$, $\pi_2(\xi_1, \xi_2)$ are derived from

$$\dot{\xi}_2 = \dot{\pi}_4. \tag{5.7}$$

and

$$\frac{1}{m_t}\Big(\bar{f} - K_t\xi_1 - C_t\xi_2 - K(t)\xi_1\Big) = \frac{1}{m_2}\Big(-K_2(\xi_1 - \pi_1) - C_2(\xi_2 - \pi_2) - K(t)\xi_1\Big) \tag{5.8}$$

The mapping functions selected are

$$\pi_1 = \Big(-m_2 \frac{\big(K(t)+K_t\big)}{K_2 m_t} + 1 \Big) \xi_1 + \alpha_1 e_p + \alpha_2 \int e_p dt + \alpha_3 K(t) \xi_2 + \alpha_4 K(t) \xi_1, \quad (5.9)$$

$$\pi_2 = \Big(-m_2 \frac{\big(K(t)+K_t\big)}{K_2 m_t} + 1 \Big) \xi_2 - \alpha_1 K(t) \xi_2 + \alpha_2 e_p + \alpha_3 K(t) \dot{\xi}_2 + \alpha_4 K(t) \xi_2. \quad (5.10)$$

and $\bar{f}$ is defined as

$$\bar{f} = \Big(-\frac{C_2}{K_2} \Big(K(t) + K_t \Big) + C_t \Big) \xi_2 + u \quad (5.11)$$

The four unknowns α_1, α_2, α_3, α_4 are found out by substituting π_1, π_2, $\bar{f}$ in (5.8).

To check the asymptotic stability of the target system, the target system dynamics are compared with a single mass system dynamics (5.12) in the same way as shown in Chapter 3. From the Lagrangian formulation the dynamics of a single mass are

$$\begin{aligned} \dot{\xi}_1 &= \xi_2 \\ \dot{\xi}_2 &= -E^{'} - \xi_2 R \end{aligned} \quad (5.12)$$

where E is the potential energy function and R is the damping function and a dash represents differentiation with respect to the state vector.

Comparing (5.4) and (5.12) gives

$$E^{'} = \frac{1}{m_t} \left(\frac{m_t K(t)}{m_2} + K_t + K(t) \right) \xi_1, \quad (5.13)$$

$$R = \frac{C_2}{K_2} \Big(K(t) + K_t \Big), \quad (5.14)$$

and

$$E = \frac{1}{2m_t} \left(\frac{m_t K(t)}{m_2} + K_t + K(t) \right) {\xi_1}^2. \quad (5.15)$$

A Lyapunov function is defined as a generalized energy function

$$V_{i\&i} = \frac{1}{2}{\xi_2}^2 + E. \tag{5.16}$$

The target system dynamics will have an asymptotically stable equilibrium at the origin if the following conditions are satisfied by the Lyapunov function defined in (5.16)

$$V(0,0) = 0 \tag{5.17a}$$

$$V(\xi_1, \xi_2) > 0, \text{ in } D - \{0\}. \quad D \to \mathbb{R}^p \tag{5.17b}$$

$$\dot{V}(\xi_1, \xi_2) < 0, \text{ in } D - \{0\}. \tag{5.17c}$$

where $V(\xi_1, \xi_2)$ is the energy function, and D is the subset of $\mathbb{R}^p$ in which the Lyapunov function is defined.

As a result

$$\dot{V}_{i\&i}(\xi_1, \xi_2) = -R{\xi_2}^2. \tag{5.18}$$

The first two conditions (5.17a) and (5.17b) are satisfied by the Lyapunov function defined in (5.16). The third condition (5.17c) where $\dot{V}_{i\&i}(\xi_1, \xi_2)$ should be negative definite, is satisfied when R is positive. As can be seen from (5.14), R is always positive. Therefore, the selected target system has an asymptotically stable equilibrium at the origin.

The error between the off-the-manifold dynamics and the mapping functions is defined as

$$z = x_1 - \pi_1 \tag{5.19}$$

and the manifold is defined as

$$\mathscr{M} = -k_1 z - k_2 \dot{z} \tag{5.20}$$

where $\dot{z} = x_2 - \pi_2$. The gains k_1 and k_2 are chosen in such a way that $(s^2 + k_2 s + k_1)$ is Hurwitz. The last step in the I & I methodology is to compute the control law, which is done using

$$\ddot{z} = \dot{x}_2 - \dot{\pi}_2 \tag{5.21}$$

and

$$\ddot{z} = \frac{1}{m_1}\Big(f_a - f_{sa} - K_1 x_1 - C_1 x_2 - K_2(x_1 - x_3) - C_2(x_2 - x_4)\Big) - \frac{\partial \pi_2}{\partial x_3}\dot{x}_3 - \frac{\partial \pi_2}{\partial x_4}\dot{x}_4. \tag{5.22}$$

The control signal f_a is given by

$$f_a = \left(-k_1 z - k_2 \dot{z} + \frac{\partial \pi_2}{\partial x_3}\dot{x}_3 + \frac{\partial \pi_2}{\partial x_4}\dot{x}_4 \right) m_1 + K_1 x_1 + C_1 x_2 + K_2(x_1 - x_3) + C_2(x_2 - x_4) \tag{5.23}$$

where

$$\frac{\partial \pi_2}{\partial x_3} = -\alpha_2 K(t) - \alpha_3 \frac{1}{m_2}\Big(K_2 + K(t)\Big), \tag{5.24}$$

and

$$\frac{\partial \pi_2}{\partial x_4} = -\frac{m_2}{K_2 m_t}\Big(K(t) + K_t\Big) + 1 + (\alpha_4 - \alpha_1)K(t) - \alpha_3 \frac{C_2}{m_2} \tag{5.25}$$

The next step is to design a controller for the semi-active device, and here the sliding mode controller is used in the same way as in Chapter 3, so instead of showing the complete controller design, only the final results are presented.

The control signal is given as

$$f_{sa} = f_n - \frac{m_2}{\lambda_2}\Big(K_{smc}\text{sgn}(S)\Big) \tag{5.26}$$

where K_{smc} is a design parameter and strictly positive and f_n is given as

$$f_n = \frac{m_2}{\lambda_2}\Bigg(-\lambda_1(x_4-\xi_2)\Bigg) + m_2\ddot{\xi}_2 + K_2(x_3-x_1) + C_2(x_4-x_2) + K(t)x_3. \tag{5.27}$$

So, the controller will be switched-on, when the relative velocity v_r across the MR damper and the control signal f_{sa} have opposite signs and will be switched-off otherwise. This condition is imposed on f_{sa} in (5.28) and is called the passivity constraint.

$$f_{sa} = \begin{cases} f_n - \dfrac{m_2}{\lambda_2}\Big(K_{smc}\text{sgn}(S)\Big) & f_{sa}v_r < 0 \\ 0 & f_{sa}v_r > 0 \end{cases} \tag{5.28}$$

where $v_r = x_4 - x_2$.

For the second pantograph-catenary model shown in Figure 5.1c, the state space equations given in (5.1) are the same with only one change. The term $K(t)x_3$ is replaced with $K_s(x_3 - x_{cat})$. An additional equation

$$K_{cat}x_{cat} + K_s(x_{cat} - x_3) = 0 \tag{5.29}$$

is introduced because of the pantograph shoe.

As x_{cat} is considered to be unknown, in order to replace x_{cat}, (5.29) is used. From (5.29)

$$x_{cat} = \frac{K_s}{K_{cat} + K_s}x_3 \tag{5.30}$$

Eventually in (5.1) the time varying stiffness term $K(t)$ is replaced with $K_s - \dfrac{{K_s}^2}{K_{cat} + K_s}$. After designing the hybrid controller for both the pantograph-catenary models, the simulation results are shown in the next section.

5.4 Simulation Results

Figure 5.3 shows the contact force in an open-loop with an uplift force of 100 N. At 100 km/h, the contact force is around 100 N as shown in Figure 5.3a. The open-loop performance can be further improved, with tuning of passive damper. When the train speed in increased from 100 km/h to 300 km/h, it can be seen in Figure 5.3b, that the it is not possible to keep the contact force around 100 N and there is also loss of contact between 1.5 and 2.5 second. It can be concluded from the open-loop results that the passive devices can give satisfactory results in low speed rails/trams where the top speed is around 70-80 km/h, but for high speed trains the passive devices are not sufficient enough.

Table 5.1 shows the pantograph-catenary system parameters. The gains designed for the controllers are shown in Table 5.2. To introduce the actuator dynamics in the simulation; a second order low-pass filter with the cutoff frequency of 50 Hz is incorporated in the simulation with saturation limits of $\pm$ 250 N for both the active actuator and the semi-active device.

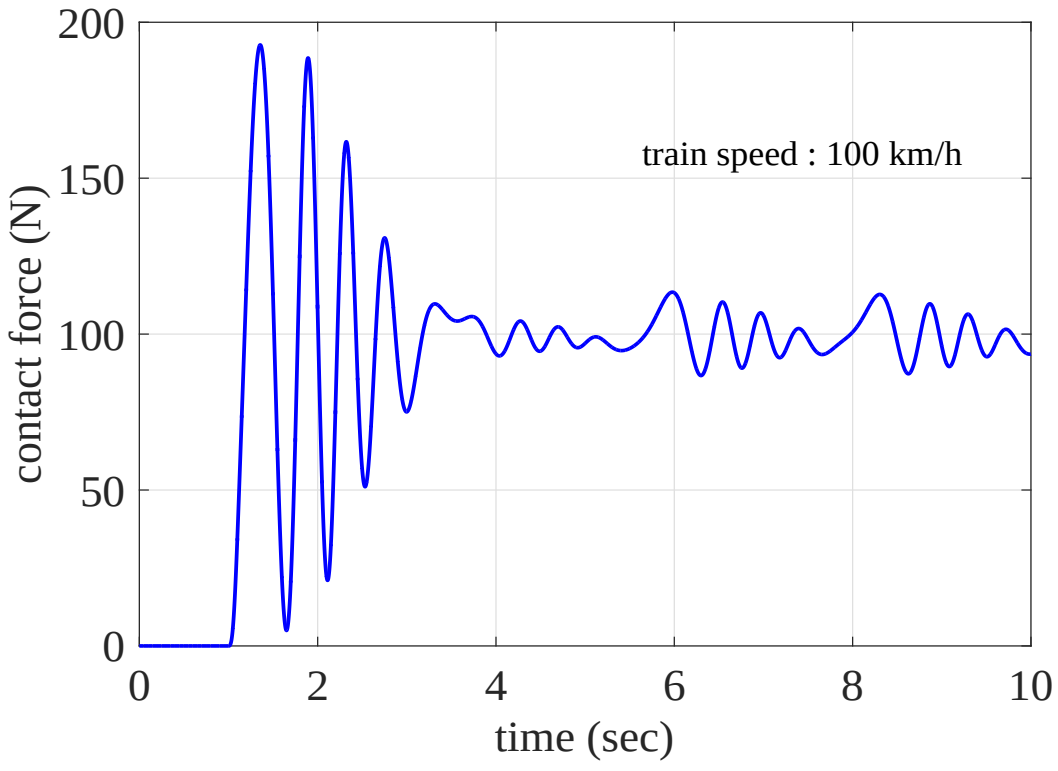

(a)

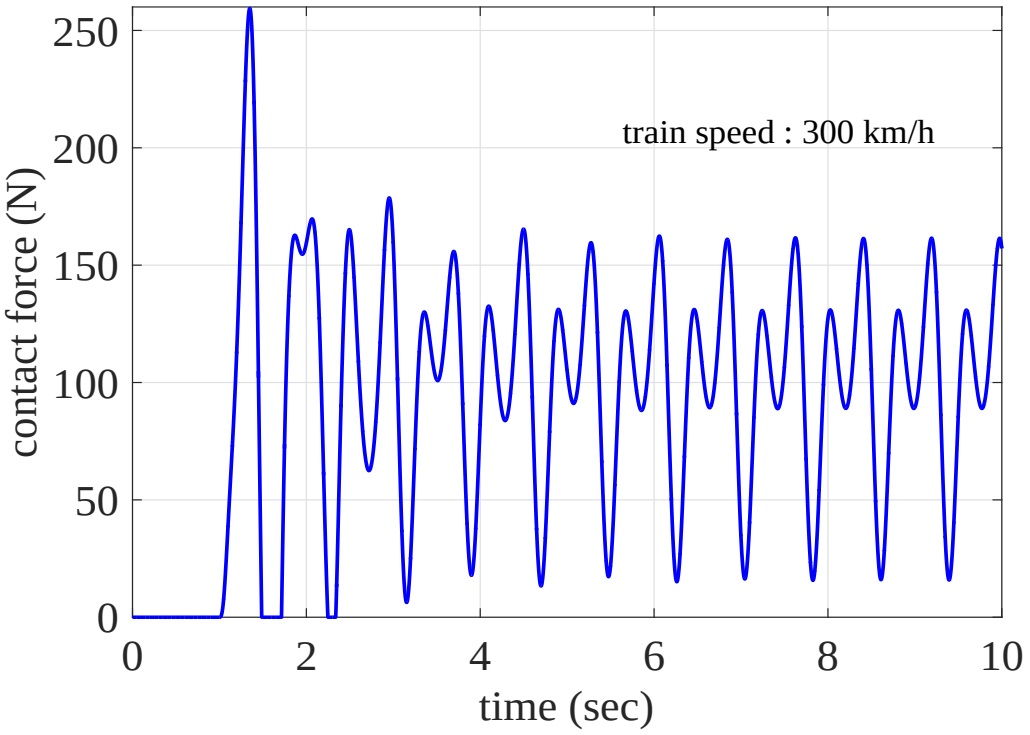

(b)

Fig. 5.3 *Contact force in open-loop with an uplift force of 100 N (a) with train speed of 100 km/h, (b) with train speed of 300 km/h*

Table 5.1 Pantograph-catenary system parameters

Parameters	Notations	Values
Catenary	K_0	3.6 kNm^{-1}
	α_s	0.5
	L	65 m
	K_{cat}	1535 kNm^{-1}
Pantograph shoe	K_s	82.3 kNm^{-1}
Pantograph head	m_2	8 kg
	C_2	120 Nsm^{-1}
	K_2	10 kNm^{-1}
Pantograph frame	m_1	12 kg
	C_1	30 Nsm^{-1}
	K_1	100 Nm^{-1}

Table 5.2 Controller gains

PI controller	I&I controller	SMC controller
$K_p = 10$	$k_a = 5000$	$K_{smc} = 10$
$K_v = 1.1$	$k_b = 450$	$\lambda_1 = 1$
$K_i = 70$		$\lambda_2 = 1$

Figure 5.4 shows the contact force in the actual and target systems under normal conditions with a constant train speed of 300 km/h. The reference contact force is 100 N. It can be seen that the actual system is following the target system. The oscillations in the steady state shows a very small variation of $\pm$ 1 N in the contact force. These oscillations are influenced by the speed of the train because the catenary is modeled as a time varying stiffness, where one of the factor affecting the stiffness is the train speed.

To check the performance of the controller against variable train speed, a speed profile is generated as shown in Figure 5.5a. Figure 5.5b shows the contact force in the actual and target system for the variable train speed. Again the performance of the controller is satisfactory.

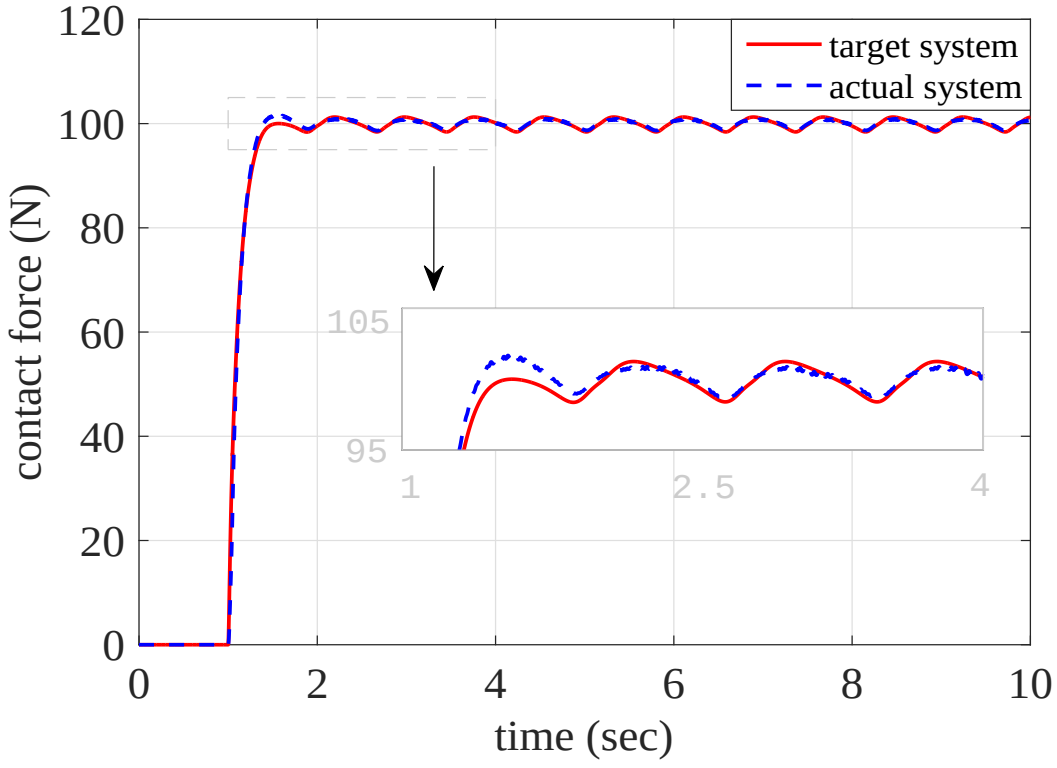

Fig. 5.4 *Contact force in actual and target systems under normal conditions, where the solid red line represents target system data, the dashed blue line represents the actual system data*

The manifold with off-the-manifold dynamics is shown in Figure 5.6. The sliding surface with error dynamics is shown in Figure 5.7. It can be seen that both off-the-manifold dynamics and error dynamics are converging onto the manifold and the sliding surface respectively. Figures 5.8 shows the active and semi-active control signals in the hybrid controller. To check the robustness of the controller, band-limited white noise is added to mass m_2 at time 5 second, and the results are shown in Figure 5.9a. In the first case the amplitude of the band-limited white noise is 10% of the saturation limits of the active actuator. Then it is increase to 30% and finally to 50%. In all the three cases shown in Figure 5.9a, performance of the controller against band-limited white noise is good.

Figure 5.9b shows the saturation effects and bandwidth consideration of the active actuator and semi-active device. A step disturbance signal with an amplitude of 50 N is added to mass m_2 at time 5 second. In this case, the hybrid controller performed well. Then the amplitude of the step disturbance signal is increased to 150 N and now it is not possible for the hybrid controller to keep the contact for constant between pantograph and catenary. In the last case the amplitude of the step disturbance signal is increased to 250 N, which is equal to the saturation limits of the active actuator and semi-active device. It can be seen in Figure 5.9b, that the contact between pantograph and catenary is lost.

Figure 5.10 shows the contact force in the actual and target systems for the second case where the catenary is modelled as a constant stiffness. It can be seen that there are no oscillations in the steady state at 100 N because the catenary is modelled as a constant stiffness. The hybrid control methodology using active actuator and semi-active device has minimized the oscillations between the pantograph and catenary by keeping the contact force between them constant. One of the advantages of using the proposed hybrid controller is that a semi-active device can easily be mounted on the pantograph upper arm without compromising the weight and the size. To assist the semi-active device and to achieve the desired performance, an active actuator is placed at the base of the pantograph.

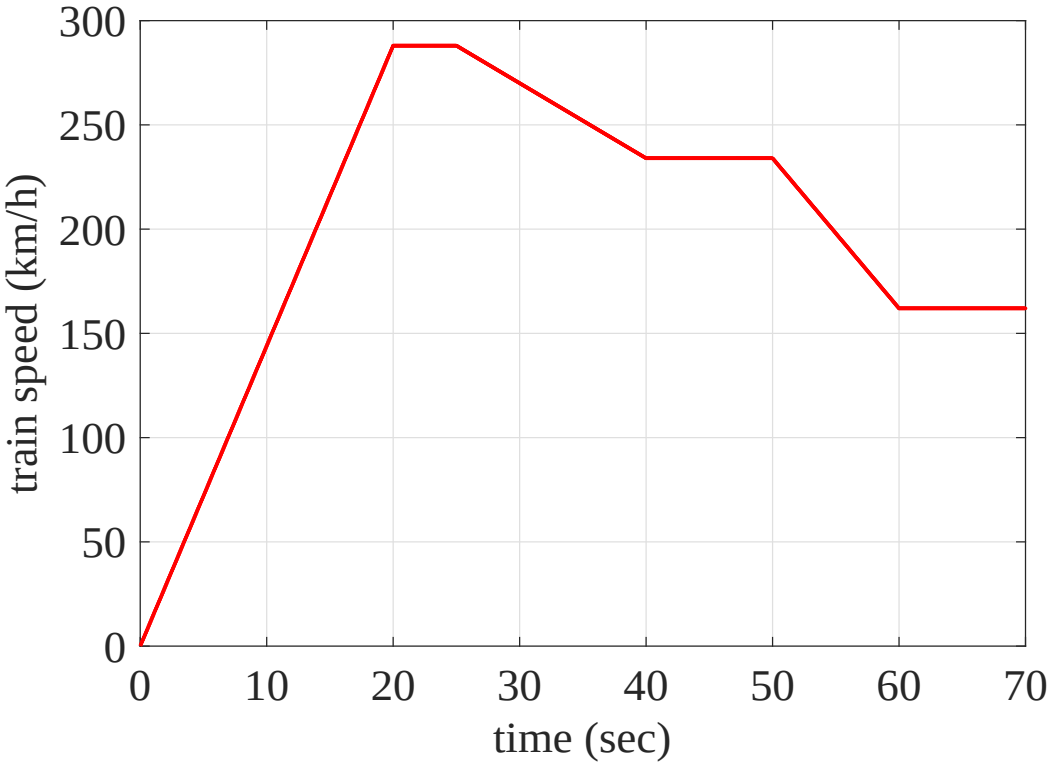

(a)

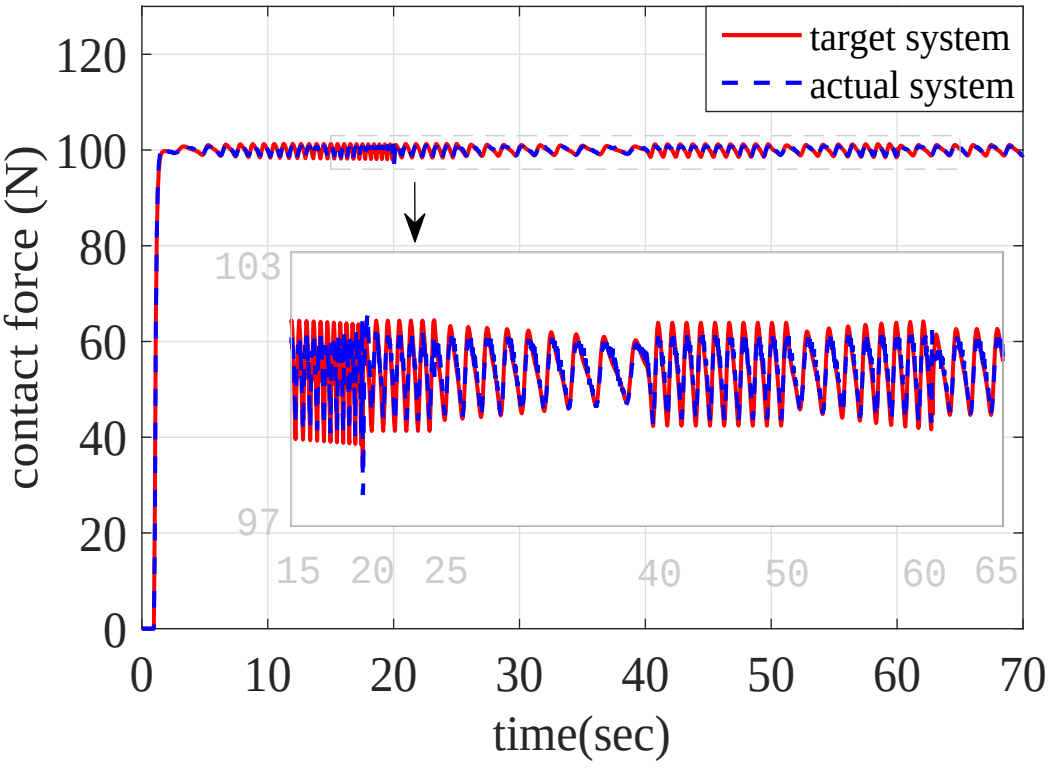

(b)

Fig. 5.5 *Contact force in actual and target systems with train speed profile, where the solid red line represents target system data, the dashed blue line represents the actual system data (a) train speed profile (b) contact force in actual and target system*

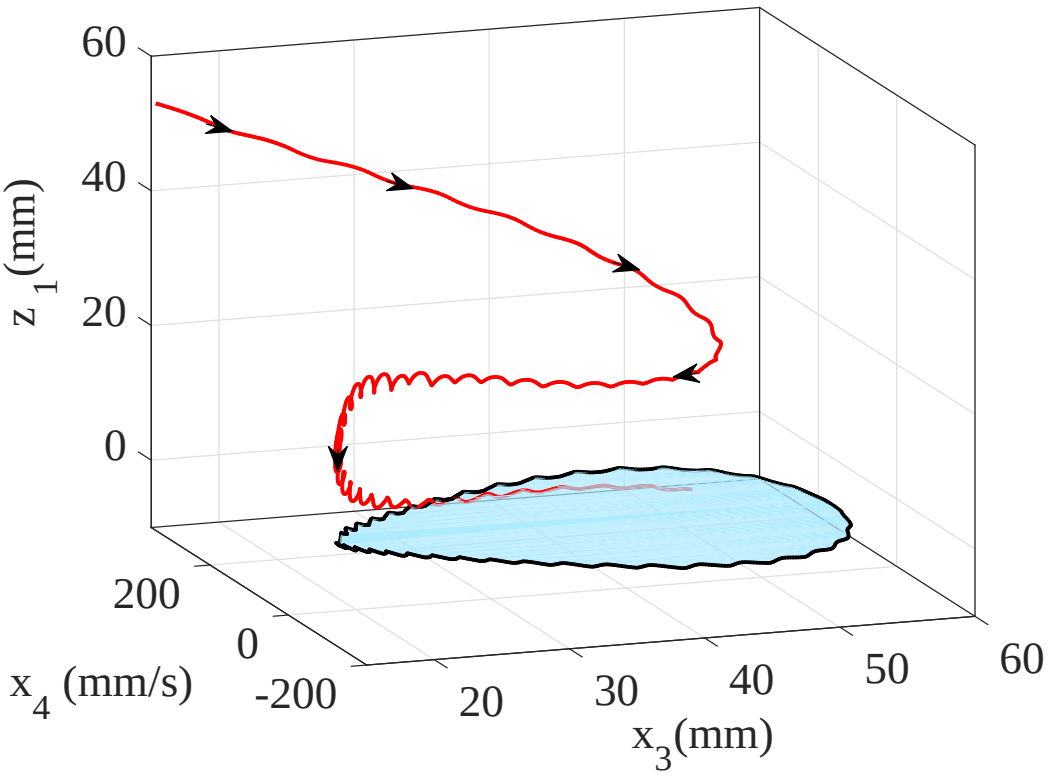

(a)

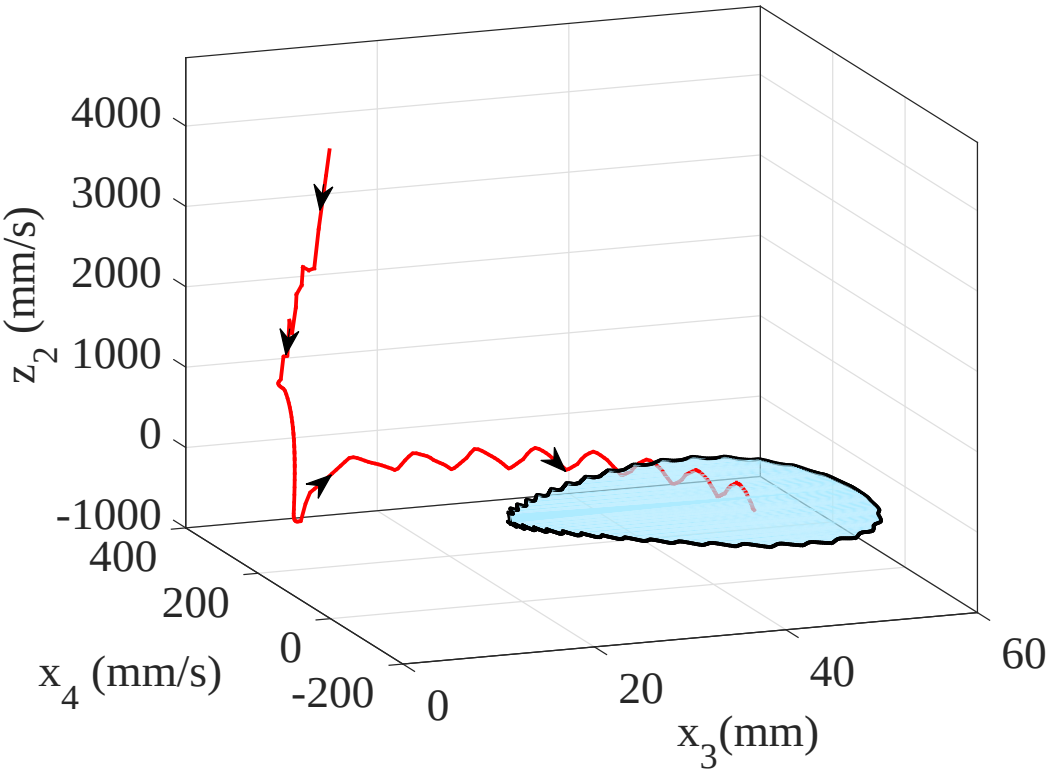

(b)

Fig. 5.6 *Manifold with off-the-manifold dynamics*

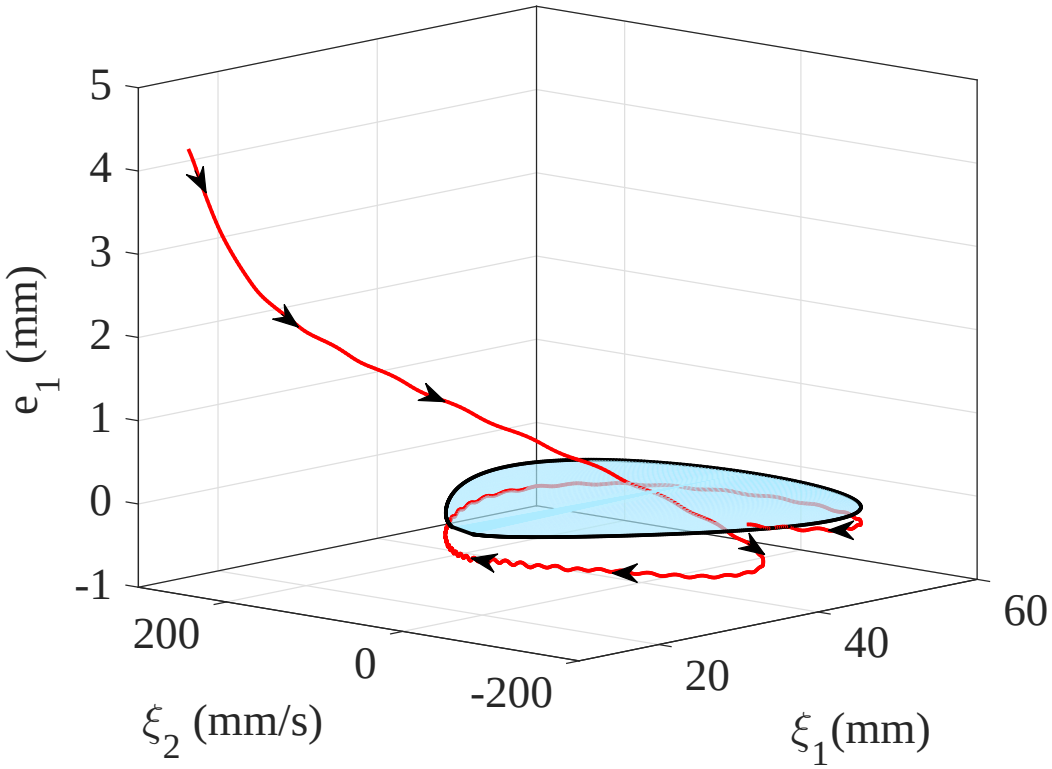

(a)

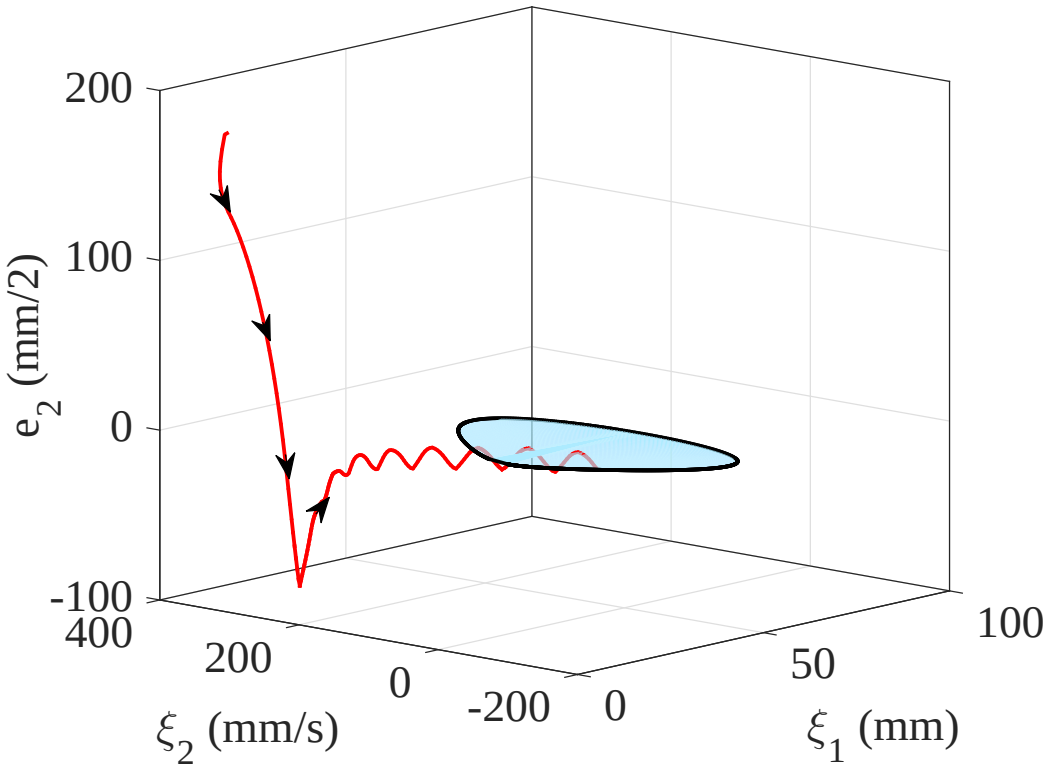

(b)

Fig. 5.7 *Sliding surface with error dynamics*

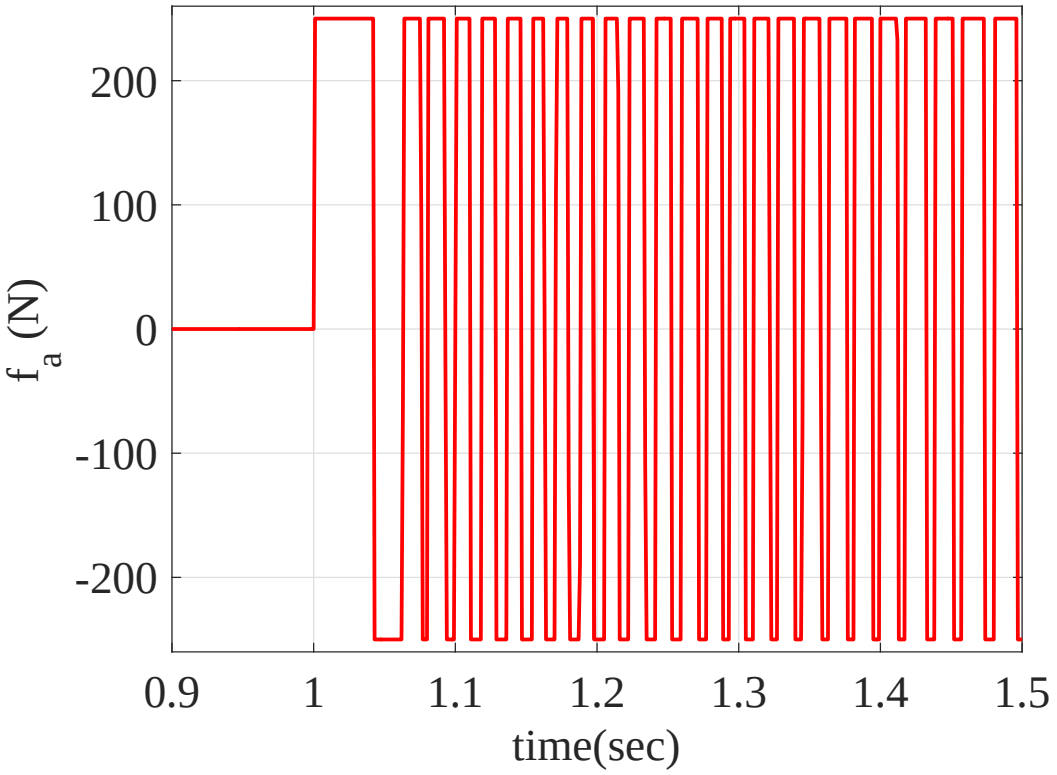

(a)

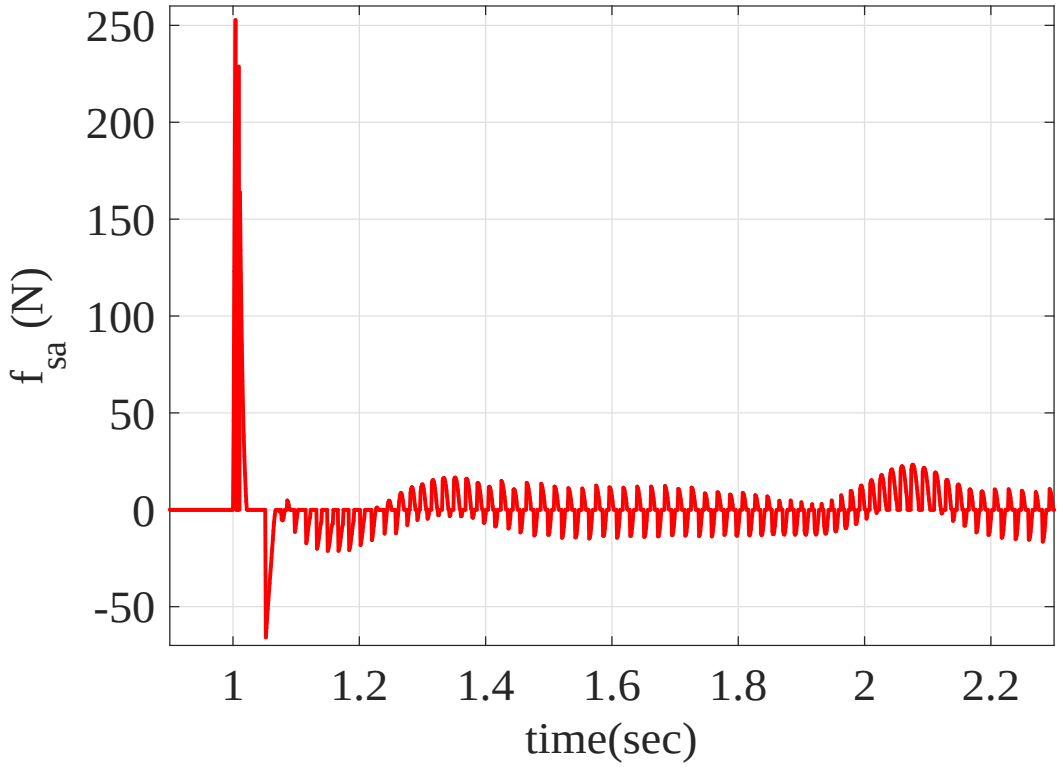

(b)

Fig. 5.8 *Active & semi-active control signals in hybrid controller, (a) active control signal, (b) semi-active control signal*

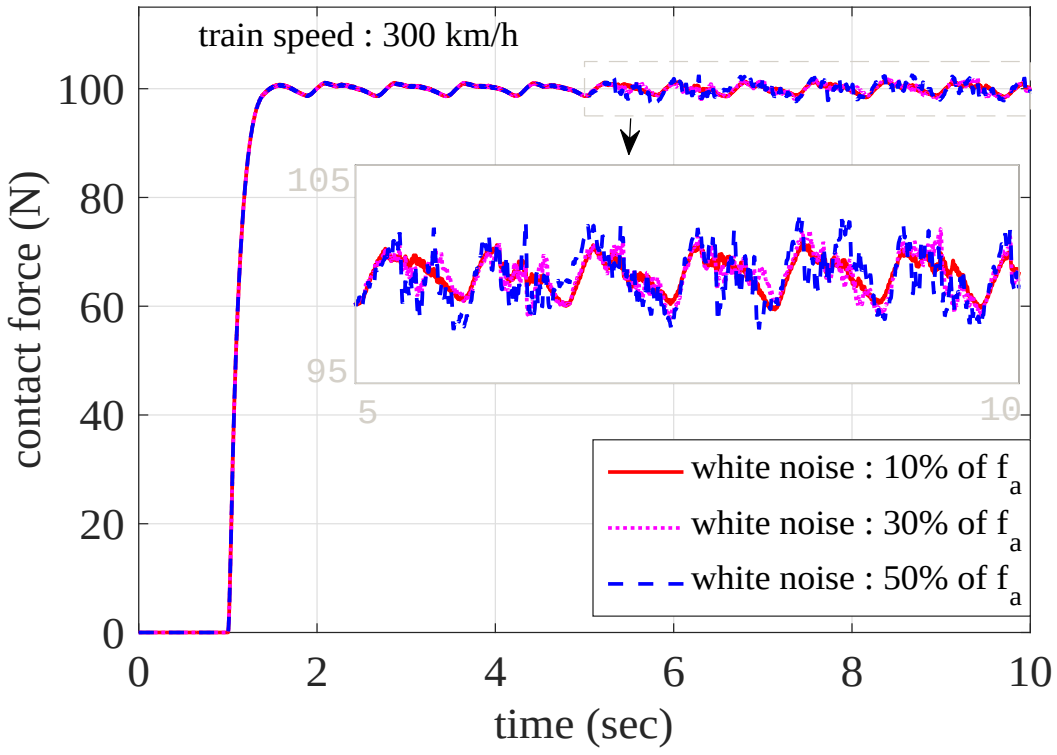

(a)

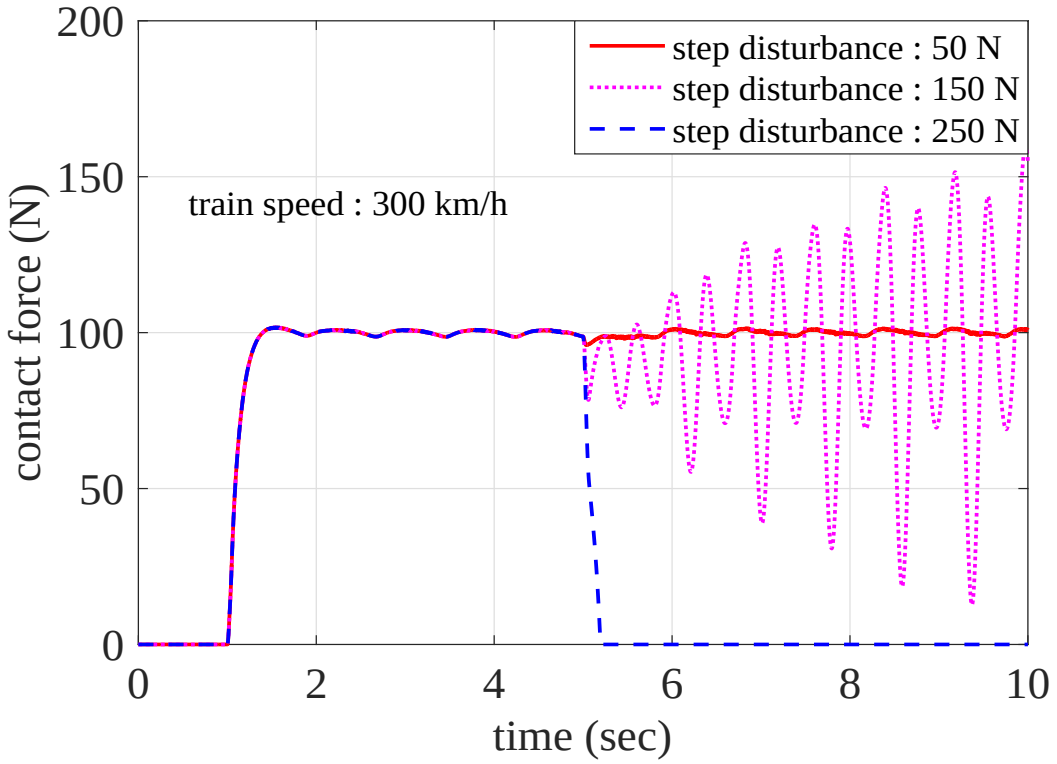

(b)

Fig. 5.9 *Contact force in actual system with band-limited white noise and step disturbance (a) with band-limited white noise introduced to mass m_2 at time 5 second, (b) with step disturbance introduced to mass m_2 at time 5 second*

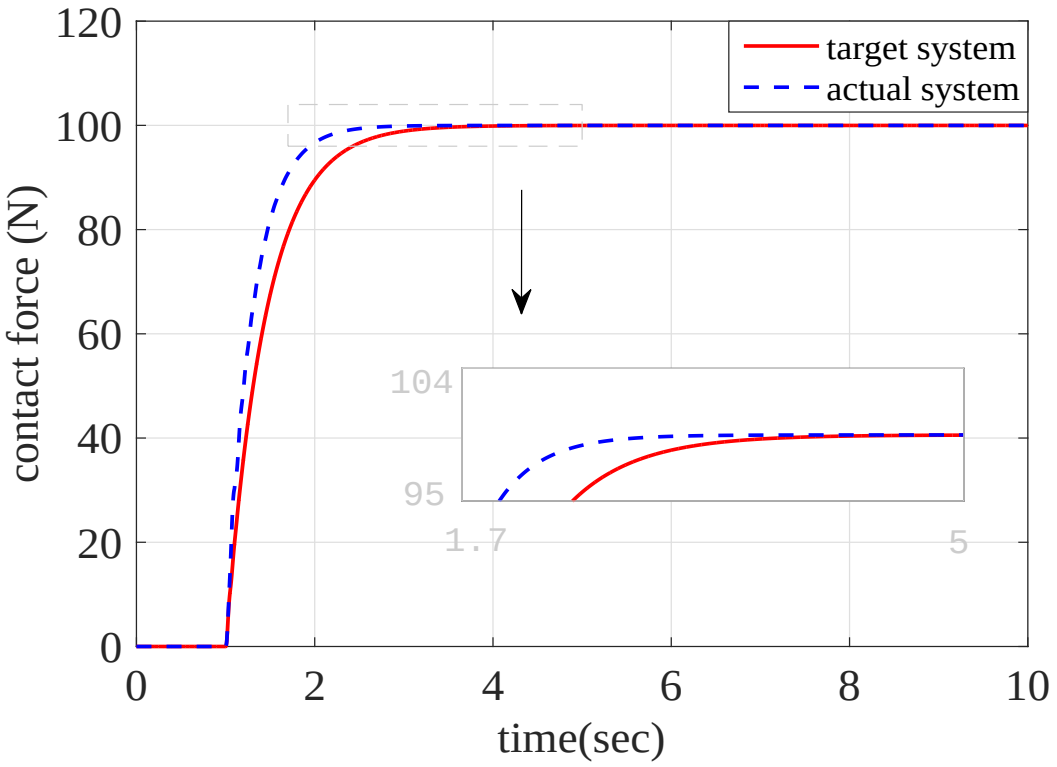

Fig. 5.10 *Contact force in actual and target systems for 2-DOF system with constant catenary stiffness, where the solid red line represents target system data, the dashed blue line represents the actual system data*

5.5 Summary

In this Chapter, an application of the hybrid controller is demonstrated. The hybrid control methodology, presented in Chapter 3, is implemented on a high-speed pantograph-catenary system. The control objective is to keep a constant contact force between the pantograph and catenary. The proposed controller has shown promising results both under normal conditions and in the presence of band-limited white noise, which demonstrates the robustness of the controller. Then the robustness was also checked against variable train speed with different slope variations and the results are satisfactory.

Two models of the pantograph-catenary system, one with time varying stiffness representing the catenary behaviour and other with a constant stiffness are used for the validation of the controller.

Chapter 6

Reduced Order Observer – Design Methodology and Validation

6.1 Introduction

Sensors are often the most expensive elements of a system, so to reduce the overall cost, the number of sensors ideally needs to be reduced. In some situations, it is difficult to place a sensor at a specific location, because of the environmental conditions or the structural design. It is often not possible to measure all the states of a dynamical system. The states are mostly required for control or monitoring purposes. Low-quality sensors can also add feedback noise to the system and degrade the overall performance of the controller. Some actuators available in the market have pre-installed sensors to measure the displacement or speed, but the cost of such actuators tends to be very high. Furthermore, to obtain the velocity, the displacement signal needs to be differentiated. Filtering needs to be done before differentiating which adds phase delay and ultimately affects the controller performance.

The solution to all these problems is to use an observer [149–151]. In this Chapter a reduced order observer using the notion of an invariant manifold will be presented and the system under consideration is the same as described in Chapter 3, so rather than assuming perfect measurements the states of the system will be observed. The

concept of an observer design was started in 1958 by Kalman and Bertram [152]. In 1960 further work was done by Kalman and then later in 1961 by Kalman and Bucy. In 1964 Luenberger introduced a new design methodology for an observer design [153]. The approach was deterministic rather than stochastic, and the observer had a reduced order as compared to the original system.

For nonlinear systems, the theory of linear observer design has been extended e.g. extended Luenburger observer [154, 155] or extended Kalman filter [156, 157]. As a result, the estimation is limited to a small domain and requires high computation power. In 1973 Thau [158] and then in 1975 Kou [159] were the first to attempt nonlinear techniques for the observer design. Since then a lot of work has been done on the observer design using nonlinear theory but mostly limited to certain classes of system that cannot typically be generalised to broader classes of systems.

The observers based on Lyapunov theory give sufficient conditions for the existence of the observer for nonlinear systems [160–162]. It may be possible for the low-order nonlinear systems to satisfy the conditions presented in the theorems based on Lyapunov theory but it is hard to find higher order nonlinear systems that can meet those conditions [163]. The observers based on extended linearization techniques linearize the error dynamics through a nonlinear output injection function [164–166]. This type of observer works locally at a fixed point but for multi-input-multi-output systems, the design methodology can be very complicated.

For nonlinear observers, models based on Lie-algebraic theory have also been used as described in the literature [167, 168]. In these techniques, the problems linked with nonlinear observer design have been dealt with by using linear techniques that exploit linear observer theory. One of the advantages of using Lie algebraic theory over the extended linearization techniques is that in the former case the observer is valid in any region where the transformation exists, whereas in the latter case the observer is designed at a fixed point. This method can also be used to create an observer for multi-input-multi-output systems. The down side of this technique is that the nonlinear

system must satisfy both a non-generic condition along with the finding of a necessary state transformation, which is not an easy task.

Generally, there are two ways to deal with observer design in nonlinear systems [19]. If the system nonlinearities are a linear function of unmeasured states or are monotonic, then observers based on linear theory can be used, or passivity can be exploited. Alternatively, the observer requires an existence of an attractive and invariant manifold. These types of observers are comprised of a linear filter and nonlinear output mapping functions. The theory of sliding mode has also been used to design observers for both linear and nonlinear systems [169, 170].

The observer design in the sliding mode methodology resembles the one proposed in this Chapter up to the extent of defining an asymptotically stable surface, which is called the sliding surface in the former and a manifold in the latter. In the sliding mode observer, the sliding surface is defined in terms of the error between the estimated and known states. A discontinuous/switching function is defined to bring the error dynamics to the sliding surface [171, 172]. Whereas in the proposed approach the observer design is reduced to make the error dynamics asymptotically stable, which depends on the definition of the mapping functions. The sliding mode observer is known for its insensitivity to parameter variation and disturbance rejection but the observer matching condition restricts the applicability of the sliding mode observer, and the system has to be minimum phase [173, 174]. This means that all the zeros of the system should be in the left half plane, or in other words the internal dynamics of the system need to be stable for the design of the first order sliding mode observer. To overcome this issue higher order sliding mode observers are proposed [175, 176]. However, the technique proposed in the present contribution could be extended, in a similar fashion for non-minimum phase systems [19].

There are mainly two types of sliding mode observer. The models based on equivalent control methods are the Utkin observers and the type based on Lyapunov methods are the Walcott and Zak observers [177]. The Utkin sliding mode observers [178] do not have a static observer gain. The disadvantage of not having a static observer

gain is that the state estimation can be performed only with the bounded error and not asymptotically. The Walcott and Zak observers have a static observer gain and the error is reduced based on system uncertainty. Another disadvantage of traditional sliding mode observers is the high-frequency switching action.

The theory for the observer developed by Astolfi *et al.* [19], has been implemented on many systems, such as the ball and beam system, the range estimation in a vision system and the magnetic levitation system. The present contribution builds upon these previous studies by demonstrating an application of the observer to a real mechanical system both in an open loop and closed loop, so that the robustness to parameter variation, external disturbance and measurement noise, can be explored for the first time. Therefore, the idea presented by Astolfi *et al.* is further extended to systems with nonlinear stiffness. In this work a reduced order observer using the notion of an invariant manifold has been designed for a 2-DOF mass-spring-damper system to estimate the displacement and velocity of one of the masses. In addition, a comparative study is presented with an observer based on the off-line solution of the Riccati equation for systems with Lipschitz type nonlinearity.

In [179–182] the observer designs based on the solution of the Riccati equation are proposed for systems with Lipchitz type nonlinearity. In the above mentioned literature, the only test performed to check the validity of the observer is that of different initial conditions given to the actual system, and it is shown that the observer is converging. In addition to that, the robustness of the observer against parameter variation, measurement noise or external disturbance is also not being discussed. In this Chapter in addition to the initial condition test, both the proposed observer and the observer based on the off-line solution of the Riccati equation are tested for robustness against parameter variation, measurement noise and external disturbance.

The approach presented in this Chapter requires the existence of a manifold that should be invariant and attractive [183–187]. The manifold is made invariant by a nonlinear filter and attractive by the proper selection of mapping functions. To prove the validity of the proposed observer, it is compared with a very well known nonlinear

observer based on Lipschitz type non-linearity presented in [188], which relies on the off-line solution of the Riccati equation. The reason for this comparison is that the system under consideration has a Lipschitz type nonlinearity.

In Section 6.2 the proposed observer design methodology is presented. The proposed observer design is applied to the example system in Section 6.3. The example system is the same as described in Chapter 3, so the states of the system will be observed instead of assuming perfect measurements. In Section 6.4 an observer based on Lipschitz type non-linearity is designed for the same example system. Simulation and experimental results with discussion are presented in Section 6.5 and Section 6.6 respectively. Finally, the summary is presented in Section 6.7.

6.2 Proposed Observer Design Methodology

Consider a nonlinear, time-varying system described as

$$\dot{\eta} = f(\eta, y, t), \tag{6.1}$$

$$\dot{y} = h(\eta, y, t), \tag{6.2}$$

where $\eta \in \mathbb{R}^q$ is the unmeasured state, $y \in \mathbb{R}^z$ is the measurable output, an over-dot represents differentiation with respect to time, $f(\eta, y, t)$ and $h(\eta, y, t)$ are nonlinear functions. It is assumed that $f(\eta, y, t)$ and $h(\eta, y, t)$ are forward complete, *i.e.* trajectories starting at time t_0 are defined for all times $t \geq t_0$.

Let $\hat{\eta} \in \mathbb{R}^s$ represent the observer state. Then the dynamical system

$$\dot{\hat{\eta}} = \alpha_o(\hat{\eta}, y, t), \tag{6.3}$$

is called an observer for the system (6.1)-(6.2), if there exist mappings

$$\beta : \mathbb{R}^s \times \mathbb{R}^z \times \mathbb{R} \to \mathbb{R}^s,$$

$$\phi : \mathbb{R}^q \to \mathbb{R}^s,$$

with ϕ left invertible, such that the manifold

$$\mathscr{M}_t = \{(\eta, y, \hat{\eta}) \in \mathbb{R}^q \times \mathbb{R}^z \times \mathbb{R}^s : \ \beta(\hat{\eta}, y, t) = \phi(\eta)\}, \tag{6.4}$$

has the following properties [19]:

1. All trajectories of the extended system (6.1)-(6.3) that start on the manifold $\mathscr{M}_t$ at time t remain there for all future times, $\tau > t$ i.e. $\mathscr{M}_t$ is positively invariant.

2. All trajectories of the extended system (6.1)-(6.3) that start in a neighborhood of $\mathscr{M}_t$ asymptotically converge to $\mathscr{M}_t$.

A mapping function $\Psi(x, y, t) : \ \mathbb{R}^l \times \mathbb{R}^z \times \mathbb{R} \to \mathbb{R}^s$ is left invertible with respect to x, if there exists another mapping $\Psi^L : \ \mathbb{R}^s \times \mathbb{R}^z \times \mathbb{R} \to \mathbb{R}^l$ such that $\Psi^L(\Psi(x, y, t), y, t) = x$ for all $x \in \mathbb{R}^l$ and for all y, t.

So from the above definition of left invertibility, the estimate of η is given by $\phi^L(\phi(\eta))$ and the estimate on the manifold is given by $\phi^L(\beta(\hat{\eta}, y, t))$, as the estimation error $\hat{\eta} - \eta$ is zero on the manifold.

Proposition :

Consider the system (6.1)-(6.3), and suppose that there exist mappings, $\beta : \mathbb{R}^s \times \mathbb{R}^z \times \mathbb{R} \to \mathbb{R}^s$ and $\phi : \mathbb{R}^q \to \mathbb{R}^s$, with ϕ left invertible, such that the following conditions hold.

(A1) The mapping function β should be chosen such that $\det\left(\dfrac{\partial \beta}{\partial \hat{\eta}}\right) \neq 0$.

(A2) Because the off-the-manifold trajectories are given as

$$z = \beta(\hat{\eta}, y, t) - \phi(\eta), \tag{6.5}$$

the z dynamics are then given as

$$\dot{z} = \frac{\partial \beta}{\partial \hat{\eta}} \alpha_o(\hat{\eta}, y, t) + \frac{\partial \beta}{\partial y} h(\eta, y, t) + \frac{\partial \beta}{\partial t} - \frac{\partial \phi}{\partial \eta} f(\eta, y, t). \tag{6.6}$$

On the manifold, z and $\dot{z}$ will converge to zero and then the function $\alpha_o(\hat{\eta}, y, t)$ will be an observer for the system (6.1)-(6.2), given by

$$\alpha_o(\hat{\eta}, y, t) = \left(\frac{\partial \beta}{\partial \hat{\eta}}\right)^{-1} \left(- \frac{\partial \beta}{\partial y} h(\phi^L(\beta(\hat{\eta}, y, t)), y, t) - \frac{\partial \beta}{\partial t} + \frac{\partial \phi}{\partial \eta} \Big|_{\eta = \phi^L(\beta(\hat{\eta}, y, t))} f(\phi^L(\beta(\hat{\eta}, y, t)), y, t) \right). \tag{6.7}$$

For dynamics that are not on the manifold (i.e. $z \neq 0$), then substituting the function $\alpha_o(\hat{\eta}, y, t)$ from (6.7) in (6.6) and making sure that (A1) holds, gives

$$\dot{z} = \frac{\partial \beta}{\partial y} \left(h(\eta, y, t) - h(\phi^L(\phi(\eta) + z), y, t) \right) - \frac{\partial \phi}{\partial \eta} f(\eta, y, t) + \frac{\partial \phi}{\partial \eta} \Big|_{\eta = \phi^L(\phi(\eta) + z)} f\left(\phi^L(\phi(\eta) + z), y, t\right). \tag{6.8}$$

The mapping functions should be selected in such a way that (6.8) has a (locally) asymptotically stable equilibrium at $z = 0$, uniformly in η, y, t , where ϕ^L is the left inverse of ϕ and z is the distance between system trajectories and the manifold.

It can be seen from (6.7) that (A1) should hold for the existence of function $\alpha_o(\hat{\eta}, y, t)$. (A2) should hold for the asymptotic convergence of off-the-manifold trajectories towards the manifold and making sure that the distance z is going to zero. The function $\alpha_o(\hat{\eta}, y, t)$ renders the manifold invariant and (A2) makes the manifold attractive. So the problem of observer design has been reduced into making the $\dot{z}$ dynamics asymptotically stable.

6.3 Proposed Observer Design for the Example System

The purpose is to design an observer that will operate efficiently for this closed loop system. More specifically, an observer that can estimate the displacement and velocity for one of the two degrees-of-freedom is a suitable solution in this case. The equation of motion for the two degree-of-freedom system presented in Chapter 3 is given by (6.9), where X_1 and X_2 represent the displacement of mass m_1 and m_2 respectively, f_a represents the force of the active actuator, f_{sa} represents the force of the semi-active device (MR damper), m_1, m_2 represent the masses, K_1, K_2 are the linear spring stiffness, K_3 is the nonlinear spring stiffness, C_1 is the damping coefficient and U_d is an excitation signal.

$$\begin{bmatrix} m_1 & 0 \\ 0 & m_2 \end{bmatrix} \begin{bmatrix} \ddot{X}_1 \\ \ddot{X}_2 \end{bmatrix} + \begin{bmatrix} C_1 & 0 \\ 0 & 0 \end{bmatrix} \begin{bmatrix} \dot{X}_1 \\ \dot{X}_2 \end{bmatrix} + \begin{bmatrix} K_1+K_2 & -K_2 \\ -K_2 & K_2 \end{bmatrix} \begin{bmatrix} X_1 \\ X_2 \end{bmatrix} = \begin{bmatrix} -K_3 \\ 0 \end{bmatrix} X_1^3 + \begin{bmatrix} f_a - f_{sa} \\ f_{sa} - U_d \end{bmatrix} \tag{6.9}$$

The system can be represented in state space form as

$$\begin{aligned} \dot{x}_1 &= x_2, \\ \dot{x}_2 &= \frac{1}{m_1}\Big(f_a - f_{sa} - K_1 x_1 - C_1 x_2 - K_2(x_1 - x_3) - K_3 x_1^3\Big), \\ \dot{x}_3 &= x_4, \\ \dot{x}_4 &= \frac{1}{m_2}\Big(f_{sa} - K_2(x_3 - x_1) - U_d\Big), \end{aligned} \tag{6.10}$$

where x_1 and x_2 are the unknown states representing the displacement and velocity of mass m_1 respectively; x_3 and x_4 are the known states representing the displacement and velocity of mass m_2, respectively.

Following the observer design methodology presented in Section 6.2, the mapping functions $\phi(x_1, x_2)$ and $\beta(\hat{\eta}, x_3, x_4)$ can be defined as

$$\phi(x_1,x_2) = \begin{bmatrix} x_1 \\ x_2 \\ K_3 x_1^3 \end{bmatrix}; \quad \beta\left(\hat{\eta},x_3,x_4\right) = \begin{bmatrix} \beta_1\left(\hat{\eta},x_3,x_4\right) \\ \beta_2\left(\hat{\eta},x_3,x_4\right) \\ \beta_3\left(\hat{\eta},x_3,x_4\right) \end{bmatrix} \tag{6.11}$$

where $\hat{\eta}$ represents the observer states. The mapping $\phi(x_1,x_2)$ is defined in terms of the unknown states, in such a way that the rank of the matrix is equal to the number of rows; hence the condition of left invertibility is satisfied. The mapping $\beta\left(\hat{\eta},x_3,x_4\right)$ is defined in terms of the known states and the observer states.

Here z represents the distance between system trajectories and the manifold, such that

$$z = \beta\left(\hat{\eta},x_3,x_4\right) - \phi(x_1,x_2). \tag{6.12}$$

The error dynamics are then given as

$$\dot{z} = \frac{\partial\beta}{\partial\hat{\eta}}\dot{\hat{\eta}} + \frac{\partial\beta}{\partial x_3}\dot{x}_3 + \frac{\partial\beta}{\partial x_4}\dot{x}_4 - \dot{\phi}(x_1,x_2), \tag{6.13}$$

which becomes

$$\dot{z} = \frac{\partial\beta}{\partial\hat{\eta}}\dot{\hat{\eta}} + \frac{\partial\beta}{\partial x_3}x_4 + \frac{\partial\beta}{\partial x_4}\frac{1}{m_2}\Big(f_{sa} - K_2(x_3 - x_1)\Big) - \begin{bmatrix} x_2 \\ \dot{x}_2 \\ 3K_3x_1^2x_2 \end{bmatrix}, \tag{6.14}$$

leading to

$$\dot{z} = \frac{\partial \beta}{\partial \hat{\eta}} \dot{\hat{\eta}} + \frac{\partial \beta}{\partial x_3} x_4 + \frac{\partial \beta}{\partial x_4} \frac{1}{m_2} \Big(f_{sa} - K_2(x_3 - (\beta_1 - z_1)) \Big) - \begin{bmatrix} \beta_2 - z_2 \\ \frac{1}{m_1} \Big(f_a - f_{sa} - K_1(\beta_1 - z_1) - C_1(\beta_2 - z_2) - K_2(\beta_1 - z_1 - x_3) - (\beta_3 - z_3) \Big) \\ 3K_3(\beta_1 - z_1)^2(\beta_2 - z_2) \end{bmatrix} \tag{6.15}$$

Selection of the mapping functions is a non-trivial task. If the $\beta(\hat{\eta}, x_3, x_4)$ mapping function is selected in such a way that (A1) holds then the observer dynamics can be selected as in (6.7) to give

$$\dot{\hat{\eta}} = \left(\frac{\partial \beta}{\partial \hat{\eta}} \right)^{-1} \left(- \frac{\partial \beta}{\partial x_3} x_4 - \frac{\partial \beta}{\partial x_4} \frac{1}{m_2} \Big(f_{sa} - K_2(x_3 - \beta_1) \Big) \right) + \left(\frac{\partial \beta}{\partial \hat{\eta}} \right)^{-1} \begin{bmatrix} \beta_2 \\ \frac{1}{m_1} \Big(f_a - f_{sa} - K_1\beta_1 - C_1\beta_2 - K_2(\beta_1 - x_3) - \beta_3 \Big) \\ 3K_3\beta_1^2\beta_2 \end{bmatrix} \tag{6.16}$$

Then the error dynamics become

$$\dot{z} = \frac{\partial \beta}{\partial x_4} \frac{1}{m_2} \Big(- K_2 z_1 - C_2 z_2 \Big) - \begin{bmatrix} -z_2 \\ \frac{1}{m_1} \Big((K_1 + K_2) z_1 + C_1 z_2 + C_2 z_2 + z_3 \Big) \\ -3K_3 x_1^2 z_2 \end{bmatrix} \tag{6.17}$$

Now the mapping function $\beta(\hat{\eta}, x_3, x_4)$ needs to be selected in such a way that (A1) and (A2) are satisfied. The $\beta(\hat{\eta}, x_3, x_4)$ mapping function is selected as

$$\beta(\hat{\eta}, x_4) = \begin{bmatrix} \hat{\eta}_1 & \hat{\eta}_2 & \hat{\eta}_3 + \dfrac{3K_3 m_2 \upsilon x_4}{C_2} \end{bmatrix}^{\intercal}, \tag{6.18}$$

where υ is a constant.

1. The first condition that needs to be satisfied by the $\beta(\hat{\eta}, x_3, x_4)$ mapping function is $\det\left(\dfrac{\partial \beta}{\partial \hat{\eta}}\right) \neq 0$. For the function given in (6.18) we have

   $$\det\left(\frac{\partial \beta}{\partial \hat{\eta}}\right) = 1$$

   Therefore the first condition is satisfied.

2. The second condition is that the error dynamics

   $$\dot{z} = \begin{bmatrix} z_2 \\ -\dfrac{1}{m_1}\Big((K_1 + K_2)z_1 + (C_1 + C_2)z_2 + z_3\Big) \\ -\dfrac{3K_2K_3\upsilon z_1}{C_2} - 3K_3\upsilon z_2 + 3K_3 x_1^2 z_2 \end{bmatrix} \tag{6.19}$$

   should have an asymptotically stable equilibrium at $z = 0$. As the error dynamics are nonlinear, to analyze the stability, Lyapunov function is used. Let

   $$V(z) = \frac{1}{2}\left(z_1^2 + z_2^2 + z_3^2\right) \tag{6.20}$$

   as a Lyapunov function, which is positive definite.

   Then

   $$\dot{V}(z) = -\left(\frac{C_1 + C_2}{m_1}\right) z_2^2 - \left(\frac{K_1 + K_2}{m_1} - 1\right)|z_1||z_2| - \left(\frac{3K_2K_3\upsilon}{C_2}\right)|z_1||z_3| - \left(3K_3\upsilon + \frac{1}{m_1}\right)|z_2||z_3| < 0 \tag{6.21}$$

As

$$V(0) = 0 \tag{6.22a}$$

$$V(z) > 0, \text{ in } D - \{0\} \tag{6.22b}$$

$$V(z) \text{ is radially unbounded} \tag{6.22c}$$

$$\dot{V}(z) < 0, \text{ in } D - \{0\}. \tag{6.22d}$$

Hence the equilibrium point $z = 0$ is global asymptotic stability, where D is the subset of $\mathbb{R}^p$ in which the Lyapunov function is defined.

In the next section the proposed observer is compared with an observer based on Lipschitz type nonlinearity.

6.4 Observer Design Based on Lipschitz Type Nonlinearity

For comparison purposes a nonlinear observer based on the off-line solution of the Riccati equation is designed for the system under consideration. This method is very well known for the class of systems that have Lipschitz type nonlinearity. The example system in this Chapter has a cubic stiffness, which is locally Lipschitz. As there is a limit on its growth due to the mechanical constraint, which makes it globally Lipschitz. Consider a system of the form

$$\begin{aligned} \dot{x} &= Ax + g(t,u,y) + f(t,u,x) \\ y &= Cx \end{aligned} \tag{6.23}$$

where $x \in \mathbb{R}^n$ is the system state, $y \in \mathbb{R}^z$ is the system measurable output, $u \in \mathbb{R}^m$ is the input, A and C are constant matrices, $g : \mathbb{R} \times \mathbb{R}^m \times \mathbb{R}^z \to \mathbb{R}^v$, $f : \mathbb{R} \times \mathbb{R}^m \times \mathbb{R}^v \to \mathbb{R}^v$, and an over-dot represents the differentiation with respect to time. The nonlinear function

$f(t,u,x)$ is assumed to be globally Lipschitz in x with a Lipschitz constant γ. A and C are assumed to be observable.

For the system in (6.23) the observer is defined as

$$\dot{\hat{x}} = A\hat{x} + g(t,u,y) + f(t,u,\hat{x}) + L(y - C\hat{x}) \tag{6.24}$$

where $\hat{x}$ represents the observer state, $L \in \mathbb{R}^{n\times z}$ is the observer gain matrix. The error dynamics are represented as

$$\dot{\tilde{x}} = (A - LC)\tilde{x} + f(t,u,x) + f(t,u,\hat{x}) \tag{6.25}$$

where $\tilde{x} = x - \hat{x}$.

Now the algorithm below presents a method to choose L which will make the error dynamics stable

1. Set ε to a positive value.
2. Solve the following Algebraic Riccati Equation (ARE)

$$AP + PA^{\intercal} + P\left(\gamma^2 I - \frac{1}{\varepsilon}C^{\intercal}C\right)P + I + \varepsilon I = 0. \tag{6.26}$$

3. If P is symmetric and positive definite, then setting

$$L = (\frac{1}{2\varepsilon})PC^{\intercal} \tag{6.27}$$

   in (6.24) gives stable error dynamics (6.25).

4. If not, set $\varepsilon = \dfrac{\varepsilon}{2}$ and go to step 2. If ε is below some precision value, abandon method.

The 2-DOF mass-spring-damper system (5.1) can be represented as

$$\dot{x} = Ax + f(x) + g(y)u \tag{6.28}$$

where

$$A = \begin{bmatrix} 0 & 1 & 0 & 0 \\ -\dfrac{(K_1+K_2)}{m_1} & -\dfrac{(C_1+C_2)}{m_1} & \dfrac{K_2}{m_1} & \dfrac{C_2}{m_1} \\ 0 & 0 & 0 & 1 \\ \dfrac{K_2}{m_2} & 0 & -\dfrac{K_2}{m_2} & 0 \end{bmatrix}; \quad g = \begin{bmatrix} 0 & 0 \\ \dfrac{1}{m_1} & -\dfrac{1}{m_1} \\ 0 & 0 \\ 0 & \dfrac{1}{m_2} \end{bmatrix}$$

$$f = \begin{bmatrix} 0 \\ 0 \\ 0 \\ -K_3 x_1^3 \end{bmatrix}; \quad C = \begin{bmatrix} 0 & 0 \\ 0 & 0 \\ 1 & 0 \\ 0 & 1 \end{bmatrix}^{\mathsf{T}}$$

A function $f(x)$ is said to be globally Lipschitz if there exists a constant γ such that for all $x_a, x_b \in \mathbb{R}^n$, the following holds,

$$|f(x_a) - f(x_b)| \leq \gamma |x_a - x_b| \tag{6.29}$$

To find the Lipschitz constant for the system under consideration, (6.29) is used as

$$|f(x_{1a}) - f(x_{1b})| \leq |K_3 x_{1a}^3 - K_3 x_{1b}^3|$$

$$|f(x_{1a}) - f(x_{1b})| \leq \gamma |x_{1a} - x_{1b}| \tag{6.30}$$

where $\gamma = |K_3||x_{1a}^2 + x_{1a}x_{1a} + x_{1b}^2|$. As there is a constraint on $x_1 \leq 27.5$ mm because of the mechanical design, this puts a saturation limit on the amplitude of nonlinearity and makes the system globally Lipschitz. The Lipschitz constant $\gamma = 7.56$ is computed using (6.30).

To compute the observer gain matrix L, the algorithm described above is used, ε is set to 1, and P is computed by solving the Riccati equation given in (6.26) using Matlab resulting in

$$P = \begin{bmatrix} 2.6699 & -0.1297 & -0.7979 & 0.0098 \\ -0.1297 & 0.0189 & -0.0039 & 0.0101 \\ -0.7979 & -0.0039 & 2.0582 & -0.1985 \\ 0.0098 & 0.0101 & -0.1985 & 0.0477 \end{bmatrix} \tag{6.31}$$

P is symmetric and positive definite, hence L is computed using (6.27), and the result is that

$$L = \begin{bmatrix} -0.3990 & -0.0020 & 1.0291 & -0.0993 \\ 0.0049 & 0.0051 & -0.0993 & 0.0238 \end{bmatrix}^{\mathsf{T}} \tag{6.32}$$

After designing the observers using both the proposed approach and the observer based on Lipschitz type nonlinearity, the simulation results are shown in the next section.

6.5 Simulation Results and Discussion

After designing observers for the 2-DOF mass-spring-damper system using the proposed technique and the method based on Lipschitz type nonlinearity, simulations were carried out using Matlab/Simulink to check the performance of both the observers under different conditions. Figures 6.1 shows the actual and estimated displacement and velocity of mass m_1 respectively under different conditions. Under normal conditions i.e. without any parameter variation or any phase change in the excitation signal, the performance of both the observers is satisfactory as shown in Figure 6.1a. In Figure 6.1b delay has been added to the phase of the excitation signal and the performance of the proposed observer is better than the observer based on Lipschitz type nonlinearity. Figure 6.1c shows the same signals but with the varied system parameters. Both the

masses m_1 and m_2 are increased by 25% and again the proposed observer is performing better.

To check the performance of both the observers against measurement noise, band-limited white noise is added to the acceleration of mass m_2. Both the observers are estimating well, but at some points, the proposed observer performance is better, as shown in Figure 6.2a. Now the band-limited white noise is added to the displacement of mass m_2. In this case, again the performance of the proposed observer is impressive, whereas, on the other hand, the observer based on Lipschitz type nonlinearity is not performing well as shown in Figure 6.2b. To further check the robustness of both the observers against different disturbances; a ramp, step, sinusoidal and random signals are used. Figure 6.3a and Figure 6.3b show the performance of both observers against step and ramp disturbance signals respectively introduced at mass m_2 for a period of one second and starting at one second. Both the disturbance signals start at one second and ending at two second. Again the proposed observer out-performed the other.

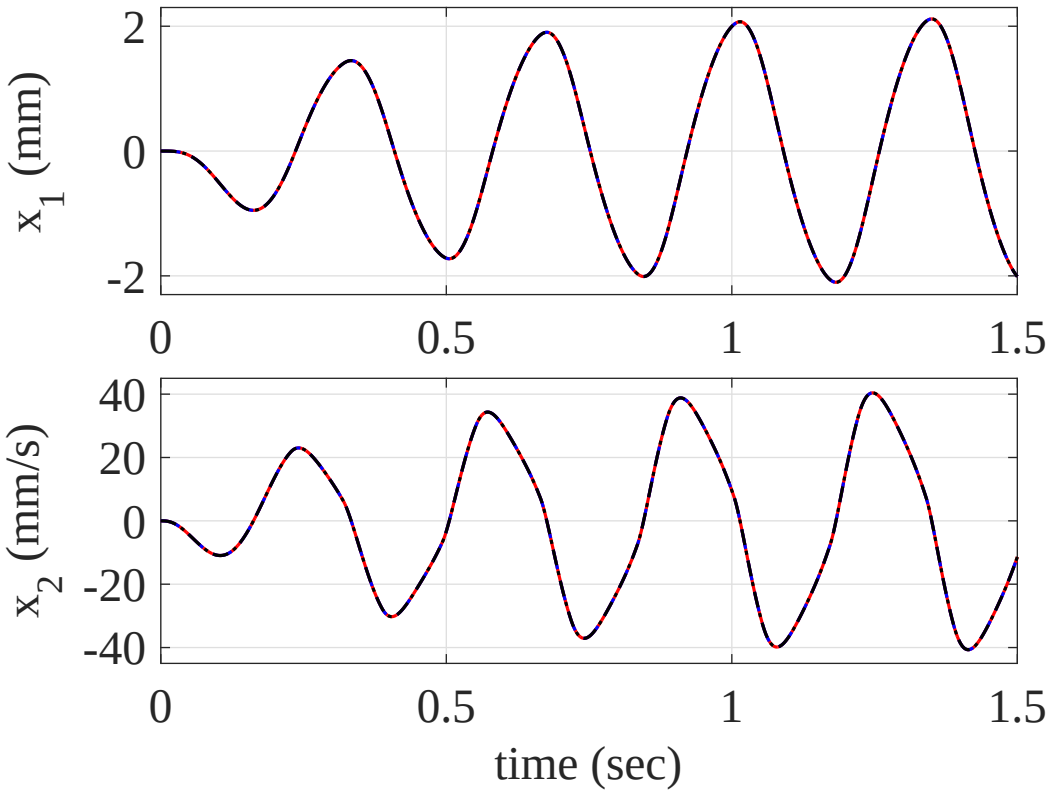

(a)

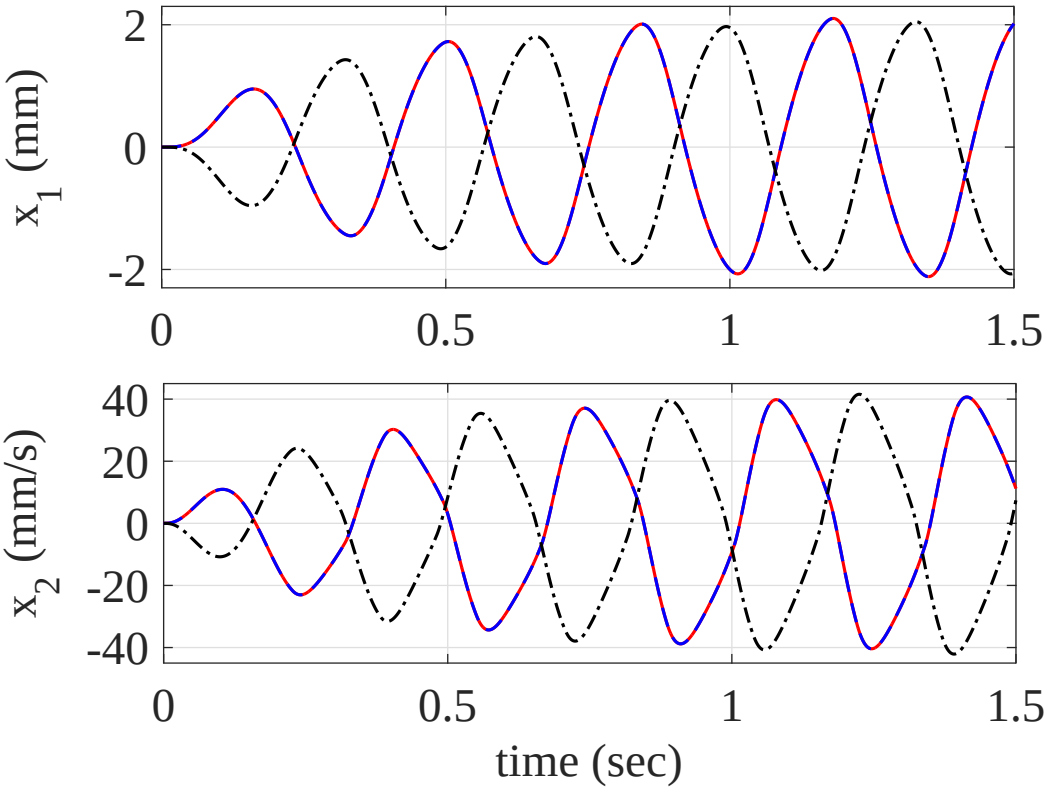

(b)

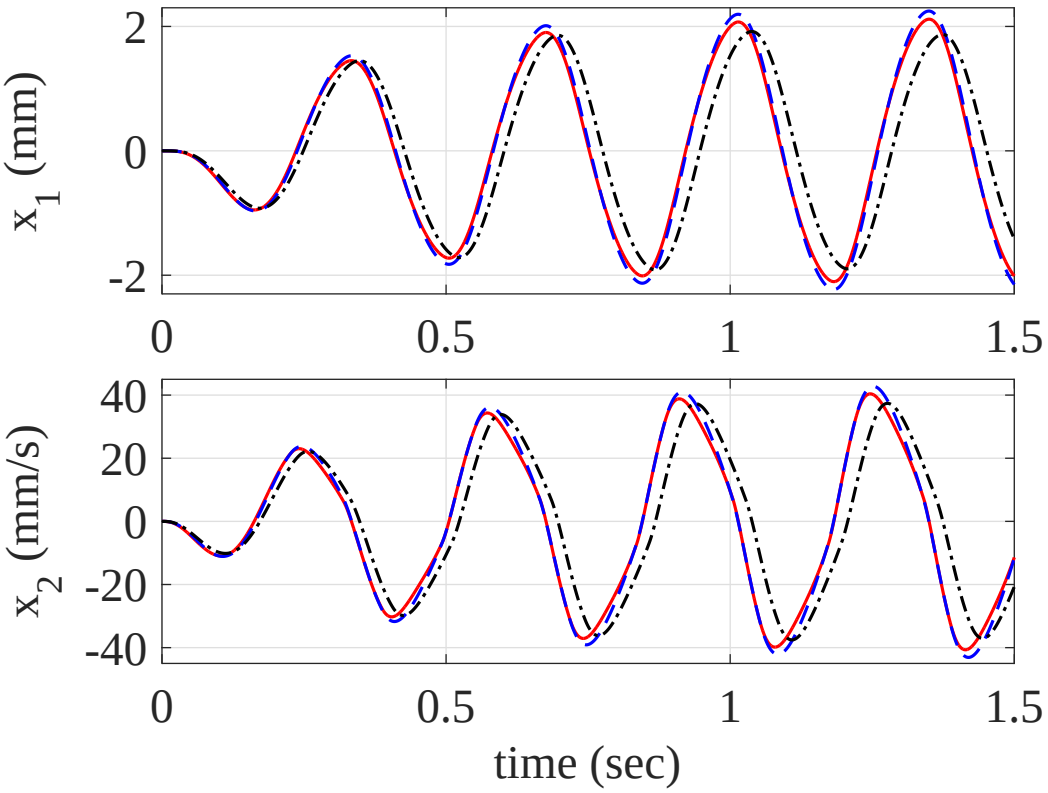

(c)

Fig. 6.1 *Simulated actual and estimated displacement and velocity of mass m_1. The solid red line represents actual measurements, the dashed blue line represents the estimated measurements using the proposed observer, the dash-dot black line represents the estimated measurements using the observer based on Lipschitz type nonlinearity, (a) under normal conditions, (b) with phase delay in the excitation signal, (c) with 25% increase in both the masses.*

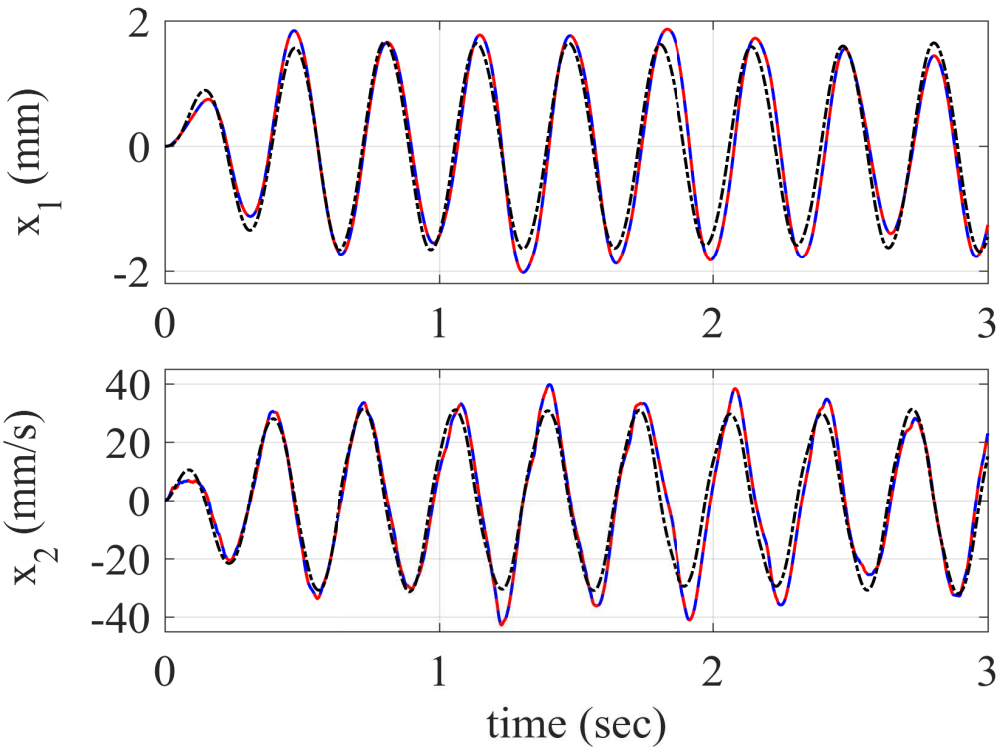

(a)

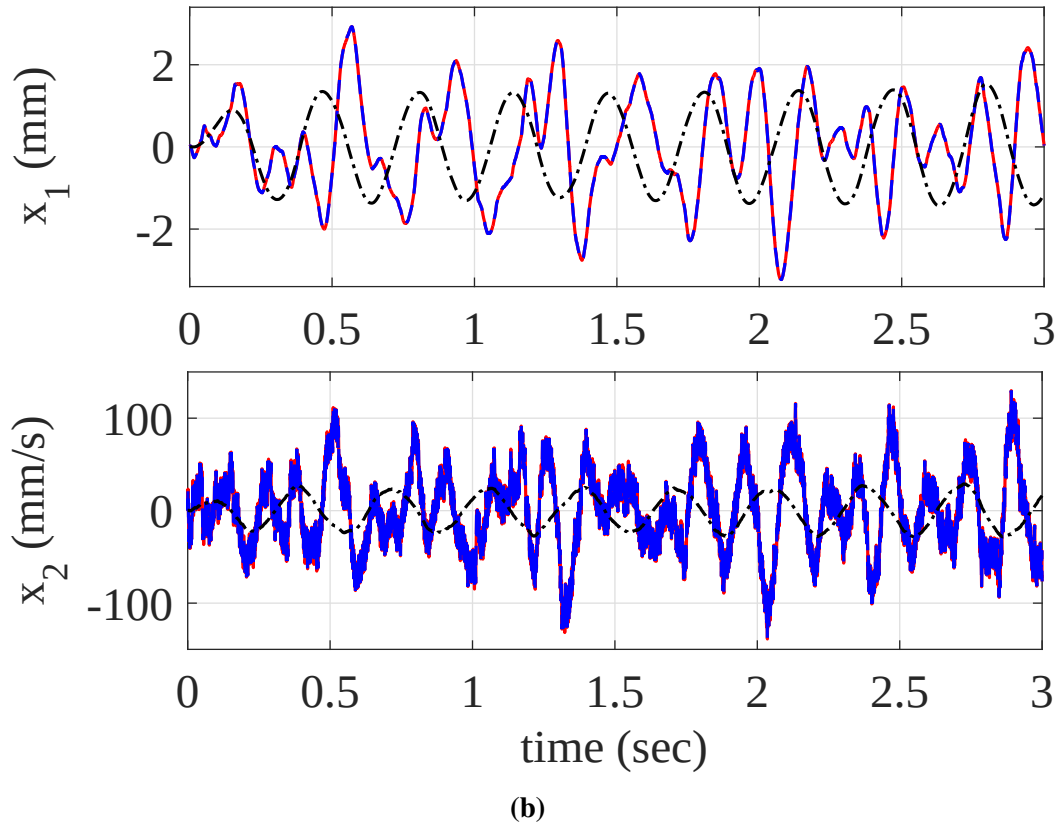

(b)

Fig. 6.2 *Simulated actual and estimated displacement and velocity of mass m_1 with measurement noise (band-limited white noise). The solid red line represents actual measurements, the dashed blue line represents the estimated measurements using the proposed observer, the dash-dot black line represents the estimated measurements using the observer based on Lipschitz type nonlinearity, (a) Band-limited white noise is added to the acceleration of mass m_2, (b) Band-limited white noise is added to the displacement of mass m_2.*

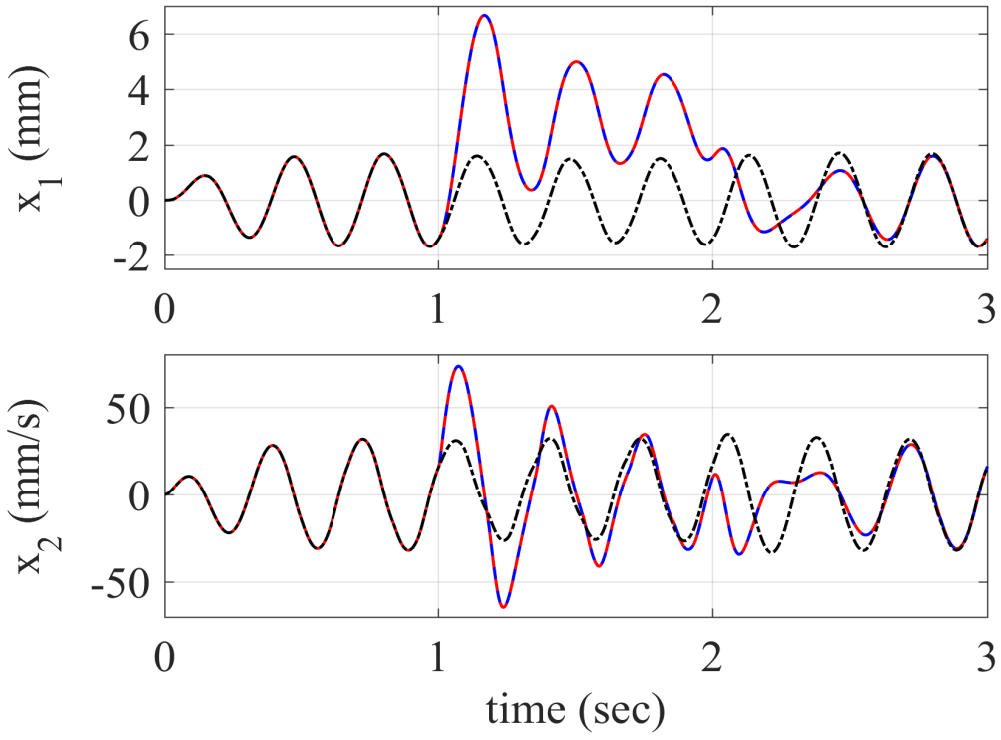

(a)

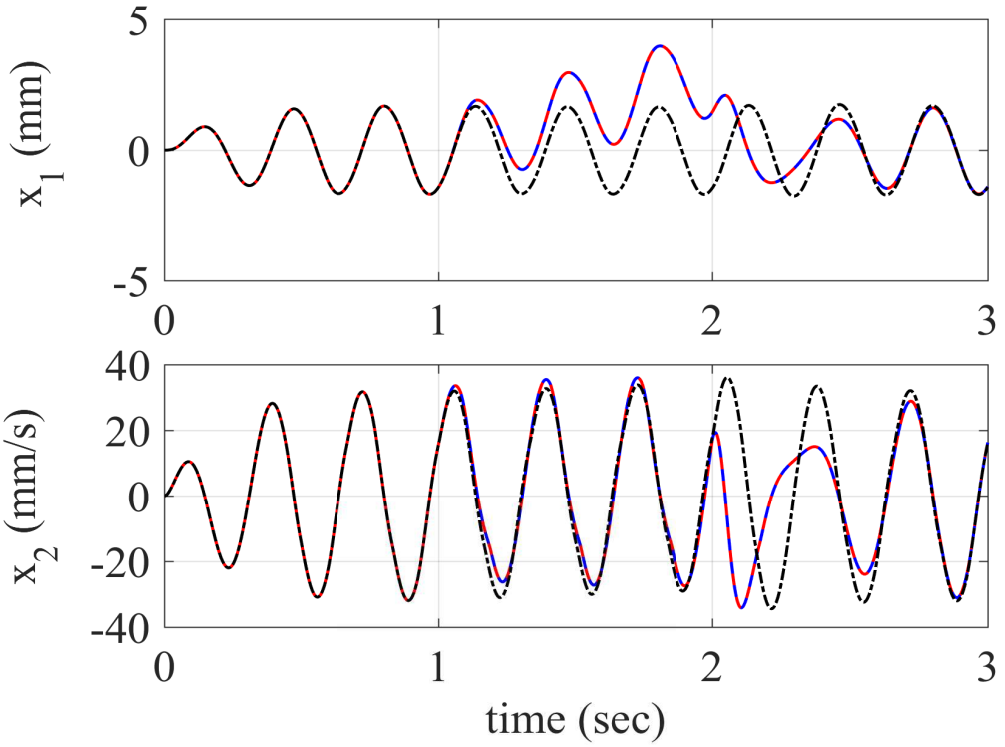

(b)

Fig. 6.3 *Simulated actual and estimated displacement and velocity of mass m_1 with step and ramp disturbance signals introduced at mass m_2 for a period of one second and starting at one second. The solid red line represents actual measurements, the dashed blue line represents the estimated measurements using the proposed observer, the dash-dot black line represents the estimated measurements using the observer based on Lipschitz type nonlinearity, (a) with step disturbance signal, (b) with ramp disturbance signal.*

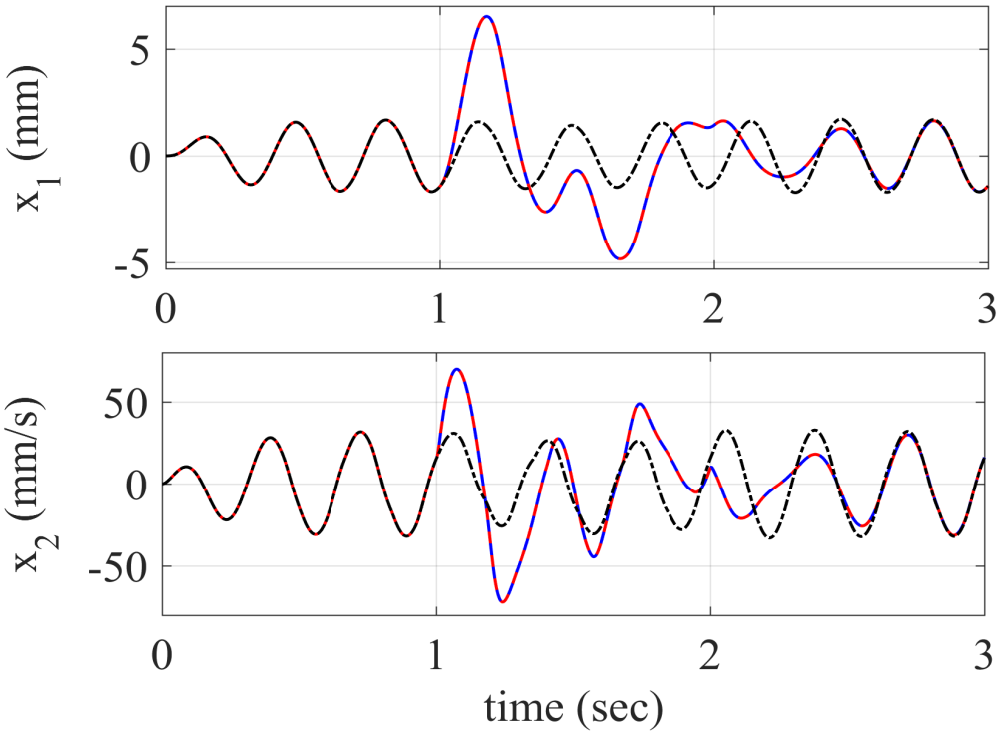

(a)

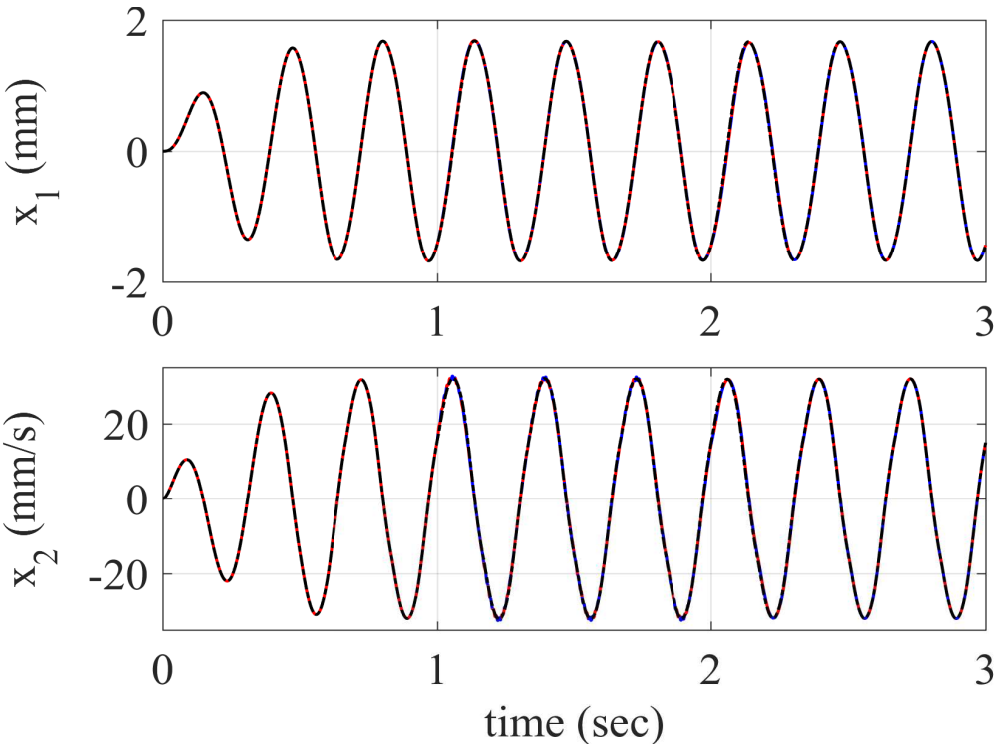

(b)

Fig. 6.4 *Simulated actual and estimated displacement and velocity of mass m_1 with sinusoidal disturbance signal at mass m_2 for a period of one second and starting at one second. The solid red line represents actual measurements, the dashed blue line represents the estimated measurements using the proposed observer, the dash-dot black line represents the estimated measurements using the observer based on Lipschitz type nonlinearity, (a) with sinusoidal disturbance of 1 Hz, (b) with sinusoidal disturbance of 100 Hz.*

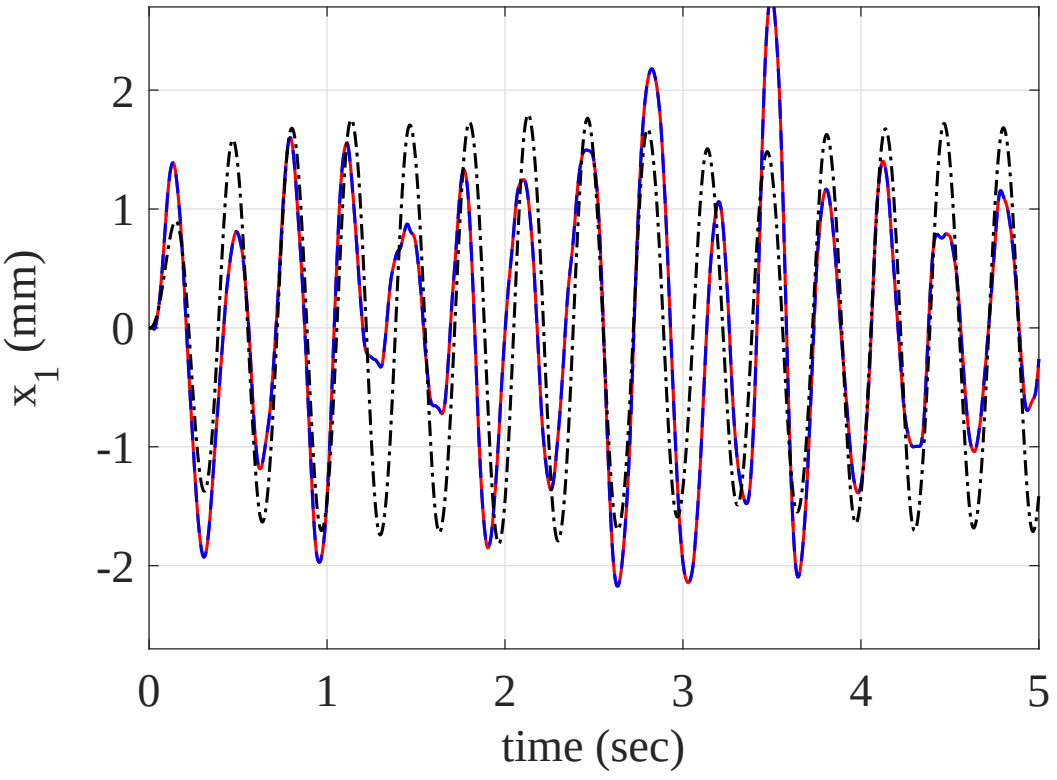

(a)

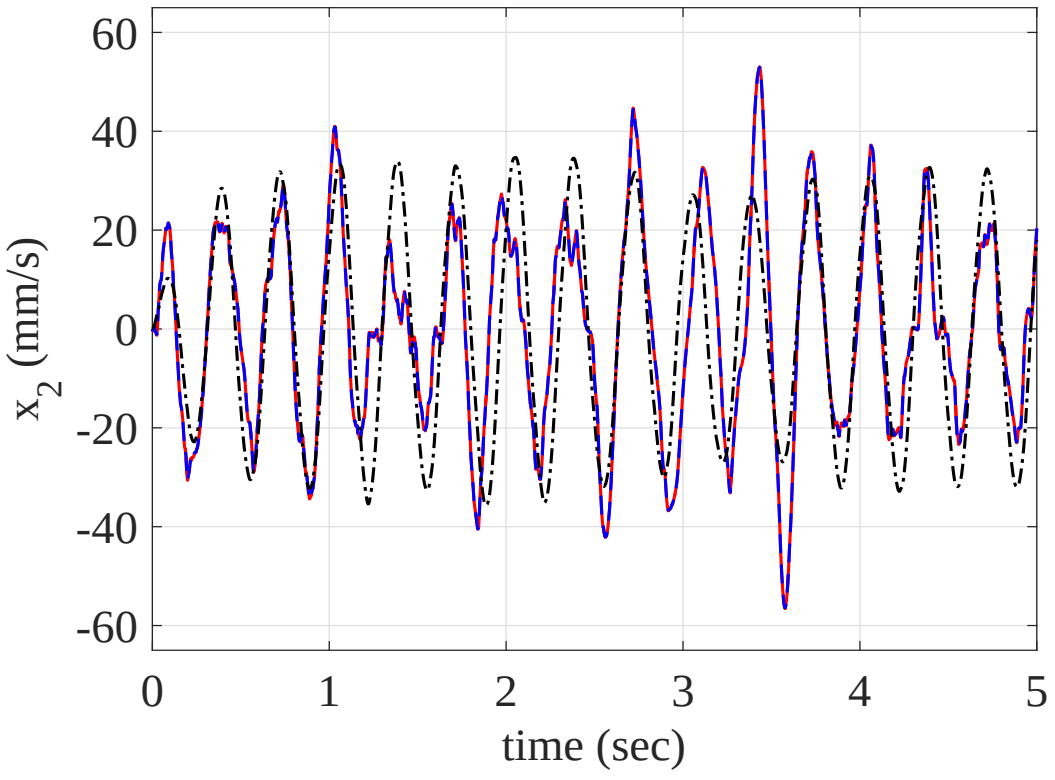

(b)

Fig. 6.5 *Simulated actual and estimated displacement and velocity of mass m_1 with random disturbance signal at mass m_2. The solid red line represents actual measurements, the dashed blue line represents the estimated measurements using the proposed observer, the dash-dot black line represents the estimated measurements using the observer based on Lipschitz type nonlinearity, (a) actual and estimated displacement of mass m_1, (b) actual and estimated velocity of mass m_1.*

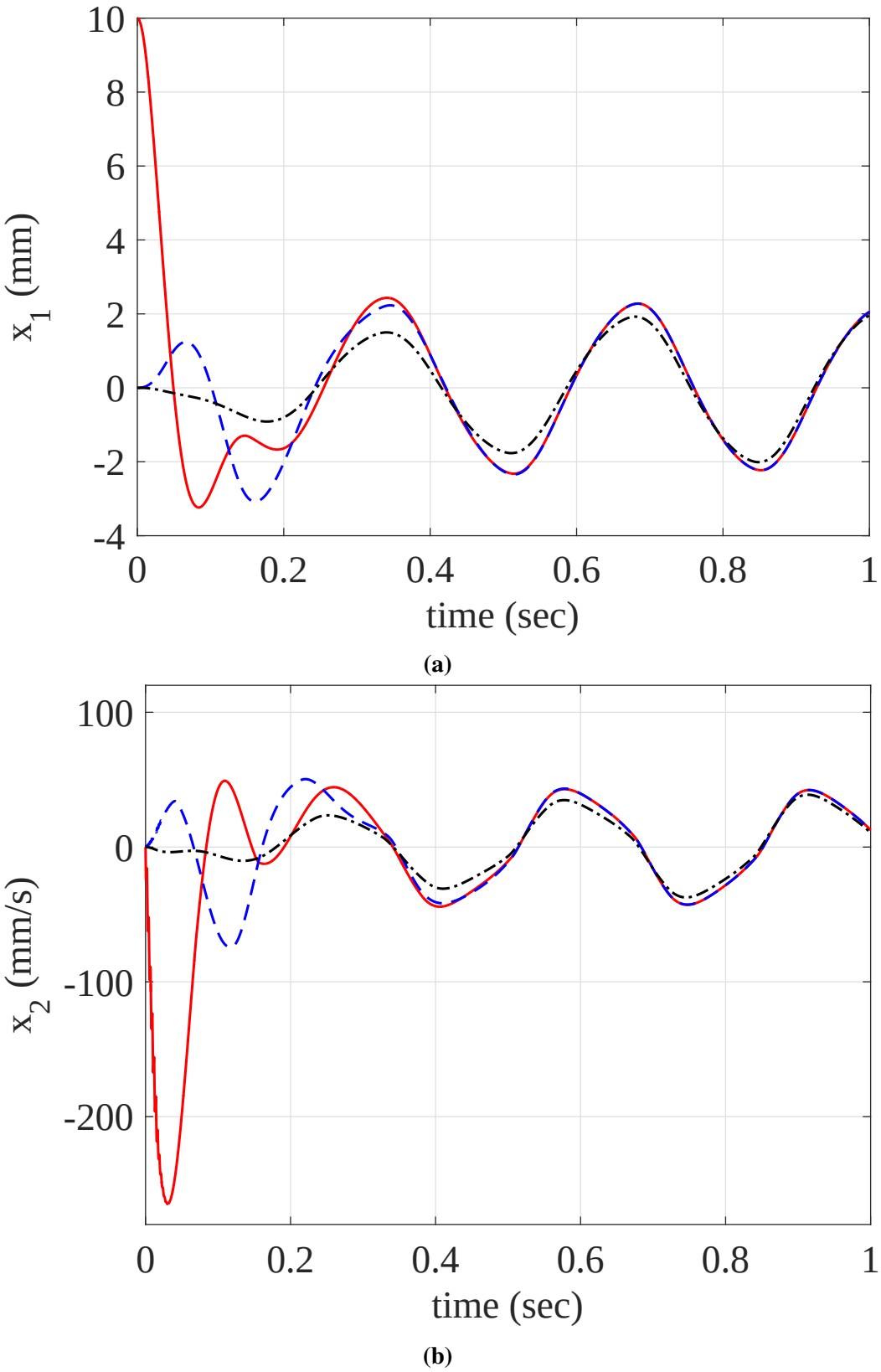

Fig. 6.6 *Simulated actual and estimated displacement and velocity of mass m_1 with different initial conditions. The solid red line represents actual measurements, the dashed blue line represents the estimated measurements using the proposed observer, the dash-dot black line represents the estimated measurements using the observer based on Lipschitz type nonlinearity, (a) actual and estimated displacement of mass m_1, (b) actual and estimated velocity of mass m_1.*

In Figure 6.4a and Figure 6.4b, a sinusoidal disturbance of 1 Hz and 100 Hz is introduced at mass m_2 respectively for a period of one second and starting at one second. At low-frequency sinusoidal disturbance, the proposed observer is performing better whereas at high-frequency sinusoidal disturbance both the observers are performing well. In Figure 6.5 a random disturbance is introduced at mass m_2, and again the proposed observer estimation is quite good as compared to the observer based on Lipschitz type nonlinearity.

In Figure 6.6 different initial conditions are given to the actual system. The converging rate of the proposed observer is faster than the observer based on Lipschitz type nonlinearity. Robustness of the observer is an important aspect, especially when it needs to be used in the closed-loop control system. The results shown here demonstrate the potential of the proposed observer in terms of robustness to both parameter variation and phase change in the excitation signal.

6.6 Experimental Results and Discussion

In the experimental test, the excitation signal is generated by rotating unbalanced masses driven by a brushless DC motor, whose speed is controlled by a separate motor speed controller. The speed controller keeps the speed of the motor close to the desired speed but there is a small amount of variation, so it is not a perfect single frequency sine wave, and the phase is also unknown. Figure 6.7 shows the actual and estimated displacement and velocity of mass m_2 respectively under three different conditions.

As mentioned earlier, the phase of the excitation signal is not known, so after doing several trials, results are selected such that the phase of the excitation signal generated experimentally best matched the phase applied to the simulation results. In this case, both the observers are estimating quite well as shown in Figure 6.7a. In Figure 6.7b the excitation signal has deliberately introduced phase delay and then in Figure 6.7c both the masses m_1 and m_2 are increased by 25% in addition to the phase delay. In both cases, the proposed observer continues to perform well, which experimentally validates the simulation results.

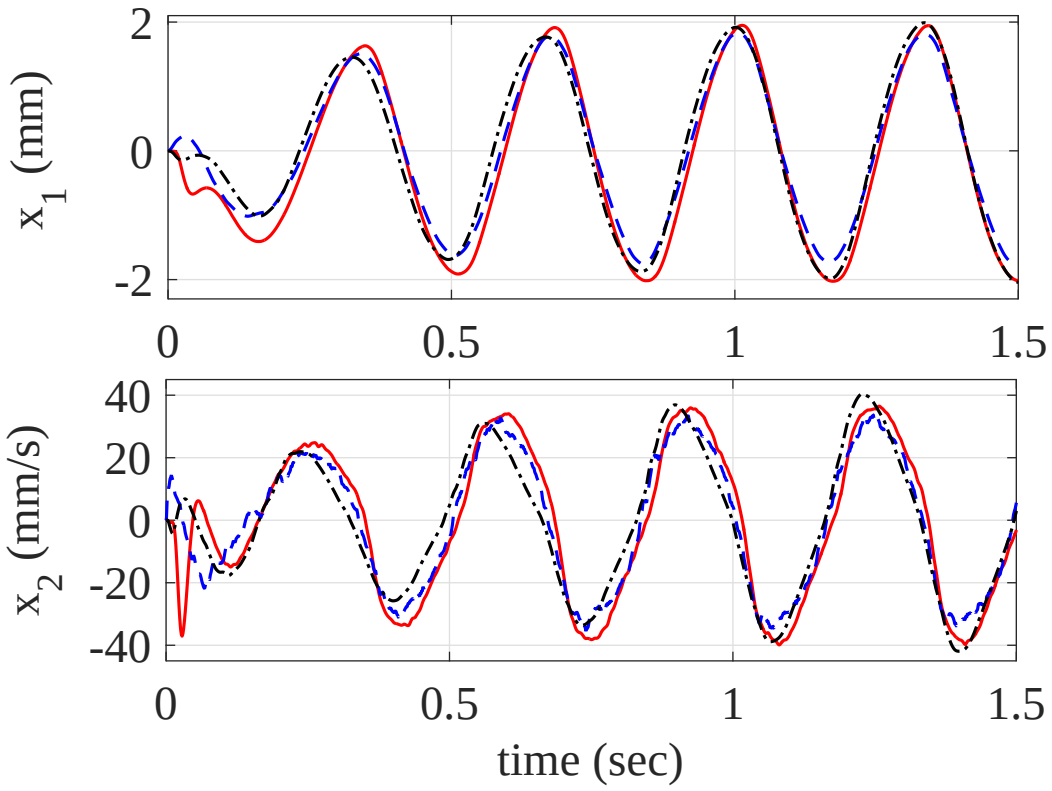
2
0
-2
x1 (mm)
0
0.5
1
1.5
40
20
0
-20
-40
x2 (mm/s)
0
0.5
1
1.5
time (sec)

(a)

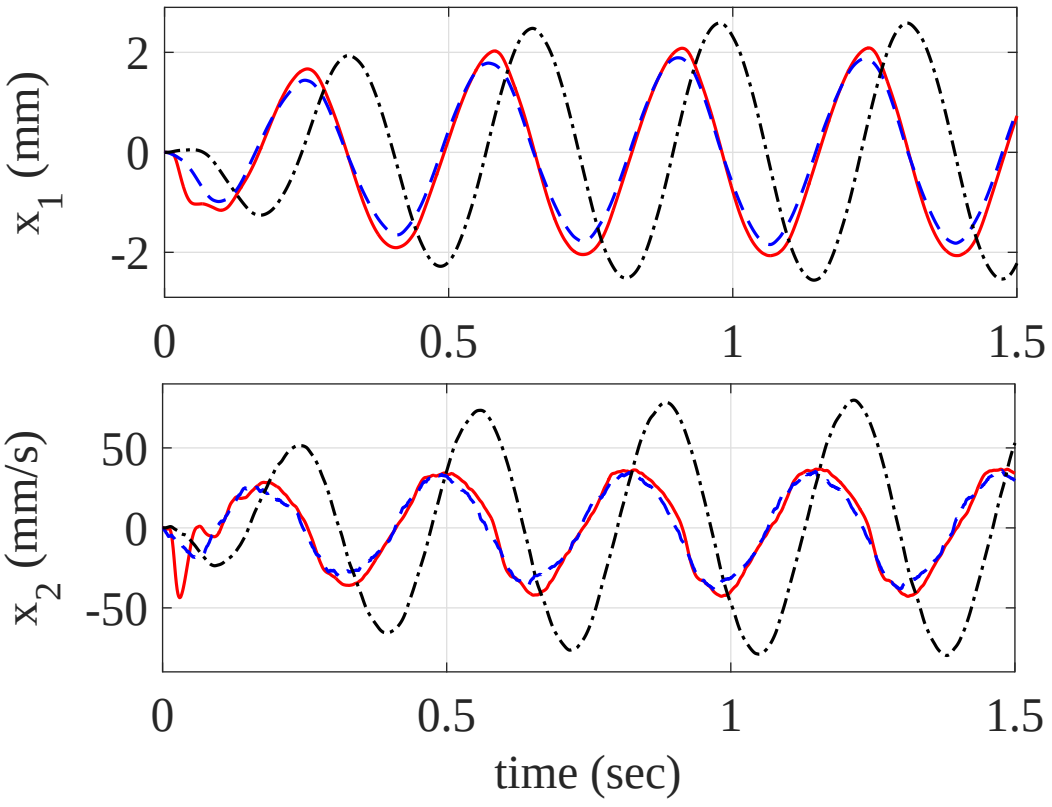
2
0
-2
x1 (mm)
0
0.5
1
1.5
50
0
-50
x2 (mm/s)
0
0.5
1
1.5
time (sec)

(b)

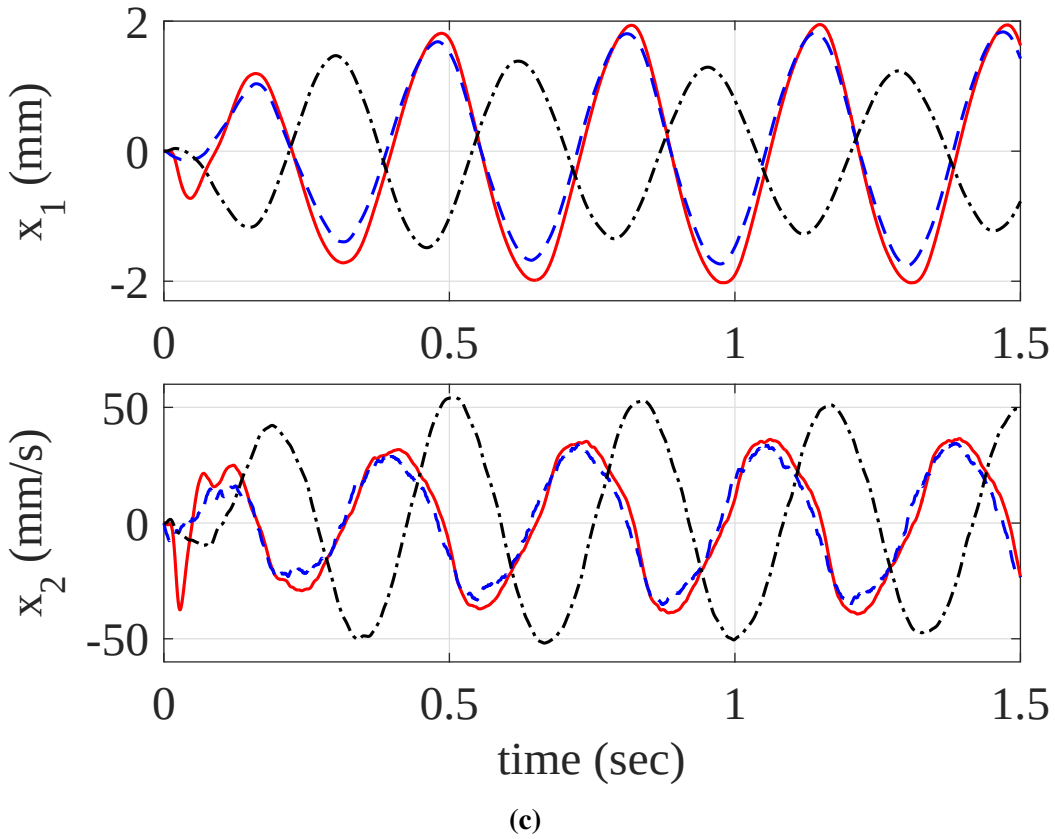

(c)

Fig. 6.7 *Experimental actual and estimated displacement and velocity of mass m_1. The solid red line represents actual measurements from the LVDT, the dashed blue line represents the estimated measurements using the proposed observer, the dash-dot black line represents the estimated measurements using the observer based on Lipschitz type nonlinearity, (a) under normal conditions, (b) with phase delay in the excitation signal, (c) with 25% increase in both the masses.*

For quantitative analysis, a performance index is defined in terms of the absolute value of the radius of the phase planes shown in Figure 6.8. This demonstrates the deterioration in performance for both the observers, with the parameter variation and phase change in the excitation signal. The phase planes in Figure 6.8 are plotted using experimental data. The error is increased from 0.5 mm to 3 mm for the observer based on Lipschitz type nonlinearity in both the scenarios as shown in Figures 6.8b and 6.8c, but for the proposed observer, the error remains almost the same in all the cases.

To further check the robustness of both the observers to parameter variation, a comparison is summarised in Table 6.1. Simulation results are used to investigate a broader range of parameter variations. It can be concluded that the proposed observer is robust to the parameter variation, measurement noise, different type of external distur-

Table 6.1 Comparison of observers based on parameter variation

System parameters (25% increase)	Proposed observer error (*mm*)	Lipschitz based observer error (*mm*)
m_1 & m_2	0.13	0.96
K_1 & K_2	0.18	1.04
C_1 & C_2	0.05	0.5

bances and phase change in the excitation signal for the range and type of parameters considered in this study.

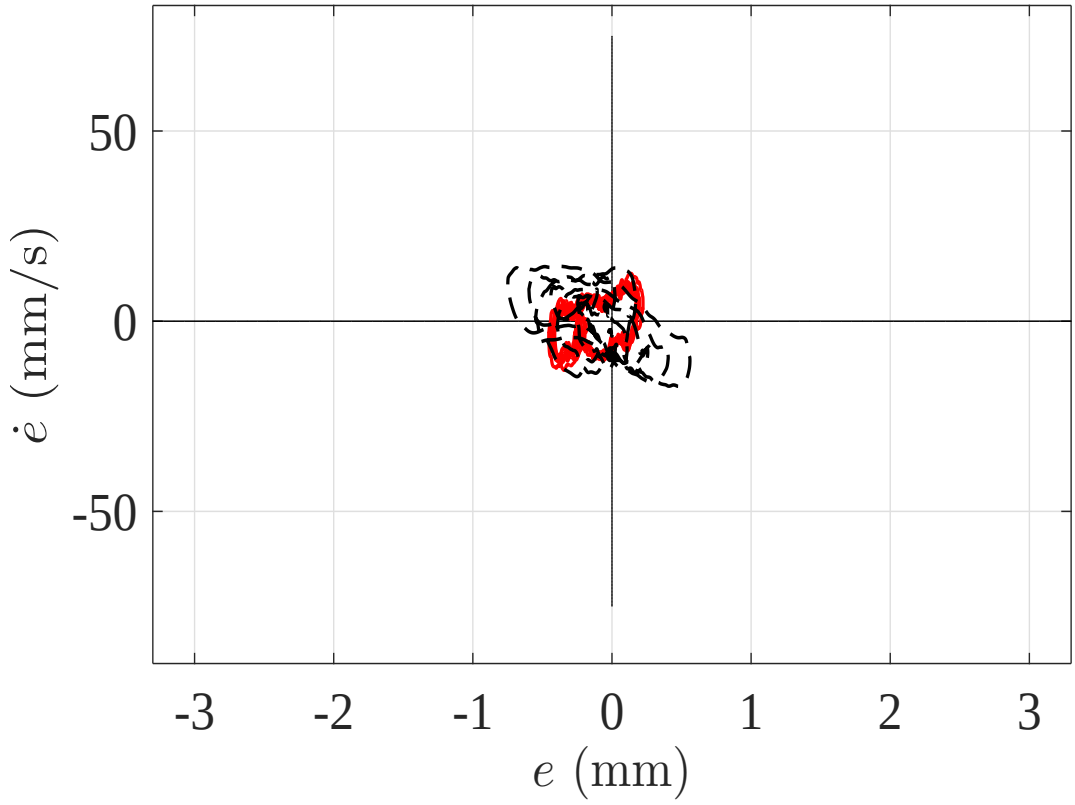

(a)

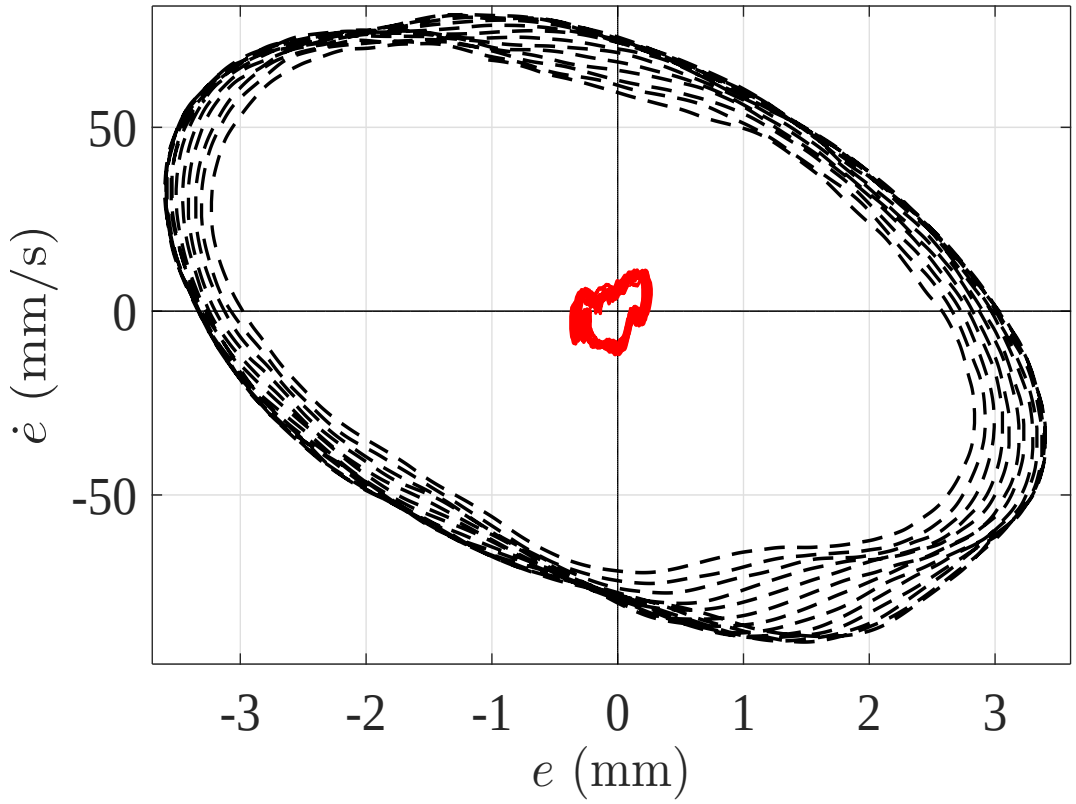

(b)

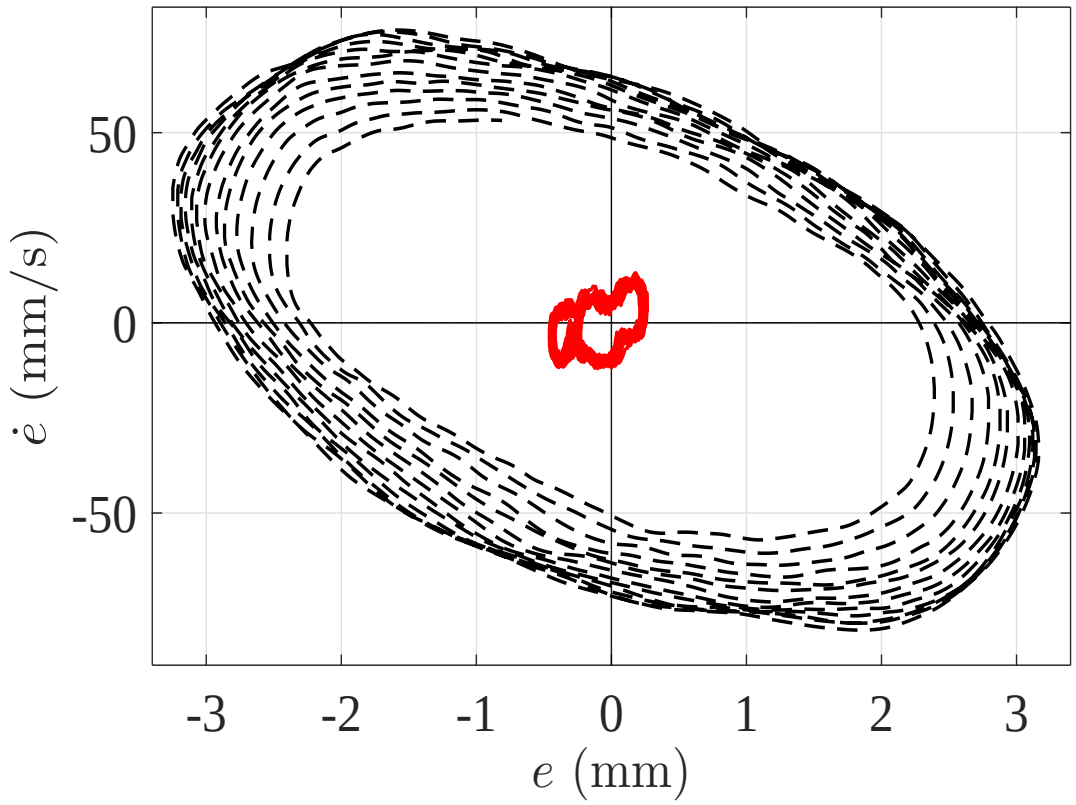

(c)

Fig. 6.8 *Error dynamics in experiment, where the solid red line represents the error dynamics in the proposed observer and the dashed black line represents the error dynamics in the observer based on Lipschitz type nonlinearity, (a) under normal conditions, (b) with 25% increase in both the masses, (c) with phase delay in the excitation signal*

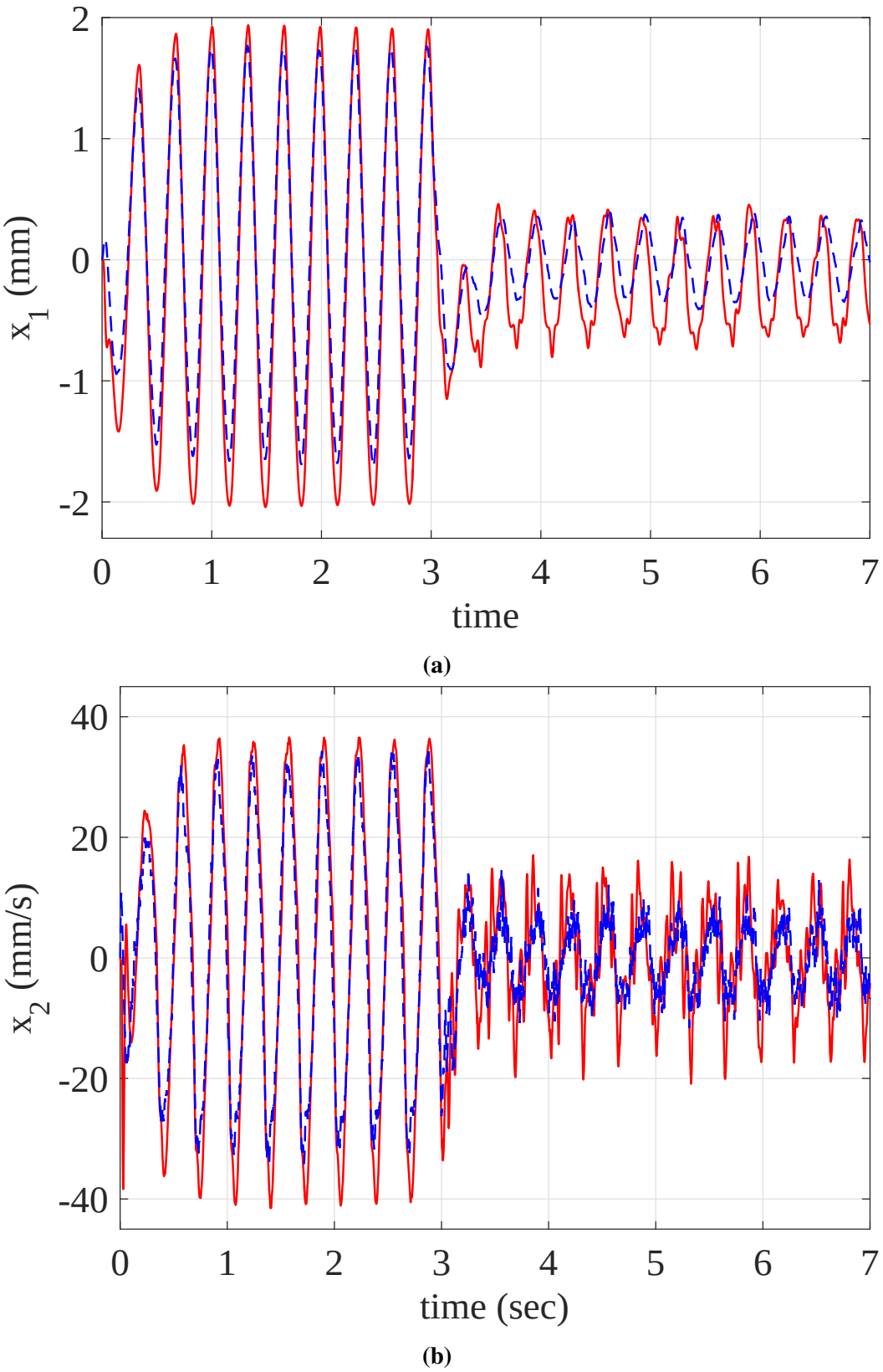

Fig. 6.9 *Experimental actual and estimated displacement and velocity of mass m_1 with hybrid active & semi-active controller, where the solid red line represents actual measurement from LVDT, the dashed blue line represents the estimated measurement using the proposed observer. The hybrid controller is switched on at time 3 seconds. (a) actual and estimated displacement of mass m_1, (b) actual and estimated velocity of mass m_1.*

The final step is to check the performance of the proposed observer as part of a closed loop control system in the experimental setup. The controller used a hybrid combination of a semi-active device and an active control actuator to suppress vibrations. Figure 6.9 shows the actual and estimated displacement and velocity of mass m_1 in the closed loop system. The results show excellent agreement.

6.7 Summary

One of the major issues with nonlinear observers is that most of them did not give a structural design methodology and if they do, then some of the conditions are very hard to meet. Secondly, most of them are designed for a particular class of systems, like the one that is used for comparison purposes, it is only applicable to the systems that have Lipschitz type nonlinearity and satisfies the globally Lipschitz conditions. The proposed observer is not restricted to any class of system as long as an invariant manifold exists and it also provides a structured design methodology. Robustness is a fundamental property, especially when the observer needs to be used in a closed loop control system because the performance of the controller depends on the estimated signals. A qualitative analysis has been performed based on the performance index defined in Section 6.6. It is shown that the proposed observer is robust to the parameter variation, measurement noise, different type of external disturbances and phase change in the excitation signal, whereas there is an increase in the error in all the scenarios for the observer based on Lipschitz type nonlinearity.

To conclude a method to design a reduced order observer for a nonlinear system has been presented. A systematic design method for the observer has been explained in detail. Then the performance of the proposed observer was tested using a 2-DOF example system. As part of this process, the proposed observer was compared with a well-known observer based on Lipschitz type non-linearity. Based on this comparison, the conclusion is that the new observer has a clear performance benefit, with significant potential to be extended to a wider range of nonlinear systems beyond the one considered here.

The proposed observer was shown to have a better performance for the parameters and inputs selected in the example 2-DOF system. In particular, the robustness of the proposed observer against parameter variation and excitation signal for the example 2-DOF system is shown to be better in both simulation and experiment. Finally, the proposed observer was found to perform well when tested in a closed loop with a hybrid active and semi-active controller system.

Chapter 7

Conclusions and Future Work

7.1 Summary of Thesis

The summary of the thesis is as follows:

- The motivation, background, effects of vibration in different fields and thesis outline have been presented in Chapter 1.

- In Chapter 2 the literature review was presented in detail with linear and nonlinear systems being discussed. Then the passive damping devices used for the vibration suppression and vibration isolation were discussed. The semi-active devices were discussed and MR damper was described in detail. A comparison between MR and ER dampers was presented. Active control devices were then discussed briefly. After that, the control strategies used alongside these actuators for vibration suppression were presented. In the end the I & I and SMC control methodologies were introduced and the literature related to both I & I, and SMC were described in detail.

- The hybrid control methodology was illustrated in Chapter 3. The I & I control method has been used to design the controller for the active actuator and SMC has been used to design the controller for the semi-active device. After the analytical design, the performance of the controller was tested in simulation, and the results

were presented. Then the dynamics of both the active actuator and the semi-active device was introduced, and the simulations were repeated.

- In Chapter 4 the experimental setup was presented. For practical implementation, HIL testing was performed for the hybrid controller validation. The results from HIL testing has shown good results in achieving the control objectives. The switching time of the semi-active controller has been reduced to a large extent by the hybrid active & semi-active controller because the active actuator injects the desired energy as the semi-active controller switches off, following which the semi-active device returns to the dissipative region. In the end, a comparison was made with some benchmark controllers and the proposed controller performance was better than the other controllers.

- To illustrate the effectiveness of the proposed hybrid controller, the possible application was discussed in Chapter 5. The hybrid controller was implemented to keep the contact force constant in the pantograph-catenary system of high-speed trains. A detailed derivation was given after which the simulation results were presented.

- A reduced order observer using a notion of the invariant manifold was designed for the same 2-DOF system in Chapter 6. The analytical design of the observer was described in detail. All the derivations were presented along with the simulation results. After validation and satisfactory results, the observer was implemented in practice using HIL both in open loop and closed loop with the hybrid controller. A comparison has also been made with a benchmark observer based on the Lipschitz type nonlinearity.

7.2 Key Conclusions

The conclusions of the thesis is as follows:

- Semi-active devices have a lot of advantages; however, the downside of such devices is the passivity constraint, i.e., they can only operate in the dissipative energy regions. To deal with this problem, an idea has been presented in which an active actuator can assist the semi-active device to achieve the performance close to a fully active system. The fully active system is the reference/target system. The results obtained both in the simulation and experiment have reinforced the proposed idea.

- In order to achieve the goal of an active actuator assisting the semi-active device, the control techniques selection is done accordingly. The selected control method needs to be robust and cater for the nonlinearities. The I & I methodology fits well in these circumstances. In this control technique a reduced order target system needs to be defined, and then the higher order system dynamics are immersed into the lower order target system. The semi-active device is located at the point where the vibration needs to be controlled, the SMC control methodology has been chosen for the controller design of the semi-active device. The SMC control method comes under the umbrella of the I & I methodology. The two controllers complement each other as they are trying to achieve the same target system.

- After the analytical design of the controller, it has been validated in the simulation without the actuator dynamics. To implement the controller in practice, the actuator dynamics need to be first incorporated into the simulation. For that purpose, the unified MR damper model has been used along with the current controller which converts the SMC control signal to current control signal. The ultimate goal is to perform the HIL testing, in which one DOF will be simulated and represented by the hydraulic actuator. The hydraulic actuator model provided by the manufacturer has been used in the simulation and is controlled by an Instron controller. The model of the Instron controller utilised in the simulation is also

provided by the manufacturer. After making all these changes, the simulations were run again, and the results were very close to the one without the actuator dynamics.

- After the satisfactory simulation results, the hybrid active & semi-active controller has been validated using HIL testing in which an active actuator is assisting the semi-active device to achieve performance close to that of a fully active system. HIL testing has shown promising results. The switching time of the semi-active controller has been reduced to a large extent by the hybrid active & semi-active controller because the active actuator injects the desired energy as the semi-active controller switches off, following which the semi-active device returns to the dissipative region.

- The proposed control technique has been compared with semi-active and hybrid active & passive controllers. For a quantitative analysis of the three controllers, a performance index is defined as an absolute value of the radius of error dynamics phase plane. It was shown that when the proposed hybrid active & semi-active controller is turned on, the error is reduced by 88%. In comparison, for the other two controllers i.e. hybrid active & passive and semi-active, the error is reduced by 73% and 41% respectively. The proposed hybrid active & semi-active controller has reduced the error by 92%, and the other two controllers have reduced the error by 68%, when the amplitude of the excitation signal has been increased from 70 N to 1000 N. Therefore the performance of the proposed hybrid active & semi-active controller is better than the other two controllers in both the cases of low and high amplitude excitation signals. In the case of the high amplitude excitation signal, the performance index of the proposed hybrid active & semi-active controller has been further increased by 4%.

- In high-speed trains, the contact force between pantograph and catenary ideally needs to be constant. The proposed hybrid controller was implemented to keep the contact force constant. It has shown promising results both under normal

conditions and in the presence of the band-limited white noise, which demonstrates the robustness of the controller. Then the robustness was also checked against variable train speed with different slope variations and the results were satisfactory.

- A method to design a reduced order observer for a nonlinear system has been presented. One of the major issues with nonlinear observers is that most of them did not give a structural design methodology and if they do, then some of the conditions are very hard to meet. Secondly, most of them are designed for a particular class of systems. The proposed observer is not restricted to any class of system as long as an invariant manifold exists and it also provides a structured design methodology. Both simulations and experiments have shown promising results. A comparison has also been made with a benchmark observer based on Lipschitz type nonlinearity. Based on this comparison, the proposed observer has a clear performance benefit, with significant potential to be extended to a wider range of nonlinear systems beyond the one considered here. In particular, the robustness of the proposed observer against parameter variation and excitation signal for the example 2-DOF system is shown to be better in both simulation and experiment. Finally, the proposed observer was found to perform well when tested in a closed-loop with a hybrid active and semi-active controller.

7.3 Summary of Original Contribution

The summary of the contribution is as follows:

- A novel hybrid active and semi-active controller has been presented where an active actuator is assisting a semi-active device.

- I & I and SMC control strategies were combined to achieved the desired performance.

- The proposed hybrid controller was validated both in simulation and practice using HIL testing.
- A comparison of the controller has been made with some benchmark controllers and based on the performance index, the proposed controller performance was better than the other two controllers.
- To further illustrate the effectiveness of the proposed hybrid controller, it has been used to keep the contact force constant between the pantograph and catenary in high-speed trains.
- A reduced order observer based on the notion of an invariant manifold has been designed and to illustrate the performance, first the observer was tested in simulation. After satisfactory results from simulations, the observer was tested in practice using HIL testing. The proposed observer has shown robust performance to the parameter variation, measurement noise, different type of external disturbances and phase change in the excitation signal for the range and type of parameters considered in this study.
- A comparison of the proposed observer was made with a benchmark observer based on Lipschitz type nonlinearity. The proposed observer has shown promising results in comparison to the observer based on Lipschitz type nonlinearity.

7.4 Recommendations for Future Work

Following are the suggestions for future work:

- In this work it is shown using hybrid control that an active actuator can assist the semi-active device using an example 2-DOF system. This work can be further extended by implementing it on n-DOF system. Further work can be done to optimize the location of the semi-active device in case of n-DOF system. In the same context, more than one semi-active device can be deployed in n-DOF system, and the hybrid controller can be exploited to consider how many semi-active

devices can be assisted by a single active actuator and that how the performance is effected by increasing the degree of freedom in the system.

- In Chapter 4, HIL testing is performed using the test rig, in which one DOF is simulated. The test rig can be build as a complete 2-DOF system and the same tests can be repeated along with new tests to further validate the hybrid controller. In Chapter 5, practical application for the hybrid controller is presented and the results are shown in the simulation. A test rig emulating the pantograph-catenary system can be manufactured to test the hybrid controller.

- In the present work, I & I along with the SMC is used to design the controller for active actuator and semi-active device respectively. A common target system is defined for both the controllers. One possible extension of the current work is that other control techniques can also be explored to achieve a similar or better performance, in which an active actuator can assist the semi-active device.

- The focus of current work is on vibration suppression using hybrid active and semi-active control. Although in Chapter 5, the controller is also used to keep the contact force constant between pantograph and catenary of a high speed train. The work can be further extended to position control in flexible structures, robotics and elastic drive systems.

- The goal of the hybrid controller is to make the actual system behave as close to the target system as possible. One possible extension of the work can be to define different target system in order to analyze the behavior and limitations of the hybrid controller. A comparison can be made that which target systems are possible to achieve and which are not.

- The MR damper can potentially be replaced with a semi-active inerter or varying stiffness device and using the proposed hybrid controller a comparison can be made that which of the semi-active device is more appropriate for vibration suppression in different situations.

A final area for future work is that of helicopter vibrations. The author has begun a preliminary study in this area, which is briefly summarised below.

7.4.1 Helicopter Vibrations

The helicopter has its importance in the aerospace industry because of its unique abilities of take-off, landing, hover, etc. The flight experience of a helicopter for both the crew and the passengers is not pleasant as compared to aeroplanes because of the vibrations in the cabin. The primary sources of cabin vibrations are the rotor blade vibrations induced by the aerodynamics loads and the inertial loads at harmonics frequencies. These cabin vibrations are passed on to the crew members and the passengers through seats. The passengers have short-term exposure to these vibrations, but the crew members have long-term exposure. It has adverse effects both in short and long term.

In the short term, it can cause fatigue, discomfort, headache, operational safety, etc. In the long term, it can affect the spinal cord and the neck, which can lead to long-lasting damages. Hence it is vital to control this vibration. In the literature lot of work has been done to control these vibrations. Passive devices are used to damp the vibrations, and they are also used as vibration isolation devices, but the problem with the passive devices is that they can only be tuned to a particular frequency, however in a helicopter the vibrating frequency spectrum is broad, so the passive devices are not that efficient, and another issue is that they add lot of weight to the structure, which is very crucial to the aerospace industry. There are two main approaches to vibration control in a helicopter. The first is the overall vibration control or in other words, global vibration control. The second is local vibration control, in which the vibration is controlled locally in any part of the structure.

In this application, the local vibration control is demonstrated, which is the aircrew seat vibration control. In [189] the adaptive control has been proposed for vibration suppression in the helicopter aircrew seat. Further details are presented in [190], where the seat is modelled as a 2-DOF system and the human upper body is modelled as a 4-DOF system. The system with a bio-dynamics model is shown in Figure 7.1.

where m_f, k_f, c_f, are the mass, stiffness coefficient and damping coefficient of the seat frame respectively, f_a is the active actuator force, m_c, k_c, are the mass and stiffness coefficient of the seat cushion respectively, f_{sa} is the semi-active device force, mp_1, kp_1, cp_1, are the mass, stiffness coefficient and damping coefficient of lower torso of the bio-dynamics model respectively, mp_2, kp_2, cp_2, are the mass, stiffness coefficient and damping coefficient of the viscera of the bio-dynamics model respectively, mp_3, kp_3, cp_3, are the mass, stiffness coefficient and damping coefficient of the upper torso of the bio-dynamics model respectively, mp_4, kp_4, cp_4, are the mass, stiffness coefficient and damping coefficient of the head and neck of the bio-dynamics model respectively, z_0, z_f, z_c, zp_1, zp_2, zp_3, zp_4 represent the displacements of the helicopter floor, seat frame, seat cushion, lower torso, viscera, upper torso, head and neck respectively.

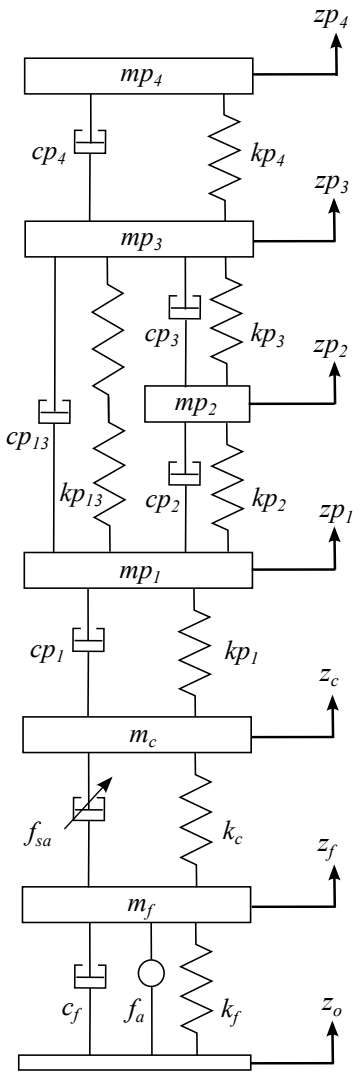

Fig. 7.1 *Helicopter crew seat model including the bio-dynamics model*

The proposed hybrid active and semi-active controller can be used in this application to suppress the aircrew seat vibration. An active actuator is connected between the seat and the helicopter floor, and the seat cushion is considered to be made of a semi-active device so that its damping properties can be changed. In this case, the vibrations are coming from the ground or helicopter floor in contrast to the system used in Chapter 3 where the vibrations were introduced from the top. The ultimate goal is to control the vibrations that are transmitted to the aircrew helmet. A comparison of the simulation and test fight results in an open-loop presented in [190], is shown in Figure 7.2, where a sine sweep excitation signal is given as an input.

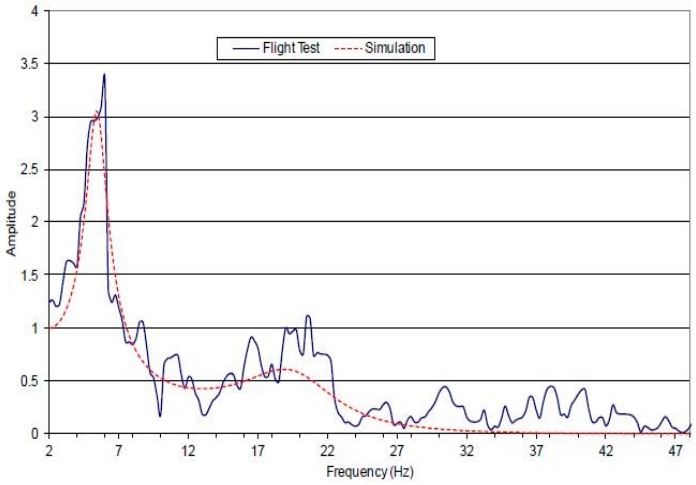

Fig. 7.2 *Open-loop helicopter aircrew helmet frequency response in simulation and flight test [190]*

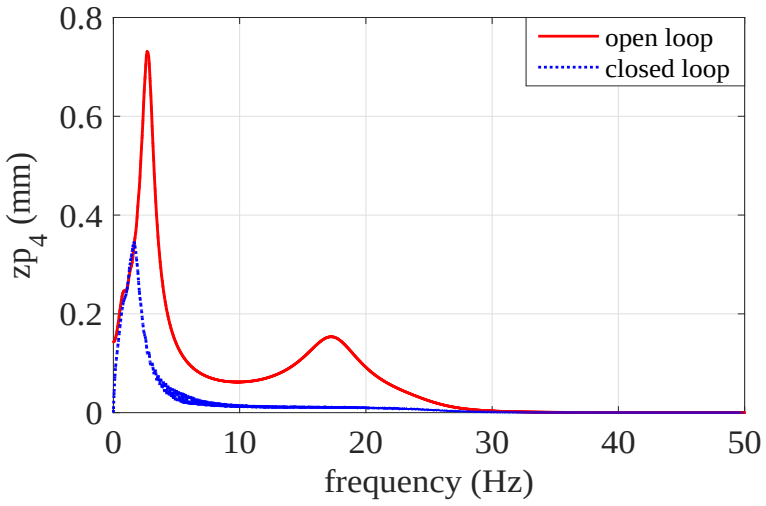

Fig. 7.3 *Frequency response of the aircrew helmet, where the solid red line represents the open-loop response, the dashed blue line represents the closed-loop response*

The hybrid active and semi-active controller is implemented to control the vibrations transmitted to the bio-dynamics model. A sinusoidal chirp signal with a frequency ranging from 0.1-50 Hz is given as a helicopter floor disturbance. Figure 7.3, shows the frequency response of the aircrew helmet in an open and closed-loop. It can be seen that the system resonates at 2.68 Hz and 17.3 Hz in an open-loop. With the hybrid controller, the amplitude has been decreased from 0.73 mm to 0.12 mm at first resonant frequency. At the second resonant frequency the amplitude has been decreased from 0.17 mm to 0.009 mm. These are just preliminary result. In the future work all the tests presented in [190] can be performed with the proposed hybrid controller and a comparison can be made with the adaptive controller presented in [190].

References

[1] A. Preumont, "Vibration control of active structures: an introduction," *Springer*, vol. 179, 2011.

[2] M. J. Crocker, "Handbook of noise and vibration control," *John Wiley & Sons*, 2007.

[3] D. I. Jones, "Handbook of viscoelastic vibration damping," *John Wiley & Sons*, 2001.

[4] C. C. Fuller, S. Elliott, and P. A. Nelson, "Active control of vibration," *Academic Press*, 1996.

[5] L. L. Beranek and I. L. Vér, "Noise and vibration control engineering," *John Wiley & Sons*, 1992.

[6] D. Gómez, J. Marulanda, and P. Thomson, "Sistemas de control para la protección de estructuras civiles sometidas a cargas dinámicas," *Dyna*, vol. 75, no. 155, pp. 77–89, 2008.

[7] R. Manley, "Vibrations in aircraft: A series of articles covering the general principles for aeronautical engineers," *Aircraft Engineering and Aerospace Technology*, vol. 16, no. 4, pp. 100–102, 1944.

[8] M. Azizan and M. Fard, "The influence of vibrations on vehicle occupant fatigue," in *Internoise Conference*, vol. 62, pp. 1–15, 2014.

[9] J. J. d'Azzo and C. D. Houpis, "Linear control system analysis and design: conventional and modern," *McGraw-Hill Higher Education*, 1995.

[10] T. Kaczorek, "Linear control systems: analysis of multivariable systems," *John Wiley & Sons, Inc.*, 1992.

[11] S. Sastry, "Nonlinear systems: analysis, stability, and control," *Springer New York*, 1999.

[12] H. M. Zhou, X. J. Zheng, and Y.-H. Zhou, "Active vibration control of nonlinear giant magnetostrictive actuators," *Smart Materials and Structures*, vol. 15, no. 3, p. 792, 2006.

[13] S. A. Fazelzadeh and S. M. Jafari, "Active control law design for flutter suppression and gust alleviation of a panel with piezoelectric actuators," *Smart Materials and Structures*, vol. 17, no. 3, p. 035013, 2008.

[14] I. Diaz and P. Reynolds, "Robust saturated control of human-induced floor vibrations via a proof-mass actuator," *Smart Materials and Structures*, vol. 18, no. 12, p. 125024, 2009.

[15] T. Fujita, "Application of hybrid mass damper with convertible active and passive modes using hydraulic actuator to high-rise building," *American Control Conference*, vol. 1, pp. 1067–1072, 1994.

[16] T. Fujinami, Y. Saito, M. Morishita, Y. Koike, and K. Tanida, "A hybrid mass damper system controlled by H-infinity control theory for reducing bending-torsion vibration of an actual building," *Earthquake Engineering & Structural Dynamics*, vol. 30, no. 11, pp. 1639–1653, 2001.

[17] H. Kim and H. Adeli, "Hybrid control of smart structures using a novel wavelet-based algorithm," *Computer-Aided Civil and Infrastructure Engineering*, vol. 20, no. 1, pp. 7–22, 2005.

[18] M. Rao, T. Ram, and A. Purushottam, "Analysis of passive and semi active controlled suspension systems for ride comfort in an omnibus passing over a speed bump," *International Journal of Research & Reviews in Applied Sciences*, vol. 5, no. 1, 2010.

[19] A. Astolfi, D. Karagiannis, and R. Ortega, "Nonlinear and adaptive control with applications," *Springer Science & Business Media*, 2007.

[20] C. T. Chen, "Linear system theory and design," *Oxford University Press, Inc.*, 1995.

[21] H. Kwakernaak and R. Sivan, "Linear optimal control systems," *Wiley-interscience New York*, 1972.

[22] A. Isidori, "Nonlinear control systems," *Springer*, 1995.

[23] Z. Vukic, "Nonlinear control systems," *CRC Press*, 2003.

[24] M. Krstic, I. Kanellakopoulos, and P. V. Kokotovic, "Nonlinear and adaptive control design," *Wiley*, 1995.

[25] S. Lefschetz, "Stability of nonlinear control systems," tech. rep., DTIC Document, 1965.

[26] K. Zhou, J. C. Doyle, K. Glover, *et al.*, "Robust and optimal control," *Prentice Hall New Jersey*, vol. 40, 1996.

[27] G. C. Goodwin, "A brief overview of nonlinear control," *Centre for Integrated Dynamics and Control Bildirisi, Department of Electrical and Computer Engineering, The University of Newcastle, Australia*, 2002.

[28] P. Watts, "On a method of reducing the rolling of ships at sea," *Trans. INA*, vol. 24, 1883.

[29] H. Frahm, "Device for damping vibration of bodies," 18 Apr. 1911. U.S. Patent No. 989,958.

[30] J. Ormondroyd, "Theory of the dynamic vibration absorber," *Journal of American Society of Mechanical Engineers*, vol. 50, pp. 9–22, 1928.

[31] J. Den Hartog, "Mechanical vibrations," *McGraw-Hill Book Company, New York*, pp. 122–169, 1956.

[32] P. A. Irwin and B. Breukelman, "Recent applications of damping systems for wind response," in *Proceedings of the Sixth World Congress of the Council on Tall Buildings and Urban Habitat, Melbourne, Australia, February*, 2001.

[33] T. Datta, "A state-of-the-art review on active control of structures," *ISET Journal of Earthquake Technology*, vol. 40, no. 1, pp. 1–17, 2003.

[34] A. R. Klembczyk, "Introduction to shock and vibration isolation and damping systems," in *IMAC-XXVII: Conference & Exposition on Structural Dynamics*, pp. 58–66, 2009.

[35] A. Levant, A. Pisano, and E. Usai, "Output-feedback control of the contact-force in high-speed-train pantographs," in *Proceedings of the 40th IEEE Conference on Decision and Control*, vol. 2, pp. 1831–1836, 2001.

[36] A. Rachid, "Pantograph catenary control and observation using the LMI approach," in *50th IEEE Conference on Decision and Control and European Control Conference (CDC-ECC)*, pp. 2287–2292, 2011.

[37] S. Shin, K. Eum, and J. Um, "Contact force control of pantograph-catenary system using block pulse function," in *Proceedings of the 7th World Congress on Railway Research (WCRR)*, pp. 4–8.

[38] M. C. Smith, "Synthesis of mechanical networks: the inerter," *IEEE Transactions on Automatic Control*, vol. 47, no. 10, pp. 1648–1662, 2002.

[39] M. Z. Chen, C. Papageorgiou, F. Scheibe, F. C. Wang, and M. C. Smith, "The missing mechanical circuit element," *IEEE Circuits and Systems Magazine*, vol. 9, no. 1, pp. 10–26, 2009.

[40] M. C. Smith and F. C. Wang, "Performance benefits in passive vehicle suspensions employing inerters," *Vehicle System Dynamics*, vol. 42, no. 4, pp. 235–257, 2004.

[41] C. Papageorgiou and M. C. Smith, "Positive real synthesis using matrix inequalities for mechanical networks: application to vehicle suspension," *IEEE Transactions on Control Systems Technology*, vol. 14, no. 3, pp. 423–435, 2006.

[42] F. C. Wang, M. K. Liao, B. H. Liao, W. J. Su, and H. A. Chan, "The performance improvements of train suspension systems with mechanical networks employing inerters," *Vehicle System Dynamics*, vol. 47, no. 7, pp. 805–830, 2009.

[43] F. C. Wang, C. W. Chen, M. K. Liao, and M. F. Hong, "Performance analyses of building suspension control with inerters," in *46th IEEE Conference on Decision and Control*, pp. 3786–3791, 2007.

[44] I. F. Lazar, S. A. Neild, and D. J. Wagg, "Design and performance analysis of inerter-based vibration control systems," in *Dynamics of Civil Structures, Volume 4*, pp. 493–500, Springer, 2014.

[45] I. Lazar, S. Neild, and D. Wagg, "Inerter-based vibration suppression systems for laterally and base-excited structures," *Proceedings of EURODYN 2014*, pp. 1525–1530, 2014.

[46] D. Karnopp, M. J. Crosby, and R. Harwood, "Vibration control using semi-active force generators," *Journal of Engineering for Industry*, vol. 96, no. 2, pp. 619–626, 1974.

[47] W. Patten, C. Mo, J. Kuehn, and J. Lee, "A primer on design of semiactive vibration absorbers (sava)," *Journal of Engineering Mechanics*, vol. 124, no. 1, pp. 61–68, 1998.

[48] F. Jabbari and J. E. Bobrow, "Vibration suppression with resettable device," *Journal of Engineering Mechanics*, vol. 128, no. 9, pp. 916–924, 2002.

[49] A. Agrawal, J. Yang, and W. He, "Applications of some semiactive control systems to benchmark cable-stayed bridge," *Journal of Structural Engineering*, vol. 129, no. 7, pp. 884–894, 2003.

[50] K. W. Min, H. S. Kim, S. H. Lee, H. Kim, and S. K. Ahn, "Performance evaluation of tuned liquid column dampers for response control of a 76-story benchmark building," *Engineering Structures*, vol. 27, no. 7, pp. 1101–1112, 2005.

[51] Y. Kitagawa, H. Tamai, and M. Takeshita, "Characteristics of piezoelectric dampers and their application to tall buildings as a smart structural system," in *13th World Conference on Earthquake Engineering*, 2004.

[52] Q. Feng and M. Shinozuka, "Use of a variable damper for hybrid control of bridge response under earthquake," in *Proc., US Nat. Workshop on Struct. Control Res.,, USC Publ. No. CE-9013*, 1990.

[53] B. Spencer, S. Dyke, M. Sain, and J. Carlson, "Phenomenological model for magnetorheological dampers," *Journal of Engineering Mechanics*, vol. 123, no. 3, pp. 230–238, 1997.

[54] K. D. Weiss and J. D. Carlson, "A growing attraction to magnetic fluids," *Machine Design*, vol. 66, no. 15, pp. 61–64, 1994.

[55] J. Rabinow, "The magnetic fluid clutch," *Transactions of the American Institute of Electrical Engineers*, vol. 67, pp. 1308–1315, 1948.

[56] M. F. Clutch and J. Rabinow, "Technical news bulletin," *National Bureau of Standards*, vol. 32, no. 4, pp. 54–60, 1948.

[57] R. Jacob, "Magnetic fluid torque and force transmitting device," 1951. US Patent No. 2,575,360.

[58] M. Schwartz, "Smart materials," *CRC Press*, 2008.

[59] J. D. Carlson, D. Catanzarite, and K. St. Clair, "Commercial magneto-rheological fluid devices," *International Journal of Modern Physics B*, vol. 10, pp. 2857–2865, 1996.

[60] J. P. Lynch, "Active structural control research at Kajima corporation," *The National Science Foundation's Summer Institute in Japan Program, Research Project*, vol. 17, p. 11, 1998.

[61] S. Dyke, B. Spencer Jr, P. Quast, M. Sain, D. Kaspari Jr, and T. Soong, "Experimental verification of acceleration feedback control strategies for an active tendon system," *Technical Report of National Center for Earthquake Engineering Research, NCEER-94*, vol. 24, 1994.

[62] X. Song, "Cost-effective skyhook control for semiactive vehicle suspension applications," *Open Mechanical Engineering Journal*, vol. 3, pp. 17–25, 2009.

[63] M. Ahmadian, X. Song, and S. C. Southward, "No-jerk skyhook control methods for semiactive suspensions," *Journal of Vibration and Acoustics*, vol. 126, no. 4, pp. 580–584, 2004.

[64] Y. T. Choi and N. M. Wereley, "Biodynamic response mitigation to shock loads using magnetorheological helicopter crew seat suspensions," *Journal of Aircraft*, vol. 42, no. 5, pp. 1288–1295, 2005.

[65] K.-S. Hong, H.-C. Sohn, and J. K. Hedrick, "Modified skyhook control of semi-active suspensions: A new model, gain scheduling, and hardware-in-the-loop tuning," *Journal of Dynamic Systems, Measurement, and Control*, vol. 124, no. 1, pp. 158–167, 2002.

[66] G. Priyandoko, M. Mailah, and H. Jamaluddin, "Vehicle active suspension system using skyhook adaptive neuro active force control," *Mechanical Systems and Signal Processing*, vol. 23, no. 3, pp. 855–868, 2009.

[67] M. Ahmadian and C. A. Pare, "A quarter-car experimental analysis of alternative semiactive control methods," *Journal of Intelligent Material Systems and Structures*, vol. 11, no. 8, pp. 604–612, 2000.

[68] Y. Liu, T. Waters, and M. Brennan, "A comparison of semi-active damping control strategies for vibration isolation of harmonic disturbances," *Journal of Sound and Vibration*, vol. 280, no. 1, pp. 21–39, 2005.

[69] S. Dyke, B. Spencer Jr, M. Sain, and J. Carlson, "Modeling and control of magnetorheological dampers for seismic response reduction," *Smart Materials and Structures*, vol. 5, no. 5, p. 565, 1996.

[70] L. M. Jansen and S. J. Dyke, "Semiactive control strategies for MR dampers: comparative study," *Journal of Engineering Mechanics*, vol. 126, no. 8, pp. 795–803, 2000.

[71] B. Sapiński, "Fuzzy control for MR damper in a driver's seat suspension," *Journal of Theoretical and Applied Mechanics*, vol. 43, no. 1, pp. 179–201, 2005.

[72] R. E. Kalman, "Contributions to the theory of optimal control," *Bol. Soc. Mat. Mexicana*, vol. 5, no. 2, pp. 102–119, 1960.

[73] C. Albert, "The analysis and synthesis of linear servomechanisms," *Technology Press, MIT, Cambridge, MA.*, 1943.

[74] N. Wiener, "Extrapolation, interpolation, and smoothing of stationary time series," *MIT Press Cambridge*, vol. 2, 1949.

[75] R. E. Kalman and R. S. Bucy, "New results in linear filtering and prediction theory," *Journal of Basic Engineering*, vol. 83, no. 1, pp. 95–108, 1961.

[76] M. G. Safonov and M. Athans, "Gain and phase margin for multiloop LQG regulators.," tech. rep., DTIC Document, 1976.

[77] J. Doyle, "Guaranteed margins for LQG regulators," *IEEE Transactions on Automatic Control*, vol. 23, pp. 756–757, 1978.

[78] S. Emelyanov, "Variable structure control systems," *Moscow, Nouka*, 1967.

[79] I. U. Vadim, "Survey paper variable structure systems with sliding modes," *IEEE Transactions on Automatic control*, vol. 22, no. 2, 1977.

[80] V. I. Utkin, "Variable structure systems- present and future," *Automation and Remote Control*, vol. 44, no. 9, pp. 1105–1120, 1984.

[81] J. Y. Hung, W. Gao, and J. C. Hung, "Variable structure control: a survey," *IEEE Transactions on Industrial Electronics*, vol. 40, no. 1, pp. 2–22, 1993.

[82] K. D. Young, V. I. Utkin, and U. Ozguner, "A control engineer's guide to sliding mode control," *IEEE Transactions on Control Systems Technology*, vol. 7, no. 3, pp. 328–342, 1999.

[83] X. Yu and O. Kaynak, "Sliding-mode control with soft computing: A survey," *IEEE Transactions on Industrial Electronics*, vol. 56, no. 9, pp. 3275–3285, 2009.

[84] G. Song and H. Gu, "Active vibration suppression of a smart flexible beam using a sliding mode based controller," *Journal of Vibration and Control*, vol. 13, no. 8, pp. 1095–1107, 2007.

[85] F. Piltan, B. Boroomand, A. Jahed, and H. Rezaie, "Methodology of mathematical error-based tuning sliding mode controller," *International Journal of Engineering*, vol. 6, no. 2, pp. 96–112, 2012.

[86] V. Q. Nguyen and S. B. Choi, "A robust vibration control for a multi-active mount system subjected to broadband excitation," *Smart Materials and Structures*, vol. 20, no. 5, p. 055002, 2011.

[87] K. C. Lu, C. H. Loh, J. N. Yang, and P. Y. Lin, "Decentralized sliding mode control of a building using MR dampers," *Smart Materials and Structures*, vol. 17, no. 5, p. 055006, 2008.

[88] B. Assadsangabi, M. Eghtesad, F. Daneshmand, and N. Vahdati, "Hybrid sliding mode control of semi-active suspension systems," *Smart Materials and Structures*, vol. 18, no. 12, p. 125027, 2009.

[89] J. l. Yao, W. k. Shi, J. q. Zheng, and H. p. Zhou, "Development of a sliding mode controller for semi-active vehicle suspensions," *Journal of Vibration and Control*, vol. 19, no. 8, pp. 1152–1160, 2013.

[90] A. Levant, "Sliding order and sliding accuracy in sliding mode control," *International Journal of Control*, vol. 58, no. 6, pp. 1247–1263, 1993.

[91] G. Bartolini, A. Pisano, E. Punta, and E. Usai, "A survey of applications of second-order sliding mode control to mechanical systems," *International Journal of Control*, vol. 76, no. 9-10, pp. 875–892, 2003.

[92] G. Bartolini, A. Pisano, and E. Usai, "Second-order sliding-mode control of container cranes," *Automatica*, vol. 38, no. 10, pp. 1783–1790, 2002.

[93] G. Bartolini, A. Ferrara, A. Levant, and E. Usai, "On second order sliding mode controllers," *Variable Structure Systems, Sliding Mode and Nonlinear Control*, pp. 329–350, 1999.

[94] A. Levant, "Higher-order sliding modes, differentiation and output-feedback control," *International Journal of Control*, vol. 76, no. 9-10, pp. 924–941, 2003.

[95] G. Bartolini, A. Ferrara, and E. Usani, "Chattering avoidance by second-order sliding mode control," *IEEE Transactions on Automatic Control*, vol. 43, no. 2, pp. 241–246, 1998.

[96] G. Bartolini, A. Ferrara, E. Usai, and V. I. Utkin, "On multi-input chattering-free second-order sliding mode control," *IEEE Transactions on Automatic Control*, vol. 45, no. 9, pp. 1711–1717, 2000.

[97] I. Boiko, L. Fridman, A. Pisano, and E. Usai, "Analysis of chattering in systems with second-order sliding modes," *IEEE Transactions on Automatic Control*, vol. 52, no. 11, pp. 2085–2102, 2007.

[98] C. Kim and P. Ro, "A sliding mode controller for vehicle active suspension systems with non-linearities," *Proceedings of the Institution of Mechanical Engineers, Part D: Journal of Automobile Engineering*, vol. 212, no. 2, pp. 79–92, 1998.

[99] J. Shi, X. Li, and J. Zhang, "Feedback linearization and sliding mode control for active hydropneumatic suspension of a special-purpose vehicle," *Proceedings of the Institution of Mechanical Engineers, Part D: Journal of Automobile Engineering*, vol. 224, no. 1, pp. 41–53, 2010.

[100] Y. M. Sam, J. H. Osman, and M. Ghani, "A class of proportional-integral sliding mode control with application to active suspension system," *Systems & Control Letters*, vol. 51, no. 3, pp. 217–223, 2004.

[101] C. Y. Lai and W.-H. Liao, "Vibration control of a suspension system via a magnetorheological fluid damper," *Journal of Vibration and Control*, vol. 8, no. 4, pp. 527–547, 2002.

[102] M. El-Kafafy, S. M. El-Demerdash, and A.-A. M. Rabeih, "Automotive ride comfort control using MR fluid damper," *Engineering*, vol. 4, p. 179, 2012.

[103] A. Bondarev, S. Bondarev, N. Kostyleva, and V. I. Utkin, "Sliding modes in systems with asymptotic state observers," *Avtomatika i Telemekhanika*, no. 6, pp. 5–11, 1985.

[104] K. D. Young and U. Ozguner, "Frequency shaping compensator design for sliding mode," *International Journal of Control*, vol. 57, no. 5, pp. 1005–1019, 1993.

[105] K. D. Young and S. V. Drakunov, "Sliding mode control with chattering reduction," in *American Control Conference*, pp. 1291–1292, 1992.

[106] W. C. Su, S. Drakunov, U. Ozguner, and K. D. Young, "Sliding mode with chattering reduction in sampled data systems," in *Proceedings of the 32nd IEEE Conference on Decision and Control*, pp. 2452–2457, 1993.

[107] V. I. Utkin and H. Lee, "Chattering problem in sliding mode control systems," in *IEEE International Workshop on Variable Structure Systems*, pp. 346–350, 2006.

[108] B. Cardoso, A. Moreira, B. Menezes, and P. Cortizo, "Analysis of switching frequency reduction methods applied to sliding mode controlled DC-DC converters," in *IEEE Seventh Annual Conference Proceedings of Applied Power Electronics*, pp. 403–410, 1992.

[109] K. J. Kim, J. B. Park, and Y. H. Choi, "Chattering free sliding mode control," in *IEEE International Joint Conference SICE-ICASE*, pp. 732–735, 2006.

[110] P. Kachroo and M. Tomizuka, "Chattering reduction and error convergence in the sliding-mode control of a class of nonlinear systems," *IEEE Transactions on Automatic Control*, vol. 41, no. 7, pp. 1063–1068, 1996.

[111] I. Boiko, L. Fridman, and R. Iriarte, "Analysis of chattering in continuous sliding mode control," in *Proceedings of the IEEE American Control Conference*, pp. 2439–2444, 2005.

[112] A. Bartoszewicz, "Discrete-time quasi-sliding-mode control strategies," *IEEE Transactions on Industrial Electronics*, vol. 45, no. 4, pp. 633–637, 1998.

[113] H. Lee and V. I. Utkin, "Chattering suppression methods in sliding mode control systems," *Annual Reviews in Control*, vol. 31, no. 2, pp. 179–188, 2007.

[114] V. Parra Vega and G. Hirzinger, "Chattering-free sliding mode control for a class of nonlinear mechanical systems," *International Journal of Robust and Nonlinear Control*, vol. 11, no. 12, pp. 1161–1178, 2001.

[115] H.-T. Yau and C.-L. Chen, "Chattering-free fuzzy sliding-mode control strategy for uncertain chaotic systems," *Chaos, Solitons & Fractals*, vol. 30, no. 3, pp. 709–718, 2006.

[116] V. I. Utkin, "Sliding modes in control and optimization," *Springer*, vol. 116, 1992.

[117] V. I. Utkin, J. Guldner, and M. Shijun, "Sliding mode control in electro-mechanical systems," *CRC Press*, vol. 34, 1999.

[118] W. Perruquetti and J. P. Barbot, "Sliding mode control in engineering," *CRC Press*, 2002.

[119] A. Astolfi and R. Ortega, "Immersion and invariance: a new tool for stabilization and adaptive control of nonlinear systems," *IEEE Transactions on Automatic Control*, vol. 48, no. 4, pp. 590–606, 2003.

[120] D. Karagiannis, A. Astolfi, and R. Ortega, "Nonlinear stabilization via system immersion and manifold invariance: survey and new results," *MMS*, vol. 3, no. 4, pp. 801–817, 2005.

[121] A. Astolfi, D. Karagiannis, and R. Ortega, "Towards applied nonlinear adaptive control," *Annu. Rev. Control*, vol. 32, no. 2, pp. 136–148, 2008.

[122] A. Astolfi and D. Karagiannis, "Nonlinear and adaptive control with applications," *Springer Science & Business Media*, 2007.

[123] B. Zhao, B. Xian, Y. Zhang, and X. Zhang, "Nonlinear robust adaptive tracking control of a quadrotor UAV via immersion and invariance methodology," *IEEE Transactions on Industrial Electronics*, vol. 62, no. 5, pp. 2891–2902, 2015.

[124] P. Santhanapipatkul and W. Khovidhungij, "Nonlinear controller design for active suspension systems using the immersion and invariance method," *World Congress*, vol. 16, no. 1, pp. 1934–1934, 2005.

[125] T. Wimbock, C. Ott, and G. Hirzinger, "Immersion and invariance control for an antagonistic joint with nonlinear mechanical stiffness," *Proceedings of 49th IEEE Conference on Decision and Control*, pp. 1128–1135, 2010.

[126] W. Dib, G. Kenné, and F. Lamnabhi-Lagarrigue, "An application of immersion and invariance to transient stability and voltage regulation of power systems with unknown mechanical power," *Proceedings of 48th IEEE CDC*, pp. 7837–7842, 2009.

[127] I. U. Khan and R. Dhaouadi, "Vibration suppression in elastic drive systems using the immersion and invariance methodology," *3rd IEEE International Conference on Electric Power and Energy Conversion Systems*, pp. 1–6, 2013.

[128] B. Spencer Jr and S. Nagarajaiah, "State of the art of structural control," *Journal of Structural Engineering*, vol. 129, no. 7, pp. 845–856, 2003.

[129] T. Soong and B. Spencer Jr, "Supplemental energy dissipation: state-of-the-art and state-of-the-practice," *Engineering Structures*, vol. 24, no. 3, pp. 243–259, 2002.

[130] D. Demetriou, N. Nikitas, and K. D. Tsavdaridis, "A novel hybrid semi-active mass damper for lightweight steel structural applications," in *The 8th International Conference on Advances in Steel Structures*, 2015.

[131] D. Demetriou and N. Nikitas, "A novel hybrid semi-active mass damper configuration for structural applications," *Applied Sciences*, vol. 6, no. 12, p. 397, 2016.

[132] I. U. Khan, D. Wagg, and N. D. Sims, "Improving the vibration suppression capabilities of a magneto-rheological damper using hybrid active and semi-active control," *Smart Materials and Structures*, vol. 25, no. 8, p. 085045, 2016.

[133] I. U. Khan, D. Wagg, and N. D. Sims, "Hybrid active and semi-active control for vibration suppression in flexible structures," in *Dynamic Systems and Control Conference*, American Society of Mechanical Engineers, 2016.

[134] I. U. Khan, D. Wagg, and N. D. Sims, "Nonlinear robust observer design using an invariant manifold approach," *Control Engineering Practice*, vol. 55, pp. 69–79, 2016.

[135] I. U. Khan, D. Wagg, and N. D. Sims, "Hybrid active and semi-active control for pantograph-catenary system of high-speed train," in *27th International Conference on Noise and Vibration, ISMA*, 2016.

[136] I. U. Khan and R. Dhaouadi, "Robust control of elastic drives through immersion and invariance," *IEEE Transactions on Industrial Electronics*, vol. 62, no. 3, pp. 1572–1580, 2015.

[137] G. M. Kamath, M. K. Hurt, and N. M. Wereley, "Analysis and testing of bingham plastic behavior in semi-active electrorheological fluid dampers," *Smart Materials and Structures*, vol. 5, no. 5, p. 576, 1996.

[138] N. D. Sims, N. Holmes, and R. Stanway, "A unified modelling and model updating procedure for electrorheological and magnetorheological vibration dampers," *Smart Materials and Structures*, vol. 13, no. 1, p. 100, 2004.

[139] P. Brezas, M. C. Smith, and W. Hoult, "A clipped-optimal control algorithm for semi-active vehicle suspensions: Theory and experimental evaluation," *Automatica*, vol. 53, pp. 188–194, 2015.

[140] C. K. Ide, S. Olaru, P. Rodriguez Ayerbe, and A. Rachid, "A nonlinear state feedback control approach for a pantograph-catenary system," in *17th IEEE International Conference System Theory, Control and Computing (ICSTCC)*, pp. 268–273, 2013.

[141] R. Garg, P. Mahajan, P. Kumar, and V. Gupta, "Design and study of active controllers for pantograph-catenary system," in *IEEE Conference and Expo Transportation Electrification Asia-Pacific (ITEC Asia-Pacific)*, 2014.

[142] P. Mahajan, R. Garg, V. Gupta, and P. Kumar, "Design of controller for pantograph-catenary system using reduced order model," in *6th IEEE Power India International Conference (PIICON)*, pp. 1–6, 2014.

[143] E. Karakose and M. T. Gencoglu, "Adaptive fuzzy control approach for dynamic pantograph-catenary interaction," in *15th IEEE International Symposium MECHATRONIKA*, pp. 1–5, 2012.

[144] Y. J. Huang and T. C. Kuo, "Discrete pantograph position control for the high speed transportation systems," in *IEEE International Conference on Networking, Sensing and Control*, vol. 2, pp. 932–936, 2004.

[145] E. Karakose and M. T. Gencoglu, "An investigation of pantograph parameter effects for pantograph-catenary systems," in *IEEE International Symposium on Innovations in Intelligent Systems and Applications (INISTA)*, pp. 338–343, 2014.

[146] N. Mokrani and A. Rachid, "A robust control of contact force of pantograph-catenary for the high-speed train," in *2013 European Control Conference (ECC)*, pp. 4568–4573, 2013.

[147] A. Pisano and E. Usai, "Contact force estimation and regulation in active pantographs: an algebraic observability approach," *Asian Journal of Control*, vol. 13, no. 6, pp. 761–772, 2011.

[148] N. Mokrani, A. Rachid, and M. A. Rami, "A tracking control for pantograph-catenary system," in *54th IEEE Annual Conference on Decision and Control (CDC)*, pp. 185–190, 2015.

[149] N. Kazantzis and C. Kravaris, "Nonlinear observer design using Lyapunov's auxiliary theorem," *Systems & Control Letters*, vol. 34, no. 5, pp. 241–247, 1998.

[150] J. Yao, Z. Jiao, and D. Ma, "Extended-state-observer-based output feedback nonlinear robust control of hydraulic systems with backstepping," *IEEE Transactions on Industrial Electronics*, vol. 61, no. 11, pp. 6285–6293, 2014.

[151] M. Ruderman and M. Iwasaki, "Observer of nonlinear friction dynamics for motion control," *IEEE Transactions on Industrial Electronics*, vol. 62, no. 9, pp. 5941–5949, 2015.

[152] R. E. Kalman, "A new approach to linear filtering and prediction problems," *Journal of Fluids Engineering*, vol. 82, no. 1, pp. 35–45, 1960.

[153] D. G. Luenberger, "Observing the state of a linear system," *IEEE Transactions on Military Electronics*, vol. 8, no. 2, pp. 74–80, 1964.

[154] M. Zeitz, "The extended Luenberger observer for nonlinear systems," *Systems & Control Letters*, vol. 9, no. 2, pp. 149–156, 1987.

[155] M. G. Price and G. Cook, "Identification/observation using an extended Luenberger observer," *IEEE Transactions on Industrial Electronics*, vol. IE-29, no. 4, pp. 279–287, 1982.

[156] M. Boutayeb and D. Aubry, "A strong tracking extended Kalman observer for nonlinear discrete-time systems," *IEEE Transactions on Automatic Control*, vol. 44, no. 8, pp. 1550–1556, 1999.

[157] P. Mercorelli, "A two-stage augmented extended Kalman filter as an observer for sensorless valve control in camless internal combustion engines," *IEEE Transactions on Industrial Electronics,*, vol. 59, no. 11, pp. 4236–4247, 2012.

[158] F. Thau, "Observing the state of non-linear dynamic systems," *International Journal of Control*, vol. 17, no. 3, pp. 471–479, 1973.

[159] S. R. Kou, D. L. Elliott, and T. J. Tarn, "Exponential observers for nonlinear dynamic systems," *Information and Control*, vol. 29, no. 3, pp. 204–216, 1975.

[160] P. Vaclavek and P. Blaha, "Lyapunov-function-based flux and speed observer for AC induction motor sensorless control and parameters estimation," *IEEE Transactions on Industrial Electronics*, vol. 53, no. 1, pp. 138–145, 2005.

[161] H. Chaoui, N. Golbon, I. Hmouz, R. Souissi, and S. Tahar, "Lyapunov-based adaptive state of charge and state of health estimation for lithium-ion batteries," *IEEE Transactions on Industrial Electronics*, vol. 62, no. 3, pp. 1610–1618, 2015.

[162] A. Nikoobin and R. Haghighi, "Lyapunov-based nonlinear disturbance observer for serial n-link robot manipulators," *Journal of Intelligent and Robotic Systems*, vol. 55, no. 2-3, pp. 135–153, 2009.

[163] C. Lageman, R. Mahony, and J. Trumpf, "State observers for invariant dynamics on a Lie group," in *18th International Symposium on Mathematical Theory of Networks and Systems*, p. 8, 2008.

[164] S. E. Talole, J. P. Kolhe, and S. B. Phadke, "Extended-state-observer-based control of flexible-joint system with experimental validation," *IEEE Transactions on Industrial Electronics*, vol. 57, no. 4, pp. 1411–1419, 2010.

[165] S. Li, J. Yang, W.-H. Chen, and X. Chen, "Generalized extended state observer based control for systems with mismatched uncertainties," *IEEE Transactions on Industrial Electronics*, vol. 59, no. 12, pp. 4792–4802, 2012.

[166] Y. Huang, K. Xu, J. Han, and J. Lam, "Flight control design using extended state observer and non-smooth feedback," in *Proceedings of the IEEE Conference on Decision and Control*, vol. 1, pp. 223–228, 2001.

[167] D. Maithripala, J. M. Berg, and W. Dayawansa, "An intrinsic observer for a class of simple mechanical systems on a Lie group," in *Proceedings of the IEEE American Control Conference*, vol. 2, pp. 1546–1551, 2004.

[168] C. Lageman, J. Trumpf, and R. Mahony, "Gradient-like observers for invariant dynamics on a Lie group," *IEEE Transactions on Automatic Control*, vol. 55, no. 2, pp. 367–377, 2010.

[169] C. Edwards and C. P. Tan, "Sensor fault tolerant control using sliding mode observers," *Control Engineering Practice*, vol. 14, no. 8, pp. 897–908, 2006.

[170] F. Nollet, T. Floquet, and W. Perruquetti, "Observer-based second order sliding mode control laws for stepper motors," *Control Engineering Practice*, vol. 16, no. 4, pp. 429–443, 2008.

[171] J. J. Slotine, J. Hedrick, and E. Misawa, "On sliding observers for nonlinear systems," *Journal of Dynamic Systems, Measurement, and Control*, vol. 109, no. 3, pp. 245–252, 1987.

[172] C. Edwards, S. K. Spurgeon, C. P. Tan, and N. Patel, "Sliding-mode observers," in *Mathematical Methods for Robust and Nonlinear Control*, pp. 221–242, Springer, 2007.

[173] K. Kalsi, J. Lian, S. Hui, and S. H. Zak, "Sliding-mode observers for uncertain systems," in *American Control Conference*, pp. 1189–1194, 2009.

[174] L. Fridman, Y. Shtessel, C. Edwards, and X.-G. Yan, "Higher-order sliding-mode observer for state estimation and input reconstruction in nonlinear systems," *International Journal of Robust and Nonlinear Control*, vol. 18, no. 4-5, pp. 399–412, 2008.

[175] L. Fridman, A. Levant, and J. Davila, "Observation of linear systems with unknown inputs via high-order sliding-modes," *International Journal of Systems Science*, vol. 38, no. 10, pp. 773–791, 2007.

[176] T. Floquet and J. P. Barbot, "A canonical form for the design of unknown input sliding mode observers," in *Advances in Variable Structure and Sliding Mode Control*, pp. 271–292, Springer, 2006.

[177] B. Walcott and S. Zak, "Observation of dynamical systems in the presence of bounded nonlinearities/uncertainties," in *25th IEEE Conference on Decision and Control*, no. 25, pp. 961–966, 1986.

[178] S. Drakunov and V. I. Utkin, "Sliding mode observers. tutorial," in *Proceedings of the 34th IEEE Conference on Decision and Control*, vol. 4, pp. 3376–3378, 1995.

[179] F. Zhu and Z. Han, "A note on observers for Lipschitz nonlinear systems," *IEEE Transactions on Automatic Control*, vol. 47, no. 10, pp. 1751–1754, 2002.

[180] W. Zhang, H. Su, H. Wang, and Z. Han, "Full-order and reduced-order observers for one-sided Lipschitz nonlinear systems using Riccati equations," *Communications in Nonlinear Science and Numerical Simulation*, vol. 17, no. 12, pp. 4968–4977, 2012.

[181] A. Zemouche, M. Boutayeb, and G. I. Bara, "Observers for a class of Lipschitz systems with extension to H-infinity performance analysis," *Systems & Control Letters*, vol. 57, no. 1, pp. 18–27, 2008.

[182] Q. P. Ha and H. Trinh, "State and input simultaneous estimation for a class of nonlinear systems," *Automatica*, vol. 40, no. 10, pp. 1779–1785, 2004.

[183] I. U. Khan and R. Dhaouadi, "Nonlinear reduced order observer design for elastic drive systems using invariant manifolds," in *IEEE International Conference on Mechatronics (ICM)*, pp. 58–63, 2015.

[184] F. Morbidi, G. L. Mariottini, and D. Prattichizzo, "Observer design via immersion and invariance for vision-based leader–follower formation control," *Automatica*, vol. 46, no. 1, pp. 148–154, 2010.

[185] D. Karagiannis, D. Carnevale, and A. Astolfi, "Invariant manifold based reduced-order observer design for nonlinear systems," *IEEE Transactions on Automatic Control*, vol. 53, no. 11, pp. 2602–2614, 2008.

[186] G. Besancon and A. Ticlea, "An immersion-based observer design for rank-observable nonlinear systems," *IEEE Transactions on Automatic Control*, vol. 52, no. 1, pp. 83–88, 2007.

[187] A. Astolfi, R. Ortega, and A. Venkatraman, "A globally exponentially convergent immersion and invariance speed observer for mechanical systems with non-holonomic constraints," *Automatica*, vol. 46, no. 1, pp. 182–189, 2010.

[188] S. Raghavan and J. K. Hedrick, "Observer design for a class of nonlinear systems," *International Journal of Control*, vol. 59, no. 2, pp. 515–528, 1994.

[189] V. Wickramasinghe, C. Yong, and D. Zimcik, "Development of an active suspension system for adaptive vibration control of helicopter seats," *NA TORTOA VT-170/RSM-025 on Active Suspension Technologies for Military Vehicles and Platforms*, 2010.

[190] V. K. Wickramasinghe, *Dynamics Control Approaches to Improve Vibratory Environment of the Helicopter Aircrew*. PhD thesis, Carleton University Ottawa, 2012.

Appendix A

Abstracts of Published Work

Improving the vibration suppression capabilities of a magnetorheological damper using hybrid active and semi-active control

Smart Materials and Structures Journal

vol. 25, no. 8, p. 085045, 2016

I.U. Khan, D.Wagg, N.D. Sims

University of Sheffield, Department of Mechanical Engineering,

S1 3JD, Sheffield, United Kingdom

Abstract

This paper presents a new hybrid active & semi-active control method for vibration suppression in flexible structures. The method uses a combination of a semi-active device and an active control actuator situated elsewhere in the structure to suppress vibrations. The key novelty is to use the hybrid controller to enable the magneto-rheological damper to achieve a performance as close to a fully active device as possible. This is achieved by ensuring that the active actuator can assist the magneto-rheological damper in the regions where energy is required. In addition, the hybrid active & semi-active controller is designed to minimize the switching of the semi-active controller. The control framework used is the immersion and invariance control technique in combination with sliding mode control. A two degree-of-freedom system with lightly damped resonances is used as an example system. Both numerical and experimental results are generated for this system, and then compared as part of a validation study. The experimental system uses hardware-in-the-loop to simulate the effect of both the degrees-of-freedom. The results show that the concept is viable both numerically and experimentally, and improved vibration suppression results can be obtained for the magneto-rheological damper that approach the performance of an active device.

Nonlinear robust observer design using an invariant manifold approach

Control Engineering Practice Journal

vol. 55, pp. 69–79, 2016

I.U. Khan, D.Wagg, N.D. Sims

University of Sheffield, Department of Mechanical Engineering,

S1 3JD, Sheffield, United Kingdom

Abstract

This paper presents a method to design a reduced order observer using an invariant manifold approach. The main advantages of this method are that it enables a systematic design approach, and (unlike most nonlinear observer design methods), it can be generalized over a larger class of nonlinear systems. The method uses specific mapping functions in a way that minimises the error dynamics close to zero. Another important aspect is the robustness property which is due to the manifold attractivity: an important feature when an observer is used in a closed loop control system. A two degree-of-freedom system is used as an example. The observer design is validated using numerical simulation. Then experimental validation is carried out using hardware-in-loop testing. The proposed observer is then compared with a very well known nonlinear observer based on the off-line solution of the Riccati equation for systems with Lipschitz type nonlinearity. In all cases, the performance of the proposed observer is shown to be very high.

Hybrid active and semi-active control for pantograph catenary system of high-speed train

International Conference on Noise and Control, ISMA 2016

Leuven, Belgium, 19-21 September, 2016.

I.U. Khan, D.Wagg, N.D. Sims

University of Sheffield, Department of Mechanical Engineering,

S1 3JD, Sheffield, United Kingdom

Abstract

In this paper a new hybrid control methodology using active actuator and semi-active device is proposed to minimize the oscillations between the pantograph and catenary by keeping the contact force between them constant. One of the advantage of using the proposed hybrid controller is that a semi-active device can easily be mounted on the pantograph upper arm without compromising the weight and the size. As the performance of a semi-active device is restricted because of the passivity constraint. To assist the semi-active device and to achieve the desired performance an active actuator is placed at the base of the pantograph. Immersion and invariance (I & I) methodology is used to design the controller for the active actuator and sliding mode control (SMC) is used to design the controller for the semi-active device. Simulations show promising results.

Hybrid active and semi-active control for vibration suppression in flexible structures

Dynamic Systems and Control Conference, DSCC 2016

Minneapolis, Minnesota, USA, 12-14 October, 2016.

I.U. Khan, D.Wagg, N.D. Sims

University of Sheffield, Department of Mechanical Engineering,

S1 3JD, Sheffield, United Kingdom

Abstract

A new hybrid control methodology is presented for vibration suppression in flexible structures, where an active actuator is used to assist a nearby semi-active device to achieve a control performance close to that of a fully active system. The clipping phenomenon, typical of semi-active control, is reduced to a large extent by the proposed hybrid controller. The immersion and invariance methodology along with sliding mode control is used to create the hybrid controller. The result is that as the semi-active controller switches off in the hybrid controller, the active actuator injects the required energy into the system. A two degree of freedom system with cubic stiffness is used as an example system. Both simulation and experiment data are presented to demonstrate the usefulness of the proposed idea. The proposed hybrid controller shows robust results as compared to just using a semi-active controller.

Appendix B

Sliding Mode Control

In order to explain the SMC, consider a nonlinear system of the form

$$\dot{x}^{(n)} = f(x,t) + g(x,t)u(t) \tag{B.1}$$

Where x represents the states of the system up to $n-1$ derivative, n represents the order of differentiation, u is the control input, $f(x,t)$ and $g(x,t)$ are nonlinear function of x and t. It is assumed that these nonlinear functions are not exactly known, but the upper bound on both the functions are known. The estimation error in $f(x,t)$ and $g(x,t)$ can be expressed as

$$|\hat{f}(x,t) - f(x,t)| \leq F(x,t) \tag{B.2}$$

$$|\hat{g}(x,t) - g(x,t)| \leq G(x,t) \tag{B.3}$$

Where $\hat{f}(x,t)$ and $\hat{g}(x,t)$ represent the estimation of $f(x,t)$ and $g(x,t)$ respectively. The error signal $e(t)$, is defined in terms of the actual signal, x and the reference signal, x_r.

$$e(t) = x - x_r \tag{B.4}$$

The sliding surface $S(x,t)$, is defined as

$$S(x,t) = \left(\frac{d}{dt} + \lambda\right)^{(n-1)} e(t) \tag{B.5}$$

Where $\lambda > 0$ determines that how fast the error dynamics will decay. On the sliding surface the error dynamics are given by the equation.

$$\left(\frac{d}{dt} + \lambda\right)^{(n-1)} e(t) = 0 \tag{B.6}$$

In order to derive the control law, (B.5) will be used and $\dot{S}$ will be computed. As the error will go towards zero on the sliding surface, $\dot{S}$ will also go to zero.

Defining S in terms of error dynamics as $S = e^{(n-1)} + ... + \lambda^{(n-1)} e$

Differentiating S gives

$$\dot{S} = e^{(n)} + ... + \lambda^{(n-1)} \dot{e}$$

$$\dot{S} = x^{(n)} - {x_r}^{(n)} + ... + \lambda^{(n-1)} \dot{e}$$

$$\dot{S} = f(x,t) + g(x,t)u - {x_r}^{(n)} + ... + \lambda^{(n-1)} \dot{e} \tag{B.7}$$

Computing $\hat{u}$ from (B.7) gives

$$\hat{u} = \frac{1}{\hat{g}(x,t)} \left(-\hat{f}(x,t) + {x_r}^{(n)} - ... - \lambda^{(n-1)} \dot{e} \right) \tag{B.8}$$

When $\dot{S} = 0$, then the control signal is given by (B.8). To add the robustness property to the controller a second part is added to it.

$$u_{rb} = \hat{u} - \frac{K}{\hat{g}(x,t)} \mathrm{sgn}(x) \tag{B.9}$$

where

$$\text{sgn}(x) = \begin{cases} +1 & x > 0 \\ -1 & x < 0 \end{cases} \tag{B.10}$$

and the Lyapunov stability theorem has been used to make sure that the sliding surface has asymptotic stable origin, towards which the system dynamics will slide. The Lyapunov function is defined as

$$V = \frac{1}{2}S^2 \tag{B.11}$$

To make sure that the system dynamics will reach in finite time on the sliding surface another condition is imposed, which is given as

$$V \leq -\eta_{smc}|S| \tag{B.12}$$

Appendix C

Controller Gain Design

SMC Controller Gain Design

To find the reaching phase time for the sliding surface, the relationship between S and V_{smc} is used as

$$\dot{V}_{smc} = -\eta_{smc}|S| \tag{C.1}$$

Substituting S in the above equation using the relation $V_{smc} = \frac{1}{2}S^2$ gives

$$\dot{V}_{smc} = -\eta_{smc}\sqrt{2V_{smc}} \tag{C.2}$$

$$\frac{dV_{smc}}{\sqrt{V_{smc}}} = -\eta_{smc}\sqrt{2}dt$$

Integrating the above equation gives

$$\int_{V_{smc}(0)}^{V_{smc}(T)} \frac{1}{\sqrt{V_{smc}}} dV_{smc} = -\eta_{smc}\sqrt{2}\int_0^T dt$$

$$2\sqrt{V_{smc}(T)} - 2\sqrt{V_{smc}(0)} = -\eta_{smc}\sqrt{2}(T-0) \tag{C.3}$$

At time T the sliding surface will be reached and $S(T) = 0$ which leads to $V_{smc}(T) = 0$

$$2\sqrt{V_{smc}(0)} = \eta_{smc}\sqrt{2}T$$

$$T = \frac{\sqrt{2V_{smc}(0)}}{\eta_{smc}} \tag{C.4}$$

where

$$V_{smc}(0) = \frac{1}{2}S(0)^2$$

and

$$S(0) = \lambda_1 e_1(0) + \lambda_2 \dot{e}_1(0)$$

λ_1, λ_2 for the sliding surface S, should be chosen in such a way that $x^2 + \lambda_2 x + \lambda_1$ is Hurtwiz polynomial.

PI Controller Gain Design

In order to find the equations for the controller gains, the closed loop transfer function of the PI controller with the target system shown in Figure C.1, is given as

$$G_{cl} = \frac{\frac{K_p K_i}{m_t s^3}}{1 + \frac{K_p K_i}{m_t s^3} + \frac{K_i}{m_t s^2} + \frac{K_v}{m_t s}} \tag{C.5}$$

Rearranging (C.5), gives

$$G_{cl} = \frac{\frac{K_p K_i}{m_t}}{s^3 + \frac{K_v}{m_t}s^2 + \frac{K_i}{m_t}s + \frac{K_p K_i}{m_t}} \tag{C.6}$$

The denominator of (C.6) can be written in factor form as

$$\delta = (s^2 + 2\zeta\omega_n s + \omega_n^2)(s + a) \tag{C.7}$$

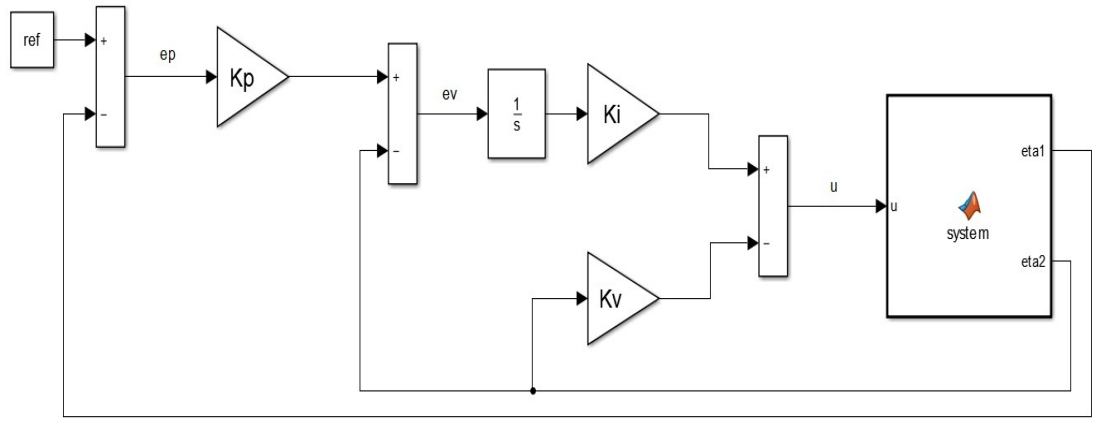

Fig. C.1 PI controller block diagram

leads to

$$\delta = s^3 + (a + 2\zeta\omega_n)s^2 + (2\zeta\omega_n a + \omega_n^2)s + a\omega_n^2 \tag{C.8}$$

Comparing (C.8) and denominator of (C.6) gives

$$a + 2\zeta\omega_n = \frac{K_v}{m_t}$$

$$2\zeta\omega_n a + \omega_n^2 = \frac{K_i}{m_t}$$

$$a\omega_n^2 = \frac{K_p K_i}{m_t}$$

Finally the controller gains are given as

$$K_p = \frac{a\omega_n}{2\zeta a + \omega_n} \tag{C.9}$$

$$K_i = m_t(2\zeta\omega_n a + \omega_n^2) \tag{C.10}$$

$$K_v = m_t(a + 2\zeta\omega_n) \tag{C.11}$$

Index